9 November 2007 | $10

# Science

AAAS

Volume 318, Issue 5852


## COVER

All-sky projection of highest-energy cosmic rays detected by the Pierre Auger Observatory (open circles) that are correlated with the positions of nearby quasars (crosses), a measure of the local galaxy distribution. The supergalactic and Milky Way planes are marked. The background shows a composite image of a nearby galaxy (M82) observed by NASA's Spitzer, Hubble, and Chandra space observatories. See page 938.

***Composite image: Kelly Krause/Science (figure: Auger Collaboration; photo: NASA/JPL-Caltech/STScI/Chandra X-ray Center/Univ. of Arizona/ESA/AURA/Johns Hopkins Univ.)***

## DEPARTMENTS



## EDITORIAL



## NEWS OF THE WEEK



## NEWS FOCUS




## LETTERS



## BOOKS *ET AL.*



## POLICY FORUM



## PERSPECTIVES





CONTENTS continued >>

Science



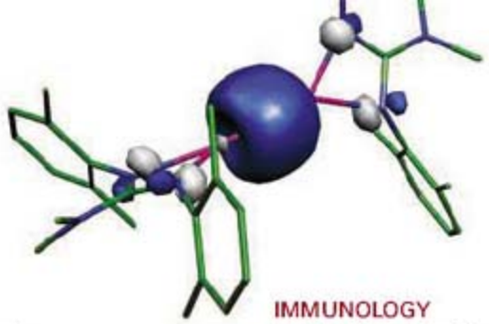

## SCIENCE EXPRESS

www.sciencexpress.org

CHEMISTRY

**Stable Magnesium(I) Compounds with Mg-Mg Bonds**
*S. P. Green, C. Jones, A. Stasch*
Controlled reduction of a magnesium compound coordinated by bulky nitrogen-based ligands yields the previously elusive +1 oxidation state of the element.
10.1126/science.1150856

MEDICINE

**The Obesity-Associated *FTO* Gene Encodes a 2-Oxoglutarate–Dependent Nucleic Acid Demethylase**
*T. Gerken* et al.
A gene that affects an individual's risk of obesity codes for a protein that removes methyl groups from DNA, although how this function regulates obesity is unclear.
10.1126/science.1151710

IMMUNOLOGY

**DUBA: A Deubiquitinase That Regulates Type I Interferon Production**
*N. Kayagaki* et al.
Interferon secretion in response to viral infection is reduced by an enzyme that removes ubiquitin chains from proteins, an effect that could inhibit autoimmune disease.
10.1126/science.1145918

ECOLOGY

**Asymmetric Mating Interactions Drive Widespread Invasion and Displacement in a Whitefly**
*S.-S. Liu* et al.
The success of the invasive whitefly in China and Australia is the result of reproductive suppression of native populations by the invader.
10.1126/science.1149887

## TECHNICAL COMMENT ABSTRACTS



## REVIEW



## BREVIA



944

## RESEARCH ARTICLES



## REPORTS



CONTENTS continued >>

Science



970

## REPORTS *CONTINUED...*



SPECIAL FEATURE

## Managing a Productive Laboratory

*www.sciencecareers.org*



AAAS
ADVANCING SCIENCE, SERVING SOCIETY

**SCIENCE (ISSN 0036-8075) is published weekly on Friday, except the last week in December, by the American Association for the Advancement of Science, 1200 New York Avenue, NW, Washington, DC 20005.** Periodicals Mail postage (publication No. 484460) paid at Washington, DC, and additional mailing offices.  The title SCIENCE is a registered trademark of the AAAS. Domestic individual membership and subscription (51 issues): $142 ($74 allocated to subscription). Domestic institutional subscription (51 issues): $710; Foreign postage extra: Mexico, Caribbean (surface mail) $55; other countries (air assist delivery) $85. First class, airmail, student, and emeritus rates on request. Canadian rates with GST available upon request, GST #1254 88122. Publications Mail Agreement Number 1069624. SCIENCE is printed on 30 percent post-consumer recycled paper. **Printed in the U.S.A.**

**Change of address:** Allow 4 weeks, giving old and new addresses and 8-digit account number. **Postmaster:** Send change of address to AAAS, P.O. Box 96178, Washington, DC 20090–6178. **Single-copy sales:** $10.00 current issue, $15.00 back issue prepaid includes surface postage; bulk rates on request.  The identification code for *Science* is 0036-8075. *Science* is indexed in the *Reader's Guide to Periodical Literature* and in several specialized indexes.

Printed on 30% post-consumer recycled paper.

CONTENTS continued >>

Paris Hilton stresses mice out.

## SCIENCENOW

www.sciencenow.org DAILY NEWS COVERAGE

**Stress, Pain, and Paris Hilton**
A cardboard cutout of the reality show star reveals a curious gender difference in mice.

**Robot Dearest?**
Children show affinity for interactive machines.

**Planting RNA on the Farm**
Modifying crops with small RNAs can be a turnoff to pests.

The essential skills of management.

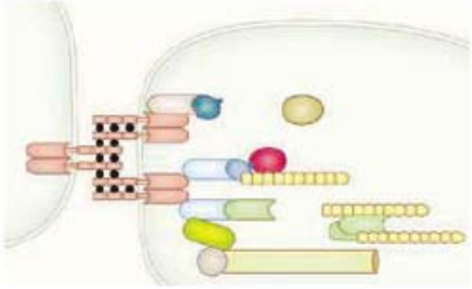

Regulating adherens junction integrity.

## SCIENCE'S STKE

www.stke.org SIGNAL TRANSDUCTION KNOWLEDGE ENVIRONMENT

**PERSPECTIVE: The Role of Intracellular Calcium and RhoA in Neuronal Migration**
*C. H. Faux and J. G. Parnavelas*
Do calcium signals coordinate neuronal migration?

**PERSPECTIVE: Tumbling, An Interactive Way to Move Forward**
*H. Sano, S. Ricardo, R. Lehmann*
Border cells use multiple mechanisms to move as a collective unit.

**REVIEW: Dual Regulation of Endothelial Junctional Permeability**
*Y. A. Komarova, D. Mehta, A. B. Malik*
Inflammatory mediators both disrupt and help repair the endothelial barrier.

## SCIENCECAREERS

www.sciencecareers.org CAREER RESOURCES FOR SCIENTISTS

*>> Managing a Productive Laboratory feature, page 993*

**GLOBAL: Special Feature—Lab Management**
*J. Austin*
*Science* Careers offers primers on managing people and resources in a laboratory.

**GLOBAL: Laughter in the Lab**
*I. S. Levine*
When used wisely, humor can defuse difficult situations and increase productivity.

## SCIENCEPODCAST

Download the 9 November *Science* Podcast to hear about extragalactic high-energy cosmic rays, the invasive success of whiteflies, choosing the next Mars rover landing site, and more.
www.sciencemag.org/about/podcast.dtl

CREDIT: (SCIENCE CAREERS) JOHANNA BLESS; (SCIENCE NOW) VAUGHN YOUTZ/ZUMA PRESS

***Separate individual or institutional subscriptions to these products may be required for full-text access.***

EDITED BY STELLA HURTLEY AND PHIL SZUROMI

## << Speedier Yellowstone Uplift

The Yellowstone caldera is the remnant of three giant eruptions 640,000 years ago, as well as numerous smaller eruptions prior to 70,000 years ago. The region is still very active and experiences earthquakes, heat flow, and ground deformation, as well as hydrothermal activity. **Chang *et al.*** (p. 952) present satellite radar and global positioning satellite measurements which show that the caldera underwent a period of accelerated uplift between 2004 and 2006. The highest rate of about 7 centimeters per year is more than three times faster than uplift rates measured since the 1920s. The uplift may reflect ongoing magma recharge and fluid redistribution.

## Energizing Cosmic Rays

Cosmic rays are energetic particles that are accelerated by magnetic fields in space. A very small fraction of the cosmic rays that penetrate Earth's atmosphere have tremendous energies, exceeding tens of EeV (1 EeV is $10^{18}$ electron volts). Their presence is puzzling because cosmic rays should lose energy very quickly as they travel through space, and so these highest-energy particles would not be expected to survive the journey. **The Pierre Auger Collaboration** (p. 938; see the cover and the news story by **Cho**) detected 80 of the highest-energy cosmic rays and located their directions in the sky by combining two detection techniques. The most energetic cosmic rays originate statistically from areas of the sky that are populated by nearby active galactic nuclei, which themselves trace galaxy-rich regions that include the supergalactic plane. Thus, the cosmic rays' huge energies might be explained if they were accelerated around giant galactic black holes lying within 75 megaparsecs of the Milky Way.

## Morning Methane Mist

When the Huygens probe landed on Titan, it descended through clouds of methane and landed on a damp surface wetted by methane mist. Larger fluvial channels suggest that Titan's weather may become stormier and has prompted the need for understanding of its atmospheric methane cycles. **Ádámkovics *et al.*** (p. 962, published online 11 October) used terrestrial telescopes to map areas of high-infrared methane opacity in Titan's lower troposphere. These studies revealed methane clouds and droplets below 15 kilometers altitude and methane drizzle below 5 kilometers. These phenomena are seen preferentially on the morning side of the leading hemisphere, which suggests that diurnal temperature gradients may contribute to variations in methane relative humidity, as well as to winds and topography. Thus, morning drizzle is widespread and may be the dominant mechanism for returning from the atmospheric methane to the surface.

CREDITS (TOP TO BOTTOM): ROBERT B. SMITH/UNIVERSITY OF UTAH; ARAKAWA ET AL.

## Thrown for a Dislocation Loop

The migration behavior of vacancies and self-interstitial atoms are of importance in understanding radiation damage effects in materials and mechanical responses to applied stresses (see the Perspective by **Wirth**). **Arakawa *et al.*** (p. 956) show that for α-iron, defect loops can migrate even under a zero-stress condition. Motion arises through the formation of double kinks, and fluctuations in their number drives the motion of loop defects; their diffusion rate depends on the loop size. These observations help directly confirm many of the effects associated with the migration of radiation-induced defects and dislocations loops. Prior simulation studies have indicated that small vacancy loops would not undergo one-dimensional (1D) migration in face-centered cubic metals. **Matsukawa and Zinkle** (p. 959) use in situ transmission electron microscopy observations of gold foil specimens that contained a large number of vacancies and observed vacancy loops showing 1D oscillatory motion. A prismatic, highly mobile vacancy-type dislocation loop can spontaneously transform into a stacking fault tetrahedron.

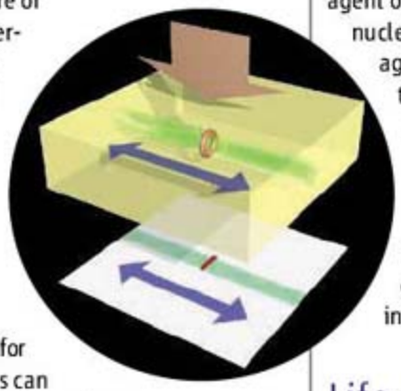

## Straining to Understand Prion Diseases

Mammalian prion diseases are infectious lethal neurodegenerative disorders. The pathogenic agent of prion diseases is thought to lack nucleic acids, but instead relies on the propagation of a pathological conformation of the prion protein, an endogenous glycoprotein. **Collinge and Clarke** (p. 930) review several aspects of prion diseases, including how prion strains can be generated and maintained and suggest a model for how prion propagation involves the generation of toxic intermediates.

## Life and Death Decisions

How do cells determine whether to live or die after exposure to stressors that cause misfolding of intracellular proteins? **Lin *et al.*** (p. 944) find that the IRE1 signaling branch of the unfolded protein response plays a key role in promoting cell survival after protein misfolding in the endoplasmic reticulum (ER). Human cells shut off IRE1 signaling after prolonged ER protein misfolding in order to enhance cell survival.

*Continued on page 885*

Donald Kennedy is the Editor-in-Chief of *Science*.

# Bill Golden

THE SCIENTIFIC COMMUNITY LOST A REMARKABLE RESOURCE WHEN WILLIAM T. GOLDEN, for years the treasurer of the American Association for the Advancement of Science (AAAS) among many other things, passed away on 7 October of this year at the age of 97. Bill had a stunning career, well positioned at the juncture of the science he loved and the public interest to which he was so dedicated. He will be missed for many reasons, not least because he was a treasury of knowledge and recollection about science and public policy.

The list of his commitments is not merely long; it's full of high spots. For half a century, he was a major authority on the history and practice of giving science advice to the U.S. government. His book *Science Advice to the President* was first published by AAAS in 1980, is now in its second edition, and is required reading for anyone seriously interested in the evolution of science policy. Bill first dipped into personal involvement in science right after his release from active wartime Navy service, and he didn't stop for a moment until his death.

It seems safe to say that the scientific community in the United States has never had a stronger or more resolute supporter. But that would unfairly exclude his importance to international science, which he served in multiple ways, among which two are especially significant. In the early 1990s, he established and served as the organizer and leader of the Carnegie Group, an association of science advisers and ministers from the G7 nations. These candid sessions had a positive effect on scientific coordination among these countries, and according to the late D. Allan Bromley, former Science Adviser to President George H. W. Bush, the Carnegie Group would not have existed without Golden.

In the early years of the Clinton administration, Bill saw the need for more scientific input to the Department of State, and with others, succeeded in managing a feat that not only required his personal ingenuity but cost him something as well. He persuaded Secretary of State Albright to request a National Academies study on the role of science, technology, and health in foreign affairs. State and the Academies worked together on the study, Bill paid for it, Secretary Albright accepted its findings, and Norman Neureiter was appointed as her science adviser. The position was a historic first and deserves to be made permanent.

I would guess that the deepest impact of Bill's vision came about through his chairmanship, with Joshua Lederberg, of the Carnegie Commission on Science, Technology, and Government. It was the brainchild of David Hamburg, president of the Carnegie Corporation of New York. Hamburg had a strategy about commissions: that nongovernment groups, if appropriately formed and supported, could have a national voice and an influence at least as great as those of groups formed by government. This one had a membership that included former President Carter and a roster of scientists, university presidents, and former government officials, but most of the real work was done by task forces assigned to work on particular problems. Well over a dozen reports were produced; they sit on my shelf and are useful enough that I still occasionally refer to them. Bill's favorite was surely the first of these, *Science and Technology in U.S. International Affairs*. He wrote the foreword with Lederburg and clearly brought the report into play at the beginning of his effort to inject science policy into the Department of State.

Do you see a certain pattern here? Golden would discover a problem, and if it was important enough, he got an early start, creating auspices under which his plan for addressing it could gain some credibility. Later, that plan could be referred to as an enabling document in the bibliography of an official study on the problem. If further studies were needed, they would get done, perhaps through Bill's financial as well as intellectual gifts. Time after time, when he saw a real need, he found a way to fill it. What an epitaph!

**– Donald Kennedy**

10.1126/science.1151940

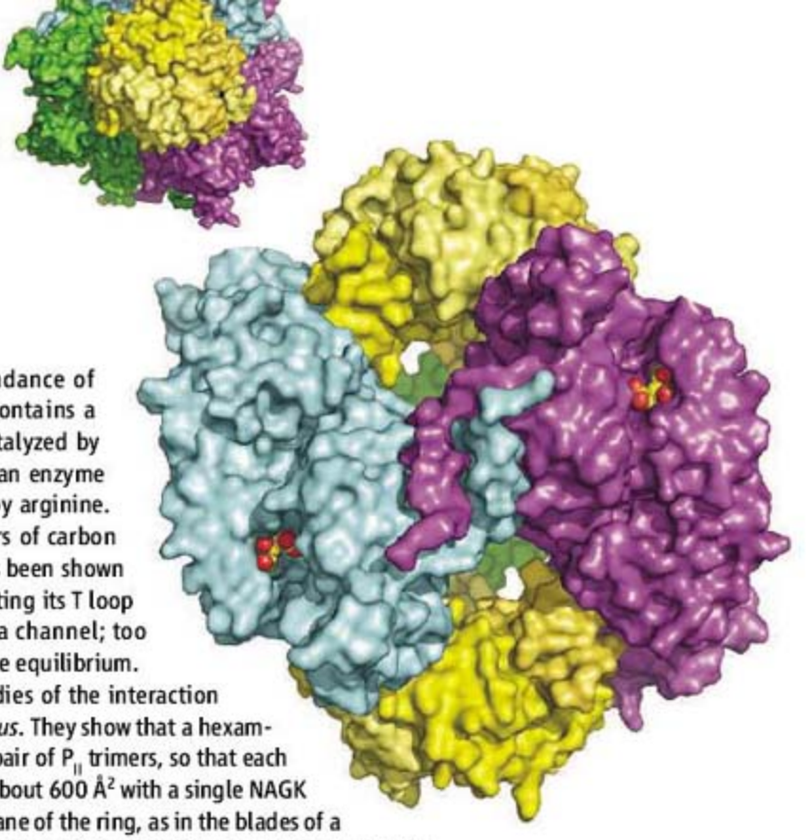

BIOCHEMISTRY

## Three Times Two Is Six

Photosynthetic organisms take advantage of an abundance of nitrogen by storing it as arginine (whose side chain contains a nitrogen-rich guanidinium group), a reaction that is catalyzed by the dimeric protein *N*-acetylglutamate kinase (NAGK)—an enzyme that is, not surprisingly, subject to feedback inhibition by arginine. $P_{II}$ proteins are one of the central metabolic coordinators of carbon and nitrogen fluxes; this protein is a homotrimer and has been shown previously to regulate ammonia influx into cells by inserting its T loop into the cytoplasmic vestibule of the trimeric ammonia channel; too much of a good thing can be hazardous to one's acid/base equilibrium.

Llácer *et al.* describe structural and biochemical studies of the interaction between $P_{II}$ and NAGK in the cyanobacterium *Synechococcus*. They show that a hexameric ring (a trimer of dimers) of NAGK is sandwiched by a pair of $P_{II}$ trimers, so that each of the six $P_{II}$ subunits makes a reversible contact covering about 600 Å$^2$ with a single NAGK subunit. Each NAGK dimer is oriented at an angle to the plane of the ring, as in the blades of a propeller, and the binding of $P_{II}$ increases the angle slightly. The arginine-binding sites are located at the interdimer surfaces, and tilting the dimers and altering the interdimer contacts reduces the binding affinity for arginine by 15-fold. Unlike its direct inhibition of the ammonia channel, the effect of $P_{II}$ binding on NAGK, though also mediated in large part by the T loop, is entirely indirect and distant from both the catalytic and allosteric sites. — GJC

*Proc. Natl. Acad. Sci. U.S.A.* **104**, 17644 (2007).

IMMUNOLOGY

## Death by Consumption

Regulatory T ($T_{reg}$) cells continue to command attention in the minds of immunologists, not least because the mechanisms by which they exert their suppressive effects remain obscure. Although one possibility is that $T_{reg}$ cells paralyze particular functions in effector T cells, Pandiyan *et al.* present evidence that they can starve their targets to death. When the two types of T cells were placed in culture together, the effector (also called the responder) CD4$^+$ T cell population eventually underwent cell death in a manner reminiscent of that seen when T cells are deprived of cytokines. It emerged that the $T_{reg}$ cells were consuming the growth factor interleukin 2 (IL-2), and possibly other cytokines as well. This depletion appeared to operate only when the two types of cells were in close proximity, suggesting that the balance between the supply of secreted cytokines and the voraciousness of the $T_{reg}$ cells might be an important factor. Cell death by cytokine withdrawal was controlled by intracellular mediators, such as the pro-apoptotic protein Bim, and Bim-deficient responder T cells were able to resist suppression by $T_{reg}$ cells. Cytokine consumption by $T_{reg}$ cells was also found to block pathogenic T cells in a mouse colitis model, suggesting that this mechanism might be broadly involved in regulating pro-inflammatory T cells. — SJS

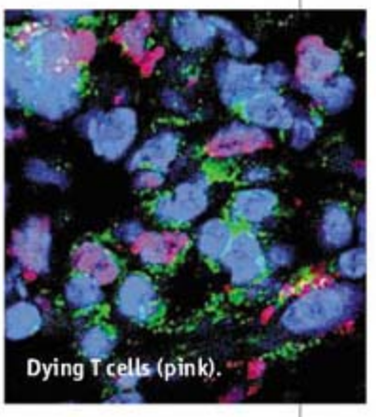

Dying T cells (pink).

*Nat. Immunol.* **8**, 1353 (2007).

CHEMISTRY

## From Pathogen to Polymer?

Diagnosing diseases would ideally entail simple, rapid, inexpensive tests with both high sensitivity and high specificity. One widely applied approach at the molecular level has been the enzyme-linked immunosorbent assay (ELISA), in which an antigen associated with the disease is induced to bind with an antibody attached to an enzyme. A substrate is then added that the enzyme can modify to elicit a visible response, such as fluorescence, for quantification. In some cases, however, ELISAs can be complicated to implement and may not offer the requisite sensitivity. Sikes *et al.* present a promising preliminary exploration of an alternative approach, in which the enzyme is replaced by a synthetic photoinitiator of free-radical polymerization. Specifically, the authors appended ~140 initiators and one or two avidin derivatives to each chain in a sample of acrylic acid/acrylamide copolymer. They then exposed a surface functionalized with biotin to this sensing polymer and detected avidin-biotin binding by adding aqueous acrylate monomers and irradiating the samples with ultraviolet light to induce polymerization where the initiators were bound. A 10-min irradiation time was sufficient to produce visible white polymer spots on samples containing as few as 1000 biotin sites: a response several orders of magnitude more sensitive than an enzyme-based assay applied to the same system. — JSY

*Nat. Mater.* 10.1038/nmat2042 (2007).

CELL BIOLOGY

## From Fat to Fusion

In diabetes, lipid droplets can often be seen to accumulate in muscle and liver cells. The extent to which individual lipid droplets interact within the cell is not very well understood. Boström *et al.* describe how such intracellular lipid droplets can grow within a cell by the fusion of individual droplets; this merging is promoted by components of the intracellular vesicle fusion machinery, which are better known as the molecular mediators of transport vesicle fusion with their target membranes. Lipid droplets from fibroblast cells in culture were isolated by cell fractionation and shown to

CREDITS (TOP TO BOTTOM): LLÁCER *ET AL.*, *PROC. NATL. ACAD. SCI. U.S.A.* **104**, 17644 (2007); PANDIYAN *ET AL.*, *NAT. IMMUNOL.* **8**, 1353 (2007)

contain several proteins, including members of the so-called SNARE family of membrane fusion proteins. In an assay of lipid droplet fusion in living cells, the knockdown of lipid-droplet–associated SNAREs reduced the number of fusion events observed by up to 75%. Furthermore, in muscle cells, the co-opting of one of the SNAREs, SNAP23, to lipid droplets (for example, by adding increasing amounts of the fatty acid oleic acid) may play a role in the development of insulin resistance by diverting the SNARE from its normal function in delivering glucose transporters to the cell surface in response to insulin. — SMH

*Nat. Cell Biol.* **9**, 1286 (2007).

PHYSICS

## Atom Gyroscopes

We terrestrials tend to get our bearings from compass readings, tracking the stars, or more recently in a digital format from global positioning systems. For the likes of satellites, orbiting telescopes, and probes navigating through deep space, the systems of choice to point the way are based on gyroscopes aligned with a distant reference star. To study predictions of general relativity such as frame dragging, the effects of which would be seen as tugs on the rotation axis of the gyros, high sensitivity of the gyroscopes to rotation is a prerequisite. In this context, atom interferometers can surpass mechanical gyroscopes or optical interferometers by orders of magnitude. Wu *et al.* report on the development of a cold-atom interferometer in which a matter wave of Rb atoms is split in two, with both halves sent around opposite paths repeatedly and brought together again to produce an interference pattern. The phase shift is sensitive to the rotation of the interferometer. — ISO

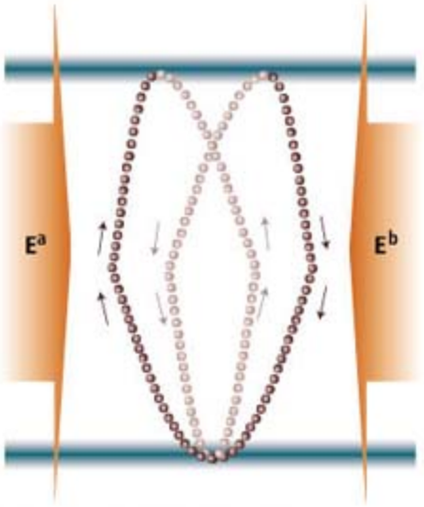


**Interfering atom paths (purple).**

CREDITS: ADAPTED FROM WU ET AL., PHYS. REV. LETT. 99, 173201 (2007)

*Phys. Rev. Lett.* **99**, 173201 (2007).

CHEMISTRY

## Picking Partners

The evolution of strategies for synthesizing complex organic molecules relied in large part on a deepening understanding of the relative reaction rates of often subtly differing functional groups. Rational assembly of larger, supramolecular structures, which are held together by an array of noncovalent interactions, is now proceeding along a similar course, with predictive principles emerging from careful systematic studies. In this vein, Aakeröy *et al.* have explored the competition between hydrogen and halogen bonding in the cocrystallization of several small aromatic building blocks. One crystallizing partner contained two nitrogen sites (pyridine and benzimidazole), each of which could potentially act as an acceptor toward either a polarized hydrogen or a halogen. The donor partners each bore an oxime (CH=NOH) group, which could interact through either the C-H or the O-H site, as well as a fluorine, bromine, or iodine substituent poised for halogen bonding. Crystallography revealed that in all three cocrystals, the benzimidazole N formed an H bond with the oxime OH. In the F- and Br-substituted systems, the pyridine N attracted the C-H group; only in the iodo case did a halogen bond form instead. — JSY

*J. Am. Chem. Soc.* **129**, 10.1021/ja073201c (2007).

CHEMISTRY

## Stages of Growth

Many important catalysts are composed of supported metal nanoparticles. Although x-ray absorption spectroscopy has been used to probe the impact of particle size and shape on chemical reactivity, it is difficult to extract information beyond the first few coordination shells, and there is a risk with this technique of radiation damage to the samples. Chupas *et al.* show that by monitoring the change in pair distribution functions from the scattering of weakly absorbed (and thus minimally damaging) high-energy x-rays, they can track the growth of $Pt^0$ nanoparticles with time. They studied the reduction of $PtCl_6^{2-}$, supported on titanium dioxide, at temperatures from 100° to 200°C. The Pt-Cl correlations decreased linearly with time without an induction period, suggesting that the reduction is not autocatalytic, as has been seen for $Pt^{4+}$ species in solution. Data collected during the heating period revealed a shift in the dominant process from reduction of the Pt ions (to make isolated metal atoms or small clusters), to rapid growth or sintering, and finally ripening of the larger clusters. — MSL

*J. Am. Chem. Soc.* **129**, 10.1021/ja076437p (2007).

www.sciencemag.org

# Science

1200 New York Avenue, NW
Washington, DC 20005
Editorial: 202-326-6550, FAX 202-289-7562
News: 202-326-6581, FAX 202-371-9227

Bateman House, 82-88 Hills Road
Cambridge, UK CB2 1LQ
+44 (0) 1223 326500, FAX +44 (0) 1223 326501

**Subscription Services** For change of address, missing issues, new orders and renewals, and payment questions: 866-434-AAAS (2227) or 202-326-6417, FAX 202-842-1065. Mailing addresses: AAAS, P.O. Box 96178, Washington, DC 20090-6178 or AAAS Member Services, 1200 New York Avenue, NW, Washington, DC 20005

**Institutional Site Licenses** please call 202-326-6755 for any questions or information

**Reprints:** Author Inquiries 800-635-7181
Commercial Inquiries 803-359-4578

**Permissions** 202-326-7074, FAX 202-682-0816z

**Member Benefits** AAAS/Barnes&Noble.com bookstore www.aaas.org/bn; AAAS Online Store http://www.apisource.com/aaas/ code MKB6; AAAS Travels: Betchart Expeditions 800-252-4910; Apple Store www.apple/eppstore/aaas; Bank of America MasterCard 1-800-833-6262 priority code FAA3YU; Cold Spring Harbor Laboratory Press Publications www.cshlpress.com/affiliates/aaas.htm; GEICO Auto Insurance www.geico.com/landing/page/go51.htm?logo=17624; Hertz 800-654-2200 CDP#343457; Office Depot https://bsd.officedepot.com/portalLogin.do; Seabury & Smith Life Insurance 800-424-9883; Subaru VIP Program 202-326-6417; VIP Moving Services http://www.vipmayflower.com/domestic/index.html; Other Benefits: AAAS Member Services 202-326-6417 or www.aaasmember.org.

science_editors@aaas.org (for general editorial queries)
science_letters@aaas.org (for queries about letters)
science_reviews@aaas.org (for returning manuscript reviews)
science_bookrevs@aaas.org (for book review queries)

Published by the American Association for the Advancement of Science (AAAS), *Science* serves its readers as a forum for the presentation and discussion of important issues related to the advancement of science, including the presentation of minority or conflicting points of view, rather than by publishing only material on which a consensus has been reached. Accordingly, all articles published in *Science*—including editorials, news and comment, and book reviews—are signed and reflect the individual views of the authors and not official points of view adopted by the AAAS or the institutions with which the authors are affiliated.

AAAS was founded in 1848 and incorporated in 1874. Its mission is to advance science and innovation throughout the world for the benefit of all people. The goals of the association are to: foster communication among scientists, engineers and the public; enhance international cooperation in science and its applications; promote the responsible conduct and use of science and technology; foster education in science and technology for everyone; enhance the science and technology workforce and infrastructure; increase public understanding and appreciation of science and technology; and strengthen support for the science and technology enterprise.

**Information for Authors**

See pages 120 and 121 of the 5 January 2007 issue or access www.sciencemag.org/feature/contribinfo/home.shtml


Flat cat?

## Rare-Tiger Photo Flap Makes Fur Fly in China

A few weeks ago, tiger researchers celebrated the news that a South China tiger (*Panthera tigris amoyensis*) had been spotted—and photographed—in the wilds of Shaanxi Province. But netizens in China and elsewhere have declared it only a "paper tiger" after scrutinizing the two available images.

Although the species has been declared "functionally extinct," reports of tiger activity in the heavily forested Qinba Mountains prompted Shaanxi officials to offer a reward to anyone able to photograph one of the tigers.

At a 12 October press conference in Xian, Zhou Zhenglong, a former hunter, told a rapt audience of his quest to photograph the beast, crawling to within 20 meters of one and snapping 71 images. When the camera's flash went off, the tiger roared and disappeared, he said.

Skeptics, citing factors such as the tiger's tame-looking expression and unreal coat color—as well as the fact that the two photos portray exactly the same tiger but differently positioned foliage—think it's more likely that someone planted a cardboard tiger in the bushes. Fu Dezhi, a botanist at the Chinese Academy of Sciences, adds that the plants are not to scale in relation to the tiger. Zhou, who was paid 20,000 yuan ($2666) for the images, says, "I guarantee with my head that the photographs are authentic."

The Shaanxi Forestry Bureau is pushing ahead with plans for a thorough survey and a tiger reserve. "It's tremendously exciting news, if it can be substantiated," says tiger expert Gary Koehler of Washington state's Department of Fish and Wildlife (*Science*, 7 September, p. 1312). But first, "they need to look for hair snags or scat" for genetic verification.

## Lean Times for Lake Superior

This fall, the water level of Lake Superior, the world's largest freshwater lake, dipped below the record it set in the Dust Bowl days of 1926. In September, the 1540-square-kilometer lake on the Canadian border was at its lowest since record-keeping began in 1860—with an average depth of 183 meters. October's level went up after several weeks of rain but was still 30 cm below the long-term average. Boats are resting on mud, docks are poking nothing but air, and fishermen and lakeside rice growers are watching their livelihoods dry up.

Some factors that explain the mess: The surface temperature of the lake has mysteriously risen 4.5°C since 1978—twice as fast as the temperature of the surrounding air. Ice, which blocks evaporation, has become rare on Superior, and precipitation has dropped 15 cm a year from the annual average of 77 cm.

But the big picture remains unclear. "We know how it's happening, but the why—I don't know," says hydrologist Cynthia Sellinger of the National Oceanic and Atmospheric Administration. One reason, experts say, is that climate models aren't very good at predicting greenhouse effects at regional scales.

## << Micromini Radio

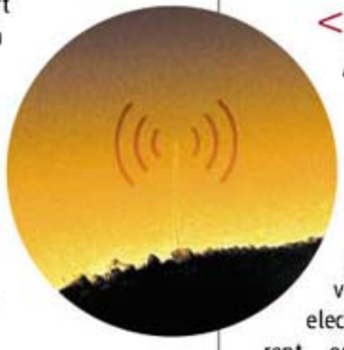

A carbon nanotube 10,000 times as thin as a human hair turns radio waves into music, acting like a tiny radio, in this image (wavy lines added) taken by researchers at the University of California, Irvine. AM radio waves cause the tube to vibrate; then an electric field forces electrons—that is, an electrical current—out of its tip. The current detects the vibrations, converting the waves to sound. This month in *Nano Letters*, Peter Burke and Christopher Rutherglen report using the device to transmit music wirelessly almost a meter from an iPod to a speaker. Scientists are finding that radio frequencies are well-suited to manipulating nanometer-sized parts, further opening up new horizons in nanotechnology.

## DINO DELIGHT

A breathtaking panorama will greet visitors to the Carnegie Museum of Natural History in Pittsburgh, Pennsylvania, when the 100-year-old Dinosaur Hall reopens on 16 November after a lengthy $36 million renovation. Created by artists Robert Walters and Tess Kissinger of Philadelphia, the mural stretches 55 meters over two walls and is 4.5 meters high. It depicts life in the Jurassic Morrison Formation of western North America—which stretches from Saskatchewan, Canada, to New Mexico—and forms a backdrop for the newly mounted skeletons in the hall, including a giant sauropod defending her baby from an attacking *Allosaurus*. "It gives you a sense of one dramatic day 150 million years ago," says curator Zhe-Xi Luo. "Everything looks so real." Walters and Kissinger are working on a second mural, of the late Cretaceous Period, for another hall that will open next year.

CREDITS (TOP TO BOTTOM): ZHOU ZHENGLONG; K. JENSEN, ZETTL RESEARCH GROUP/LBNL AND UNIVERSITY OF CALIFORNIA, BERKELEY; WALTERS AND KISSINGER/CMNH

EDITED BY YUDHIJIT BHATTACHARJEE

# MOVERS

**OLD AND THE YOUNG.** The Royal Netherlands Academy of Arts and Sciences (KNAW) has elected its youngest president ever. String theorist Robbert Dijkgraaf, 47, promises to help rejuvenate the 199-year-old academy and turn it into a forum for debates about science and society.

The leader of a high-profile group at the University of Amsterdam, Dijkgraaf is best known in his own country as a prolific newspaper columnist, op-ed writer, and TV guest who has long championed the cause of scientific literacy. He has also addressed the lack of science education in Dutch elementary schools. For instance, he spent some of the Spinoza Prize money he won in 2003 to set up a Web site where students and teachers can find fun hands-on science experiments. Besides strengthening KNAW activities in the same areas, Dijkgraaf—an art lover who interrupted his physics training for 2 years to study painting—hopes to encourage exchanges between scientists and artists.

With his playfulness and enthusiasm, Dijkgraaf is the right man to modernize the 220-member KNAW, which is "still a bit like a 19th century society sometimes," says Herman Verlinde, a Dutch physicist at Princeton University, where Dijkgraaf did a postdoc.

## ON CAMPUS

**TIME TO GO?** Fabio Mussi, Italy's research minister, wants to make room for fresh talent at the country's 62 state universities. So he's proposed lowering the official retirement age for Italian professors from 75 to 70. "Going this way, we expect to save more money to hire young researchers," says Mussi, who is 59, about reducing the retirement age in 1-year increments over the next 5 years.

The plan, which Mussi announced at a public talk last month at the Genova Science Festival, has been greeted with cheers from the young and grumbling from senior academics. Federica Migliardo, a 32-year-old physicist at the University of Messina, says it's needed to revitalize Italian science. But Armando Bazzani, a 66-year-old physics professor at the University of Bologna, predicts "there will be great resistance" when the minister introduces his plan in Parliament.

## IN PRINT

**BITE YOUR TONGUE.** Like many scholars of evolution, Oliver Curry is all for explaining the topic to a general audience. But now he wishes he hadn't shared his less-than-scientific musings with a popular entertainment channel.

In 2006, Curry, an evolutionary theorist at the London School of Economics, wrote an essay for the British Bravo TV network in which he laid out "plausible scenarios" for how humans might evolve over the next million years. Although Curry made it clear that the exercise was purely speculative, Bravo billed his ideas as serious research. That triggered a flurry of media reports forecasting, among other things, the emergence in the next millennium of a "coffee-colored" race.

Last month, Curry finally issued a statement declaring that his essay was "intended as a 'science fiction' way of illustrating some aspects of evolutionary theory." And he adds, "I do not endorse the content of these media reports."

CREDITS (TOP TO BOTTOM): BRAM BUDEL; LUCA ROSINGANA; ANNAMARIA TALAS/REAL PICTURES

Got a tip for this page? E-mail people@aaas.org

## Deaths >>

**A GIGANTIC PRESENCE.** As Indonesia's "king of paleoanthropology," Teuku Jacob ruled over a vital collection of hominid fossils. He was a formidable skeptic of the 1-meter-tall "hobbit" remains from the Indonesian island of Flores, arguing that they instead represented a diseased modern human. On 17 October, at the age of 76, the professor emeritus and former rector of Gadjah Mada University in Yogyakarta died of liver problems.

Jacob studied fossil hominids under famed paleontologist G. H. R. von Koenigswald, then found and was curator of many important specimens, particularly of *Homo erectus*. He was a key figure in the Indonesian independence movement, making nationalist radio broadcasts after World War II during the country's 4-year fight for independence from the Dutch. "He built the field up—he *was* paleoanthropology in Indonesia for quite a while," says anthropologist Russell Tuttle of the University of Chicago in Illinois, noting that Jacob trained Indonesians to study the fossils found in their country. "It was an indigenous effort."

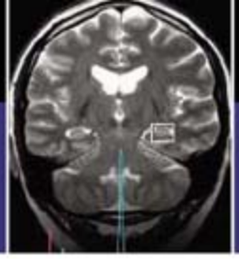

Monitoring neurogenesis 899

Planning and the hippocampus 900

ASTROPHYSICS

# Universe's Highest-Energy Particles Traced Back to Other Galaxies

Every so often, a subatomic particle crashes into Earth's atmosphere packing as much energy as a large hailstone. Physicists have struggled for decades to determine where such ultrahigh-energy cosmic rays come from, what they consist of, and how they are accelerated to energies 100 million times greater than particle accelerators have reached. Now answers may be in sight. Ultrahigh-energy cosmic rays appear to come from the neighborhoods of certain nearby churning galaxies, physicists working with the gigantic Pierre Auger Observatory in western Argentina report on page 938. The finding marks a first big step toward explaining the mysterious particles, others say.

"This is of the greatest importance," says Veniamin Berezinsky, a theorist at Gran Sasso National Laboratory in Assergi, Italy. "If it is correct, it solves one part of this puzzle completely." Alan Watson, an astrophysicist at the University of Leeds in the U.K. and spokesperson for the 300-member Auger collaboration, says, "For myself, it's deeply satisfying to have gotten to the beginning of the end of this whole riddle."

To trace the cosmic rays, the Auger team employed a detector array larger than Tokyo. When a cosmic ray hits the atmosphere, it triggers an avalanche of particles tens of kilometers long called an extensive air shower. By sampling the shower with detectors on the ground, physicists can determine its direction and, hence, the direction of the cosmic ray. The shower also causes nitrogen molecules in the air to fluoresce, so on moonless nights, special telescopes can see the showers. Because the highest energy cosmic rays arrive at a rate of less than one per square kilometer per century, the Auger team has carpeted 3000 square kilometers of Argentina's Pampa Amarilla with more than 1300 detectors and deployed four batteries of telescopes.

Physicists measure the energy of the highest energy rays in exa–electron volts (EeV). The Auger team finds that rays with energies higher than 57 EeV—of which they see 27—generally come from directions within 3° of "active galactic nuclei" (AGNs) that lie within roughly 250 million light-years of Earth. That's close enough that the particles aren't sapped of their energy by interactions with the afterglow of the big bang, the cosmic microwave background. AGNs are thought to be supermassive black holes at the hearts of galaxies that are slurping up matter and spewing radiation. The cosmic rays do not point precisely to the AGNs; presumably, our galaxy's magnetic field deflects them in transit. Details of the analysis suggest that the cosmic rays are protons.

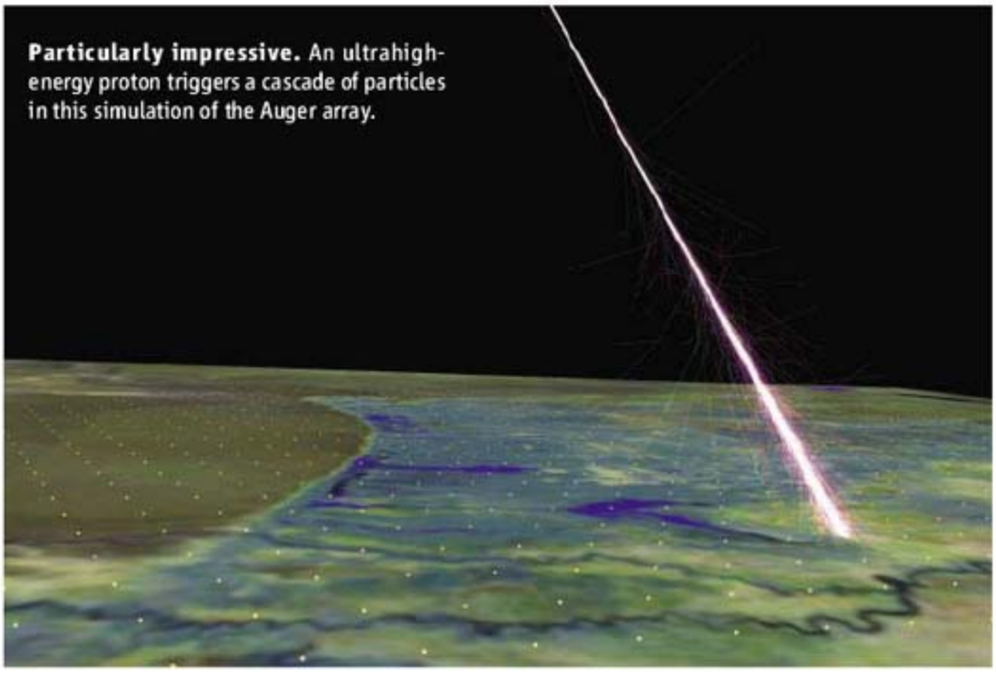

**Particularly impressive.** An ultrahigh-energy proton triggers a cascade of particles in this simulation of the Auger array.

CREDIT: SPACE VISUALIZATION LABORATORY AT THE ADLER PLANETARIUM

The results don't *prove* AGNs are sources of the rays. "Anything else that's distributed on the sky in the same way as AGNs could be the source," Watson says. For example, galaxies tend to clump, so some other sort of galaxy might be the culprit. James Cronin, a particle physicist at the University of Chicago in Illinois and co-founder of the project, says the key point is that cosmic rays do not arrive in equal numbers from all directions. Such "anisotropy" suggests that researchers are finally on the trail of the rays' origins and gives scientists a new way to view the heavens, Cronin says: "It's the beginning of an astronomy of cosmic rays at the highest energies."

Others had claimed to trace the origins of the highest energy rays before. In 2001, theorists Peter Tinyakov and Igor Tkachev of the Russian Academy of Sciences in Moscow analyzed data from Japan's Akeno Giant Air Shower Array (AGASA), a 100-square-kilometer array outside Tokyo that took data from 1993 to 2004. The highest energy rays appeared to come from objects called BL Lacs, galaxies with jets of matter and energy shooting out of them directly at Earth, they reported. That claim was disputed by researchers working with Hi-Res, twin batteries of fluorescence telescopes located in Dugway, Utah, that took data from 1997 to 2006. Last year, Hi-Res researchers argued that there was no correlation in either AGASA's data or their own but that there was correlation in their data if they included another subtype of BL Lac.

These claims suffered from a key weakness, says Todor Stanev, a theorist at the University of Delaware, Newark. The sky is full of possible sources, so by selecting the sources in just the right way, researchers can inadvertently manufacture a specious correlation, he says. The only way to guard against that is to test the claimed correlation in a new data set. That's what the Auger team did. First, researchers searched data collected from 1 January 2004 to 26 May 2006 to find a ▶

Picking a landing site on Mars
908

Genes and queens
910

correlation; then they confirmed the correlation by analyzing data collected from 27 May 2006 to 31 August 2007 using the same criteria. "The Auger collaboration has been excellent in setting the rules and not deviating from them for any reason," Stanev says.

Still, not everyone is convinced that the observation will hold up as Auger collects more data. Even with the check against the second data set, the Auger team estimates that there is a 1-in-1000 chance the correlation with AGNs is a meaningless fluke. Statistically speaking, that makes it a "three-sigma" observation, says Gordon Thomson, an experimenter at Rutgers University in Piscataway, New Jersey, and a member of the Hi-Res team. "There are many three-sigma signals that come and go," Thomson says. But he adds that Auger's claim "is sufficiently interesting that a postdoc and I are looking at our data" for a correlation with AGNs.

Spurred by their first big result, the Auger team is pushing to build a second array at least three times larger in the Northern Hemisphere, which would enable them to view the entire sky. Researchers hope to submit a proposal within a year, Cronin says. Meanwhile, theorists have a puzzle to solve: Exactly how might an AGN accelerate a proton to such mind-boggling energies? **–ADRIAN CHO**

RESEARCH CAREERS

# Postdoc Survey Finds Gender Split on Family Issues

A new survey of how young biologists view their prospects suggests that the main concern for women is not a hostile climate but insufficient time to juggle the needs of family and career. The study of 1300 postdocs at the National Institutes of Health (NIH) in Bethesda, Maryland, includes a call for more family-friendly policies at U.S. research institutions.

"What these findings are telling us is that universities and funding institutions need to tune the academic system to the needs of women," says Elisabeth Martinez, lead author and a former NIH postdoc who is now a pharmacology instructor at the University of Texas Southwestern Medical Center in Dallas. Martinez and her nine co-authors are members of the Second Task Force on the Status of NIH Intramural Women Scientists. (The first issued a report in 1992 calling for equity in pay and hiring practices.) The new report recommends that institutions set up part-time positions for principal investigators (PIs), offer grant supplements to hire qualified spouses on separate or related projects, and provide affordable childcare for all researchers.

NIH is one of the places where the system is out of whack. The share of women among its 900 tenured investigators has barely budged in the past decade, from 18% to 19%, and the figure for tenure-track positions has remained at 29%. (By comparison, women received more than 40% of the Ph.D.s in the life sciences awarded in the United States during the same time frame.)

The survey found that more than 70% of the men have their sights set on a PI position compared with only 50% of the women. (The results were published in the 29 October issue of *EMBO Reports*.) Men were also more confident—by a margin of 59% to 40%—that they would become PIs. One apparent reason for the gender discrepancy is that women appear more willing to make career sacrifices for the sake of their families (see graph). For example, 57% of female postdocs who were married but without children said that having children would influence their career choices compared with only 29% of married men without children. Similarly, 31% of married women expressed a willingness to make concessions to accommodate their spouses' careers versus 21% of the men.

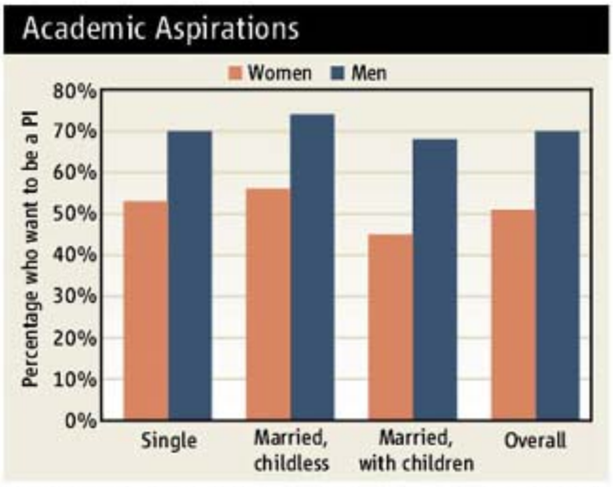


**Tough choice.** Family responsibilities seem to affect career goals of women on the academic track more than those of men.

At the same time, male and female postdocs said that they felt equally comfortable in their working environments. "Overt discrimination does not seem to be the issue," says Martinez. Three other surveys still being analyzed by the task force—of tenure-track and tenured investigators, staff scientists, and tenure-track researchers who had left NIH before getting tenure—say the same thing, reports Joan Schwartz, assistant director for intramural research at NIH and head of the task force.

Biologist Sue Rosser of Georgia Institute of Technology in Atlanta agrees that family-friendly policies are key. But she warns against underestimating how gender discrimination affects women, especially at higher rungs of the academic ladder. "It gets complicated pretty quickly," she says, adding that many female faculty members face isolation and dismissive attitudes throughout their careers.

Schwartz says NIH is already addressing some of the task force's recommendations. For example, NIH used to allow only tenured investigators to have staff scientists. Now, tenure-track researchers can request the same support if they need to work part time for short stints to take care of a child or a family member. NIH also encourages researchers to telecommute if possible, she adds.

But providing affordable childcare is another matter. More than 1000 people are on a waiting list for 350 slots available on and off campus, says Schwartz, and employees receive preference. That makes it tough on postdocs, who are technically trainees. "Building another daycare center on campus is a priority," she says, "but there's no money at the moment."

**–YUDHIJIT BHATTACHARJEE**

CREDIT: ADAPTED FROM E. D. MARTINEZ ET AL., *EMBO REPORTS* 8, 11 (2007) EUROPEAN MOLECULAR BIOLOGY ORGANIZATION)

NEUROSCIENCE

# Spying On New Neurons In the Human Brain

The realization more than a decade ago that the mammalian brain produces new neurons well into adulthood was a revolution in neurobiology. It also raised a slew of questions about the function of these new cells. In recent years, for example, scientists have debated whether newborn neurons aid learning and memory and whether aberrations in adult neurogenesis contribute to disorders such as depression (*Science*, 17 February 2006, p. 938; 8 August 2003, p. 757).

Now, researchers may have a powerful new tool to help tackle these questions: a noninvasive method for detecting neural stem cells in live animals—including humans. On page 980, a multidisciplinary team led by child neurologist Mirjana Maletic-Savatic of Stony Brook University in New York state describes the technique, which uses magnetic resonance spectroscopy to detect a biomarker for the progenitor cells that give rise to new neurons.

Other researchers are greeting the work with excitement, tempered with a healthy dose of caution. "This has the potential to open the doors to research that could not have been done in humans before," says Walter Koroshetz, deputy director of the National Institute of Neurological Disorders and Stroke in Bethesda, Maryland. "If it's validated, it's the coolest thing since sliced bread," says neurobiologist Theo Palmer of Stanford University in Palo Alto, California.

Maletic-Savatic and her colleagues began their search for a biomarker in a series of experiments with cultured mouse cells, using nuclear magnetic resonance (NMR) spectroscopy to compare the chemical makeup of neural progenitor cells from embryonic brain tissue with that of other types of cells, including mature neurons and glial cells. The NMR spectra of the neural progenitor cells had a prominent peak that was not present in the other cells, indicating high levels of a compound specific to neural progenitors. The identity of this compound isn't known, but its position on the NMR spectra, at 1.28 parts per million (ppm; the conventional unit in NMR spectroscopy), suggests that it's a fatty acid, a class of compounds that play a wide variety of roles inside cells, Maletic-Savatic says.

Encouraged by their mouse-tissue experiments, the researchers next looked for the 1.28-ppm biomarker in live rats. For this work, they turned to magnetic resonance spectroscopy, a method that works on the same principles as NMR but can be used with the scanners found in many hospitals and research centers. At first, the spectra from the live rat experiments were messy, and the peak at 1.28 ppm was a tiny blip in a sea of squiggles. But with the help of Stony Brook University engineer Petar Djurić, the researchers developed a mathematical algorithm that separated the 1.28-ppm peak from the noise. Using this approach, the researchers found relatively high levels of the 1.28-ppm biomarker in the hippocampus of adult rats, where previous studies have found neurogenesis, compared to the cerebral cortex, where neurogenesis has not been confirmed. Moreover, when the ▶

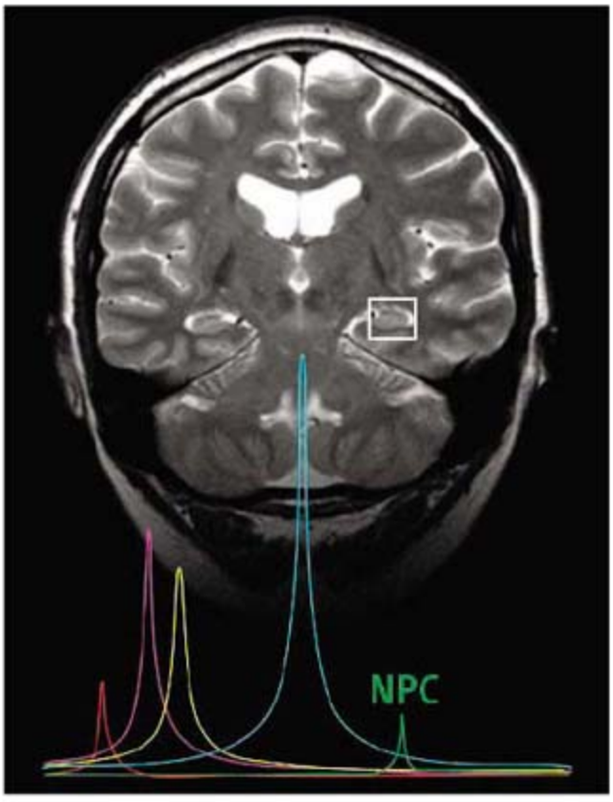


**Peak excitement.** A new method reveals a biomarker of neurogenesis (green) in the human hippocampus (box).

CREDIT: AMANDA SIERRA SAAVEDRA

## Panel's Move Has Flamingo Fans Tickled Pink

An international effort to protect Tanzania's Lake Natron, the only known breeding site for East Africa's lesser flamingos, got a boost last week when a technical advisory panel recommended rejection of the environmental-impact plan submitted by a company that wants to build a soda-ash extraction plant there.

"We suggested that they go back to the drawing board," says Lota Melamari of the Wildlife Conservation Society of Tanzania and a member of the panel, which includes representatives of conservation groups and the national parks. He said the panel's findings are expected to be endorsed by Tanzania's National Environment Management Council in its report to the environment minister, who will make the final decision on the studies the developer will be required to do.

The company, Lake Natron Resources, had requested permission to construct a large plant at the alkaline lake, which has been the only known breeding ground for East Africa's 1.5 million to 2.5 million lesser flamingos for 45 years (*Science*, 22 September 2006, p. 1724). The advisory panel found that the plan lacked several essential details, and members questioned whether its proposed mitigation strategies would protect the flamingo breeding area. The company contends that the extraction plant would not hurt or drive away the birds. **–ROBERT KOENIG**

## Judge Blocks Patent Rules

A U.S. federal judge has temporarily blocked new patent rules finalized by the U.S. Patent and Trademark Office that would limit certain patent applications. The rules, originally set to take effect last week, would have limited filed amendments that allow applicants to add information to pending applications. Last week, the Virginia district judge ruled in favor of drug giant GlaxoSmithKline, saying that the limits would have "retroactively alter[ed] the bargain" that inventors such as GSK make in trading research secrets for a patent monopoly and "provide[d] a disincentive to their filing of new patent applications for researching new pharmaceutical products." The rules will stay off the books for now. A judge will likely hear the case early next year.

Meanwhile, the Senate is set to debate a patent-reform bill that would create a new system for challenging granted patents and set certain limits on legal damages in patent suits. A similar version passed in the House in September. **–ELI KINTISCH**

researchers administered electroconvulsive shock, which increases hippocampal neurogenesis, levels of the biomarker increased as well.

Finally, the team applied the method to 11 healthy human volunteers who sat for a 45-minute scanning procedure. As predicted, the spectra revealed higher levels of the biomarker in the hippocampus than in the cortex. In addition, levels of the biomarker were considerably higher in the youngest subjects (ages 8 to 10) compared with the oldest (ages 30 to 35), consistent with previous animal studies indicating declining neurogenesis with age.

"Only time will tell how strong this method is, [but] it looks very promising," says Gerd Kempermann, a neuroscientist at the Center for Regenerative Therapies in Dresden, Germany. "The 1.28-ppm peak really seems to represent something related to progenitor cells." A crucial next step, Kempermann and others say, will be to figure out exactly what the biomarker is and whether it tracks the overall number of progenitor cells or just those that are in the process of proliferating—an important distinction for interpreting experimental findings.

In addition, some researchers are wary that the unconventional algorithm used to pull out the 1.28-ppm peak from the noisy magnetic resonance spectra could yield artifacts by amplifying noise instead. But if the new method does hold up to additional scrutiny, there's no shortage of ideas about how to use it. Maletic-Savatic hopes to investigate whether neural progenitor cells behave abnormally in disorders of brain development such as cerebral palsy and mental retardation. Palmer says that the new method could help explain the cognitive decline some children experience after receiving radiation therapy for cancer: A valid biomarker could test the hypothesis that the impairments result from radiation damage to neural progenitor cells and potentially help evaluate drugs intended to protect progenitor cells. **–GREG MILLER**

NEUROSCIENCE

# Hippocampal Cells Help Rats Think Ahead

One view of the hippocampus, based on human brain-imaging studies and other data, is that it is essential for remembering the past, as well as for imagining the future (*Science*, 19 January, p. 312). The relatively new idea that this part of the brain helps plan the future gets support from a paper in the 7 November issue of *The Journal of Neuroscience* by A. David Redish and Adam Johnson of the University of Minnesota, Minneapolis. With electrodes implanted into the brains of rats, they've captured, on the scale of single neurons, rodents thinking ahead about their routes in a maze.

"I think the paper's elegant, and it's going to be a classic," says Randy Buckner of Harvard University. "They really show a compelling example of the rats representing in their brains a series of possible futures and using that to test what they're going to do next."

In the 1930s, Edward Tolman looked at decision-making by using the T-maze, in which a rodent comes to a "choice point" and must decide whether it's better to take the left or right branch in pursuit of a food reward. "If you look at Tolman's [research], and you think about how that kind of a paradigm might be done in neural terms, you come to the conclusion that the rats probably have a neural mechanism to preplay what might happen next," says Buckner, who proposed that idea in 2006 with his Harvard colleague Daniel Carroll.

Redish and Johnson were already searching for such a decision-making mechanism by putting electrode "hats" on rats. These arrays of electrodes implanted into the brains of rats can detect the firing of 100 or so individual neurons. The rats can move freely and naturally while researchers record their brain activity. In the new work, Redish and Johnson placed rats with such hats into a modified T-maze and were able to observe cells in the CA3 area of the hippocampus as the rats walked through the maze. As the animals scurried, so-called place cells, neurons that fire in response to position, signaled where in the maze the rats were.

Such observations have been standard in the hippocampal literature for 30 years. But the data have often been confounded by additional firing, which has been dismissed as noise. The problem is that neuronal firing data, or spiking, are often averaged together, which blurs temporal resolution, explains Emery Brown of Harvard and the Massachusetts Institute of Technology. In the computational equivalent of putting another lens on a high-powered microscope, Brown and his colleague Loren Frank, who is now at the University of California, San Francisco, created an algorithm in 1998 that allowed spike ensembles to be seen at the millisecond time scale at which neuronal firing actually occurs. "If you can do the analysis at the resolution at which the spikes come in," says Brown, "you can move on to other, more important scientific questions."

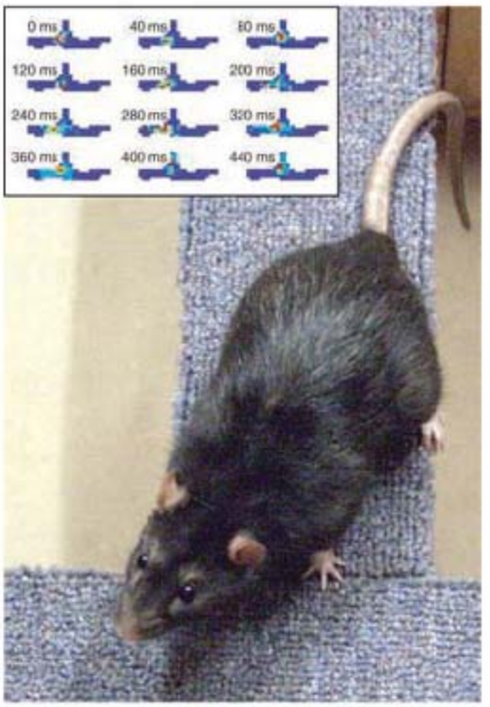


**Imagine that.** As a rat looks in one direction, neurons representing that position (*inset*) fire over a half-second period.

CREDIT: A. JOHNSON, M. VAN DER MEER, A. D. REDISH

In their new study, Johnson and Redish tweaked the algorithm and used it to reveal that the apparent noise in place-cell firings was actually signal. The additional neuronal firing corresponds to place cells representing the paths forward of where the rat is standing. The firing proceeds in a sequence lasting a few hundred milliseconds. At a choice point, when the rat pauses and looks left, place cells fire that correspond to the left path even though these cells were thought to respond only when an animal was actually at a particular place. When the rat looks right, place cells corresponding to the right path go off, again as though the rat were imagining walking the route. Cognition is faster than behavior, explains Redish: "We can now see, as Adam put it, the rat thinking faster than it walks."

If rats can visualize their routes, the next research question is, how do they decide which path to choose? There are reward pathways within the brains of rats and humans, says Buckner, who predicts that studies will link those pathways with the rats' decision-making areas. Cheese, anyone? **–KAREN HEYMAN**

Karen Heyman is a freelance writer in Santa Monica, California.

**On alert.** Nurses in a pediatric TB ward in South Africa, where drug resistance is high.

CREDIT: GIANLUIGI GUERCIA/AFP/GETTY IMAGES

TUBERCULOSIS

# Few Mutations Divide Some Drug-Resistant TB Strains

The first genome analysis of an extensively drug-resistant tuberculosis (XDR-TB) strain has found that only a small number of mutations distinguish it from a less drug-resistant strain and a drug-sensitive one. That means that clarifying the molecular basis of TB drug resistance might not be as difficult as some had expected, say the researchers from the Broad Institute and Harvard School of Public Health (HSPH). Other scientists, although welcoming the new data, say it is too soon to tell.

The analysis, to be posted this week on the Broad Institute's Web site, offers initial results of an ambitious international project that will eventually compare the complete genomes of several dozen TB strains from around the globe. A major goal is to generate enough molecular data to speed the development of better diagnostic techniques and therapies for multidrug-resistant (MDR) TB, which causes an estimated 450,000 new infections a year.

Detected only a few years ago, XDR-TB is even more challenging to treat because it is resistant to second-line as well as first-line drugs. The World Health Organization (WHO) in Geneva, Switzerland, estimates that XDR-TB infects about 27,000 people worldwide, but that number is uncertain because diagnosis is difficult and most cases go unreported. The TB isolate sequenced at Broad came from the largest reported XDR outbreak, in the town of Tugela Ferry in South Africa's KwaZulu-Natal province in 2005–2006. That outbreak killed 52 of the 53 persons it infected, all of whom were also infected with HIV. Since then, another 450 cases of MDR-TB have been reported in Tugela Ferry, and more than half are XDR cases.

Scientists at Broad and Harvard scrutinized draft genomes covering about 95% of that one XDR-TB isolate and two other strains from KwaZulu-Natal. They found that only 33 single-nucleotide polymorphisms (SNPs) separated the XDR strain from a drug-sensitive strain, and 29 SNPs distinguished the drug-sensitive strain from an MDR one. They also identified a small number of other mutations, including genome insertions and deletions. Several mutations were previously known to be associated with drug resistance.

"We were surprised and delighted to find so few differences," says project leader Megan Murray of HSPH. "This simplifies the task of investigating those mutations to determine which are related to drug resistance." Scientists also want to identify so-called compensatory mutations that enable TB bacteria to thrive despite drug-resistance mutations that might otherwise weaken them.

Sebastien Gagneux, who studies TB genomic diversity at the National Institute for Medical Research in London, told *Science* that sequencing the KwaZulu-Natal strains was important but that much more SNP data from a global collection of TB strains is needed to understand the molecular basis of drug resistance.

Clinical advances may take longer. Paul Nunn, who coordinates the drug-resistant TB team at WHO, cautions that improved diagnostic tools based on new sequence data "are probably a few years off," whereas developing a new generation of drugs would take longer.

The Broad-Harvard study comes a month after a South African group announced the first sequence of the full genome of an XDR-TB strain. But the South African data ▶

## SCIENCESCOPE

### Bee Virus Endemic

A new genetic analysis, to be published next month in the *American Bee Journal*, suggests that the virus linked to the collapse of honeybee colonies did not arrive in the United States via recently imported Australian bees. In September, a team of researchers reported online in *Science* that collapsed hives, which have affected as many as 25% of U.S. beekeepers, were much more likely than healthy hives to be infected with Israeli acute paralysis virus. They did not find the virus in bees collected before Australian bee imports began in 2005, and so suspicion fell on the Australian bees. But the team behind the new analysis found the virus in preserved bees dating back to 2002. "It seems to let the Australians off the hook," says entomologist Nicholas Calderone of Cornell University.

**–ERIK STOKSTAD**

### Oil Crunch Forecasted

The International Energy Agency (IEA) is ratcheting up its concern about peaking world oil supplies that could trigger price hikes. In its annual energy outlook released this week, the agency warns that it cannot rule out a "supply-side crunch" in world oil markets by 2015 as flagging oil production struggles to keep up with soaring demand. Major agencies such as IEA have usually assumed that Middle East oil producers would make up the shortfall between sagging global production and rising demand, says Boston University economist Robert Kaufmann. Now IEA projects even faster demand growth than it did last year. "We're really at the knife edge" between demand for oil and the world's ability to produce it, says Kaufmann. **–RICHARD A. KERR**

### Argo Ahoy

Scientists this month have fully deployed 3000 oceanographic floats around the world, completing work on an 8-year-old network designed to monitor the world's seas. Data from the floats have already helped scientists detect changes in the stratification of waters that affect major food webs and interpret the influence of global winds on climate. Climate-forecasting centers around the world also use Argo data, and as the data sets expand, climate predictions should become more accurate, says Dean Roemmich of Scripps Institution of Oceanography in San Diego, California, who co-chairs the steering committee. "This will be key to proving to the contributing countries that this effort deserves a sustained commitment," he says. Argo's $20-million-a-year budget comes from 23 countries. **–NOREEN PARKS**

have not yet been fully assembled or posted on a public Web site. The TB research lab of A. Willem Sturm of the University of KwaZulu-Natal in Durban provided the XDR isolates to both teams. The Harvard group's main South African collaborators, Tommie Victor and Rob Warren of the Centre of Excellence for Biomedical TB Research at the University of Stellenbosch in South Africa, are providing other strains for the wider Broad analysis.

The Broad team used two sequencing technologies, says institute director Eric Lander. The data were generated using Solexa sequencers—a new, massively parallel technology—and also crosschecked on more traditional sequencers. The South African team used a rival new sequencing technology, the Roche GS-FLX. Says Lander: "As the speed and efficiency of microbial sequencing skyrockets, it should be possible to extract enormous amounts of information about population variation in TB and other infectious organisms."

As part of the wider project, HSPH and Broad Institute scientists, sequencing isolates provided by international labs, are analyzing dozens of "evolved" TB strains that include several XDR and MDR isolates from the same persons or communities. Says Murray: "At the end of the day, we will have a comprehensive list of polymorphisms associated with the acquisition of drug resistance."

–ROBERT KOENIG

SCIENCE IN CHINA

# Max Planck's Asian Venture Rethinks Its Agenda

**SHANGHAI**—After an auspicious start, a unique joint venture of the science academies of China and Germany is undergoing a tough outside review that could lead to significant changes. The Partner Institute for Computational Biology (PICB), founded 2 years ago by the Chinese Academy of Sciences (CAS) and the Max Planck Society (MPG), has won praise for its scientific activities. But reviewers and others are concerned that management troubles are preventing PICB from realizing its full potential.

At a closed session on 23 October, PICB's outside scientific advisory board chewed over a range of options, including recommending greater autonomy for the institute and closing it down after its 5-year contract runs out in 2010, according to sources involved in the discussions. The board is now drafting recommendations that will be presented next month to CAS President Lu Yongxiang and MPG President Peter Gruss, who together will decide PICB's fate. Lu, in a meeting with a senior MPG official last week, "emphasized that closing PICB is not an option," says CAS program officer Fang Qiang.

The two science powerhouses have been exchanging students and faculty members since the late 1970s. PICB is their most ambitious endeavor yet, and observers say that the institute and its managing director, mathematician Andreas Dress, are making a mark. Dress has demonstrated "a lot of personal dedication and energy," says Jürgen Jost, director of the Max Planck Institute for Mathematics in the Sciences in Leipzig, Germany.

But PICB's complex management structure has caused problems from the beginning. "Neither MPG nor CAS were under the naive impression that an undertaking like a partner institute will develop straight, smoothly, and without frictions," says an MPG official. Or as Fang says, "It's like a German baby growing up in a Chinese world."

Much of the angst is over who should control PICB's purse strings. The institute has a €1.5 million ($2.2 million) budget, two-thirds of which is supplied by CAS. Spending decisions must be approved by CAS's Shanghai Institutes for Biological Sciences (SIBS), which oversees PICB. SIBS and other institutions with a hand in PICB sometimes do not see eye to eye on priorities. One recent example is Dress's aim to establish a research center on the toponome, the spatial arrangement underlying the functional organization of proteins and protein networks in cells. Dress says he struggled for months to win approval for the center from Germany's science ministry in early 2006. Since then, PICB has been waiting for SIBS, CAS, and MPG to reach an agreement to release the funds.

**Joint chiefs.** Mathematician Andreas Dress (*left*) and geneticist Jin Li were tapped to lead the Partner Institute for Computational Biology in Shanghai; it is now seeking a third director.

CREDITS: COURTESY OF PICB

One of PICB's biggest challenges, CAS and MPG officials concur, has been finding leaders. By tradition, Max Planck institutes have several directors. When MPG and CAS advertised the directorship posts in 2004, Dress, who had retired in 2003 from Bielefeld University in Germany, was invited to apply. He was appointed head of the combinatorics and geometry department. Meanwhile, a Sino-German search committee interviewed a dozen Chinese candidates but offered the job to none.

Former CAS vice president Chen Zhu, now China's health minister, then recruited geneticist Jin Li, and MPG approved him as the second director. Jin, now vice president of Fudan University in Shanghai, logs only about a week of each month at the institute. But his contributions are substantial, says Dress: "He's an excellent scientist and values the institute." Candidates for a third directorship and for Dress's job after he retires—possibly after his 3-year contract is up next year—were vetted in Shanghai last month.

Management issues aside, "scientifically, the institute has done quite a good job," says Fang. PICB's scholarship has drawn praise. Highlights include a new computer method for mapping protein networks in cells that was published in *Nature Biotechnology* in October 2006 and a conference dedicated to the 400th anniversary of the Chinese translation of Euclid's *Elements* (*Science*, 2 November, p. 733).

Noting such achievements, MPG and CAS officials at last month's meeting forcefully argued against dissolving the institute, sources say. "We are willing to try new things," says Fang, who notes that Lu last week floated the idea of encouraging PICB to expand the number of junior scientist groups (it currently has two) in order to cultivate future leaders. A trickier issue for Lu and Gruss is whether, and how, a precocious young institute with two masters can be granted more freedom to run its own affairs.

–RICHARD STONE

EVOLUTIONARY GENOMICS

# Fruit Fly Blitz Shows the Power of Comparative Genomics

To the uninitiated, one fruit fly is like any other—all equally pesky and deserving a good swat. But in reality, these insects are quite diverse, with species that differ from each other, genetically speaking, more than a platypus differs from a primate. A consortium of about 250 researchers harnessed this diversity and in a blast of reports this week demonstrated the analytical power of comparative genomics.

The group has sequenced 10 genomes from different fruit fly species; combining these with existing DNA data, they have done a 12-way comparison to track the evolution of genes, regulatory regions, entire pathways, and cellular processes. Having these patterns in hand makes it easier to spot similar features in the genomes of other species, including humans, researchers report in more than 40 research papers in the 8 November issue of *Nature* and in other journals.

"This work has really increased the sophistication of what we can learn from comparative sequence analysis," says genomicist Elliott H. Margulies of the National Human Genome Research Institute (NHGRI) in Bethesda, Maryland. As project co-leader Michael Eisen of Lawrence Berkeley National Laboratory in California points out, the comparison "allows you to map where [genetic] changes occur along the tree, and that allows you to study the process of evolution, not just the product."

*Drosophila melanogaster*, the lab standard, has powered genetics studies for almost a century. In 2000, its genome became the second animal genome sequenced, but partly because it was one-of-a-kind, it was hard to decipher. Subsequent comparisons between the human and mouse genomes and, in 2003, between the genomes of four yeast species drove home the value of comparative genomics. Immediately, *Drosophila* enthusiasts appealed to NHGRI to support an even larger multispecies comparison in fruit flies.

NHGRI approved a plan to look at 12 *Drosophila* species that diverged between a half-million and 60 million years ago. Each has its own lifestyle and geographic distribution—and each has a distinct evolutionary relatedness to *D. melanogaster*. The genomes proved quite varied, ranging in size from 130 million to 364 million bases, with 13,683 to 17,325 genes. The amount of DNA taken up by transposable elements, or repeated regions of DNA, varied by an order of magnitude, the consortium reports in the 8 November issue of *Nature*.

From this material, the researchers pieced together evolutionary stories. Probing a biological pathway as it changes from one species to the next "lets you see where there's evolutionary pressure driving the change," says Andrew Clark of Cornell University. His group looked at the impact of pathogens. They examined the repertoire of genes involved in recognizing microbes, signaling an invader's presence, and producing toxins to thwart attacks—245 genes in *D. melanogaster* alone and 1200 across the 12 species.

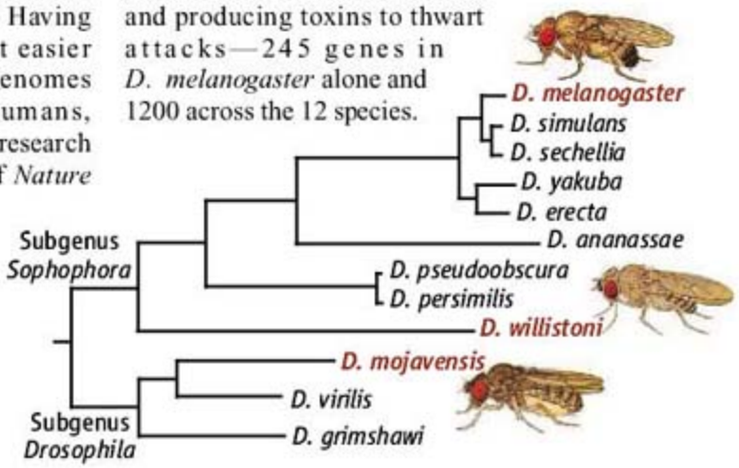


**Fruit flies galore.** By sequencing *Drosophila* species of varying degrees of relatedness, genomicists have learned much more about genome structure and evolution.

In many fruit fly species, some families of genes that code for antimicrobial peptides have been expanded, Clark and other researchers found. The expansion makes sense, as a fly with multiple copies of the right genes can produce more toxin and mount a stronger defense, Clark explains. Although the group didn't find quite as many duplicated pathogen-recognition genes, these were the fastest evolving, reflecting the need for ever-changing defenses as microbes constantly come up with ways to evade detection, Clark and colleagues reported online 8 November in *Nature Genetics*.

The evolutionary analyses yielded surprises as well. For example, Clark's team found that a new gene called *drosomycin*, which codes for an antifungal compound, appears only in *D. melanogaster* and its close relatives. There are no clues, however, as to how this gene came to be. Another surprise came from the species *D. willistoni*: It doesn't seem to have genes to make proteins containing selenium—proteins that researchers had thought were common to all animals.

Manolis Kellis of the Broad Institute in Cambridge, Massachusetts, led an assessment of how each type of gene or regulatory region changed—or didn't change—from one species to the next, revealing specific evolutionary patterns, or signatures. Kellis and others have incorporated those telltale patterns into software to look for the same patterns in other species to pinpoint each type of DNA. "This allows us to assign function" to some regions "through computation alone," says Margulies.

Based on a common pattern of insertions, deletions, base usage, and substitutions, Kellis and his colleagues detected 192 undiscovered protein-coding genes as well as 150 that do not follow standard rules. Typically, protein-coding genes have a "stop" sequence that signals the end of the gene. But in these 150 cases, protein-coding sequences extended beyond the "stop." "It's always a little humbling that the assumptions we are taught in school do not apply across all genes," says Ewan Birney of the EMBL European Bioinformatics Institute in Hinxton, U.K.

With these new tools, which are particularly useful for recognizing regulatory DNA, Kellis and his colleagues have pieced together a fruit fly gene regulatory network that incorporates 81 microRNAs and 67 transcription factors. "The methodology and principles are absolutely general, and they are applicable to any genome," says Kellis. Others say that the model still needs refining to reconcile it with experimental results. But geneticist Rama Singh of McMaster University in Hamilton, Canada, is quite pleased with this beginning. Because many fruit fly and human genes are equivalent, the network "is going to tell us a lot about humans," he predicts.

The analysis bodes well for the utility of bird, marsupial, and reptile sequences in analyzing the human genome. It also argues for sequencing and comparing all the primates, says Birney: "The take-home message is that there are a lot of clear wins from doing this sort of evolutionary genomics."

–ELIZABETH PENNISI

SOURCE: ADAPTED FROM A. STARK *ET AL.*, *NATURE* (19 OCTOBER 2007); ILLUSTRATIONS: S. L. MARTIN, UNIVERSITY OF TEXAS PUBLICATION, NO. 4313 (1 APRIL 1943) AND NO. 4445 (1 DECEMBER 1944)

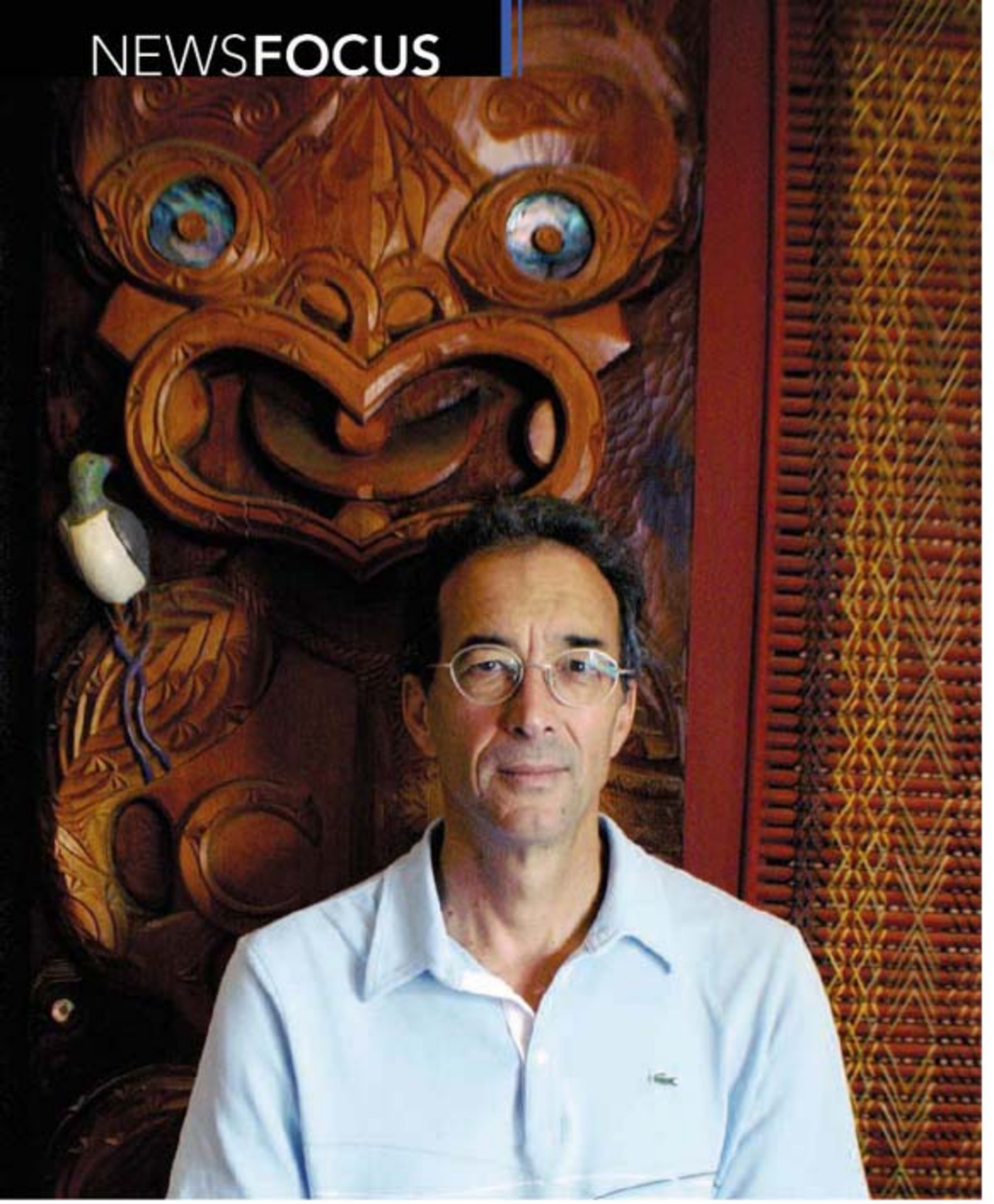

**Navigator.** Biologist Michael Walker stands in front of a carving of Turi, a legendary Maori canoe pilot.

CREDIT: J. BOHANNON/SCIENCE

# Seeking Nature's Inner Compass

**Michael Walker has navigated cultures and courted controversy in his quest to prove that life forms possess a single organ for perceiving magnetic fields—a sensor based on magnetite**

**AUCKLAND, NEW ZEALAND**—Michael Walker slips off his shoes and enters an enormous Maori ceremonial room, the University of Auckland's Tānenuiarangi Hall. Padding across long wooden planks, the biologist explains the significance of each of dozens of painted wooden carvings on the walls and pillars. "This is Turi," he says, pointing out a highly stylized humanoid with a green bird on its shoulder. "He was the skipper of a canoe which sailed to New Zealand from the Cook Islands." For that unrivaled feat, Turi gained a place among the gods.

The colonization of New Zealand about 1000 years ago, the last of the great Polynesian migrations, is a marvel of navigation. The first Maori visitors traversed thousands of kilometers of ocean with nothing but the sun and stars to guide them. How did those pioneers manage to get here?

Indeed, how does any creature find its way across featureless expanses such as the Pacific Ocean? The question fascinates Walker and has come to define his career. Competing theories have been proposed to explain the uncanny orienteering of animals as diverse as birds, bees, and fish. A decade ago, Walker's team galvanized the field with the discovery of an organ that may function as an internal compass: a string of magnetic crystals in the nose of trout (*Science*, 5 February 1999, p. 775). "Walker is definitely a pioneer," says biophysicist Thorsten Ritz of the University of California, Irvine. Now Walker believes he is on the verge of clinching the case that magnetite is the universal animal compass that scientists have been seeking for a century. But the belief makes Walker a maverick: Most others in the field are convinced that animals have more than one navigation organ.

## A hybrid mind

Walker had to chart his own path to scientific success. His mother is of European ancestry, his father a famous Maori leader, "and I kept those halves of my life separate and parallel," he says. There was the Walker who donned shirt and tie and keenly devoured his physics textbooks. And there was the Walker whose Maori grandmother taught him mythology and the lunar system for planting and fishing. The result, he says, was "a hybrid mind."

It wasn't until after a Pacific odyssey of his own—a Ph.D. at the University of Hawaii followed by 5 years of postdoctoral research in California—that "the halves finally came together," Walker says. The fusion was triggered by his mentoring of Maori science students after returning to his alma mater, the University of Auckland, in 1990. Many of his students struggle with cultural dissonance. Walker, 53, is now helping them embrace both cultures (see sidebar on p. 907).

Having a hybrid mind can at times produce "discomfort in your own skin," says Walker, but it has advantages. "It has helped me to be aware that there's always more than one way to do things," he says. For instance, he points out that New Zealand's first European visitor, the 18th century English explorer James Cook, crossed the ocean with the help of a magnetic compass, tracking his ship's position

on a two-dimensional grid. Along the way, Cook met Maori navigators who could island-hop more reliably using polar coordinates based on star-zenith positions and known distances between islands. Walker has sailed the Pacific using both systems.

He has put that experience to use in his research on biological navigation. "Animals are similar in that they use different strategies on different scales of time and space," he says. A bird winging its way back to its nest uses visual cues, from the position of the sun to the lay of the land. But the same bird at sea will die without more guidance. The sun indicates a heading, but over a long haul even the slightest cross-breeze will cause vast displacements. How does the bird know it has been blown off course?

### The sixth sense

In the 1860s, Russian zoologist Alexander von Middendorff first noticed that some birds migrate along fixed paths, later recognized as Earth's magnetic field lines. But it took another century before behavioral biologists demonstrated that animals can detect magnetic fields. Sure enough, attaching a magnet to a pigeon's beak interferes with its return to the roost. For a snack reward, fish can be trained to respond to magnetic fields. And a lobster transplanted from sea bottom to an aquarium orients itself toward home like a compass with claws.

In principle, Earth's magnetic field provides enough information for an animal to cross an ocean, by fin or wing, without going astray. From most places on the planet's surface, the magnetic field points north, so knowing which direction you are facing is the easy part. Changes in a field's intensity or angle, which generally grow stronger and steeper toward the poles, reveal latitude.

Gauging longitude is trickier. One approach is to note the sun's position as it rises and sets. Because Earth spins on an axis off kilter from its magnetic axis, the sun's intersection with the horizon changes systematically the farther east or west you go. For underwater animals, there is a mesh of north-south magnetic ridges on the ocean floor—created by the spreading crust and the periodic reversal of Earth's magnetic poles—that can be memorized.

But a long-standing riddle is whether animals can detect such subtle fluctuations. "For a magnetoreception organ to work, it must be amazingly fine-tuned," says Ritz. Not only is Earth's magnetic field faint—hundreds of times weaker than that of a child's bar magnet—but for an animal to track its position using field variations, it must detect changes as small as 1% of that signal.

Several possible mechanisms emerged in the 1970s. One bona fide contender is a biological compass made of magnetite. Also known as lodestone, magnetite is the most magnetic form of iron oxide and occurs naturally in rocks. Living cells can make their own tiny magnetite crystals. Some mud-loving bacteria make magnetite for orientation, and similar crystals have been found in a multitude of higher organisms. Magnetite may serve other functions, such as locking up excess iron, says Kenneth Lohmann of the University of North Carolina, Chapel Hill, who's an expert on turtle migration. "But it's very hard to imagine these crystals aren't there for magnetic detection."

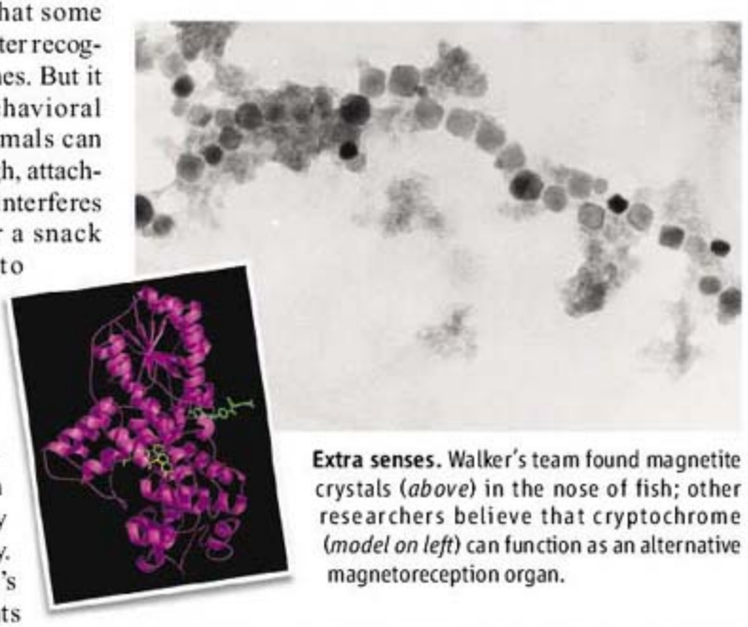

**Extra senses.** Walker's team found magnetite crystals (*above*) in the nose of fish; other researchers believe that cryptochrome (*model on left*) can function as an alternative magnetoreception organ.

Enter Walker, who had already made a name with his innovative behavioral studies of fish in controlled magnetic fields. He became wedded to the magnetite model during a postdoc stint in California, where he bounced the idea off biophysicist Joseph Kirschvink of the California Institute of Technology in Pasadena. With his geosciences background, Kirschvink is the physics Yin to Walker's biology Yang. After the duo extracted magnetitelike crystals from a tuna (*Science*, 18 May 1984, p. 751), Walker was convinced that they were on the trail of the real biological compass.

The magnetite model surged with two studies of rainbow trout that Walker's team published in *Nature* in 1997 and 2000. "We studied the fish as if it were a rock," he says. Working their way through the head in thin, frozen slices under a magnetic force microscope—a geologist's tool—the researchers found a group of cells in the nose laden with strings of magnetite crystals. Crucially, the cells are wired to the brain via a nerve sensitive to magnetic fields. "This is really the first truly new type of sensory cell to be discovered in a long while," says Kirschvink, who was not an author of the *Nature* papers. "If there is ever a Nobel Prize for magnetic field perception, Walker's name will be on it."

### And a seventh?

Others are not convinced that this is the full story. An alternative mechanism for magnetoreception, known as the radical-pair model, has gained a strong following over the past decade. The idea is that besides using magnetite to detect the push and pull of Earth's magnetic field, animals also keep track of it with a chemical reaction.

It was only theoretical until 1998, when a candidate magnetoreceptor called cryptochrome was discovered in the eyes of animals as diverse as fruit flies and mice. When light strikes this protein, it produces two possible intermediate states differing in the configuration of a single electron. Their ratio depends on the orientation of cryptochrome—and hence, the orientation of the organism—relative to the ambient magnetic field. Because cryptochrome is in the retina, Ritz and others have proposed that it feeds magnetic information to the brain through the optic nerves. Birds, for example, may "see" Earth's magnetic field with a few quick turns of the head.

"Many pieces of the puzzle that never fit well with the magnetite model have started to make a lot of sense," says Ritz. One of these is that some animals, particularly birds and amphibians, do not seem to be sensitive to polarity; reversing a field's north and south poles in the lab often has no effect on behavior. "That is a prediction of the radical-pair mechanism," says Ritz, "because it only detects displacement from the north-south axis, not a flipping of the axis."

A 2004 study in *Nature* by Ritz and others provided another test. The cryptochrome compass, but not magnetite, should be disrupted by certain frequencies of electromagnetic fields. Birds exposed to these frequencies were disoriented. "That

CREDITS (TOP TO BOTTOM): COURTESY OF MICHAEL WALKER; SEZGIN OZGUR AND AZIZ SANCAR/UNIVERSITY OF NORTH CAROLINA

## A Home for Maori Science

**Future scientists.** Melanie Cheung (*center*) and fellow graduate students at the University of Auckland.

**AUCKLAND, NEW ZEALAND**—A meeting of Maori scientists begins like no other. In a sun-drenched conference room at the University of Auckland, a couple of dozen researchers filter in, smile, and press foreheads together in a *hongi* greeting. A flowing speech in the Maori tongue introduces the newcomers. Only then does the language switch to English and the topic to science.

This is Horizons of Insight, New Zealand's National Institute of Research Excellence for Maori Development and Advancement—known here as the Maori Research Centre. Today, graduate students on center grants are giving an update on their work.

The Maori are a success story among post-colonial indigenous peoples, but they still face serious problems. Among New Zealanders, Maori citizens are burdened with a disproportionately high rate of poverty, drug abuse, and violent crime. Maori students are far less likely than those of European ancestry to finish an undergraduate degree, let alone enter graduate school. And among those who do, few choose science. Boosting Maori academic success is a necessary starting point for equality, the center's co-director, Michael Walker (see main text), and others argue. That's the raison d'être of the 5-year-old center, which aims to improve the social and environmental health of Maori communities as well as support Maori Ph.D. students. When the center started, it hoped to boost the number of Maori Ph.D. students from a few dozen enrolled in 2002 to at least 500 in 5 years. They pulled it off ahead of schedule, chalking up the 500th Maori Ph.D. student last year.

One of the center's high achievers, Melanie Cheung, walks to the head of the long table.

Her project on Huntington's disease began traditionally enough, she says. To investigate what might be going wrong in the brains of patients who suffer from Huntington's, she planned to develop a model using lab-grown neurons. Her hypothesis is that faulty mitochondria, the cellular dynamos, are a key part of the puzzle.

Then Maori custom intervened. To grow neurons, she must extract cells from the brains of cadavers. But in Maori culture, she says, "the head and brain are *tapu*," a sacred body part that must not be tampered with.

Rather than bagging the project, Cheung turned to her community for advice. She discussed the problem with her family, then with the elders of her tribe, the Ngati Rangitihi. Some implored her not to "mess with *tapu*," she says. Others dismissed Huntington's as "a white man's disease." But the elders "supported the purpose of the work," she says, and invited Cheung's team, including her Ph.D. adviser, Richard Faull, to take part. The confab lasted an entire day, with a song following every speech. Not only did Cheung allay her tribe's worries about the project, "now they wholeheartedly support it," she says.

Although the elders could not change the brain's status as *tapu*, they created rituals that are now part of her daily lab routine. Before and after isolating and culturing neurons, she says a prayer to "acknowledge the person who has passed, the gift that their family has given us." She also learned a song about creation. "Sometimes I sing, sometimes I don't," she says. "It depends if there are other researchers around, and if I feel the need. These processes are about keeping me culturally safe."

What may seem like an extra burden has proved to be a boon. When Cheung started her Ph.D., cases of Huntington's disease were unknown among the Maori. But after engaging her tribe, "people started coming forward," she says. Four likely cases have been diagnosed, and genetic counselors are working with Maori communities for the first time.

Cheung's efforts at bridging the cultures are ongoing. "In February, we are returning to visit my tribe with our entire research group of 60 or so people and their families," she says. The tribe is eager for an update on their progress.

Cultural engagement like this is not only a happy outcome of the Maori Research Centre's grants, says Walker: "It's required." Every project includes an element of community service, he says. "You have to give back."

**–J.B.**

result is very difficult to explain if birds are only using magnetite to orient themselves," says biologist Henrik Mouritsen of the University of Oldenburg, Germany.

Walker doesn't buy it. He labels the reported effect of cryptochrome-targeted radiation on orientation as "noise" rather than evidence of an alternative magnetic sense. The cryptochrome model, he says, is only supported in birds and amphibians, implying that it has been gained and lost repeatedly during vertebrate evolution, whereas magnetite—and, Walker argues, its compass function—has remained constant. The idea that evolution has maintained a second organ for magnetoreception is "absurdity," he says.

Walker's uncompromising position frustrates many colleagues. "He completely misrepresents the field," grumbles John Phillips, a magnetoreception researcher at Virginia Polytechnic Institute and State University in Blacksburg, "only citing papers that support his view and ignoring the rest." Phillips argues that the evidence for the radical-pair model is at least as solid as is the evidence for magnetite. "Both systems have been maintained because they do different things," he says. Cryptochrome is the more reliable compass for determining a heading, Phillips says, whereas magnetite may be used for mapping displacements en route. Mouritsen, who also studies magnetoreception in birds, agrees: "Whether or not the story is parsimonious, the evidence shows that there are two systems for sensing magnetic fields."

Kirschvink, like Walker, dismisses the two-magnetoreceptor hypothesis. "That simply does not make sense," he says. Walker enjoys the jousting. "This is all vigorous scientific debate," he says. "It drives the development of theory and experiment, and peer review winnows things out."

The issue may be resolved soon. Mouritsen and Phillips, with cryptochrome-knockout mice in hand, are confident that the detailed behavioral studies will prove the radical-pair model beyond a doubt. Meanwhile, Walker, Kirschvink, and others just landed a $1.4 million grant from the Human Frontier Science Program. The grant will allow them to do ultrafine structural studies of fish magnetite that could reveal exactly how it works.

Is Walker reaching the end of his odyssey? Perhaps. But whatever he finds in the nose of the fish, says Ritz, "there will be a truly wonderful story."

**–JOHN BOHANNON**

CREDIT: J. BOHANNON/SCIENCE

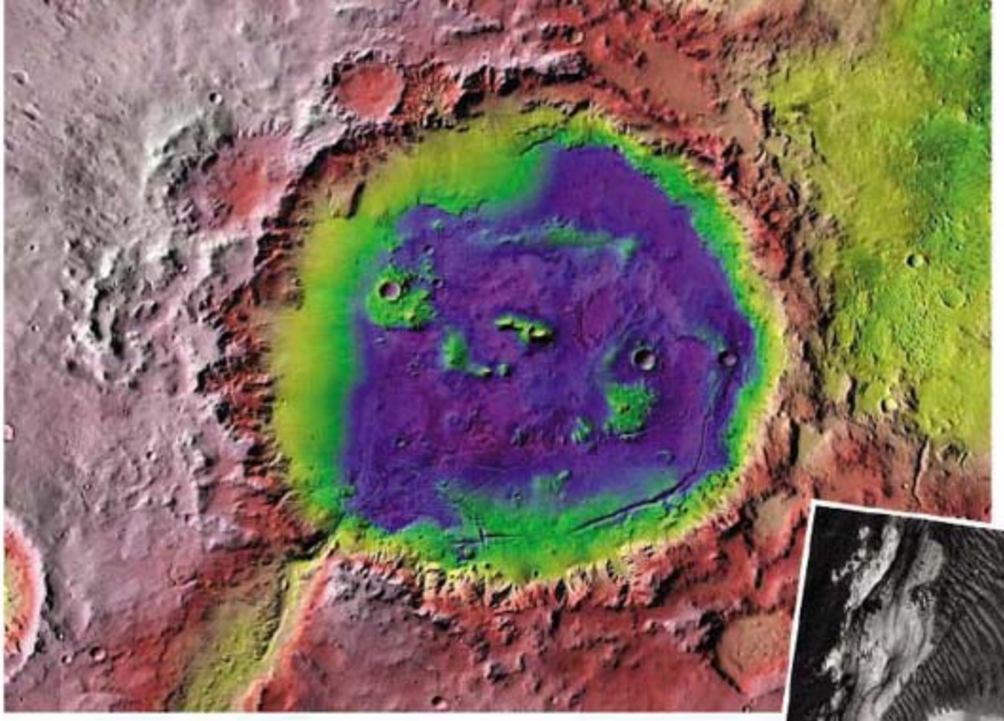

PLANETARY SCIENCE

# Majority Rules in Finding A Path for the Next Mars Rover

**A few dozen self-selected planetary scientists are voting their way through a minefield of fiscal and scientific uncertainty in the pursuit of martian life**

**PASADENA, CALIFORNIA**—When it comes to exploring Mars, geologists love rocks. Engineers looking to land the next Mars rover hate them. Throw in rover mission cost overruns, a crucial design failure, a severely limited understanding of Mars, and a rush to launch 2 years from now, and the Mars exploration community has a lot to talk about.

Scientists in a small planetary town hall meeting here are helping sort out where the billion-dollar Mars Science Laboratory (MSL) rover should be landed in NASA's drive to understand life beyond the home planet. After dozens of sometimes boisterous votes by a grab bag of specialists, most of their proposed landing sites lay on the cutting-room floor. "Is there anything like this elsewhere in science?" asked a meeting organizer in an aside. Not likely.

At the end of the MSL landing site selection workshop,* participants had pared their 51 proposed sites to six for further consideration by NASA. It was a painful if democratic process. The same procedure had gone wrong once before, sending the Spirit rover to what looked like an ancient lakebed but turned out to be a barren lava plain. And this time researchers are not just "following the water" on Mars in search of past environments conducive to life. They are also hunting for places that might still harbor organic matter from past or present life. That raised the bar for candidate landing sites, as did the tighter constraints mission engineers had to place on where MSL can land.

In the end, the majority-rules approach fared well. "We've pretty much captured all the types" of landing sites while getting down to just six, says geochemist David Des Marais of NASA's Ames Research Center in Mountain View, California. "A lot of people subverted their interests [in a particular site] to the science. This degree of community participation is one reason the Mars program has been so successful." In 9 months, planetary scientists will return to see if they can agree on a single landing site that's both safe and exciting.

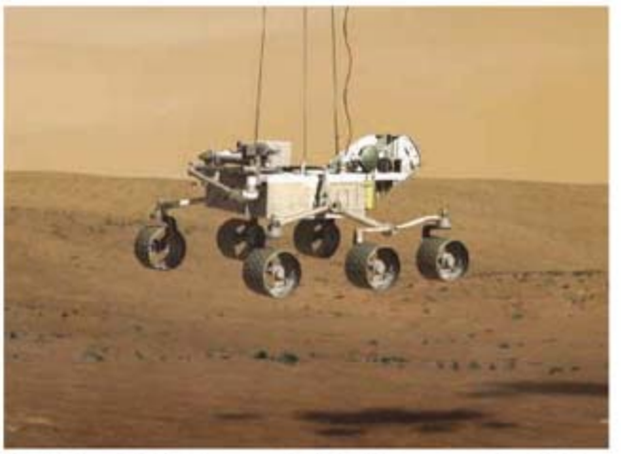

**Touchdown.** MSL (*above*) can land in tight quarters like 150-km Holden crater (*top*), where water once entered from lower left.

CREDITS (TOP TO BOTTOM): NASA/JPL; NASA/JPL/UNIVERSITY OF ARIZONA; NASA/JPL

### A new challenge

Five craft, all American, have successfully landed on Mars. The first—two Viking landers that set down on roaring retrorockets in 1976—went in nearly blind on a wing and a prayer. The two latest—the Opportunity and Spirit rovers that rolled onto the martian surface encased in airbags—benefited from years-long analyses of landing hazards and the prospects for good science (*Science*, 17 January 2003, p. 326). In four workshops, interested planetary scientists proposed 185 landing zones for the Mars Exploration Rover (MER) mission and then pared their list to the safest-looking, most scientifically interesting two on the basis of the latest observations from Mars. More-detailed imaging from orbiting spacecraft, for example, allowed accurate estimates of the abundance of mission-ending boulders too small to be seen from orbit. And better spectroscopy pointed to an enticing site loaded with the mineral hematite that forms only in water.

This community-supported selection process reaped considerable rewards. The rovers landed safely on opposite sides of the planet to find landing conditions much as predicted. And Opportunity roved across plenty of hematite, although the mineral had formed in briny groundwater rather than on the postulated lakebed. Spirit, on the other hand, was in for a surprise. For all the analysis of geologic features on the floor of giant Gusev crater, Spirit landed not on the expected ancient lakebed but on a vast lava plain devoid of signs of water. Only by chance did it eventually reach nearby hills that harbored enigmatic water-altered rock.

This time around, NASA is sending the Humvee of rovers to Mars. MSL, which is slated to rove for two Earth years, weighs in at three-quarters of a ton (more than four times the mass of Opportunity or Spirit), boasts nine instruments (each developed specially for this mission, including a rock-zapping laser chemical analyzer), and runs on nuclear power. Even the landing system is brand-new. In a landing scenario

* Second MSL Landing Site Workshop, 23–25 October, sponsored by the NASA-appointed Mars Landing Site Steering Committee and the MSL Project.

variously described by scientists as "exciting" or "scary," the rover—only one this time—will descend the final 1500 meters hanging by cables from a rocket-festooned descent stage. All this for $1.7 billion.

Mars scientists would have happily settled for a couple of more modest rovers like Opportunity and Spirit (at $410 million each), but that isn't the NASA way, they explain; each new mission must be bigger and obviously better. MSL is clearly in the NASA spirit. "This has been a very ambitious task," MSL project manager Richard Cook of the Jet Propulsion Laboratory (JPL) in Pasadena, California, said at the workshop. Engineers speak of the number of miracles required on a project, he said, and "on MSL, it seems we have more than our share."

### Whittling down

Not all of the required miracles came through. At the project's most recent NASA review, it appeared that MSL would exceed its budget by $50 million to $100 million, NASA's Mars program scientist Michael Meyer told *Science*. As a result, the project ended up economizing on rover instrumentation, among various cuts, and reducing the number of candidate landing sites it would scrutinize from 12 to five. "We have become painfully aware how complex and time-consuming it is to select and certify a landing site," said Cook, and consequently expensive. New imaging revealing fields of lander-destroying boulders recently required relocation of the Phoenix landing site.

The heart of the MSL winnowing process was almost 2 days of 15-minute presentations, discussion, and voting in a Pasadena hotel. Anyone with a site to propose (and the money to travel) could make their PowerPoint pitch to the assembled dozen members of the MSL steering committee, other proposers, a handful of invited outside experts, and interested planetary scientists and their grad students. Discussion followed, with one eye on the prospects for doing science and the other on the engineering constraints. Then came the voting: a show of hands for green, yellow, or red on four science-related questions for each site. With considerable good-humored joshing, voters expressed their opinions on each site "as a potential habitat for life, past or present."

Yellows predominated. Although strictly speaking, the voting was on the science potential, not the rover's physical capabilities, new engineering restrictions were at times factored in. For example, mission engineers had planned on using an exotic dry lubricant to keep the driving and steering systems and the instrument-laden rover arm operating down to −150°C, far below the −50°C limits of the MERs. But in testing, the new dry lubricant failed after just 20% of its required lifetime, MSL mission manager Michael Watkins of JPL said at the workshop. Returning to a wet lubricant made one site impossible and put any sites poleward of 25°S in jeopardy.

The rover's mobility hasn't worked out quite as expected, either. At the first workshop, many scientists proposed "go-to" landing sites. In these, MSL would land somewhere in a smooth, safe, 20-kilometer-diameter landing zone and then drive beyond the landing zone to interesting but unlandably rough geology.

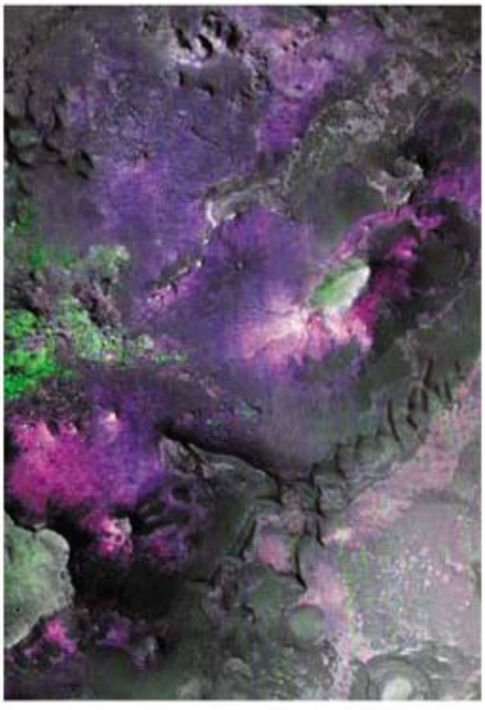

**Go-to.** MSL might rove into rugged terrain with clays (blue and magenta) denoting past water.

CREDIT: NASA/JPL/JHU APL/UNIVERSITY OF ARIZONA/BROWN UNIVERSITY (J. MUSTARD)

But at this workshop, Watkins reported that on further consideration, project engineers expect MSL's driving to be "MER-like," something like 200 meters per day rather than the expected 500 meters per day. MSL, it turns out, must charge its batteries with its radioisotope thermoelectric generator and use them to drive, rather than driving directly from the RTG. "We need prime science within 10 kilometers" of the center of the landing zone, said Watkins. That eliminated a few sites and sent proposers scrambling to find interesting geology in their landing zones.

Some attendees wondered out loud whether the geologists might be squinting at their images a bit too hard. This could be "Gusev all over again," said spectroscopist Steven Ruff of Arizona State University in Tempe. Some geologists were interpreting layered rock as sediments laid down under lake water, he said, without discussing less interesting but quite plausible alternatives, such as blankets of volcanic ash. Such concerns helped eliminate exquisitely layered basins with no sign that water ever flowed there.

Mineralogy rather than geology ended up being the prime criterion. Most attendees took the detection of clays—the product of the watery alteration of igneous rocks—as a sign that water had long been in contact with rock there. That would bode well for life. Clays are also adept at preserving organic matter over the eons. So any site without at least a hint of clay was out of the running.

This was a bit too much for some. Many of the geobiochemists and astrobiologists—the smallest contingent in the crowd—felt that people were leaning on the clays far too much. Having clays is nice, they said, but it's not everything. Clays that formed within the ancient Mars crust, for example, are far less promising signposts of early life than clays in a river delta formed in a crater lake. Astrobiologist Dawn Sumner of the University of California, Davis, pointed to Vernal Crater, which had fared poorly in initial voting because a thin dust layer blocks any spectral signature, so researchers couldn't tell whether clay was present. But Vernal's proposer, planetary scientist Carlton Allen of NASA's Johnson Space Center in Houston, Texas, had drawn attention to what appeared to be lake deposits, lake shorelines, channels, and even hot-spring deposits, the first proposed on Mars. "These things are really important," said Sumner. "I voted all green" on Vernal. Nonetheless, a revote kept Vernal out of the top 10.

In a final afternoon session, the workshop got down to a final six by demoting four sites to "purgatory" because they held too little promise of traces of life or their landing zones were just too boring. The remaining six push the engineering limits, although those limits remain flexible. The project asked that two of the final five landing zones be demonstrably safe, but at this point in the hazard analysis, none of the current batch is. Three are former crater lakes, the workshop's obvious favorite type of site, even though two of them are so far south that the rover would likely have to hibernate one-third of the time, beginning on landing. And two others are the crustal-clay sites so popular with the geologists but shunned by astrobiologists. Still, "it turned out better than I would have expected," says Sumner. They ended up with a diverse suite of sites whose riskiness will "poke the engineers to find what we really want."

**–RICHARD A. KERR**

GENETICS

# Who's the Queen? Ask the Genes

**Biologists are finding that in some social insects nature, not nurture, determines whether offspring become workers or royalty**

In 1712, the English scholar Joseph Warder dedicated his treatise, *The True Amazons: Or, The Monarchy of Bees*, to Queen Anne, citing the caste divisions of the hive—the queen built for breeding and the workers tending her and her brood, foraging, and dying to defend their home—as evidence that nature adored royalty. But much of what entomologists have learned since then has made the lives of bees and other social insects seem closer to the American dream: Given the right nurturing—a diet of royal jelly in honeybees, or being reared at a certain temperature in some ants—any female grub in a beehive or in an ant's nest can grow up to be queen.

At least this nurture-over-nature paradigm was the prevailing wisdom, backed by theory that argued that any gene that required a developing insect to become a sterile worker would be committing evolutionary suicide. But a few years ago, social-insect research was rocked by the discovery that in some ant species, workers and queens are determined by their genes—in other words, born, not made. And this was discovered not in some obscure rain forest species but in harvester ants, which are ubiquitous across the southern United States, have been studied for decades, and are even sold online for ant farms.

"Harvester ants are the poster child for ant research," says Sara Helms Cahan of the University of Vermont in Burlington, one of the co-discoverers of genetic caste determination (GCD). "Imagine what the other 11,999 species might be up to." Indeed, several more examples of GCD have popped up among other ant species. Researchers such as Helms Cahan are now tackling a raft of questions about this mode of life, trying to unravel these ants' evolutionary history, exactly what genes determine castes in the insects, and what, if any, evolutionary advantage GCD confers.

The trait, it turns out, is not confined to ants. A report on page 985 shows that a species of termite also uses genes to split breeders from workers. "This is probably the first clear-cut example of how caste is determined in termites," says Nathan Lo of the University of Sydney, Australia, a member of the team behind the discovery. And some believe that many more strange genetic and reproductive systems await discovery in social insects.

## Lucky ants

It took some luck to reveal harvester ants' odd genetics. "We found it by sheer accident," says ecologist Deborah Gordon of Stanford University in Palo Alto, California. The ants' natural history is normal enough: A single queen founds each nest and gives birth to all the colony's workers, sterile females that give harvester ants their name by gathering seeds for food. The queen also produces the next generation of reproductives: males and daughter queens, neither of which work. As in all ants, wasps, and bees, males of harvester ant species develop from unfertilized eggs and so have half as many chromosomes as females. After summer rains, males and prospective queens leave the nest on swarmlike mating flights. Males die after mating; queens found new colonies and can live for more than 20 years.

Five years ago, three teams, including Gordon's, Helms Cahan's, and one led by Jennifer Fewell of Arizona State University in Tempe, independently noticed that in some nests of the red harvester ant (*Pogonomyrmex barbatus*) and in other nests containing the rough harvester ant (*P. rugosus*), all the workers carry two different versions of a gene at certain DNA markers, whereas the queens in these colonies have identical pairs of genes at the same markers. This was weird, as genes should be spread about between the two castes at random in a colony in which any female can supposedly become a queen or worker.

Further genetic analysis of workers and queens showed that these ants were in fact neither *P. barbatus* nor *P. rugosus* but a hybrid of the two species. More complicated still, the hybrid population consists of two strains. In each nest, the queen and her daughter queens are purebred members of one strain or the other, whereas the workers are a cross between the two strains. The only way this system could work, the various research groups concluded, was if queens used sperm from males of their own strain to make more queens and sperm from the other strain to make workers, with each ant's caste decided not by its upbringing but by the combination of genes it receives from its parents. So queens must mate with males of both strains to raise a functioning colony.

Subsequent work has found that harvester ants with this GCD dominate a strip of desert from western Texas to eastern Arizona. (Other ants in this genus appear to use diet to determine caste.) So far, eight genetically distinct hybrid strains have been found, coexisting in four pairs of dependent strains, suggesting that hybridization has occurred—and GCD evolved—more than once.

**Queen me?** These red harvester ants need the right genes to become a queen.

CREDIT: ALEX WILD 2007

Mating between species is often a dead end because it leads to sterile offspring, but two aspects of ant biology allow *Pogonomyrmex* to get around this. Queens with GCD that have mated with only the other strain do not lose all their reproductive options: They can still produce males from unfertilized eggs. And workers are already condemned not to reproduce, so the sterility of interstrain offspring is moot.

**Strained relations.** Rough harvester ants (*above*) and red harvester ants have hybridized.

Even so, GCD seems a perilously fragile reproductive system, says evolutionary biologist Peter Nonacs of the University of California, Los Angeles. Each nest competes with those presided over by queens of its partner strain for food and territory yet also depends on the males of that strain for its survival. And strains cannot evolve together by swapping genes, because genes from one strain will never end up in a queen from the other. "It's such an odd way to have a social system. One would think there'd be great selective disadvantages and that it'd break down, but it hasn't," says Nonacs.

The origin of GCD in ants is almost as mysterious as its advantages. The obvious hypothesis, favored by Helms Cahan, is that the hybrid strains are descended from ancient crossings between the two parental species. The presence of genes from both species in each strain lends weight to this idea, as does the fact that within each pair, one strain's genes are more similar to *P. rugosus*, whereas the other is closer to *P. barbatus* (even though the two strains in each pair look alike physically). Helms Cahan has found that colonies with GCD grow more quickly than those of either pure *P. barbatus* or *P. rugosus* and that their workers are more aggressive than those of the parent species. "I wouldn't be surprised if they had an ecological advantage," she says. Hybrid plants often grow well, she points out, something long exploited by plant breeders.

Fewell has a different view of how GCD arose. Based on analyses of DNA from ant mitochondria—an energy-generating structure inside the cell with its own small genome—she believes that the oldest of the eight known strains with GCD is most closely related to *P. barbatus*. This species, she suggests, evolved an "egoistic" gene that made its bearers more likely to become queens. Such a gene would aid its carriers but would also create selection for worker-producing genes to prevent colony extinction. GCD might be a way to cope with egoistic genes, not something that gives a competitive advantage, she says, and the crossing with *P. rugosus* might be a later event not directly related to GCD's origin.

So far, biologists have spotted only genetic markers of caste determination; the actual genes behind it are unknown. But finding those genes in harvester ants could reveal those that control the developmental pathways of social insects in general. "*Pogonomyrmex* is going to be a very good model to look at mechanisms of caste determination," says Laurent Keller of the University of Lausanne, Switzerland.

Since GCD was discovered in harvester ants, it has been found in a number of other species. The southern fire ant (*Solenopsis xyloni*) uses sperm from males of a close relative to make workers and sperm of its own species to make queens. There are also genetic differences between the types of workers in leaf-cutting and army ant colonies. These workers come in various shapes and sizes, called subcastes, specialized for jobs such as soldiering, foraging, and nest maintenance. Like harvester ants, queens of these species mate with many males, and William Hughes of the University of Leeds, U.K., and his colleagues have found that in leaf-cutting ants, the offspring of different males are biased toward becoming a particular kind of worker, suggesting that a worker's genetic makeup predisposes her toward joining a particular subcaste. At the most extreme, more than 90% of a male leaf-cutting ant's offspring can develop into one subcaste. Hughes is now looking for genetic differences between queens and workers in leaf-cutting ants.

## Hidden complexity

Inspired by the discoveries in ants, Lo and colleagues at Ibaraki University in Japan looked for GCD in termites. Unlike ants and bees, termite societies have both male and female workers, and each colony has a king and a queen. It was thought that pheromones from other nest members controlled what termite larvae developed into, although no one had ever identified such caste-determining chemicals.

Working with the Japanese termite species *Reticulitermes speratus*, Lo and his colleagues examined this question by depriving colonies of their king and queen, which induces some larvae and normally sterile workers to become fertile creatures called neotenics. Through crossbreeding experiments between male and female neotenics, the team established that a single gene on the X chromosome controls caste in this termite species. The gene comes in two forms, dubbed A and B. Two A's in a female make a queen, whereas males with a B gene become kings. AB females and A males become workers.

When a queen with her two A's mates with a king and his B gene, all their offspring will be sterile workers. Lo believes this helps prevent cheating in the nest. *Reticulitermes* workers only become reproductives if the king or queen dies, removing a chemical signal that suppresses worker development. In contrast, in other termite species, all workers have the potential to become reproductives, placing a drain on the colony's resources. "They just sit around being looked after," says Lo.

Lo suggests that GCD is likely relatively rare in ants, the result of unusual circumstances such as hybridization, but that it may be common among termites because of the king-queen system and its associated genetics. It's still unclear how widespread GCD is in social insects, says ant expert Andrew Bourke of the University of East Anglia in Norwich, U.K. "There's a lot of hidden complexity that it's taking modern molecular techniques to discover," he says.

**Know your place.** The termite *Reticulitermes speratus* uses genes to prevent workers from becoming royal freeloaders.

Now that insect researchers have spotted some of this complexity, they may start finding more. "People have been a bit blind," Keller says. "They read something in a textbook, and then when the data doesn't fit that model, they throw out the data." The discoveries so far are just the beginning, he predicts: "I think that 5 to 10% of ant species will turn out to have very weird modes of reproduction." What Warder would have made of such royal perversity is anyone's guess.

**–JOHN WHITFIELD**

John Whitfield, a science writer in London, is author of *In the Beat of a Heart: Life, Energy, and the Unity of Nature*.

CREDITS (TOP TO BOTTOM): ALEX WILD 2007; YOSHINOBU HAYASHI ET AL.

# LETTERS

*edited by Jennifer Sills*

## Speaking Out About U.S. Science Output

I WAS AMAZED BY J. MERVIS'S NEWS OF THE WEEK STORY "U.S. OUTPUT FLATTENS, AND NSF wonders why" (3 August, p. 582). Not by the conclusion that U.S. science productivity is flattening out, but because apparently nobody interviewed by the NSF could identify the reason. Had the question been posed of almost any working scientist I know, the simple and accurate answer would have been that the number of papers that are written is diminishing because scientists are able to spend less time writing papers! Instead, we spend ever-more time on the increasingly burdensome administrative requirements of conducting science legally, and on writing, rewriting, and re-rewriting grant applications as the NIH's pay line drops to catastrophically low levels. As the number of hours in a day is finite and unchanging, something has to give. If I didn't have to spend the rest of this month ignoring various half-complete manuscripts and rewriting a grant application, I'd be able to explain in more detail.

**JOHN P. MOORE**

Department of Microbiology and Immunology, Weill Medical College, Cornell University, New York, NY 10065, USA.

CREDIT: IMAGES.COM/CORBIS

THE REGULATORY BURDEN THAT ACCELERATED around 1990 is finally affecting the output of U.S. researchers (J. Mervis, "U.S. output flattens, and NSF wonders why," News of the Week, 3 August, p. 582). Increased funding is reduced by the cost of regulatory compliance: expensive security systems for animals, superfluous accreditation, excessive requirements for cage sterilization, verification of sterility using cultures, and signatures at every step. And, of course, the regulatory documentation takes time away from documenting the research itself. Because of the monumental effort required to gain approval to use animal or human subjects in research, discouraged investigators avoid pursuing experiments that require new approvals, even if the idea may take only a few days to test.

The fault lies not with committee members trying to maintain compliance while still permitting research to proceed, but rather with regulations that aim to prevent not only harm, but the appearance of harm, or even the possibility of harm no matter how unlikely. Even an experiment in which participants must listen to a snippet of song and judge its familiarity is subject to stringent requirements intended to protect those participants from harm.

Science is an exploration of the unexpected, and these constraints are suffocating. We must expect creative students to look to other careers when they see how science is done today. They are replaced by those who are comfortable with bureaucracy and who do not know that science used to be accompanied by enthusiasm and spontaneity. The only mystery is why the flat output line has not yet turned down.

**RICKYE S. HEFFNER**

Department of Psychology, University of Toledo, Toledo, OH 43606, USA.

THE NEWS OF THE WEEK STORY " U.S. OUTPUT flattens, and NSF wonders why" by J. Mervis (3 August, p. 582) states that "the total output of U.S. scientists stopped growing in the early 1990s and hasn't budged since then." This conclusion is based on publication productivity data from 1992 and 2001. Had more recent data been used, at least one university, Drexel, would have shown a 130% increase in publication productivity. Specifically, in 2002 Drexel faculty published 502 articles; in 2006 the number grew to 1165, according to data from Thompson Scientific Web of Science. Drexel's productivity has not only budged, but surged.

The decrease shown in the article for MCP Hahnemann University and Drexel University requires context. For starters, MCP and Drexel are one and the same university. When Drexel acquired the academic units of the bankrupt Allegheny University of the Health Sciences in 1998, it formed an exigent entity called MCP Hahnemann University, which by design was dissolved in 2002 and no longer exists.

The compelling reason why Drexel and MCP show a decline in faculty publications during 1992 to 2001 is because of the profound shift in attention, energy, and resources on the part of both faculties as they worked toward the common goal of integrating the nation's largest private medical school, a college of nursing and health professions, and a school of public health into a consolidated, fully integrated university. This formidable and unprecedented undertaking was a success, and research and publishing are now thriving at Drexel University.

Telling a story "by the numbers" alone can sometimes mean a tale half-told. Drexel and likely other universities accept NSF's challenge to step up productivity and are already meeting it.

**STEPHEN W. DIRECTOR**

Office of the Provost, Drexel University, Philadelphia, PA 19104, USA.

## Threats to Privacy Protection

W. W. LOWRANCE AND F. S. COLLINS RAISE excellent points in their Policy Forum "Identifiability in genomic research" (3 August, p. 600). Assuring privacy protections in both genomic research and medicine practice is of urgent concern.

A recent *Scientific American* article (*1*) describes how even deidentified data can be used to reidentify individuals, specifically when bits of information exist in public databases. The article recounts the work of Lantanya Sweeney, who runs the Data Privacy

Laboratory at Carnegie Mellon University. Her research found that reidentifying personal information is simpler than one might have imagined. In one case, a banker cross-referenced information in publicly available hospital discharge records against his client list to determine whether any of his clients had cancer. If they did, he called in their loans. In another case, Sweeney found a way to reidentify patients with Huntington disease even after all information about the patients had been deleted from their records. She combined known sequencing data indicating the presence of the disease with hospital discharge records, which included patients' ages, and succeeded in accurately linking 90% of the Huntington disease patients with DNA records on file.

Privacy involves more than the deidentification of personal information, as illustrated by the 2004 U.S. Appeals case *Northwestern Memorial Hospital vs. John Ashcroft*. The case centered on Ashcroft's attempt to subpoena roughly 45 Northwestern Memorial Hospital patient records for use in an upcoming trial in the Southern District of New York to challenge the constitutionality of the Partial-Birth Abortion Ban Act of 2003. Although patient records would have been anonymized prior to release, patients nonetheless protested against Ashcroft's access on grounds that anonymization did not fully protect their privacy. The hospital went to court to block Ashcroft, and the patients prevailed. The court determined that Northwestern Memorial Hospital was not required to comply with a subpoena from the Justice Department for abortion patients' medical records. Importantly, the court stated, "Even if there were no possibility that a patient's identity might be learned from a redacted medical record, there would be an invasion of privacy. If Northwestern Memorial Hospital cannot shield its abortion patients' records from disclosure in judicial proceedings, moreover, the hospital will lose the confidence of its patients, and persons with sensitive medical conditions may be inclined to turn elsewhere for medical treatment" (*2*).

**CAROL ISAACSON BARASH**

Genetics, Ethics, and Policy Consulting, Inc., Boston, MA 02130, USA. E-mail: cbarash@gepci.com

**References**

1. C. Walter, *Sci. Am.* **297**, 92 (July 2007).
2. *Northwestern Memorial Hospital vs. John Ashcroft*, 362 F.3d 923 (7th Cir. 2004); available at http://fl1.findlaw.com/news.findlaw.com/hdocs/docs/abortion/nwmhash40604opn.pdf.

## Potent Questions About India's Polio Vaccine

IN THEIR REPORT "NEW STRATEGIES FOR THE elimination of polio from India" (17 November 2006, p. 1150), N. Grassly *et al.* discuss the use of trivalent oral polio vaccine (OPV) in India for supplementary immunizations against type 1 poliovirus. During the past 5 years, OPV efficacy in relation to confirmed cases of type 1 paralytic poliovirus and number of doses (Grassly *et al.*'s Fig. 3) suggests that poor-quality vaccine lots are being dispensed during primary and supplementary immunization. The chances of any recipient receiving adequate immunization against three poliovirus serotypes depend on the quality of OPV available locally. Suboptimal immunizing doses or missed immunizations would lead to individuals who do not respond to multiple OPV doses.

Assays for the total viral content (*1*) of the vaccine dose are biased in favor of type 1 poliovirus. Potency assays on tri- or univalent lots retrieved from field usage would be more reliable than any cumulative thermal color changes observed by vaccine vial monitors. Vaccine vial monitors are just physical indicators of temperature. They do not indicate the period (duration) of exposure to such a temperature. Furthermore, they do not indicate the extent of exposure to sunlight and would not indicate the biological activity in the vaccine vial container (*2*). Inadvertent use of poor immunogenicity lots (*3*) and brutal handling of OPV aliquots (*4*) are widespread.

It is at least possible that the apparent absence of genetically divergent vaccine-derived polioviruses correlates with field usage of poor-quality OPV.

**SUBHASH C. ARYA AND NIRMALA AGARWAL**

Sant Parmanand Hospital, 18 Alipore Road, Delhi 110054, India. E-mail: subhashji@hotmail.com

**References**

1. World Health Organization Manual of laboratory methods for testing of potency of final vaccines used in the WHO Expanded Programme on Immunization (WHO BLG/95.1, Geneva, 1995).
2. VVM for all, Technical Session on Vaccine Vial Monitors (World Health Organization, Geneva, 2002) (downloaded on 23 November 2006 from www.childrensvaccine.org/files/Getting_started_with_VVMs.pdf).
3. S. A. Omilabu, A. O. Oyefolu, O. O. Ojo, R. A. Audu, *Afr. J. Med. Med. Sci.* **28**, 209 (1999).
4. N. K. Goel, H. M. Swami, S. P. Bhatia, *Ind. J. Public Health* **48**, 200 (2004).

### Response

ARYA AND AGARWAL ARE CONCERNED ABOUT the potency of trivalent oral polio vaccine (OPV) administered to children in India and the possibility of low potency contributing to low efficacy of this vaccine in Uttar Pradesh. This concern seems to flow from several misunderstandings about the testing, distribution, and use of OPV in India.

All OPV released for use in India is tested by the producer and, subsequently, by a national reference laboratory before release. All batches released in India are potent according to international standards. Titers of each individual Sabin virus and a total titer are evaluated. A specific, internationally agreed-

## CORRECTIONS AND CLARIFICATIONS

**News of the Week**: "Is battered Arctic Sea ice down for the count?" by R. A. Kerr (5 October, p. 33). The caption for the graphic should have noted more fully that the analysis rendered in the plot was different from the analysis discussed in the text. A particular year's sea ice area differed in the two analyses, but the long-running downward trend and the sharp decline in 2007 were the same.

## TECHNICAL COMMENT ABSTRACTS

### COMMENT ON "A G Protein–Coupled Receptor Is a Plasma Membrane Receptor for the Plant Hormone Abscisic Acid"

Christopher A. Johnston, Brenda R. Temple, Jin-Gui Chen, Yajun Gao, Etsuko N. Moriyama, Alan M. Jones, David P. Siderovski, Francis S. Willard

Liu *et al.* (Reports, 23 March 2007, p. 1712) reported that the *Arabidopsis thaliana* gene *GCR2* encodes a seven-transmembrane, G protein–coupled receptor for abscisic acid. We argue that GCR2 is not likely to be a transmembrane protein nor a G protein–coupled receptor. Instead, GCR2 is most likely a plant homolog of bacterial lanthionine synthetases.

Full text at www.sciencemag.org/cgi/content/full/318/5852/914c

### RESPONSE TO COMMENT ON "A G Protein–Coupled Receptor Is a Plasma Membrane Receptor for the Plant Hormone Abscisic Acid"

Xigang Liu, Yanling Yue, Wei Li, Ligeng Ma

Our study provided experimental evidence that GCR2 is a membrane-associated abscisic acid receptor that interacts with the G protein α subunit GPA1 in *Arabidopsis*. Although we cannot rule out GCR2 as a lanthionine synthetase homolog, our data indicate that it may define a new type of nonclassical G protein–coupled receptor.

Full text at www.sciencemag.org/cgi/content/full/318/5852/914d

upon benchmark titer is used to assess potency (for example, each dose must contain titers of Sabin serotype 1 virus that exceed $10^6$ tissue culture infective doses). Thus, the suggestion that assays used to assess potency are somehow biased and misleading is incorrect.

After testing, vaccine is distributed in a refrigerated "cold chain" throughout the country. Each vial of vaccine includes a vaccine vial monitor (VVM), which indicates cumulative heat exposure over time. The VVM is calibrated to alert the vaccinator when the vial has become exposed to enough heat over time to reduce potency to a level that would hinder the protective effect.

## Letters to the Editor

Letters (~300 words) discuss material published in *Science* in the previous 3 months or issues of general interest. They can be submitted through the Web (www.submit2science.org) or by regular mail (1200 New York Ave., NW, Washington, DC 20005, USA). Letters are not acknowledged upon receipt, nor are authors generally consulted before publication. Whether published in full or in part, letters are subject to editing for clarity and space.

(Arya and Agarwal incorrectly state that VVMs do not measure heat exposure over time.) Thus, although the VVM does not directly measure potency, it provides information about the main factor that affects potency. Vaccine vials whose VVMs indicate that they have not been maintained at the correct temperature are discarded. This system ensures that only potent oral polio vaccine is administered to children in India. Monitoring data shows only a very small minority of vaccine vials observed in the field indicate overexposure to heat (less than 1%) (*1*). In addition, a recent laboratory evaluation of monovalent and trivalent OPV retrieved from the field in Uttar Pradesh during the 2006 mass immunization campaigns demonstrated adequate potency in all vials with VVMs indicating potency [a sample of 345 vials from 69 districts (*2*)].

Arya and Agarwal cite an article about a Nigerian measles immunization program, which is of negligible relevance to a discussion of the Indian polio immunization program, and an article about the cold chain in Chandigarh, which, although in India, is an area that eliminated wild polio virus transmission years ago with the trivalent vaccine. Thus, neither of these references supports a serious concern about the cold chain capacity in India as a potential cause for reduced vaccine effectiveness.

Finally, the assertion that the absence of genetically divergent vaccine-derived polio virus (VDPV) is consistent with use of poor-quality vaccine is not true. The most important risk factor for development of circulating VDPV is low population immunity levels. If the vaccine was poorly immunogenic, low population immunity would result, and one would be likely to see more, not fewer, episodes of circulating VDPV.

**NICHOLAS C. GRASSLY,[1] JAY WENGER,[2] R. BRUCE AYLWARD[3]**

[1]Department of Infectious Disease Epidemiology, Imperial College London, Norfolk Place, London W2 1PG, UK. [2]National Polio Surveillance Project, World Health Organization, R. K. Khanna Tennis Stadium, Africa Avenue, Safdarjung Enclave, New Delhi, 110029, India. [3]Global Polio Eradication Initiative, World Health Organization, 20 Avenue Appia, CH 1211 Geneva 27, Switzerland.

### References

1. National Polio Surveillance Project, data available at www.npsuindia.org.
2. Ministry of Health and Family Welfare, Government of India, New Delhi; data available at www.npsuindia.org.

SOCIAL SCIENCES

# Arguing for Computational Power

**Daniel Diermeier**

Nearly every book on agent-based models (including *Generative Social Science*) features advanced praise on the dust cover that highlights the tremendous promise of agent-based modeling. Agent-based modeling, however, is now at least 35 years old—counting from the publication of Thomas Schelling's *Micromotives and Macrobehavior* (*1*)—and its impact on mainstream research in the three major social sciences (economics, sociology, and political science) has been limited in contrast to, say, that of game theory. Before the reader jumps to conclusions about conspiracies among scientific elites that rigidly hold on to existing views, it is worth keeping in mind that over the past 15 years, the supposed fortress of orthodoxy, theoretical economics, has been revolutionized at least twice: first by the introduction of evolutionary game theory and more recently by the birth of behavioral economics and neuroeconomics. Agent-based models have had no similar impact.

Joshua Epstein's book is a clear and highly illuminating response to this challenge. Much of *Generative Social Science* is not new. Indeed, most of the book is essentially an anthology of previous work by Epstein (an economist at the Brookings Institution) and his coauthors. It should be noted that having all these contributions in one place is not only useful but pleasing. It is a delight to reacquaint oneself with such gems as the work on the culture, population, and behavior of the Anasazi and the consideration of civil violence.

For the reader mainly interested in what is new in agent-based modeling, the first two chapters are by far the most interesting. Epstein's main argument is that agent-based models have been both misinterpreted and evaluated by the wrong standards. He contends that (i) contrary to common belief, agent-based models do satisfy our standards of scientific theories; (ii) according to many explanatory criteria, agent-based models outperform more traditional models given those explanatory standards; and (iii) they exemplify a different type of explanatory criteria appropriate for "generative social science." The generative standard is epitomized in the slogan "if you didn't grow it, you didn't explain it."

This generative approach, of course, is not new. It has predecessors in Chomskyan linguistics and even Thomas Hobbes's *Elements* (*2*). There is, however, some tension between arguments (i) and (ii), which presuppose a more traditional model of explanation, and argument (iii), which offers a rather different model of explanation. This is not just a philosophical exercise as, on closer inspection, much of Epstein's argument depends on whether we indeed accept generative explanations as somehow superior. The author, however, does not provide any reasons why a generative approach is superior.

To see some of the possible problems, consider the converse of the generativist claim: "If you grew it, you explained it." In the agent-based tradition, considerable emphasis is placed on the fact that "simple" rules lead to the "emergence" of "complex" behavior. Epstein provides a nice, somewhat tongue-in-cheek, discussion of the vagueness and ambiguity of emergence in the agent-based modeling community, but the generativist slogan rests itself on the importance of simple rules. Suppose, for example, that one provides a generative model of biological organisms using micro-rules that violate basic principles of physics. Would we consider this an explanation? I think not. (Moves toward pragmatist accounts of explanation should be resisted; they may let agent-based models off the hook, but they also absolve rational choice–based theories.) My sense is that many of the rules used in agent-based models have that feature. They are too simple to be plausible. This is particularly important in the economic context, where we can easily devise strategies that would be able to outperform the proposed rules.

**Generative Social Science**
Studies in Agent-Based Computational Modeling

***by Joshua M. Epstein***

Princeton University Press, Princeton, NJ, 2006. 378 pp. plus CD. $49.50, £29.95. ISBN 9780691125473. Princeton Studies in Complexity.

Dropping the fixation with a generativist approach and simple rules may offer some promising directions for agent-based modeling—for example in its relation to game theory, which plays the role of the ancien régime to Epstein's revolution. Epstein argues that the central solution concept in noncooperative game theory, Nash equilibrium, cannot provide an explanation of how equilibrium states can be attained. The focus on Nash equilibrium and its static properties, however, seems quite outdated. The issue of how players converge on equilibria has been the subject of an extremely active and influential research area, evolutionary game theory. This approach is not generative in the sense of Epstein, because the underlying rules are not simple. Rather,

CREDIT: GEORGE J. GUMERMAN/SANTA FE INSTITUTE

**Scene for simulations.** The Artificial Anasazi Project used archaeological data from Long House Valley, northeastern Arizona, to evaluate the results of an agent-based model of settlement patterns and demographic behavior on a landscape of annual variations in potential maize production.

The reviewer is at the Northwestern Institute on Complex Systems and the Kellogg School of Management, 2001 Sheridan Road, Leverone Hall 585, Northwestern University, Evanston, IL 60208–2009, USA. E-mail: d-diermeier@kellogg.northwestern.edu

they build on insights from psychology and incorporate learning, adaptation, and so forth.

Unfortunately, much of evolutionary game theory is solely concerned with foundational questions, e.g., how to characterize Nash equilibrium (or its refinements) in terms of adaptive mechanisms. Much less work has focused on using the proposed dynamic models directly to explain social phenomena. Given, on the one hand, the computational difficulties to doing that and, on the other hand, the rich modeling capabilities offered by agent-based models, there seems to be ample room for collaboration and convergence. Perhaps such efforts offer a more fruitful direction than the ongoing argument over which approach is right.

Epstein's book is a concise and well-articulated defense of agent-based modeling. *Generative Social Science* is essential reading for anyone seriously interested in the foundations and the practice of agent-based modeling. In my view it does not settle the questions, but stating them clearly and providing a clear and provocative argument is no minor achievement.

**References**

1. T. C. Schelling, *Micromotives and Macrobehavior* (Norton, New York, 1978).
2. T. Hobbes, *The Elements of Law Natural and Politic* (1640); www.efm.bris.ac.uk/het/hobbes/elelaw.

10.1126/science.1142510

EVOLUTION AND BEHAVIOR

# Simple Maths for a Perplexing World

**Daniel J. Rankin**

Charles Darwin famously remarked that those versed well in mathematics are endowed with something akin to an extra sense. In the past half century, mathematics has brought a great deal of insight into evolutionary biology, and perhaps for this reason hoards of mathematicians and physicists flock to biology to apply their insight. The depth and range of topics dealt with in Richard McElreath and Robert Boyd's *Mathematical Models of Social Evolution* keenly demonstrate how far that extra sense can bring us.

The reviewer is at the Department of Behavioural Ecology, Institute of Zoology, University of Bern, Wohlenstrasse 50a, CH-3032 Hinterkappelen, Switzerland. E-mail: daniel.rankin@esh.unibe.ch

The book begins with the analogy that mathematics is like Latin: everyone knows a few words, but very few people can understand a sentence. The analogy is a good one, as mathematics takes a back seat in most biology programs. McElreath and Boyd (anthropologists at, respectively, the University of California, Davis, and the University of California, Los Angeles) hope for nothing less than a reformation in evolutionary biology, and like Martin Luther (who translated the Bible from Latin into the vernacular), they succeed very well in conveying their ideas to the perplexed. Simply flicking through the book without reading the details is enough to panic anyone with even a slight phobia of equations: the book is packed with squiggles, little letters, and strange-looking symbols. Taking the plunge, however, reveals that the authors have explained each step of the chosen models as clearly as possible. These widely used models are elegant in their mathematical simplicity, and at times the prose reads like a bedtime story, prompting the reader to think "how simple!"

**Mathematical Models of Social Evolution**
A Guide for the Perplexed
*by Richard McElreath and Robert Boyd*
University of Chicago Press, Chicago, 2007.
428 pp. $62.50, £39.50.
ISBN 9780226558264.
Paper, $25, £16.
ISBN 9780226558271.

Each chapter is followed by a guide to the relevant literature, and a detailed appendix covers some of the most useful techniques in mathematical biology. Classic topics such as animal conflict, sex allocation, and dispersal are discussed. Disappointingly, the authors neglect a few well-used approaches, including simulations (which they dismiss from the start), standard optimization theory, and dynamic programming. Those interested in such tools will find Hanna Kokko's recent book (*1*) helpful.

Much of the mathematical theory of social evolution theory stems from the work of W. D. Hamilton, and his results feature prominently in the book. The two chapters devoted to cooperation and reciprocity introduce both game theoretical and inclusive fitness techniques for approaching these problems. These chapters offer a comprehensive introduction to what increasingly seems a mammoth field on its own; clearly, the tool box that the authors use in their day-to-day research is immense. Hamilton (*2*) noted that altruistic behaviors could evolve if the cost ($c$) that an altruist paid was less than the benefit of the recipient, weighted by the relatedness coefficient ($r$): $c < rb$, known as Hamilton's rule. One long-standing issue in the field of social evolution concerns what role group selection (where an individual's fitness depends on the success of the group) plays in the evolution of altruism—a question recently addressed in (*3*, *4*). In their chapter on selection among groups, the authors use an elegant model to show that both kin selection and group selection approaches to altruism yield Hamilton's rule. As they remark: "There is only one world out there. It would be bad if changing the way we did the accounting of genes changed the answer."

One of the most interesting topics McElreath and Boyd cover is social learning (learning from observing and copying others). Many animals have the ability to copy each other; thus, behaviors can be transmitted by learning from other animals as well as by genes. In the introductory chapter, the authors discuss a simple model that allows one to calculate the frequency of copied behaviors when animals estimate payoffs to others in deciding whether to imitate another individual and which behavior to copy. In their chapter on animal communication, the authors consider such cultural inheritance in a fictitious species that inhabits a changing environment. Using a model of gene-culture coevolution (which allows both genes and culturally inherited traits to evolve), they then examine the conditions under which social learning can evolve. They show that for more predictable environments, social learning is favored over individual learning (learning purely from one's own experience). The field of cultural evolution is still fertile ground, and the ideas presented in the authors' discussion of social learning will spur many a biologist to think more about the role of cultural transmission in evolutionary change.

*Mathematical Models of Social Evolution* will no doubt reward psychologists, sociologists, and economists interested in evolutionary theory. Anyone desiring a thorough, yet down-to-Earth, introduction to modeling in social evolution couldn't do much better than to read this book. Using little more than high school mathematics, McElreath and Boyd show how one can take a big step toward understanding many perplexing evolutionary processes.

**References**

1. H. Kokko, *Modelling for Field Biologists and Other Interesting People* (Cambridge Univ. Press, Cambridge, 2007).
2. W. D. Hamilton, *J. Theor. Biol.* **7**, 1 (1964).
3. K. R. Foster, T. Wenseleers, F. L. W. Ratnieks, *Trends Ecol. Evol.* **21**, 57 (2006).
4. L. Lehmann, L. Keller, S. West, D. Roze, *Proc. Natl. Acad. Sci. U.S.A.* **104**, 6736 (2007).

10.1126/science.1150194

ENVIRONMENTAL SCIENCE

# Rethinking Desalinated Water Quality and Agriculture

Damage to crops after irrigation with extremely pure water from the world's largest reverse-osmosis desalination plant reveals a need for revised treatment standards.

U. Yermiyahu,[1] A. Tal,[2]* A. Ben-Gal,[1] A. Bar-Tal,[3] J. Tarchitzky,[4] O. Lahav[5]

With almost half of humanity suffering insufficient access to potable water (*1*) and water scarcity for agriculture considered to be a global crisis (*2*), seawater desalination has emerged as a feasible solution. Between 1994 and 2004, world desalination capacity increased from 17.3 to 35.6 million $m^3$/day (*3*). At present, seawater desalination provides 1% of the world's drinking water (*4*).

Desalinized water is increasingly considered a source of water for agriculture as well. With 69% of the global water supply going to irrigation (*5*), present freshwater resources may soon be insufficient to meet the growing demand for food. A recent report (*6*) concludes that, although the costs of desalination remain prohibitively expensive for full use by irrigated agriculture, for high-value cash crops like greenhouse vegetables and flowers, its use may be economically feasible.

In a few countries, desalinized brackish water (whose price is typically a third of desalinated seawater) is already widely used by farmers. For instance, ~22% of water desalinated in Spain goes to agricultural irrigation (*6*). An Australian survey found that 53% of the population envisioned desalinated water usage for irrigation of vegetables as highly likely (*7*). In Israel, the promise of new, profitable crop options has inspired farmers to request allocations of relatively higher priced desalinized waters.

In December 2005, a new seawater desalination plant was opened in Ashkelon, on Israel's southern Mediterranean coast. Its 100,000,000 $m^3$/year production makes it the largest reverse-osmosis (RO) desalination facility presently in operation worldwide (*8*). It is also the world's first desalination facility to produce potable water from seawater at a price below \$0.55/$m^3$ (*9*). Although the Ashkelon facility was designed to provide water for human consumption, because of relatively modest population densities in southern Israel, a substantial percentage of the desalinated seawater was delivered to farmers. Recent evaluation of the effect of the plant's desalinized water on agriculture, however, produced some surprising, negative results. Changing these outcomes will require modifying future water management orientation and revision of desalination standards.

**WATER-QUALITY PARAMETERS AFTER DESALINATION**

| Parameter | Water from Ashkelon desalination plant | Recommendation for domestic and agricultural usage |
|---|---|---|
| EC (dS/m) | 0.2–0.3 | <0.3 |
| [$Cl^-$] (mg/liter) | 15–20 | <20 |
| [$Na^+$] (mg/liter) | 9–10 | <20 |
| [$Ca^{2+}$] (mg/liter) | 40–46 | 32–48* |
| [$Mg^{2+}$] (mg/liter) | 0 | 12–18 |
| [$SO_4^{2-}$-S] (mg/liter) | 20–25 | >30 |
| [B] (mg/liter) | 0.2–0.3 | 0.2–0.3 |
| Alkalinity (mg/liter as $CaCO_3$) | 48–52 | >80* |
| CCPP (mg/liter as $CaCO_3$) | 0.7–1.0 | 3–10* |
| pH | 8.0–8.2 | <8.5* |

**Value based on the new Israeli recommendations for desalinated water.*

### Effects of Desalinization

When farmers receive desalinized water, the lowered salinity is perceived as a bonus, because the salts (especially $Na^+$ and $Cl^-$) damage soils, stunt plant growth, and harm the environment. Salinity in water is measured by its electrical conductivity (EC). The EC of water produced at the Ashkelon desalination plant is 0.2 to 0.3 dS/m, replacing water from a national distribution system with an EC higher by a factor of three to five.

Boron (B) concentration in seawater averages 4.5 mg/liter and is slightly higher in the Mediterranean Sea. At these concentrations, B does not constitute a threat to human health (*10*) but is highly toxic to many crops (*11*). Boron in neutral and acidic environments readily passes through the RO membranes. Without additional treatment, B in Mediterranean seawater after RO will reach 2 mg/liter, which is toxic for all but the most tolerant crops (*11*). Toxicity symptoms in orchards were observed after irrigation with effluent originating from desalinated municipal water in Eilat with ~1.2 mg/liter B produced. Concentrations of 2 mg/liter B in irrigation water also caused reductions in yields in peanuts and tomatoes in the Negev region (*12*, *13*).

Desalination not only separates the undesirable salts from the water, but also removes ions that are essential to plant growth. Desalinized water typically replaces irrigation water that previously provided basic nutrients like calcium ($Ca^{2+}$), magnesium ($Mg^{2+}$), and sulfate ($SO_4^{2-}$) at levels sufficient to preclude additional fertilization of these elements.

Although water from Israel's national water carrier typically contains dissolved $Mg^{2+}$ levels of 20 to 25 mg/liter, water from the Ashkelon plant has no $Mg^{2+}$. After farmers used this water, $Mg^{2+}$ deficiency symptoms appeared in crops, including tomatoes, basil, and flowers, and had to be remedied by fertilization. Current Israeli drinking water standards set a minimum $Ca^{2+}$ level of 20 mg/liter. The postdesalination treatment in the Ashkelon plant uses sulfuric acid to dissolve calcite (limestone), resulting in $Ca^{2+}$ concentration of 40 to 46 mg/liter. This is still lower

[1]Agricultural Research Organization, Gilat Research Center, Mobile Post Negev 2, 85280 Israel. [2]Mitrani Department of Desert Ecology, Blaustein Institutes of Desert Research, Ben-Gurion University of the Negev, Sede Boqer Campus, 84990 Israel. [3]Institute of Soil, Water, and Environmental Sciences, Agricultural Research Organization, The Volcani Center, Post Office Box 6, Bet Dagan, 50250 Israel. [4]Extension Service, Ministry of Agriculture, Post Office Box 25, Bet Dagan, 50250, Israel. [5]Faculty of Civil and Environmental Engineering, Technion, Haifa, 32000 Israel.

*Author for correspondence: E-mail alontal@bgu.ac.il

than the 45 to 60 mg/liter found in typical Israeli freshwaters. Other posttreatment processes, such as dissolving $CaCO_3$ with gaseous $CO_2$, planned in future local desalination plants, will produce a $Ca^{2+}$ concentration of 32 mg/liter. Calcium is not just a nutrient required by plants; its interactions with other nutrients and with growth-limiting factors, including plant disease agents, makes changes in its content and relative concentration particularly problematic (*14*, *15*).

During the desalination process, $SO_4^{2-}$ is removed completely. In the Ashkelon plant, sulfur is added coincidental to the use of sulfuric acid for dissolving calcite in the posttreatment stage. Ultimately, $SO_4^{2-}$ concentrations settle at 20 to 25 mg S/liter, similar to freshwater levels. However, sulfur deficiency could emerge as a problem in other systems where alternative methods for $Ca^{2+}$ enrichment are practiced. In intensive horticulture, the average recommended $SO_4^{2-}$ concentration in irrigation water is 58 mg S/liter, whereas the minimum concentration recommended for tomatoes is much higher: 141 mg S/liter (*16*).

Desalinated irrigation water in Israel is often blended with other water sources. As a result, the quality of the final water actually delivered to farmers is unreliable. RO water is low in dissolved substances, with little buffering capacity relative to that of freshwater. Low buffering capacity increases risks of corrosion to metal distribution pipes. It also can have a profound impact on pH (and agricultural productivity) when the water is mixed with other sources.

## Economic Factors

The cost of desalinating 1 $m^3$ of seawater at the Ashkelon plant was $0.55 in 2006; in smaller facilities, the cost using the same technology could reach $1/$m^3$. This cost includes B removal and addition of $SO_4^{2-}$, $Ca^{2+}$, and alkalinity by means of a calcite-dissolution posttreatment process. Additional enrichment of the desalinated water with $Mg^{2+}$ would raise the price further.

According to new recommendations for desalinated water in Israel (*17*), dissolved $Ca^{2+}$ concentrations should not be increased beyond 48 mg/liter. This $Ca^{2+}$ ceiling is based on economic considerations, to minimize problems related to excess hardness for users in the industrial and municipal sectors. Although magnesium is not included in local water-quality criteria, it is welcome in desalinated water not only for agricultural but also human health objectives: The World Health Organization (WHO) recommends maintaining levels of about 20 to 30 mg/liter $Ca^{2+}$ and 10 mg/liter $Mg^{2+}$ in drinking water (*18*).

To meet agricultural needs, missing nutrients might be added to desalinized water in the form of fertilizers. Supplying $Ca^{2+}$ and $Mg^{2+}$ at 24 and 12 mg/liter, respectively, costs ~$0.09/$m^3$. Direct chemical dosage at the desalination plant to increase $Mg^{2+}$ is also a relatively expensive alternative (adding ~$0.045/$m^3$ to the overall posttreatment cost when 10 mg/liter $Mg^{2+}$ is supplied as $MgCl_2$). It also results in addition of unwanted counter anions. Dissolving dolomite rock [$CaMg(CO_3)_2$] to meet $Ca^{2+}$, $Mg^{2+}$, and alkalinity criteria would only cost between $0.01 and $0.02/$m^3$ above the cost of existing calcite dissolution (*17*). Yet there are several potential problems associated with dissolved dolomite rock, most notably the relatively slow dissolution kinetics. An alternative process, where excess $Ca^{2+}$ ions (generated in the common $H_2SO_4$-based calcite dissolution posttreatment process) are replaced with $Mg^{2+}$ ions originating from seawater (extracted using specific ion-exchange resins) has been suggested. This alternative will balance $SO_4^{2-}$, $Ca^{2+}$, $Mg^{2+}$, alkalinity, and pH composition in desalinated water at a cost-effective price (*19*).

If the minerals required for agriculture are not added at the desalination plant, farmers will need sophisticated, independent control systems in order to cope with the variable water quality. Such systems can involve farm-scale water storage facilities, water-quality monitoring equipment, and fertilizer-pumping facilities capable of reacting to input water quality. The on-farm capital costs of such equipment are likely to reach $10,000 per agricultural unit, and associated operational costs will add additional expenses to the equation.

## Conclusions

If desalinized water was destined for agricultural use alone, simple blending strategies would be the most probable economical strategy, providing stable and high water quality. Yet, in more typical cases, where water supplies both municipal and agricultural uses, economic efficiency requires a balancing of treatment costs, drinking-water quality, and agricultural benefits. On the basis of recent Israeli experience, we recommend expanding water-quality parameters in desalination facilities that may supply water to farmers (see table, p. 920). The proposed standards are based on lessons learned during the initial operation of the Ashkelon plant and water quality guidelines that were subsequently recommended (*20*), as well as the actual agronomic consequences for local farmers discussed above (*14*, *15*). The standards are relevant for dry land regions but will probably not be cost-effective for areas where agriculture does not rely heavily on irrigation.

These expanded criteria neither contradict nor compromise the quality of the water for human consumption as defined by WHO standards (*21*). On the contrary, increased buffering capacity and higher $Ca^{2+}$ and $Mg^{2+}$ concentrations make the water more chemically and biologically stable and provide a higher amount of essential elements, which contribute to public health. Desalination facilities built today will be in place for decades, making planning now essential for long-term increased economic prosperity and agricultural productivity.

### References and Notes


1. P. H. Gleick, *The World's Water 2002–2003: The Biennial Report on Freshwater Resources* (Island Press, Washington, DC, 2002).
2. S. Postel, *Pillar of Sand: Can the Irrigation Miracle Last?* (World Watch, Washington, DC, 1999).
3. International Desalination Association (IDA), Worldwide Desalting Inventory (IDA Report no. 18, Wangnick Consulting, Gnarrenburg, Germany, 2004); www.wangnick.com.
4. European Commission, Environmental Technologies Action Plan, "Water desalination market acceleration" (EC, Brussels, 2006); http://ec.europa.eu/environment/etap/pdfs/watedesalination.pdf.
5. G. Meerganz von Medeazza, *Desalination* **169**, 287 (2004).
6. J. Martinez Beltran, S. Koo-Oshima, Eds., *Water Desalination for Agricultural Applications* (FAO, Rome, 2006).
7. S. Dolnicar, A. I. Schafer, presentation at the Proceedings of the AWWA (American Waste Water Association) Desalination Symposium, Honolulu, 7 to 9 May 2006; available at http://ro.uow.edu.au/commpapers/138 (2006).
8. A. Tal, *Science* **313**, 1081 (2006).
9. R. F. Service, *Science* **313**, 1088 (2006).
10. F. J. Murray, *Regul. Toxicol. Pharmacol.* **22**, 221 (1995).
11. R. O. Nable, G. S. Bañuelos, J. G. Paull, *Plant Soil* **193**, 181 (1997).
12. A. Ben-Gal, U. Shani, *Plant Soil* **247**, 211 (2002).
13. U. Yermiyahu, J. Zilberman, A. Ben-Gal, R. Keren, paper presented at the World Congress of Soil Science, Philadelphia, PA, 10 to 15 July 2006.
14. U. Yermiyahu *et al.*, "Irrigation of crops with desalinated water" [in Hebrew] (Report submitted to Chief Scientist, Israel Ministry of Agriculture and Rural Development, Tel-Aviv, Israel, 2007), 15 pp.
15. U. Yermiyahu, I. Shamai, R. Peleg, N. Dudai, D. Shtienberg, *Plant Pathol.* **55**, 544 (2006).
16. C. de Kreij, C. Sonneveld, M. G. Warmenhovn, N. Straver, *Guide Values for Nutrient Element Contents of Vegetables and Flowers Under Glass* (Naaldwijk, Aalsmeer, 3rd ed., Netherlands, 1992).
17. Joint Committee appointed by Israel Ministry of Agriculture and Rural Development and Israel Water Authority, "Quality of Desalinated Water for Agriculture" [Final report, in Hebrew] (Israel Government, Tel-Aviv, Israel, October 2007).
18. WHO, *Nutrients in Drinking Water* (Water Sanitation and Health Protection and the Human Environment, WHO, Geneva, 2005).
19. L. Birnhack, O. Lahav, *Water Res.* **41**, 3989 (2007).
20. O. Lahav, L. Birnhack, *Desalination* **207**, 286 (2007).
21. WHO, *Guidelines for Drinking-Water Quality* (WHO, Geneva, 3rd ed., 2004), chap. 12, annex 4.


10.1126/science.1146339

ASTRONOMY

# Mixing a Stellar Cocktail

Waves similar to those observed in Earth's atmosphere may strongly influence the internal structure of the Sun and other stars.

Corinne Charbonnel and Suzanne Talon

To simulate a star on a computer, you need equations describing the behavior of gases under the action of gravity. You must include nuclear reactions that release energy and produce elements beyond hydrogen. Furthermore, you have to describe how energy is carried through the star, either by photons, electrons, or moving matter. Finally, you must spin your star to shape the internal rotation as well as the internal distribution of chemical elements. You can then watch your theoretical star evolve and see that the model reproduces the main observational features of real stars, such as overall temperature and luminosity. However, your model will not pass all the tests. In particular, you won't predict that the interior of the Sun, the star we are most familiar with, is rotating slowly (*1*, *2*), nor will you properly describe the surface composition of Sun-like stars. What went wrong?

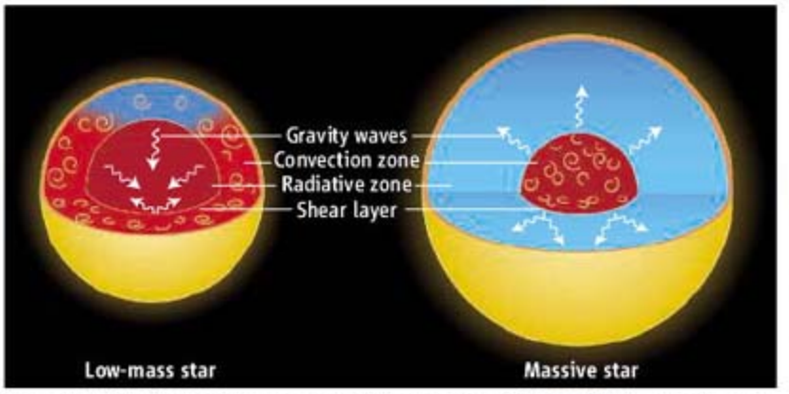


**Stirred and shaken**. Schematic view of the interior of the Sun (**left**) and of a massive star (**right**), where areas with small eddies indicate convective regions where energy is transported by large-scale motion. In radiative regions, energy is transported by photons. Red indicates fast rotation and blue indicates slow rotation. The Sun hosts a convective envelope that generates internal gravity waves traveling inward (arrows). In more massive stars hosting a convective core, gravity waves travel outward. In both cases, there is a shear layer oscillation at the frontier between the radiative and convective regions.

The most serious problem is that the models are missing a process to rigidify the internal rotation of the star and reduce the internal turbulent mixing from hydrodynamic instabilities. To better understand these effects, astrophysicists have been seeking inspiration from a new source: terrestrial atmosphere physicists. In the 1960s, atmospheric scientists were intrigued by a quasibiennial oscillation in the stratospheric wind velocity above Earth's equator. Lindzen and Holten (*3*) showed that it is caused by wave-induced momentum transport. It turns out that exactly this mechanism may be relevant to processes inside stars.

The main waves responsible for this oscillation are the so-called internal gravity waves. These waves are present in stratified media such as Earth's atmosphere, where they are excited by the turbulence of nearby regions. Such waves are an important part of several other phenomena in our atmosphere. (They are responsible, for example, for the clear-air turbulence that is feared by plane passengers and for stratospheric sudden warming caused by the dissipation of planetary waves.) Their crucial characteristic is that they produce momentum transport that cannot be modeled as a diffusive process (*4*).

In stars, the interesting property of gravity waves is that they pump angular momentum from the region where they are excited and dump it where they are damped. The nonlocal nature of this transport makes it a very efficient process to shape the internal rotation of gaseous bodies. Gravity waves are excited inside convective regions (see the figure). They travel and are damped in the radiative region over distances that depend on their wavelength and frequency. These waves can be retrograde or prograde—that is, they travel either against or with stellar rotation; the same waves also propagate radially, from the convection zone border into the radiative zone. Differential rotation induces a Doppler shift in the wave frequencies that is different for prograde and retrograde waves that convey positive and negative angular momentum respectively. The result is a local oscillating shear similar to the atmospheric quasi-biennial oscillation. This local shear then acts as a filter: small wavelength waves are all damped there, while the large wavelength waves that transport angular momentum such as to reduce differential rotation between the radiative and the convective region are favored.

The impact of gravity waves has been extensively studied in the case of the Sun, in which the convective region extends over the outer 30% in radius. The wave-induced oscillation occurs just below, at the boundary with the radiative zone, over about 2% in radius (see the figure), with a period on the order of a decade (*5*). As in all low-mass stars, the rotation of the Sun's convection zone has slowed down during its infancy. Thus, the core happened to rotate much faster than the surface. This favored retrograde waves, which caused the core of the young Sun to spin down on a time scale of a few hundred million years. In this framework, a smooth rotation profile is expected in the present Sun, consistent with helioseismological observations. Hence, the Sun has weaker hydrodynamic instabilities that lead to a surface chemical composition in agreement with spectroscopic measurements (*6*).

But how far can we trust this model? Thanks to terrestrial atmospheric physics, we understand the general properties of gravity waves, such as phase and group velocities and damping. What is still uncertain is the efficiency of wave generation by turbulent convection. To this day, stellar modelers rely on rather crude prescriptions for convection. Consequently, the spectrum of the waves excited by convective motions in stars remains elusive. To refine our knowledge of wave excitation, we await the outcome of three-dimensional simulations of convection that reproduce stellar conditions. We are not in total darkness, however, because the one-dimensional prescriptions we use reproduce the power spectrum of the solar pressure waves seen in helioseismology (*7*). In addition, the secular evolution of the interior rotation rate is not strongly dependent on the detailed wave spectrum or on the exact input rate of energy in the waves.

What about other stars? The structure and

C. Charbonnel is at the Geneva Observatory, University of Geneva, 1290 Sauverny, Switzerland, and the Laboratoire d'Astrophysique de Toulouse et Tarbes, Centre National de la Recherche Scientifique, Université Paul Sabatier Toulouse 3, 31400 Toulouse, France; S. Talon is in the Département de Physique, Université de Montréal, Montréal PQ H3C 3J7, Canada; E-mail: Corinne.Charbonnel@obs.unige.ch; talon@astro.umontreal.ca

position of convection zones vary with stellar mass and age. As a result, gravity waves are expected to alter stellar properties differently depending on the star we look at. For stars more massive than the Sun that host a convective core (see the right panel of the figure), gravity waves travel toward the surface, where they probably cause strong shears and keep the chemical composition homogeneous over a broad region (*8*). However, the influence of waves on the overall rotation and on the ultimate fate of such objects remains to be investigated. Another promising avenue is the study of evolved stars that develop convective envelopes as thick as 95% of the stellar radius. The associated gravity waves might counteract the acceleration of the contracting core toward the end of the star's life. By creating an oscillating shear deep inside the star, the waves may also modify nuclear burning in the late stages of evolution. This could help solve long-standing puzzles about the chemical patterns observed in stars at the end of their lives.

Step by step, gravity waves are gaining credibility among stellar physicists. First invoked in the synchronization of binary stars (*9*, *10*), they were soon suspected to transport particles (*11*–*15*). A major breakthrough was made 10 years ago when the impact of waves on angular momentum was demonstrated (*16*, *17*), providing a beautiful solution to the problem of the solar internal rotation (*6*). We are now in a new era in which gravity waves are becoming a key ingredient of modern stellar models.

**References and Notes**


1. W. J. Chaplin *et al.*, *Mon. Not. R. Astron. Soc.* **308**, 45 (1999).
2. S. Couvidat *et al.*, *Astrophys. J.* **597**, L77 (2003).
3. R. S. Lindzen, J. R. Holten, *J. Atmos. Sci.* **25**, 1095 (1968).
4. T. G. Shepherd, *J. Atmos. Solar-Terrestrial Phys.* **62**, 1587 (2000).
5. P. Kumar, S. Talon, J.-P. Zahn, *Astrophys. J.* **520**, 859 (1999).
6. C. Charbonnel, S. Talon, *Science* **309**, 2189 (2005)
7. P. Goldreich, N. Murray, P. Kumar, *Astrophys. J.* **424**, 466 (1994).
8. F. P. Pantillon, S. Talon, C. Charbonnel, *Astron. Astrophys.* **474**, 155 (2007).
9. J.-P. Zahn, *Astron. Astrophys.* **41**, 329 (1975).
10. P. Goldreich, P. D. Nicholson, *Astrophys. J.* **342**, 1079 (1989).
11. W. H. Press, *Astrophys. J.* **245**, 286 (1981).
12. E. Schatzman, *Astron. Astrophys.* **279**, 431 (1993).
13. J. Montalbán, *Astron. Astrophys.* **281**, 421 (1994).
14. R. J. García López, H. C. Spruit, *Astrophys. J.* **377**, 268 (1991).
15. P. A. Young, K. A. Knierman, J. R. Rigby, D. Arnett, *Astrophys. J.* **595**, 1114 (2003).
16. P. Kumar, E. Quataert, *Astrophys. J.* **475**, L143 (1997).
17. J.-P. Zahn, S. Talon, J. Matias, *Astron. Astrophys.* **322**, 320 (1997).



18. We acknowledge the financial support of the Programme National de Physique Stellaire (PNPS) of CNRS/INSU, France, and of the Swiss National Science Foundation (FNS).

10.1126/science.1148251


MATERIALS SCIENCE

# How Does Radiation Damage Materials?

Two experimental studies shed light on the dynamic behavior of the defects created by radiation damage in materials.


**Brian D. Wirth**


The often dramatic effects of particle irradiation on the properties of materials have been recognized and studied for over 60 years (*1*). These effects can be detrimental (as in structural materials degradation in nuclear reactors) or beneficial (as in the ion beam processing of semiconductors for the microelectronics industry). However, the microscopic processes that underlie these effects are not entirely understood, limiting researchers' ability to predict the consequences of irradiation. The reports by Arakawa *et al.* (*2*) and Matsukawa *et al.* (*3*) in this issue highlight the limits of knowledge about nanometer-sized dislocation loops in materials. The results should stimulate additional research to better understand these phenomena and to use the unique diffusion behavior to pattern materials at the nanoscale.

Atomic-scale computer simulations are now routinely used to study the radiation-induced formation of "Frenkel pairs" (in which an atom or ion leaves its place in the lattice, leaving a vacancy, and lodges nearby in the crystal, becoming an interstitial) and the behavior of clusters of these defects. Frenkel pair formation occurs in displacement cascades, involving a chain of atomic collisions after a high-energy particle collides with a lattice atom. Molecular-dynamics (MD) simulations can study radiation damage cascades produced by high-energy (> 20 keV) collisions as well as the structures and dynamics of defect clusters containing hundreds of vacancies or interstitials (*4*–*6*). These studies reveal that both interstitial and vacancy clusters, containing 20 or more point defects, directly form in the displacement cascades.

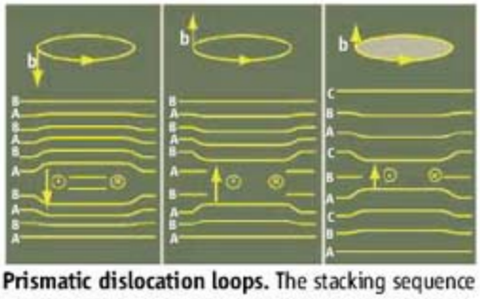


**Prismatic dislocation loops.** The stacking sequence of crystalline planes demonstrating prismatic dislocation loops formed from the clustering of the disc-shaped platelets of **(left)** two layers of interstitials, **(middle)** two layers of vacancies, and **(right)** a single vacancy layer. In a prismatic loop, the Burger's vector, which indicates the atomic displacement of the lattice, is perpendicular to the line direction of the loop periphery. The dislocation loops denoted in the left and middle panels have a perfect Burger's vector, which maintains the ABAB stacking sequence through the loop. The dislocation loop in the right panel has a faulted Burger's vector; thus, the ABCABC stacking sequence is disrupted by the loop.

The interstitial, as well as vacancy, clusters can form prismatic dislocation loops (see the figure). In both body-centered cubic (BCC) and face-centered cubic (FCC) materials, the prismatic interstitial-type loops have a perfect Burger's vector, whereas prismatic vacancy-type loops in FCC materials can be perfect or faulted. Vacancy cluster behavior is further complicated because loop, as well as void or stacking fault tetrahedra configurations are possible. The types of vacancy clusters formed during irradiation depend on the relative formation energies, which are known, and the kinetics of vacancy cluster evolutions, which are not fully understood.

MD studies of prismatic dislocation loops show that interstitial loops can diffuse along the direction of the Burger's vector without an applied stress (thermally-induced diffusion) (*5*–*7*). The loop diffusion is one-dimensional along the Burger's vector and is characterized by a standard Arrhenius diffusivity. Loops in BCC metals, like iron, containing as many as


The author is in the Nuclear Engineering Department, University of California at Berkeley, Berkeley, CA 94720, USA. E-mail: bdwirth@nuc.berkeley.edu

100 interstitials diffuse with a low activation energy and a pre-exponential factor that decreases with increasing loop size. Similar diffusion behavior occurs in FCC metals like copper, although loop diffusivity decreases for loops containing more than about 50 interstitials because the perfect dislocation separates into partial dislocations bounding a stacking fault. Few simulations of perfect vacancy loops have been performed, because they are not believed as mobile as interstitial loops.

Molecular dynamics simulations of interstitial loops containing more than a few hundred interstitials have not been performed. This is because loop migration is expected to decrease to zero as the loop size approaches that of dislocation lines observed in unirradiated materials. Such "conventional" dislocations, in the form of lines rather than loops, do not move without an applied stress. However, the size at which thermal diffusivity ceases is not well known. In the larger size limit, it is well known that the motion of dislocations in response to an applied stress controls the mechanical behavior of metals. In fact, the serrated or saw-toothed stress-strain response of BCC metals in tension tests is explained by the interaction of dislocations with nearby impurity atoms like carbon and nitrogen. The impurity atoms surrounding a dislocation are termed a "Cottrell atmosphere" (*8*), and the repeated motion of the dislocation away from the atmosphere, followed by diffusion of the impurities to, the dislocation, explains the observed stress-strain behavior.

On page 956 of this issue, Arakawa *et al.* (*2*) show that interstitial-type dislocation loops with sizes between 6 and 20 nm undergo thermally induced one-dimensional diffusion in BCC iron with a constant 1.3 eV activation barrier, independent of loop size. The authors propose that the loop diffusivity is controlled by the interaction with interstitial impurity atoms akin to the Cottrell atmospheres.

In some sense, these results agree with current knowledge, namely one-dimensional diffusion of dislocation loops controlled by the collective motion of dislocations and impurity atoms. However, these loops are larger than observed in MD simulations and yet quite small compared with conventional dislocations. Additionally, the activation energies and pre-exponential factors of loop diffusivity are larger than in MD simulations, and it is unclear whether the thermal diffusion of dislocation loops and impurities occurs by the same mechanism as the stress-driven coupled diffusion of a Cottrell atmosphere.

On page 959 of this issue, Matsukawa and Zinkle (*3*) demonstrate that prismatic vacancy-type dislocation loops with sizes between 2 and 3.4 nm undergo thermally induced one-dimensional diffusion in gold. The authors did not quantify the loop diffusivity, but estimate an activation energy of ~0.22 eV. The observation confounds the perception of low diffusivity and requires new knowledge to determine the diffusion mechanism. Additionally, and perhaps more surprising, the authors observe direct transformation of a perfect, prismatic loop into a stacking fault tetrahedron. Such a transformation, and the mechanism by which it occurs, have received limited study.

Taken together, these results expand the knowledge of dislocation loop behavior, and raise new questions about the size dependence of loop diffusion, the mechanisms controlling loop and impurity interactions, as well as possible transformation mechanisms between defect cluster configurations. This will motivate additional theoretical, computational, and experimental investigations. Yet, in this age of nanomaterials, where manipulation of the arrangement and ordering of materials across nanometer length scales is becoming routine, the articles should also stimulate innovative strategies to pattern, or self-organize, defects and solute structures as a result of one-dimensional diffusion, leading to tunable material properties.


**References**

1. E. P. Wigner, *Report for Month Ending December 15, 1942, Physics Division* (U.S. Atomic Energy Commision Report CP-387, Univ. of Chicago, Chicago, 1942).
2. K. Arakawa *et al.*, *Science* **318**, 956 (2007).
3. Y. Matsukawa, S. J. Zinkle, *Science* **318**, 959 (2007).
4. D. J. Bacon *et al.*, *J. Nucl. Mat.* **323**, 152 (2003).
5. N. Soneda, T. Diaz de la Rubia, *Philos. Mag. A* **81**, 331 (2001).
6. Y. Osetsky *et al.*, *J. Nucl. Mat.* **307**, 852 (2002).
7. J. Marian *et al.*, *Phys. Rev. B* **65**, 144102 (2002).
8. A. H. Cottrell, B. Bilby, 1949, *Proc. Phys. Soc. London A* **62**, 49 (1949).


10.1126/science.1150394

CHEMISTRY

# Enhancing Colloids Through the Surface

**Erik C. Nelson and Paul V. Braun**

Advances in colloidal surface chemistry are enabling new shapes, structures, and methods of assembly, as well as new routes to high-performance devices.

Colloidal particles are used in many consumer and industrial products, from cosmetics and pharmaceuticals to adhesives and paints. In these applications, the colloidal particles are usually spherical and have homogeneous surfaces. If their assembly could be influenced by manipulating the surface chemistry of the particles, new opportunities for colloidal materials could emerge. For example, proposed photonic applications—as chemical sensors, optical filters, or interconnects—could be realized if colloidal crystals could be assembled into new symmetries with large, defect-tolerant photonic band gaps. Surface-modified colloids and colloidal crystals may also be used in biological, microelectronic, and catalytic applications.

In a traditional colloidal system, the colloid surface is coated with charged moieties, which stabilize the colloids in solution. Upon drying, a close-packed colloidal crystal up to hundreds of layers thick with varying defect densities may form. Most colloidal systems pack into a face-centered cubic structure, but oppositely charged colloids can form ionic crystals (*1*). To create even more complex structures, the colloidal particles must exhibit directional interactions. This can potentially be achieved by chemically modifying specific regions of the colloid surface.

Systems with chemical anisotropy have great promise for forming new structures with otherwise unattainable properties (*2*). Theoretical studies by Zhang *et al.* indicate that colloids with four attractive patches on the colloid surface that form the corners of a tetrahedron can self-assemble from a disordered state into a crystal with diamond symmetry (see the first figure) (*3*). This structure is of great interest for photonic applications because of the large photonic band gap it has been proposed to possess. This structure has yet to be realized through self-assembly, but recent experimental advances in synthesizing and assembling colloids with chemically distinct patches may soon make this goal achievable.

For example, it is now possible to synthe-

The authors are in the Department of Materials Science and Engineering, Beckman Institute and Frederick Seitz Materials Research Laboratory, University of Illinois at Urbana-Champaign, Urbana, IL 61801, USA. E-mail: pbraun@uiuc.edu

size "Janus" particles with chemically distinct hemispheres. However, synthesis is only the first step toward enhancing the function of colloidal systems. Assembly must also be controlled, posing potentially more difficult problems. Such Janus colloidal particles have been shown to form minimum-energy clusters of 2 to 12 colloids (*4*), but these clusters have not yet been shown to assemble into a macroscopic crystal. Colloids with more complex patches have been patterned using multilayer colloidal crystals as a physical mask; however, the yields are low, and it is not obvious how the process can be scaled up to sufficient volumes of particles to study assembly (*5*). In another approach, microspheres of like charge were bound together with nanoparticles of opposite charge to form clusters of two to nine colloids. The loading of nanoparticles was varied to adjust the cluster surface from mostly bare to predominantly nanoparticle-covered (*6*); assembly of these particles has yet to be explored.

But it remains highly challenging to assemble more complex objects or to form assemblies with long-range order. There have been successes in directed assembly of colloids into large-scale structures. For example, Dinsmore *et al.* created complex structures by assembling colloidal crystal shells at interfaces in a water-oil emulsion (*7*). These "colloidosomes" have controlled pore sizes that can be used to selectively allow permeation of the shell by various molecular species. In another study, Hermanson *et al.* used dielectrophoresis to assemble metallic colloids into self-repairing conductive wires with millimeter-scale order (*8*). These approaches to assembling large-scale structures are promising, but do not yield structures with local order. Ligand-directed assembly may potentially provide the specificity of orientation necessary to impart both the desired local and long-range structure.

DNA is an ideal ligand for directing assembly because of its high specificity, reversibility, and unique ability to assemble structures over both the nanometer and the micrometer scale. DNA hybridization has, for example, been used to assemble gold nanoparticles (*9*) and micrometer-scale polystyrene colloids (*10*). Biancaniello and co-workers have even formed small colloidal crystals through DNA-directed assembly of polystyrene microspheres (*11*). These initial demonstrations were rather simple, but it should be possible to form much more complex structures through DNA-directed assembly. The reversibility of DNA hybridization may even allow selective defect removal.

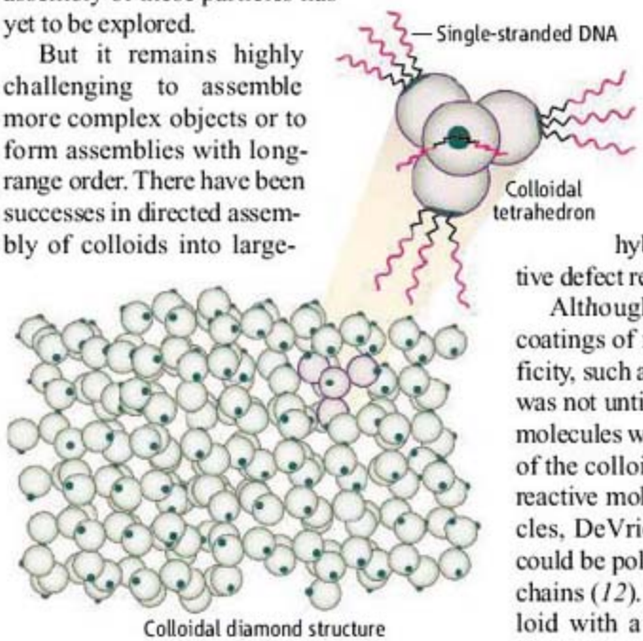


**Toward novel structures.** In a theoretical study, Zhang *et al.* have shown (*3*) that it may be possible to form diamond structures from colloids with four attractive patches. One possible functionalization to create the attractive interactions is DNA.

Although colloids with homogeneous coatings of molecules having binding specificity, such as DNA, have been synthesized, it was not until recently that individual reactive molecules were patterned on precise locations of the colloid surface. By placing individual reactive molecules at the poles of gold particles, DeVries *et al.* formed monomers that could be polymerized into linear nanoparticle chains (*12*). The authors first coated the colloid with a self-assembled monolayer and then exchanged the molecules at the poles of the colloid with reactive, functional molecules. This exchange occurs specifically at the poles of the spherical particle, where the self-assembled monolayer is unstable and easy to exchange. Similar nanoparticle chains have shown great potential for optical devices, such as waveguides (*13*).

In an interesting new approach for using surface chemistry to enhance the function of colloids, Plunkett and co-workers have synthesized colloids with reversibly photoswitchable surface charge. Upon irradiation, these colloids convert from an aggregated, oppositely charged structure to a dispersed, like-charged system, a first step toward photoreversible colloidal crystallization (see the second figure) (*14*). Such photoswitchable systems are a general route to driving colloidal assembly. For example, photoswitchable surface chemistry can also control the spatially defined adsorption of colloids onto a surface (*15*). Photoswitchable colloids could, for example, be used as switchable filters in microfluidics, in sunscreens or cosmetics that change upon light exposure, or as paints that thicken upon application.

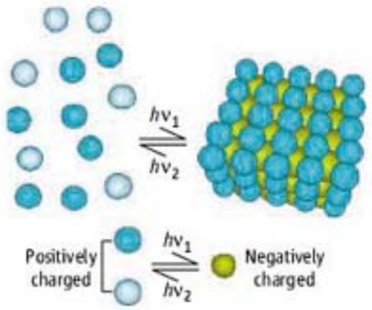


**Switchable systems.** Oppositely charged binary colloidal systems have been shown to assemble into unique ionic structures (*1*). Through appropriate surface chemistries, it may prove possible to create photoswitchable binary systems, which can convert between binary crystals and colloidal fluids when irradiated with light of different wavelengths ($h\nu_1$, $h\nu_2$).

Although advances have been made in controlling colloidal surface chemistry, critical challenges remain before exciting applications may be realized. There is still no good route for the bulk synthesis of site-specific patterned colloids. Exact control of patch size and location is difficult. General patch functionalization schemes need to be developed. Reversible interactions will also be necessary to remove defects. Here, photoswitchable systems show promise. As functionalization strategies mature, investigations into the assembly of chemically modified colloids should provide important feedback to determine the requirements for specificity, binding strength, range of interactions, and reversibility necessary to achieved the desired interactions and assembly through chemical modification of the colloid surface. Success should yield new materials for photonic and electronic applications, consumer products, and industrial systems due to the unique properties enabled by surface-modified colloids.

**References**

1. M. E. Leunissen *et al.*, *Nature* **437**, 235 (2005).
2. S. C. Glotzer, M. J. Solomon, *Nat. Mater.* **6**, 557 (2007).
3. Z. L. Zhang, A. S. Keys, T. Chen, S. C. Glotzer, *Langmuir* **21**, 11547 (2005).
4. L. Hong, A. Cacciuto, E. Luijten, S. Granick, *Nano Lett.* **6**, 2510 (2006).
5. G. Zhang, W. Dayang, H. Mohwald, *Nano Lett.* **5**, 143 (2005).
6. Y.-S. Cho *et al.*, *J. Am. Chem. Soc.* **127**, 15968 (2005).
7. A. D. Dinsmore *et al.*, *Science* **298**, 1006 (2002).
8. K. D. Hermanson *et al.*, *Science* **294**, 1082 (2001).
9. C. A. Mirkin, R. L. Letsinger, R. C. Mucic, J. J. Storhoff, *Nature* **382**, 607 (1996).
10. V. T. Milam, A. L. Hiddessen, J. C. Crocker, D. J. Graves, D. A. Hammer, *Langmuir* **19**, 10317 (2003).
11. P. L. Biancaniello, A. J. Kim, J. C. Crocker, *Phys. Rev. Lett.* **94**, 058302 (2005).
12. G. A. DeVries *et al.*, *Science* **315**, 358 (2007).
13. S. A. Maier *et al.*, *Nat. Mater.* **2**, 229 (2003).
14. K. N. Plunkett, A. Mohraz, R. T. Haasch, J. A. Lewis, J. S. Moore, *J. Am. Chem. Soc.* **127**, 14574 (2005).
15. M. Piech, M. C. George, N. S. Bell, P. V. Braun, *Langmuir* **22**, 1379 (2006).

10.1126/science.1148009

CELL SIGNALING

# mTOR, Unleashed

A mitochondrial membrane protein links two parts of a signaling pathway that is central to cell growth and proliferation.

**Christopher G. Proud**

The enzyme mammalian target of rapamycin (mTOR) integrates many different cellular signals to control cell growth and proliferation, protein synthesis and breakdown, and other processes. Dysregulation of mTOR is implicated in a range of human diseases, including cancers and cardiovascular conditions (*1*, *2*). Although analogs of the compound rapamycin (rapalogs) are in use or in clinical trials to treat such diseases, the means by which signaling through mTOR is controlled are not well understood. On page 977 of this issue, Bai *et al.* (*3*) make an important contribution to understanding how mTOR is turned on.

The drug rapamycin inhibits signaling linked to mTORC1 (*4*), a multiprotein complex that contains mTOR. mTORC1 signaling is activated by insulin and growth factors as well as by amino acids. The latter makes physiological sense: mTORC1 activates protein synthesis, for which amino acids are the precursors. However, it is still unclear how amino acids switch on mTORC1 signaling. Moreover, we still don't understand how rapamycin interferes with mTORC1 function beyond the fact that when in a complex with the protein FKBP12, the drug binds to mTORC1.

We know rather more about how insulin activates mTORC1. Rheb, a small guanosine triphosphate (GTP)–binding protein, interacts with mTORC1 (*5*, *6*). Only in a GTP-bound state (Rheb-GTP) will it activate mTOR's enzymatic activity (phosphorylating target proteins on serine and threonine residues) (*7*). However, it is puzzling that mTOR binds both to Rheb-GTP and to Rheb that is bound to guanosine diphosphate (GDP); moreover, the latter (Rheb-GDP) actually binds better to mTOR. For other small GTP-binding proteins, such as Ras, GTP enhances binding to targets or "effectors." The apparently perverse behavior of Rheb suggests that Rheb-GTP does not activate mTOR by directly binding to it—in other words, that mTOR is not the true effector for Rheb-GTP.

What, then, is the functional relationship between Rheb and mTOR? Bai *et al.* identify the protein FKBP38—a mitochondrial membrane protein—as a direct binding partner for Rheb, both in a screen for protein interactions (yeast two-hybrid system) and in cultured mammalian cells. The authors show that FKBP38 binds to mTOR within the complex mTORC1. They also demonstrate that interaction with FKBP38 displays characteristics expected of an effector of Rheb. For example, Rheb that is bound to a GTP analog associates with FKBP38 much better than does Rheb-GDP, whereas a mutant form of Rheb that does not bind to GTP cannot bind FKBP38.

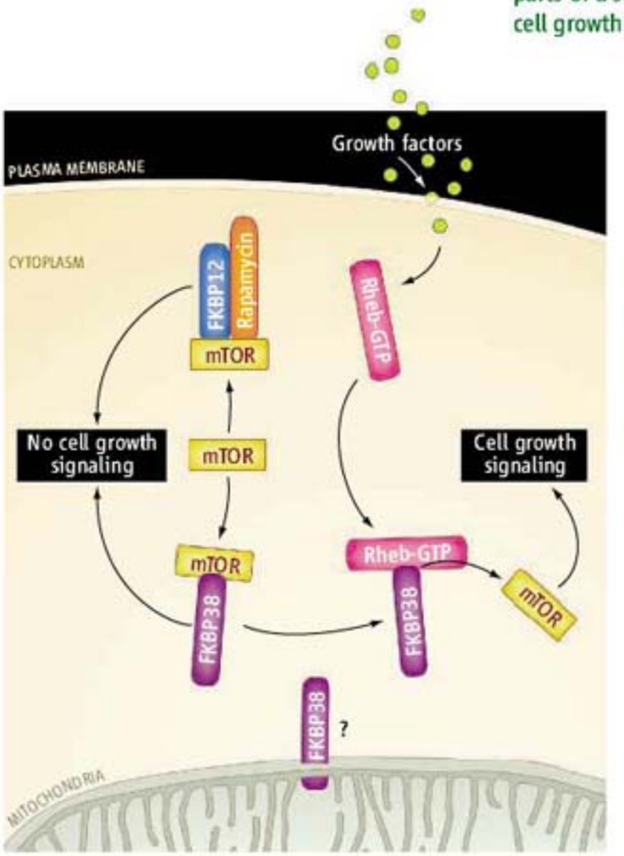


**Endogenous mTOR inhibitor.** The mitochondrial protein FKBP38 and the FKBP12-rapamycin complex each bind to mTOR (as part of mTORC1) and inhibit signaling that promotes cell growth and proliferation. GTP-bound Rheb binds to FKBP38 and induces the release and activation of mTOR. It is not yet known whether these interactions occur at the mitochondria.

These data suggested that FKBP38 may work with Rheb to control mTORC1, but in what way? Bai *et al.* found that overexpressing FKBP38 in cultured mammalian cells decreased the phosphorylation of ribosomal protein S6 kinase (S6K) and 4E binding protein 1 (4E-BP1), two well-known targets of mTORC1 (*7*). These effects were reversed by overexpressing Rheb. FKBP38 thus appears to inhibit mTORC1, and this inhibition is counteracted by Rheb. Furthermore, Rheb-GTP decreased the binding of FKBP38 to mTOR in vitro. Treating cells with serum, which contains growth factors, activated mTORC1 signaling, and this was associated with decreased binding of FKBP38 to mTOR. Thus, FKBP38 is an endogenous inhibitor of mTOR, and Rheb-GTP apparently induces the release of FKBP38 from mTOR, thereby activating mTORC1 signaling (see the figure).

This model provides a much-needed explanation for the abilities of Rheb-GTP, and in turn insulin, to activate mTORC1: By promoting the formation of Rheb-GTP (*8*), insulin alleviates the inhibition of mTORC1 by FKBP38. FKBP38 binds to a region of mTOR that apparently overlaps with another mTOR region that binds to the FKBP12-rapamycin complex. FKBP12-rapamycin precludes the binding of FKBP38 to mTOR, likely as a result of mutual competition. Thus, FKBP12-rapamycin may inhibit mTORC1 by "substituting" for FKBP38. Interestingly, an earlier study (*9*) identified FKBP38 as playing a role in controlling cell growth by the tuberous sclerosis complex proteins, which negatively regulate Rheb and mTORC1 (*8*).

However, the link between mTOR and Rheb elucidated by Bai *et al.* does raise some questions. It remains unclear how FKBP38 and FKBP12-rapamycin inhibit mTORC1 signaling. For example, it is debatable whether FKBP12-rapamycin causes the dissociation of the mTORC1 complex (*10*) or not (*11*). Because FKBP38 can be isolated from cells together with components of mTORC1, it seems that FKBP38 impairs mTORC1 signaling without disrupting this complex. Also, FKBP38 inhibits the effects of mTORC1 that are sensitive to rapamycin (such as S6K phosphorylation) but does not inhibit downstream events that are insensitive to this drug, such as the phosphorylation of certain sites in 4E-BP1 (*12*). It is unclear why this is so.

Can FKBP38 and its control by Rheb explain the regulation of mTORC1 by amino acids? Earlier studies showed that amino acids promote Rheb-mTOR interaction without altering the amount of Rheb-GTP (*13*). The

The author is in the Department of Biochemistry and Molecular Biology, University of British Columbia, 2350 Health Sciences Mall, Vancouver, British Columbia V6T 1Z3, Canada.

data of Bai *et al.* indicate that amino acids decrease the FKBP38-mTOR interaction and increase binding of FKBP38 to Rheb-GTP, consistent with FKBP38 involvement in amino acid control of mTORC1. However, decreasing the amount of FKBP38 in cells did not prevent the dephosphorylation of 4E-BP1 that occurs when cells are starved of amino acids. This suggests that the control of mTORC1 signaling by amino acids does not require FKBP38.

Although there are still important gaps in our understanding of mTOR signaling, the identification of FKBP38 as a regulator of mTOR clarifies previous observations about signaling events in this pathway. This is good news for developing alternative drugs that are not rapalogs to treat diseases that involve mTOR.


**References**

1. J. B. Easton, P. J. Houghton, *Oncogene* **25**, 6436 (2006).
2. C. H. Lee, K. Inoki, K. L. Guan, *Annu. Rev. Pharmacol. Toxicol.* **47**, 443 (2007).
3. X. Bai *et al.*, *Science* **318**, 977 (2007).
4. S. Wullschleger, R. Loewith, M. N. Hall, *Cell* **124**, 471 (2006).
5. J. Avruch *et al.*, *Oncogene* **25**, 6361 (2006).
6. X. Long, Y. Lin, S. Ortiz-Vega, K. Yonezawa, J. Avruch, *Curr. Biol.* **15**, 702 (2005).
7. X. Wang, C. G. Proud, *Physiology* **21**, 362 (2006).
8. B. D. Manning, L. C. Cantley, *Trends Biochem. Sci.* **28**, 573 (2003).
9. M. Rosner, K. Hofer, M. Kubista, M. Hengstschlager, *Oncogene* **22**, 4786 (2003).
10. D. H. Kim *et al.*, *Cell* **110**, 163 (2002).
11. E. Jacinto *et al.*, *Nat. Cell Biol.* **6**, 1122 (2004).
12. X. Wang, A. Beugnet, M. Murakami, S. Yamanaka, C. G. Proud, *Mol. Cell. Biol.* **25**, 2558 (2005).
13. X. Long, S. Ortiz-Vega, Y. Lin, J. Avruch, *J. Biol. Chem.* **280**, 23433 (2005).


10.1126/science.1150653

COMPUTER SCIENCE

# Is There Progress on Talking Sensibly to Machines?

Several research projects are closing in on ways to allow humans to effectively communicate with machines in natural language.

**Yorick Wilks**

Since the earliest days of computing, people have sought ways to communicate with computers in "natural" language, rather than program them in symbolic languages like FORTRAN and C. In the 1960s, MIT researcher Joseph Weizenbaum's ELIZA program was an entertaining simulation of a Rogerian therapist (*1*). ELIZA took words you had used and played them back, as in: "Tell me why you feel like that about your family?" It is an irony of the brief history of machine dialog programs that ELIZA is remembered and PARRY is not. PARRY ran on the early ARPAnet at Stanford in the late 1960s and was designed by Kenneth Colby, a psychiatrist who wanted to model paranoiacs and their beliefs (*2*). PARRY was paranoid about the Mafia, horse races, track betting, and Italian-Americans; if anything you typed could be linked to them, it would spew out a paragraph of invective.

PARRY was more fun than the better-remembered ELIZA, and is another example of the "Betamax principle" (*3*). PARRY was based on nothing that could be called a theory; it was closer in spirit to the principal approach for studying machine dialog today, which could be captured as "big data + small theory." That is, PARRY had a tiny matching program and a very large set of hand-crafted data: about 6000 patterns it tried to match to whatever was typed to it.

In the PARRY/ELIZA years, artificial intelligence research typically took logic to be the core of machine intelligence, and linguistics was still strongly influenced by Noam Chomsky at MIT; both AI and linguistics assumed that small sets of axioms or grammar rules explained large sets of data, i.e., proved theorems or sentences. But neither approach actually had any real data at all, only a few made-up examples, whereas PARRY at least had the large set of patterns made up by its researchers. Any match found pointed to a set of possible replies. This kind of an approach was, and is, anathema to Chomsky, who said that data gathering is like pre-Galilean physics and can have no role in formal linguistics (*4*). The underlying problem with machine dialog, viewed as a technology, was that programs based on logic or on formal linguistic grammars had had little success for more than 40 years in producing usable computational artifacts.

All this changed in 1990, with the astonishing success of Frederick Jelinek's team at IBM (*5*). Originally speech-processing engineers working on the automatic transcription of speech into written form, they decided to apply their data-driven methods to machine translation, using as data 200 million words of parliamentary proceedings in parallel English-French text. The method was a statistical one that learned from the parallel text data what translation was but without creating any rules at all. This was the first important work in applying machine learning to language processing. Jelinek and his co-workers were not completely successful, but they had a success rate of about 50% in translating sentences that the program hadn't seen before.

The field has now settled into two main traditions of research on how to produce machine conversationalists. Both schools take successful work on speech engineering, with data derived from recorded conversations (often on the phone), and seek to derive structures and rules to manage machine dialogs. One, represented by researchers like Steve Young at Cambridge University, assumes that machine learning methods from speech processing can be trained to manage dialogs directly, without intermediate quasi-linguistic structures (*6*). The second follows the route Jelinek later took and tries to recapitulate those linguistic structures but empirically, using machine learning, rather than making up rules, as linguists traditionally did (*7*).

Those in the latter camp currently believe that the infor-

**Conversational companion.** The Nabaztag rabbit (*11*) shows the feelings of a remote sender by speech, changing colors, and moving its ears. The speech is generated via a wireless Internet connection from typed input at a Web site. As an initial incarnation of a companion, the Companions project (*9*) has adapted Nabaztag to recognize speech as well.

CREDIT: NABAZTAG/VIOLET

The author is in the Department of Computer Science, University of Sheffield, Sheffield S1 4DP, UK. E-mail: y.wilks@dcs.shef.ac.uk

mation required to automatically transcribe speech to written text is simply insufficient for the larger task of creating a machine conversationalist that "understands." For example, if someone says something that contradicts his or her earlier statement, we would expect a plausible machine conversationalist to spot it. Without some structure and memory, however, it is hard to see how a system could check statements for consistency. One could never expect to learn to do that simply from data: We just do not see or hear enough sentences to have previously encountered all the inconsistencies that we could spot immediately.

At the moment, people encounter machine conversationalists only in recreational chatbots on the Web, or in simple phone transactions such as ordering travel tickets. But research systems are already much better than that, and the range of projects expected to deliver usable prototypes has expanded in recent years. These efforts range from the Defense Advanced Research Projects Agency's Cognitive Assistant that Learns and Organizes project (*8*) to the European Commission's new Companions project (*9*) to create a long-term conversational partner (see the figure). Such a Companion would learn its person's likes and dislikes, carry out Web-related tasks accordingly, and prompt reminiscences about the person's photo collection so as to build up his or her life story through conversation (*10*).

Researchers generally agree that although these large goals need more research, speech recognition technology is still not accurate enough to build a reliable machine partner capable of understanding what we say, unless it has a considerable amount of stored knowledge to enable it to understand; mere reactive chatbots will be no more help than ELIZA was. The current paradigm split in research is about how it will be possible to capture and store knowledge and language experience in large enough detail and volume to build such assistants, outside of very small domains such as recording a complicated pizza order. A long-term assistant to an astronaut on a voyage to another planet, or one to help elderly people recover their past through conversation and organize it in text and images, is a much larger goal, and one that will require better machine learning techniques than have been deployed so far.

The crux of the current research issue is this: Will a successful technology end up recreating by means of automated learning much of the linguistic and logical content that was abandoned in the 1990s? That might be closer to what our own cognitive structures seem to be. In any case, language data will remain central, and the World Wide Web has, as an unexpected benefit through chat rooms, provided researchers with potentially infinite resources of data on human conversations.

**References and Notes**

1. J. Weizenbaum, *Commun. ACM* **9**, 36 (1966).
2. K. M. Colby *et al.*, *Artif. Intell.* **2**, 1 (1972).
3. The worst can drive out the best—in the tape format wars for home video recording during the 1970s and 1980s, VHS won over Betamax.
4. www.celt.sunysb.edu/celtweb/images/Chomsky%20and%20Aronoff%20(Toledo%20Transcript).pdf
5. P. F. Brown *et al.*, *Comp. Linguistics* **16**, 79 (1990).
6. S. Young, paper presented at the International Conference on Speech and Language Processing, 16 to 20 September 2002, Denver.
7. Y. Wilks, N. Webb, A. Setzer, M. Hepple, R. Catizone, in *Recent Advances in Natural Language Processing III*, N. Nicolov, K. Bontcheva, G. Angelova, R. Mitkov, Eds. (Benjamins, Amsterdam, 2005), pp. 111–129.
8. http://caloproject.sri.com/darpa
9. www.companions-project.org
10. Y. Wilks, *Interdiscipl. Sci. Rev.* **30**, 145 (2005).
11. www.nabaztag.com
12. The author's research was sponsored by the European Commission under EC grant IST-FP6-034434 (Companions).

10.1126/science.1148895

PHYSIOLOGY

# An Integrative View of Obesity

Comparisons of responses of various cell types to excess nutrients are yielding patterns that may provide insight into the causes and consequences of obesity.

**Brent E. Wisse, Francis Kim, Michael W. Schwartz**

The World Health Organization estimates that at least 1 in 10 adults worldwide are obese, and in some western countries, a far greater percentage (25% or more) is affected (*1*). Obesity is a serious concern because it increases the risk of cardiovascular disease, type 2 diabetes, and some cancers, among other health problems. The evolution of public health policies and treatment options depends upon an improved understanding of how genetic and environmental factors interact to favor weight gain, and how excessive weight disrupts metabolism. But getting at the causes of obesity and related metabolic disorders is a formidable challenge, in part because so many body systems are affected. Because disturbances in one organ or tissue can compromise the function of several others, separating cause and effect is often difficult. Yet common themes are emerging that may offer a new viewpoint. Among these is the notion that metabolic dysfunction arises from exposure of the body's cells to an excess of nutrients (*2*). A possible extension of this view is that although the cellular consequences of nutrient excess are similar across diverse cell types, the shared nature of the underlying cellular responses can be obscured by the complexity of the events they initiate. In this light, successful identification of shared cellular responses that underlie disease requires a broad and integrative approach that may ultimately reveal more effective obesity treatment strategies.

Fundamental to understanding obesity is the fact that, like body temperature, body fat stores are ordinarily maintained within a narrow range through a process called "energy homeostasis." This process involves brain areas that control appetite and energy metabolism, as well as signals that circulate throughout the body, conveying information about the status of body fuel stores. Among the latter are nutrients themselves, such as glucose and free fatty acids, and hormones, such as insulin and leptin (*3*). Specialized neurons in the hypothalamus and other brain areas sense these factors and control both metabolic rate and the desire to eat. When circulating concentrations of these signals decrease due to weight loss, the drive to eat increases and energy expenditure declines, favoring the recovery of depleted fuel stores. Conversely, when food is consumed in amounts that exceed energy requirements, the circulating concentrations of these signals increase. In this way, homeostatic response mechanisms in the brain are poised to protect the body against changes in fat stores or swings in nutrient availability. Thus, obesity does not simply arise from the passive accumulation of excess weight; rather, it involves the active defense of an elevated level of body fat, and deciphering the causes of obesity should take this into account. Certainly, individual genetic makeup may contribute to variations in the capacity to mount these responses, and may explain why some people are protected against weight gain

The authors are in the Department of Medicine, Harborview Medical Center and University of Washington, Seattle, WA 98104, USA. E-mail: mschwart@u.washington.edu

while others are not, despite living in the same environment and eating the same food.

When energy intake exceeds energy expenditure, the resulting state of nutrient excess can trigger responses in many cell types—endothelial cells (vascular) (*4*), hepatocytes (liver) (*2*), myocytes (muscle) (*5*), adipocytes (fat) (*2*), and monocytes or macrophages (immune cells)—that could give rise to metabolic dysfunction. Among several adverse cellular responses to nutrient excess is the production of reactive oxygen species. These molecules are generated during fuel (e.g., glucose or free fatty acids) oxidation by mitochondria and from metabolic processes elsewhere in the cell. Excessive production of these molecules creates "oxidative stress," which can damage cellular structures and trigger an inflammatory response (*2*). In some cells, nutrient excess also impairs functioning of the endoplasmic reticulum (which processes newly synthesized proteins into their mature forms), giving rise to the "unfolded protein response" in this organelle. Like reactive oxygen species, this response can induce inflammation. A third cellular response to nutrient excess is the accumulation of long-chain fatty acyl coenzyme A molecules, fatty acid derivatives that are ordinarily oxidized by mitochondria to generate adenosine 5′-triphosphate (which powers many cellular processes). Making matters worse is a decrease of mitochondrial activity in response to nutrient excess. This creates a vicious cycle by further raising the concentration of these fatty acid derivatives (*5*).

Each of these responses share the ability to activate signaling pathways (such as the c-Jun N-terminal kinase and the inhibitor of kappa B kinase beta–nuclear factor kappa B pathways) (*2, 4–6*) that promote inflammation. Thus, inflammation appears to be a common endpoint. In turn, inflammation can limit further exposure to nutrients by blocking the action of insulin (*2, 5*), the hormone that stimulates target cells to take up nutrients. The enzyme phosphatidylinositol 3-OH kinase (PI3K) is part of a cell signaling pathway [the insulin receptor substrate (IRS)-PI3K pathway] that mediates insulin action and is particularly sensitive to inactivation by molecules that promote inflammation. From the perspective of an individual cell, this protective response—insulin resistance—makes sense in that it limits further nutrient uptake. With continued nutrient excess, however, neighboring cells and distant tissues that remain insulin sensitive are placed at greater risk. As insulin resistance progresses and inflammation worsens, a vicious cycle can evolve as additional pro-inflammatory factors are recruited by these cells (*2*).

In addition to regulating nutrient utilization in peripheral tissues, IRS-PI3K signaling is also implicated in the neuronal actions of insulin and leptin (*3*). As in peripheral tissues, the integrity of neuronal IRS-PI3K signaling can be undermined by nutrient excess (*7*). Studies in rodent models indicate that even short-term exposure to a highly palatable, energy-dense diet impairs the brain's response to insulin and leptin, and reduced IRS-PI3K signaling may be among several mechanisms responsible for neuronal resistance to these hormones (*7, 8*). Having lost its ability to detect an ongoing increase in body fat stores, the brain seemingly does nothing to counter it; rather, it actively defends what it perceives to be a stable, unchanging amount of body fat (*9*). Thus, impaired IRS-PI3K signaling in the hypothalamus may be a factor that contributes to the defense of elevated body weight and hence to continued exposure to nutrient excess (*3*).

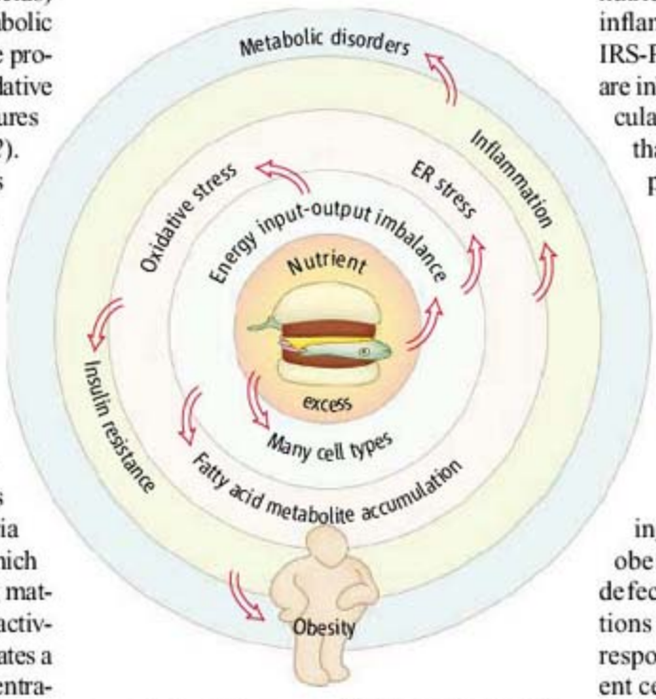


Might similar cellular responses to nutrient excess contribute to the link between obesity and type 2 diabetes? If inflammation and reduced IRS-PI3K signaling were also to occur in pancreatic β cells (which produce insulin), as has been suggested (*6*), impaired insulin secretion—which, when combined with insulin resistance, leads to type 2 diabetes—could result, because IRS-PI3K signaling is essential for the survival of these cells (*6*). This concept extends "the β cell exhaustion" hypothesis (*10*), which states that type 2 diabetes results when pancreatic β cells can no longer meet the heightened demand for insulin secretion imposed by insulin resistance. Thus, cellular consequences of nutrient excess similar to those that impair the function of other tissues could potentially contribute to the link between insulin resistance and β cell dysfunction in diabetes pathogenesis.

Nutrient excess also has deleterious effects on vascular tissue. A major function of endothelial cells that line blood vessels is to generate and release nitric oxide, a vasodilator. The IRS-PI3K signaling pathway is a key determinant of nitric oxide production and, as in other tissues, nutrient excess rapidly induces endothelial inflammation. In response, both endothelial IRS-PI3K signaling and nitric oxide generation are inhibited (*4*). Thus, the response of the vasculature to nutrient excess is reminiscent of that observed in other tissues, and offers a plausible link between nutrient excess and cardiovascular disease.

**Common threads.** Cellular responses to nutrient excess are shared across many different cell types, and may have common endpoints that are coupled to the development of obesity and its metabolic consequences. ER, endoplasmic reticulum.

Clearly, impaired IRS-PI3K signaling is not the single key to understanding obesity and its consequences. Rather, this defect illustrates how complex manifestations of metabolic disease could arise from responses that are shared across many different cell types (see the figure). In addition to research that focuses on one organ or physiological system to the exclusion of others, more integrative approaches for studying metabolic disease may ultimately inform strategies aimed at preventing or reversing obesity and its sequelae.

**References and Notes**

1. C. L. Ogden *et al.*, *JAMA* **295**, 1549 (2006).
2. G. S. Hotamisligil, *Nature* **444**, 860 (2006).
3. K. D. Niswender, D. G. Baskin, M. W. Schwartz, *Trends Endocrinol. Metab.* **15**, 362 (2004).
4. F. Kim *et al.*, *Arterioscler. Thromb. Vasc. Biol.* **25**, 989 (2005).
5. B. B. Lowell, G. I. Shulman, *Science* **307**, 384 (2005).
6. C. J. Rhodes, *Science* **307**, 380 (2005).
7. C. T. De Souza *et al.*, *Endocrinology* **146**, 4192 (2005).
8. H. Munzberg, J. S. Flier, C. Bjorbaek, *Endocrinology* **145**, 4880 (2004).
9. B. E. Levin, A. A. Dunn-Meynell, *Am. J. Physiol. Regul. Integr. Comp. Physiol.* **282**, R46 (2002).
10. S. Lillioja *et al.*, *N. Engl. J. Med.* **318**, 1217 (1988).
11. We acknowledge support from NIH grants P01-DK 068384, DK12829, NS3227, DK61384, and DK073878 and from the Diabetes Endocrinology Research Center and Clinical Nutrition Research Unit at the University of Washington.

10.1126/science.1148032

# A General Model of Prion Strains and Their Pathogenicity

John Collinge* and Anthony R. Clarke

Prions are lethal mammalian pathogens composed of aggregated conformational isomers of a host-encoded glycoprotein and which appear to lack nucleic acids. Their unique biology, allied with the public-health risks posed by prion zoonoses such as bovine spongiform encephalopathy, has focused much attention on the molecular basis of prion propagation and the "species barrier" that controls cross-species transmission. Both are intimately linked to understanding how multiple prion "strains" are encoded by a protein-only agent. The underlying mechanisms are clearly of much wider importance, and analogous protein-based inheritance mechanisms are recognized in yeast and fungi. Recent advances suggest that prions themselves are not directly neurotoxic, but rather their propagation involves production of toxic species, which may be uncoupled from infectivity.

According to the widely accepted "protein-only" hypothesis (*1*), an abnormal isoform of host-encoded cellular prion protein ($PrP^C$) is the principal, and possibly the sole, constituent of the transmissible agent or prion (*2*). It is proposed that this isoform, $PrP^{Sc}$, acts as a template that promotes the conversion of $PrP^C$ to $PrP^{Sc}$ and that the difference between these isoforms lies purely in the monomer conformation and its state of aggregation.

The human prion diseases, such as Creutzfeldt-Jakob disease (CJD), can arise sporadically, be acquired by infection, or be inherited as autosomal dominant conditions caused by mutation of the gene encoding $PrP^C$ (*3*). Human prion diseases are relatively rare, although they have occurred in epidemic form as a result of endocannibalism in recent history in Papua New Guinea, and previous epidemics may have occurred in human evolution (*4*).

Animal prion diseases include endemic scrapie of sheep and goats, chronic wasting disease of elk and deer, and transmissible mink encephalopathy (TME). Bovine spongiform encephalopathy (BSE) first appeared in the United Kingdom in the mid-1980s and rapidly evolved to a major epizootic estimated to have infected more than 2 million UK cattle. BSE has since been reported from many countries including most European Union states, the United States, Canada, and Japan. Many new animal prion diseases have since been identified, most resulting from infection with the BSE agent (*3*). These diseases can be transmitted between species by inoculation or dietary exposure, and the recognition of the novel human prion disease, variant CJD (vCJD), from the mid-1990s onward and the experimental confirmation that it is caused by the same prion strain as BSE (*5*–*7*) raised major public-health concerns (*8*). Although the number of human cases to date (around 200) has been relatively modest, key uncertainties, notably with respect to genetic effects on incubation period, allied with the widespread population exposure, suggest the need for caution (*8*). Prion infection is associated with prolonged, clinically silent incubation periods, which in humans can exceed 50 years (*9*), and secondary transmission of vCJD by blood transfusion appears to be efficient (*10*).

Prions have also assumed much wider relevance in understanding neurodegenerative and other diseases involving accumulation of misfolded host proteins ("protein-folding diseases"), and analogous processes are described in yeast and fungi. Central to understanding prion propagation remains the conundrum of prion strains—how a protein-only infectious agent can encode information required to specify distinct disease phenotypes—and also the so-called species barrier effect.

It is hypothesized that prions are self-propagating fibrillar or amyloid forms of PrP in which the ends of the propagating fibrils constitute the infectious entity and the exponential rise in prion titer is a consequence of fiber fragmentation (Fig. 1A) (*11*–*14*).

## The Species Barrier Concept

Transmission of prion diseases between different mammalian species is typically far less efficient than within species; this is known as the "species barrier" (*15*). On initial passage of prions from species A to species B, typically not all inoculated animals of species B succumb, and those that do so have much longer and more variable incubation periods than seen with transmission within the same species, where typically all inoculated animals succumb with relatively short, and remarkably similar, incubation periods. On subsequent passage of infectivity from B to B, transmission parameters resemble within-species transmissions.

Early studies argued that the barrier resides in PrP primary structure differences between the donor and recipient species. Transgenic mice expressing hamster PrP are, unlike wild-type mice, highly susceptible to Sc237 hamster prions (*16*). That sporadic and acquired CJD mostly occurs in individuals homozygous at polymorphic residue 129 of PrP supports the view that prion propagation proceeds most efficiently when the interacting $PrP^{Sc}$ and $PrP^C$ are of identical primary structure (*3*, *17*, *18*). However, prion strain type also affects ease of transmission to another species. This issue was brought into sharp focus by the behavior of the new prion strain responsible for cattle BSE. This strain is highly promiscuous, transmitting efficiently to a range of species, but maintaining its biological characteristics on passage through an intermediate species with a distinct PrP primary structure (*19*) (Fig. 1C). Perhaps the most striking example of this came from transmission studies of human prion diseases. Transmission of classical CJD prions to conventional mice is difficult or fails, whereas transgenic mice expressing human (and not mouse) PrP completely lack a species barrier (*6*, *20*). However, vCJD prions, despite having a PrP primary structure identical to that of the classical CJD prions, transmit much more readily to wild-type mice, whereas transmission to humanized mice is inefficient (*6*). Two strains propagated in the same host may thus have completely different barriers to another species; "transmission barrier" may thus be a more appropriate term (*8*).

## Prion Isolates, Strains, and Types

Multiple distinct strains of scrapie were isolated that can be propagated in lines of inbred mice and distinguished by distinct incubation periods and patterns of neuropathology (*21*). These strains cannot be encoded by differences in PrP primary structure because they can be serially propagated in inbred mice with identical PrP gene (*Prnp*) coding sequence (Fig. 1B). Furthermore, strains can be re-isolated in mice after passage in intermediate species with different PrP primary structures (*19*) (Fig. 1C). Although distinct strains of conventional pathogens can be explained by differences in their nucleic acid genome, it has been less clear how a polypeptide chain could encode multiple disease phenotypes. Some such biologically defined prion strains show biochemical differences in the propagated $PrP^{Sc}$. For two strains of TME prions, designated hyper (HY) and drowsy (DY) (*22*), limited proteolysis produced different $PrP^{Sc}$ fragment sizes, implying that the two strains have different conformations (*23*). Similarly, distinct human $PrP^{Sc}$ types have been identified by proteolytic fragment size and glycoform ratios following proteinase K digestion, and these are associated with different clinicopathological phenotypes of CJD (*5*, *24*). To be plausible candidates for the molecular basis of strain diversity, such biochemical properties need to impose their

MRC Prion Unit, Department of Neurodegenerative Disease, UCL Institute of Neurology, London WC1N 3BG, UK.

*To whom correspondence should be addressed. E-mail: j.collinge@prion.ucl.ac.uk

characteristics on a recipient PrP whether they are of the same or a different species. In studies with human prion isolates, $PrP^{Sc}$ fragment sizes following proteinase K digestion are maintained on passage in transgenic mice (*5*, *25*) and, notably, ratios of the three principal PrP glycoforms are also maintained (*5*). Transmission of human and bovine prions to wild-type mice (expressing murine $PrP^{C}$) resulted in propagation of murine $PrP^{Sc}$ with fragment sizes and glycoform ratios following protease digestion that correspond to the original inoculum (*5*), demonstrating imprinting of these biochemical characteristics onto PrP from another species. Indeed, a characteristic molecular signature of the BSE prion strain is maintained across several mammalian species, including humans (Fig. 1C) (*5*).

Further evidence that distinct prion strains are associated with different conformation states of PrP includes differential proteinase K digestion kinetics; thermal or chaotrope denaturation curves; conformation-dependent immunoassay; infrared spectroscopy and metal binding (*26*–*29*); and the use of methods to amplify $PrP^{Sc}$ or prions in vitro that show faithful propagation of strain-associated biochemical characteristics (*30*–*32*).

Prion strains are associated with consistent ratios of the three principal PrP glycoforms, which can be maintained on serial passage in hosts with the same or different PrP sequences (*5*). How might ratios be maintained? One possibility is that this reflects different, strain-specific propagation and clearance kinetics of un-, mono- and diglycosylated forms. Alternatively, individual $PrP^{Sc}$ fibrils could be composed of a regular repeating sequence of the different glycoforms, as in a linear crystal. Studies using monoclonal antibodies that precipitate native $PrP^{Sc}$, together with glycoform-specific antibodies, have shown that PrP glycoforms are physically associated in a strain-specific ratio in native $PrP^{Sc}$ (*33*); such glycosylation ratios may be important in stabilizing particular protein conformations.

A critical test of the protein-only hypothesis, both with respect to infectivity and "strain-ness," would be to produce discrete prion strains synthetically from defined components. Purified, bacterially expressed recombinant N-terminally truncated mouse PrP has been aggregated into fibrillar material and bioassayed in transgenic (Tg9949) mice expressing very high levels of the same truncated mouse PrP (*14*). After prolonged incubation periods, the Tg9949 mice develop a

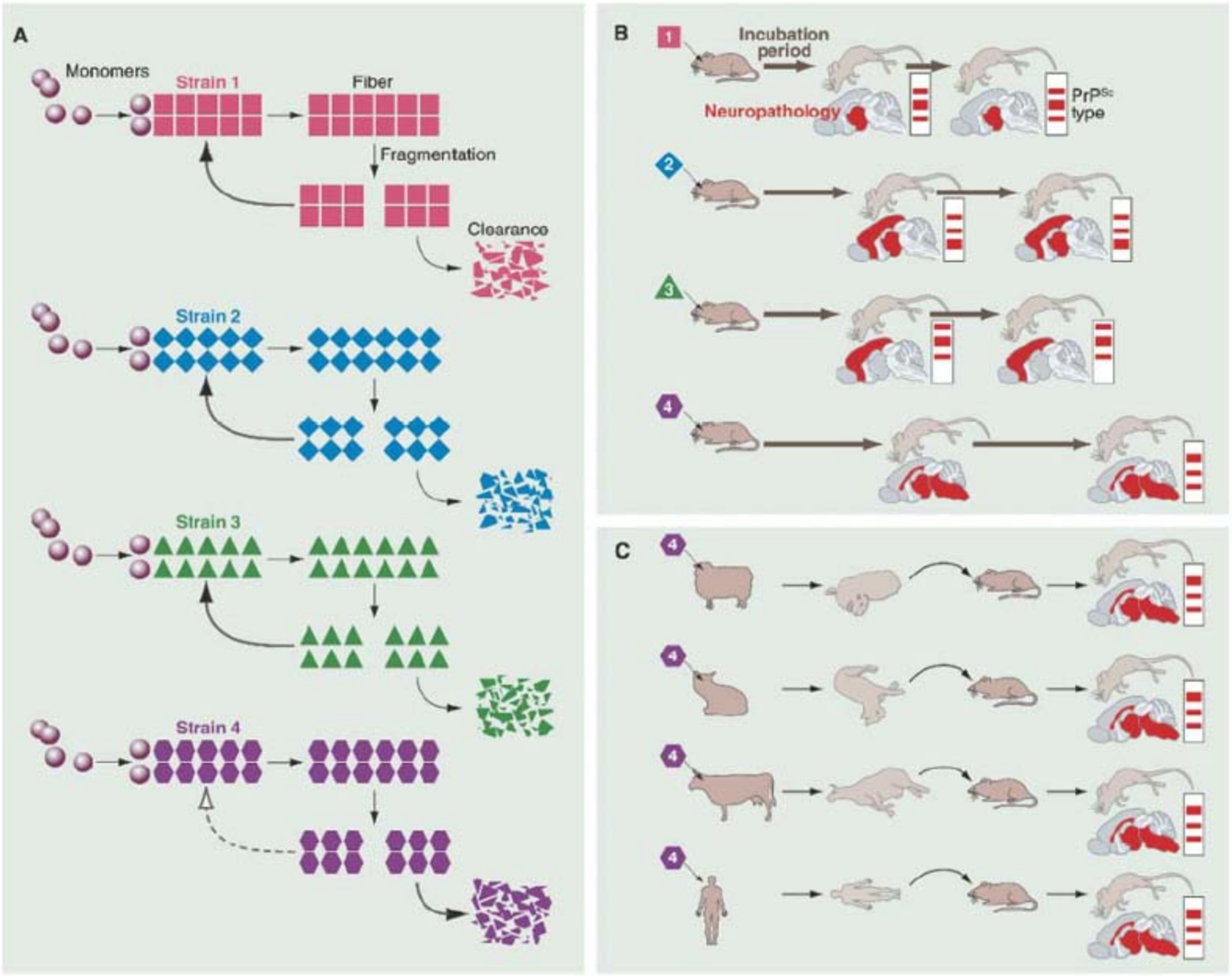


**Fig. 1.** Propagation of prion strains. **(A)** Prion propagation proceeds by recruitment of PrP monomers onto a preexisting PrP polymer template followed by fission to generate more templates in an autocatalytic manner. Distinct PrP polymer types can propagate, accounting for different strains. **(B)** Strains can be differentiated by characteristic incubation periods (length of arrow) and neuropathology (shaded brain area) when inoculated into defined inbred mice. Strain-specific $PrP^{Sc}$ fragment patterns following proteolysis are illustrated in diagrammatic Western blots (vertical bars). Both biological and biochemical strain characteristics are closely maintained on serial passage in the same host expressing the same $PrP^{C}$. **(C)** Properties of a single strain may be retained after passage in a range of different species with distinct $PrP^{C}$ sequences, when re-isolated in the original host.

prion disease transmissible to wild-type and Tg9949 mice. The transmission characteristics at both primary and second passage are consistent with production of a novel prion strain. Several "synthetic" prion strains have been described. Evaluating the strain properties of such synthetic prions on primary and second passage is complicated by the fact that primary material inoculated into mice lacks the posttranslational modifications PrP acquires in mammalian cells, notably N-linked glycosylation and C-terminal glycosylphosphatidylinositol anchor, while the putative prions then propagated in mice would be composed of processed mammalian PrP.

Though undoubtedly a major step forward, two key problems arise in the interpretation of these experiments. First, primary passage of infectivity requires transgenic mice with extremely high (~16-fold) overexpression of $PrP^C$. Spontaneous development of prion disease–like pathology is seen in other transgenic lines with high levels of $PrP^C$ expression, although this does not appear to be transmissible (*34*, *35*). Uninoculated or mock-inoculated Tg9949 mice do not appear to develop spontaneous pathology (*14*), although it has not been reported whether infectivity passageable in Tg9949 mice is present in the brains of aged un- or mock-inoculated Tg9949 mice. However, it is possible that these mice are "poised" to develop spontaneous disease and would do so if they lived long enough, and that onset of disease is simply accelerated or precipitated by inoculation of further PrP. Such a controversy is not new and continues with respect to interpretation of whether mice expressing high levels of PrP containing the murine equivalent (P101L) of the human pathogenic PrP mutation P102L (responsible for one of the inherited prion diseases) produce infectivity spontaneously. Putative prions produced de novo in such mice only infect mice expressing the same mutation at a lower level (some of which do develop spontaneous pathology at advanced age) (*36*). Prions may not then have been transmitted in this experiment; rather, this result may have represented acceleration of a spontaneous neurodegenerative disease (*37*). The general question, then, is whether the putative synthetic prions are in fact prions, or simply agents that trigger prion production in hosts that have such high levels of $PrP^C$ expression that they are close to developing spontaneous prion disease. That is, are the prions generated in the cell-free system or only in the host? This is not a purely semantic issue. For example, one would probably not want to classify an entirely unrelated agent—conceivably an environmental stress factor, for example, that up-regulated $PrP^C$ expression and achieved the same apparent effect—as being a "prion." The solution to this problem would be to show infection at first passage of wild-type animals with synthetic prions. This has not yet been reported. The second problem relates to infectious titer of the synthetic prions. The extremely prolonged incubation period at primary passage (516 ± 27 days) (*14*) could, as the authors conclude, reflect a prion strain effect. That is, the novel strain propagates only slowly in the host despite the high $PrP^C$ substrate concentration, but accepting the additional complication that the synthetic material lacks posttranslational modifications that may be important for pathogenicity.

However, there is an alternative explanation. As a prion isolate is serially diluted toward a single infectious unit per inoculum, incubation periods increase. Therefore, the long incubation periods seen with synthetic prions could simply reflect a low prion titer. With respect to the key issue of elucidating structural properties of prion strains, this is of fundamental importance. If the principal component of the synthetic material is the infectious prion, but they replicate only slowly in mice, biophysical studies can be performed to determine their structure and physical properties. Conversely, if the transmission characteristics reflect low prion titer, that would imply that the prions are only a minute fraction of the recombinant-derived protein, making physical and structural studies irrelevant (*38*). This question can be resolved, albeit laboriously, by serial titration of the synthetic prion inoculum in the transgenic mice. If the first interpretation is correct, the sample may be diluted many fold and would still produce the same incubation period. If the second is correct, even a 10-fold dilution is likely to result in nontransmission during the life span of these animals.

The recognition that certain heritable traits in yeast could be explained by conformational switching and aggregation in two yeast proteins, Ure2p and Sup35p, led to the emergence of the field of "yeast prions"; a fungal protein with prionlike properties, Het-s, has also been described (*39*). These proteins have no sequence similarity to PrP. While one can argue practical distinctions from mammalian prions, which are considered naturally infectious lethal pathogens, the study of these closely analogous phenomena has unquestionably led to rapid advances in investigating the processes of seeded fibril formation and the molecular basis of strain diversity and transmission barriers. Indeed, yeast prions are composed of protein fibrils, propagate by seeding, and possess strain diversity that is explained by distinct conformers (*40*–*45*).

## Unifying Strains and Transmission Barriers: Conformational and Kinetic Selection of Prions

Mammalian PrP genes are highly conserved, and the close similarity of PrP primary structures, and indeed folds (*46*), is presumably central to the ability of prions to cross-infect between mammalian species. Although a large number of $PrP^{Sc}$ types or "strains" are seen in the spectrum of mammalian prion diseases, presumably this number is limited by thermodynamic stability and the need to replicate at a rate above that of natural clearance in vivo. This number will constitute the theoretical portfolio of permissible and pathogenic mammalian prion strains and may be larger than the number of identified naturally occurring and experimentally derived strains. Some strains may be possible conformationally for a given PrP sequence and could be artificially synthesized, but they could not be indefinitely propagated in a normal host owing to efficient clearance. For the yeast prion [PSI+], for which the substrate protein is Sup35p, an analytical, steady-state model describing strains has been experimentally validated (*47*). This work supports a critical role of the fragmentation propensity of a prion strain in dictating its in vivo phenotype. To persist, yeast prions must propagate at a rate sufficient to compensate for the dilutional effect of cell division. Clearly, the in vivo situation in mammals is far more complex because predominantly postmitotic cells are infected and multiple cell types and tissues are involved. In the brain, clearance by cellular mechanisms to remove misfolded protein aggregates will be far more important than dilution by cell growth and division, although the situation may be different in the lymphoreticular system where prions also replicate. Mammalian prions also cause massive cell death, and cytotoxicity will be a major factor in any model of mammalian prion propagation. Also, although steady-state solutions are applicable in modeling yeast prion strains, a steady state is not reached in the mammalian central nervous system.

However, though a relatively large number of different $PrP^{Sc}$ types may be possible among the full range of mammalian PrP sequences, only a subset of these would be compatible with a given sequence (Fig. 2A). Substantial overlap between the permissible conformations for $PrP^{Sc}$ derived from species A and species B would thus result in relatively easy transmission of infection between these two species, whereas two species with no permissible $PrP^{Sc}$ conformations in common would have a large barrier to transmission. Any transmission of infectivity between such two species would require a change of strain type. According to the conformational selection model (*8*), host $PrP^C$ primary structure influences which of the portfolio of possible $PrP^{Sc}$ types are thermodynamically preferred with respect to conformation and kinetically selected during propagation. In this model, the transmission barrier is determined by the degree of overlap between the subset of $PrP^{Sc}$ types allowed or preferred by $PrP^C$ in the host and donor species. Strains and transmission barriers can therefore be considered opposite sides of the same coin.

Returning to the high cross-species pathogenicity of BSE, this strain may represent a thermodynamically highly favored $PrP^{Sc}$ conformation that is readily imprinted on PrP from a range of different species, accounting for the high promiscuity of this strain in mammals. Certainly, this strain was selected by an industrial cooking process (rendering of carcasses) involved in the recycling of infectivity that generated the UK BSE epidemic, and it is indeed known experimentally to be particularly thermostable (*48*).

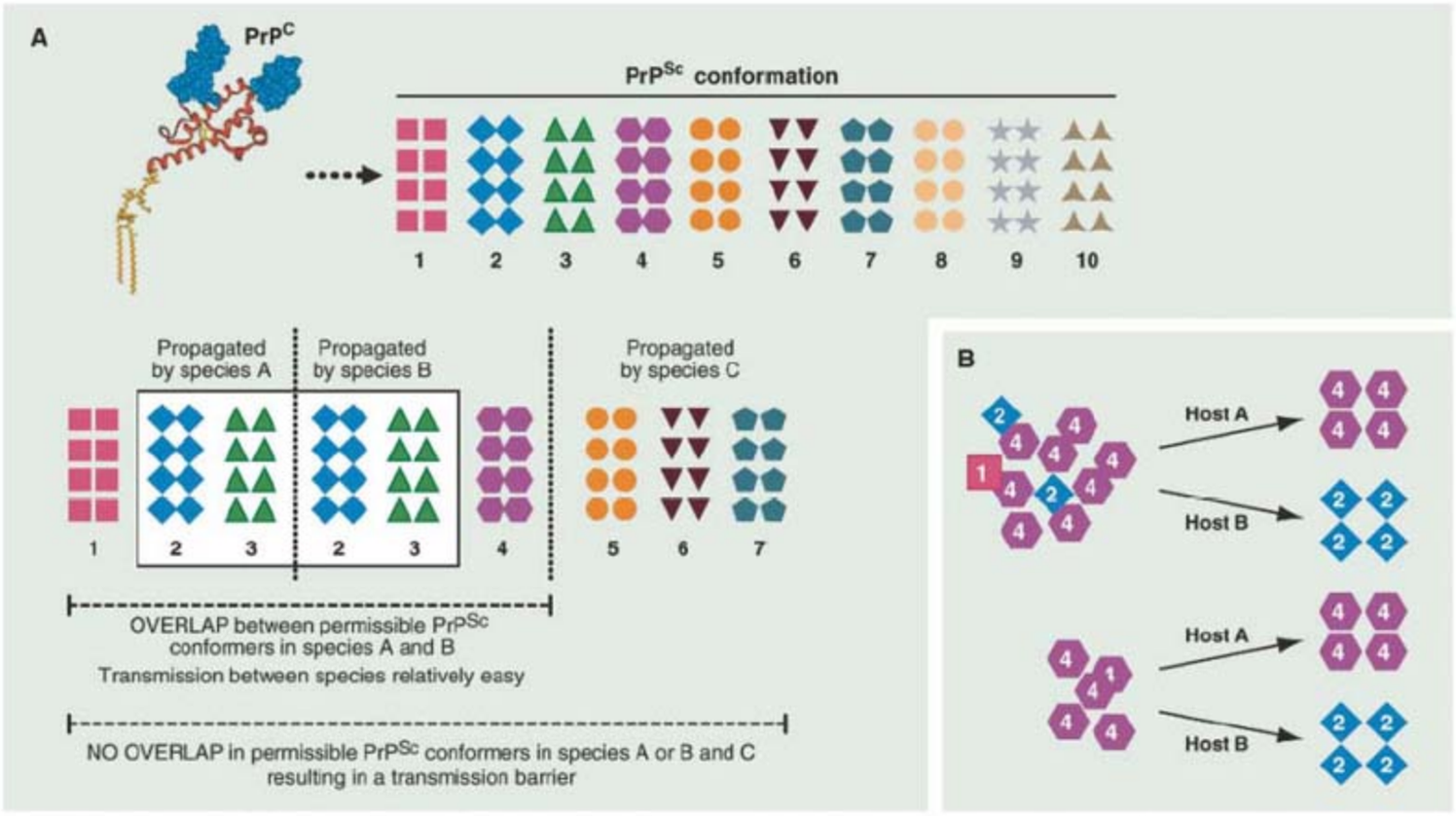


**Fig. 2.** **(A)** Conformational selection and transmission barriers. A wide range of mammalian $PrP^{Sc}$ conformations are possible, but only a subset is compatible with each individual PrP primary structure. Ease of transmission of prions between species relates to overlap of permissible $PrP^{Sc}$ conformations between PrP primary structures from the two species. Though represented as clones, prion strains may consist of an ensemble of molecules, and transmission barriers will relate to overlap of these populations. **(B)** Strain mutation. Illustration of strains as an ensemble of $PrP^{Sc}$ molecules or a clone. Strains "breed true" when propagated in host that preferentially propagates the dominant $PrP^{Sc}$ type (host A) but may change in a different host (B) that selectively propagates a minor component of the $PrP^{Sc}$ ensemble, resulting in apparent strain mutation. Alternatively, with a clonal strain, inoculation into a host (B) expressing PrP with a sequence incompatible with this $PrP^{Sc}$ conformation would only result in transmission by direct strain mutation. These alternatives are not mutually exclusive. It is possible that strain selection and mutation may occur in different tissues of the same host as well as between different hosts as a result of heterogeneity in cellular mechanisms affecting prion propagation and clearance kinetics.

Another illustration of the conformational selection model is provided by the common human PrP polymorphism (M129V), long known to be a key determinant of genetic susceptibility to prion disease. Notably, every patient with vCJD tested (~200) has been homozygous for the 129 methionine allele (a genotype seen in about a third of the normal population) because it appears that the valine 129 human PrP is not capable of adopting the $PrP^{Sc}$ conformation associated with the BSE strain (*49*). Transmission across such a barrier thus results in strain switching with propagation of a distinct and sometimes novel strain type and a different disease phenotype (*49*).

### Prion Strain Stability and Mutation

The phenomenon of strain mutation has been recognized for many years by biological strain typing methods (*50*). Classically, this occurs when a strain does not "breed true" on passage in a new host and a distinct strain is propagated. Mutation may (but does not necessarily) occur on crossing between species and also on intraspecies transmission where the PrP primary sequence of the host differs from that of the inoculum, for example, as a result of intraspecies PrP polymorphism at residue 129 in humans (*5*, *6*, *49*). In human PrP, residue 129 places constraints on which prion strains may propagate, but has no measurable effect on the folding, dynamics, and stability of $PrP^{C}$, suggesting that its effect is exerted through conformation of $PrP^{Sc}$, its precursors, or on the kinetics of their formation (*51*). Strain mutation may also occur on intraspecies transmission where host and prion donor have identical *Prnp* genes: This suggests an additional effect of background genes on strain selection (*52*, *53*). Strain mutation can be accommodated within the conformational selection hypothesis by selection of a novel $PrP^{Sc}$ conformer as a result of host $PrP^{C}$ not being able to adopt the donor $PrP^{Sc}$ conformation. However, the phenomenon poses an important question about strains. It has been long argued that strains can be biologically cloned (*50*). This is performed by serial passage at limiting dilution of an inoculum such that infection in the next host is initiated by a single prion. However, some strains are intrinsically unstable, readily reverting to another strain type, for example, the hamster DY strain (*23*). In addition, more than one strain has been isolated from some natural prion isolates, for example, sheep scrapie (*54*), and multiple $PrP^{Sc}$ types are seen in a sizable fraction of CJD brains (*55*, *56*). Certainly, a natural isolate shows considerable diversity in terms of N-terminal cleavage site, and its glycosylation is highly complex and diverse. Heat-inactivation studies also suggest heterogeneity of infectious species with thermostable subpopulations within a defined strain (*57*). Two (not mutually exclusive) possibilities can be envisaged (Fig. 2B): (i) A strain can exist as a molecular clone and strain mutation involves generation of a distinct $PrP^{Sc}$ type; (ii) strains consist of an ensemble of molecular species (containing a dominant $PrP^{Sc}$ type recognized on Western blot and preferentially propagated by its usual host) from which a less populous subspecies may be selected by an alternative host (whose propagation is most favored in that environment), resulting in a strain shift. Given the degree of molecular diversity observed in prion isolates, (ii) seems more plausible. The degree of diversity may also be strain dependent, with some strains approaching clonality in some hosts. Different cellular populations within a single host would also offer different environments for strain selection. It has long been argued that infection of a host with a "lymphotrophic strain," which rapidly colonizes

lymphoid tissues with a long latency before neuroinvasion, is in part due to the need for selection of a "neuroinvasive strain" (*58*). Indeed, differences in $PrP^{Sc}$ type in different peripheral tissues are well described in vCJD, in which prion colonization of lymphoid tissues long precedes neurological disease (*59*–*61*).

Essentially, a "prion" may be considered a rare subtype of PrP polymer that has the appropriate properties and replication kinetics to overcome and evade host defenses and propagate exponentially. Other, nascent prions are rapidly degraded in vivo and disappear. The crucial role of host selection on the ensemble that exists in a prion inoculum may be why it remains so difficult to demonstrate generation of synthetic prions. In vitro–generated "synthetic prions" may consist overwhelmingly of species that will be rapidly eliminated in a host. This would explain why highly purified PrP amyloid fibrils are apparently of low specific infectivity.

### Can Prion Infectivity and Toxicity Be Uncoupled?

What is the cause of cell death in prion neurodegeneration? $PrP^{C}$ loss of function is not a sufficient cause: PrP-null mice ($Prnp^{0/0}$) are essentially normal (*62*). That adaptation during neurodevelopment in $Prnp^{0/0}$ mice might compensate for loss of $PrP^{C}$ function, while loss of $PrP^{C}$ function in the developed brain by its sequestration to $PrP^{Sc}$ might still be deleterious, is excluded by targeted $PrP^{C}$ depletion in neurons of adult mice (*63*). However, conversion of $PrP^{C}$ to $PrP^{Sc}$ is clearly central to pathogenesis because $Prnp^{0/0}$ mice are resistant to prion disease and do not propagate infectivity (*64*, *65*). So, is $PrP^{Sc}$ neurotoxic? In vitro neurotoxicity of $PrP^{Sc}$ and short PrP peptides has been reported (*66*, *67*), but several lines of in vivo evidence argue against direct toxicity: There are prion diseases in which $PrP^{Sc}$ levels in the brain are very low (*68*–*71*); the distribution of $PrP^{Sc}$ deposits does not necessarily mirror clinical signs, and $PrP^{Sc}$ is not directly toxic to neurons that do not express $PrP^{C}$ (*64*, *65*, *72*, *73*). Furthermore, knockout of neuronal $PrP^{C}$ expression during established brain infection completely protects mice from development of clinical disease, prevents neuronal loss, and reverses early spongiform neuropathology and behavioral abnormalities (*74*, *75*). Notably, this recovery occurs despite continued $PrP^{Sc}$ production and prion replication in glial cells, such that $PrP^{Sc}$ and prion titers in brain reach levels seen in end-stage disease in conventional mice (*74*). So, do neurons need to express $PrP^{C}$ and/or replicate prions themselves for toxicity to occur? Various mechanisms have been proposed, including aberrant signaling mediated by cross-linked cell surface $PrP^{C}$ and altered $PrP^{C}$ trafficking and topology (*76*–*79*). These alternatives are challenged, however, by the phenomenon of subclinical prion infection in wild-type animals. Such carrier states are sometimes established on prion inoculation of a second species (*80*–*82*). Wild-type mice, with normal neuronal $PrP^{C}$ expression and topology, inoculated with Sc237 hamster prions propagate mouse-adapted prions and yet live a normal life span without clinical disease. Prions propagate slowly but eventually reach titers (and levels of $PrP^{Sc}$) seen in end-stage conventional clinical disease (*80*). However, second passage of these prions in mice or hamsters results in conventional transmission with short incubation periods and 100% lethality (*80*).

### Linking Prion Propagation Kinetics to Neurotoxicity

A possible explanation is that $PrP^{Sc}$ is itself relatively inert, but toxicity resides in a smaller, labile, oligomeric PrP species (named $PrP^{L}$ for lethal), generated as an intermediate or side product during prion propagation (*80*, *82*). Neurotoxicity may require a critical $PrP^{L}$ concentration that is reached during conventional infections, but the slower kinetic of increase in infective titer in the subclinically infected mice may mean that toxic $PrP^{L}$ levels are not reached (Fig. 3). This hypothesis can accommodate the notable finding that $Prnp^{+/o}$ mice (with 50% of wild-type $PrP^{C}$ expression), when inoculated with RML mouse prions, develop levels of $PrP^{Sc}$ similar to those of wild-type mice yet remain well months after their wild-type counterparts succumb in a much more prolonged incubation period (Fig. 3). Furthermore, tga20 transgenic mice, which express $PrP^{C}$ at about 10-fold the levels of wild-type mice, succumb quickly to RML prions yet have low $PrP^{Sc}$ levels at end-stage disease (*83*) (Fig. 3).

The phenomena of prion propagation and toxicity can be considered from the standpoint of classical kinetic mechanisms. A formal model must accommodate experimental observations that demonstrate an apparent split between the identity of the propagating infectious agent and toxic species. It is increasingly proposed that the toxic species in amyloid diseases are intermediates on the pathway for formation of the amyloid structures (*84*). However, in this classical sense, such intermediates that occur before the favorable polymerization phase must reach a steady state, meaning that their concentration does not rise. That is, they are part of the priming process and not part of the autocatalytic phase.

Another, more promising mechanism can be proposed (Fig. 4) that accommodates both the autocatalytic nature of mammalian prion propagation and the lack of toxicity of $PrP^{Sc}$. In the protein-only hypothesis, it is axiomatic that $PrP^{Sc}$ acts as a template for the $PrP^{C} \rightarrow PrP^{Sc}$ conversion. However, if $PrP^{Sc}$ itself is the toxic agent, then the observed decoupling between the level of $PrP^{Sc}$ and the extent of pathology is hard to explain. Without challenging the protein-only mechanism, it is plausible that during the template-assisted progression from $PrP^{C}$ to $PrP^{Sc}$ an intermediate state ($PrP^{L}$) is formed. There are then four steps in the process of $PrP^{Sc}$ formation, and in its simplest manifestation this mechanism can be written:

$$PrP^{Sc} + PrP^{C} \xrightarrow{k_1} PrP^{Sc}{:}PrP^{C} \xrightarrow{k_2} PrP^{Sc}{:}PrP^{L} \rightarrow PrP^{Sc}{:}PrP^{Sc} \rightarrow PrP^{Sc} + PrP^{Sc}$$

In this model, $PrP^{L}$ is the toxic species, and the relative levels of toxicity and infectivity are

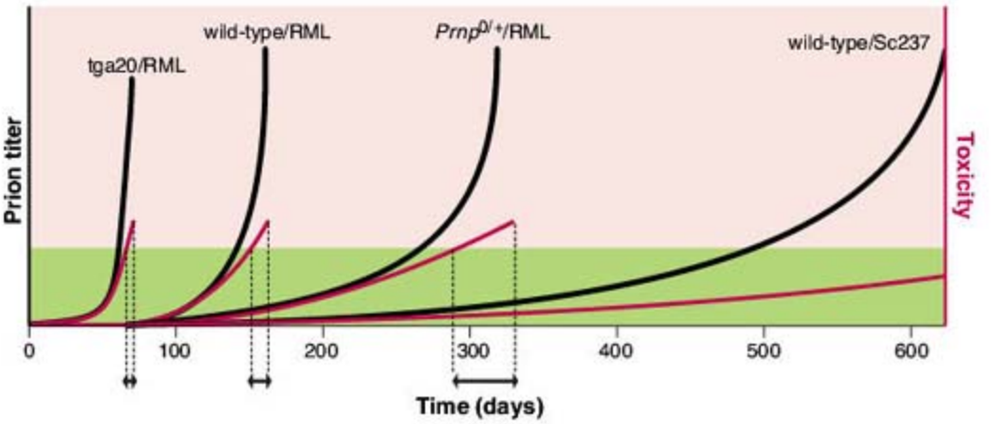


**Fig. 3.** Toxicity and prion titer. According to the proposed models illustrated in Fig. 4, toxicity is due to the buildup of a templated intermediate or side-product, $PrP^{L}$, while the infectious agent itself is not directly toxic. This graph illustrates (in a highly schematic form) the separation of the two phenomena. Prion titer is shown in black and $PrP^{L}$ concentration in red (*86*). Vertical dotted lines indicate time of onset of clinical signs and death. Green-shaded area denotes a level of $PrP^{L}$ that can be tolerated without clinical symptoms. The upper, pink-shaded region represents a level of $PrP^{L}$ that causes clinical illness; both titer and toxicity lines terminate at death of the animal. The incubation period is thus the time taken for $PrP^{L}$ levels to cross the boundary. Four host/strain combinations are exemplified: tga20 mice express $PrP^{C}$ at ~10-fold above levels seen in wild-type mice, whereas $Prnp^{0/+}$ mice express at 50% of wild-type levels. The effect of $PrP^{C}$ expression level on infection with mouse prions (RML strain) is demonstrated by the first three examples, whereas the fourth indicates wild-type mice infected with hamster (Sc237 strain) prions where prions propagate to high levels but without clinical onset during a normal life span (subclinical infection).

governed by the ratio of the initial rate of conversion ($k_1$) to the rate of maturation ($k_2$). Essentially, the proliferating, infectious $PrP^{Sc}$ acts as a catalytic surface upon which the intermediates form before they mature into the $PrP^{Sc}$ product. Consequently, their concentration will rise during the autocatalytic process because the population of the catalyst itself is rising exponentially. The difference between this model and the classical system is that formation of classical intermediates is not catalyzed by end products.

In the case of a subclinical infection, a relatively slow rate of initial conversion ($k_1$) would mean that the level of $PrP^{L}$ would be low, because its rate of loss through maturation ($k_2$) would be dominant. Thus, a large amount of $PrP^{Sc}$ or infectivity would build up, but with little toxicity (Fig. 3). By contrast, in a short-incubation disease such as RML prion infection in tga20 mice (with a high expression level of $PrP^{C}$), an increased rate of initial conversion leads to a rapid accumulation of $PrP^{L}$ and early death. In these circumstances, there is a higher probability of forming $PrP^{Sc}$:$PrP^{C}$ species through increased rates of encounter and, in turn, the level of $PrP^{Sc}$:$PrP^{L}$ is enhanced. Also, this model can explain transmission barrier (strain-adaptation) effects where primary passage is associated with very prolonged incubation periods (or indeed a subclinical infection without clinical disease in a normal life span), but where subsequent passage in the same type of host leads to a much shorter incubation period and high or complete lethality (*80*). Prion adaptation to the new host results in rapid prion propagation with an enhanced rate of initial conversion ($k_1$), which would then inevitably lead to a higher rate of formation of $PrP^{L}$ and a shorter incubation period. In this templated toxic intermediate model (Fig. 4A), the ability of a strain to propagate in a host depends on the rates of both initial conversion and of maturation; its ability to kill depends on the balance of these rates. An alternative, but related, model can be proposed in which $PrP^{Sc}$ is produced autocatalytically without toxic intermediates (Fig. 4B). However, $PrP^{Sc}$ then itself catalyzes the conversion of $PrP^{C}$ to $PrP^{L}$ as a toxic by-product. In this case, low-toxicity, high-titer infections would arise when the $PrP^{C}$-to-$PrP^{L}$ conversion rate is slow.

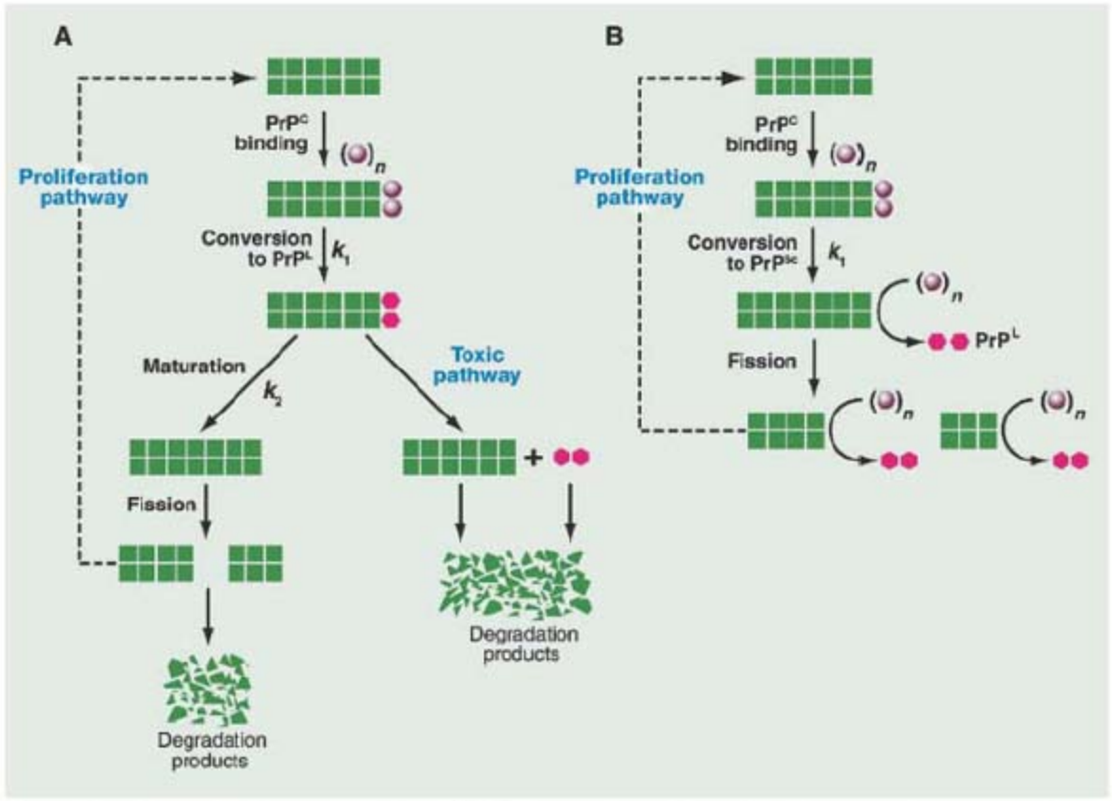


**Fig. 4.** Illustrative models for production of $PrP^{L}$: **(A)** Toxic templated intermediate. The most rudimentary model has four steps: binding, initial conversion, maturation, and fission. It is possible that $PrP^{L}$ must dissociate before it is toxic, but this is not a prerequisite. The number of $PrP^{C}$ molecules ($n$) joining, converting, and maturing per cycle does not affect the qualitative behavior of the model. **(B)** Toxic templated side product. In this model, $PrP^{Sc}$ acts as surface catalyst for the conversion of $PrP^{C}$ to $PrP^{L}$, but the latter is not an intermediate in the synthesis of $PrP^{Sc}$.

## General Model

How may all these phenomena be brought together? The recent experimental evidence for these emerging concepts now allows a general model for mammalian prions to be proposed (table S1), which accommodates the known phenomena of exponential propagation of infectivity, strain diversity and mutation, transmission barriers, and the uncoupling of infectivity from neurotoxicity, while remaining within the constraint of requiring only a single polypeptide to constitute all strains of infective and toxic species.

Essentially, the phenomena of prion disease pathogenesis can be explained in terms of the kinetics of prion propagation, determined by interplay between prion strain type (dominant $PrP^{Sc}$ polymer and its ensemble) and tissue/host environment (PrP sequence and expression level, modifier genes, and clearance mechanisms); selection of preferred conformers determines transmission barriers. Neurotoxicity is mediated by a PrP species, $PrP^{L}$, distinct from $PrP^{Sc}$ but catalyzed by it, and occurs when $PrP^{L}$ concentration passes a local toxic threshold. Rapid propagation (with a host-adapted strain and normal or high levels of host $PrP^{C}$ expression) results in severe neurotoxicity and death at strain-specific incubation periods. Slow propagation (after infection across a transmission barrier or with low host $PrP^{C}$ expression) results in low neurotoxicity and prolonged and more variable incubation periods or a persistent carrier state.

The concept of prion strain originated from biological experiments, but at a molecular level there may be quite distinct infectious PrP polymers ($PrP^{Sc}$ types) that cannot be distinguished by transmission studies in inbred laboratory mouse lines. Although in practice, the converse situation of biologically distinct prion strains associated with $PrP^{Sc}$ that cannot be biochemically differentiated by current methods will also be observed, under this general protein-only model such biochemical or biophysical differences in $PrP^{Sc}$ must exist, and the model would predict that differences would be observed with more discriminating molecular methods, challenging the historical primacy of biological classification of prion strains.

## Wider Implications

The impressive advances made in the field of yeast prions have clearly established a much wider biological importance of prion-like processes and have allowed direct experimental confirmation of molecular mechanisms proposed from work with mammalian prions. Understanding these phenomena will illuminate processes involving protein misfolding and aggregation, and protein-based inheritance, which clearly have far-reaching implications in pathobiology, aging, and the evolution of cellular processes. However, mammalian prions are distinctive. They are lethal pathogens par excellence—indeed, it is hard to think of other examples of infectious diseases with 100% mortality once the earliest clinical signs have developed.

Prions raise troubling questions in evolution. In particular, how did prions evolve as such

potent pathogens, complete with the ability to infect from the environment and travel to the brain? Conventional pathogens have evolved complex mechanisms to enable pathogenesis and evade destruction. If prions are composed purely of a polypeptide encoded by the host, how can they evolve? In essence, it seems that they had to arise de novo as an intact pathogenic system, and it is tempting to speculate that prions therefore represent malfunction of an evolved normal activity that has yet to be elucidated. That prions can encode information required to specify different discrete phenotypes opens up the possibility, perhaps likelihood, that other protein-based inheritance systems will have been exploited for benefit in mammalian evolution.

The more common neurodegenerative diseases also involve accumulation of aggregates of misfolded host-encoded proteins. It has long been speculated that some of these, and indeed other amyloidotic conditions, might be at least experimentally transmissible. Recent work has shown that brain extracts containing β-amyloid deposits taken from either Alzheimer's disease patients or transgenic mice expressing β-amyloid precursor protein (APP) induced β-amyloidosis and related pathology when injected into the brains of presymptomatic APP transgenic mice (*85*). The induced amyloidotic phenotype varied with host and source of agent, reminiscent of prion strains. It is interesting to speculate that distinct strains of β-amyloid may develop spontaneously in Alzheimer's disease and might contribute to phenotypic variability in patients. The possibility exists, therefore, that the general model proposed here may have wider relevance in other diseases involving protein misfolding and aggregation.

### References and Notes


1. J. S. Griffith, *Nature* **215**, 1043 (1967).
2. S. B. Prusiner, *Science* **216**, 136 (1982).
3. J. Collinge, *Annu. Rev. Neurosci.* **24**, 519 (2001).
4. S. Mead *et al.*, *Science* **300**, 640 (2003).
5. J. Collinge, K. C. L. Sidle, J. Meads, J. Ironside, A. F. Hill, *Nature* **383**, 685 (1996).
6. A. F. Hill *et al.*, *Nature* **389**, 448 (1997).
7. M. E. Bruce *et al.*, *Nature* **389**, 498 (1997).
8. J. Collinge, *Lancet* **354**, 317 (1999).
9. J. Collinge *et al.*, *Lancet* **367**, 2068 (2006).
10. S. J. Wroe *et al.*, *Lancet* **368**, 2061 (2006).
11. D. C. Gajdusek, *J. Neuroimmunol.* **20**, 95 (1988).
12. J. H. Come, P. E. Fraser, P. T. J. Lansbury, *Proc. Natl. Acad. Sci. U.S.A.* **90**, 5959 (1993).
13. J. T. Jarrett, P. T. J. Lansbury, *Cell* **73**, 1055 (1993).
14. G. Legname *et al.*, *Science* **305**, 673 (2004).
15. I. H. Pattison, in *Slow, Latent and Temperate Virus Infections, NINDB Monograph 2*, C. J. Gajdusek, C. J. Gibbs, M. P. Alpers, Eds. (U.S. Government Printing Office, Washington, DC, 1965), pp. 249–257.
16. S. B. Prusiner *et al.*, *Cell* **63**, 673 (1990).
17. J. Collinge, M. S. Palmer, A. J. Dryden, *Lancet* **337**, 1441 (1991).
18. M. S. Palmer, A. J. Dryden, J. T. Hughes, J. Collinge, *Nature* **352**, 340 (1991).
19. M. Bruce *et al.*, *Philos. Trans. R. Soc. London B Biol. Sci.* **343**, 405 (1994).
20. J. Collinge *et al.*, *Nature* **378**, 779 (1995).
21. H. Fraser, A. G. Dickinson, *J. Comp. Pathol.* **83**, 29 (1973).
22. R. A. Bessen, R. F. Marsh, *J. Virol.* **66**, 2096 (1992).
23. R. A. Bessen, R. F. Marsh, *J. Virol.* **68**, 7859 (1994).
24. P. Parchi *et al.*, *Ann. Neurol.* **39**, 767 (1996).
25. G. C. Telling *et al.*, *Science* **274**, 2079 (1996).
26. J. Safar *et al.*, *Nat. Med.* **4**, 1157 (1998).
27. T. Kuczius, M. H. Groschup, *Mol. Med.* **5**, 406 (1999).
28. J. Safar, F. E. Cohen, S. B. Prusiner, *Arch. Virol.* **16**, 227 (2000).
29. J. D. F. Wadsworth *et al.*, *Nat. Cell Biol.* **1**, 55 (1999).
30. D. A. Kocisko *et al.*, *Nature* **370**, 471 (1994).
31. R. A. Bessen *et al.*, *Nature* **375**, 698 (1995).
32. J. Castilla, P. Saa, C. Hetz, C. Soto, *Cell* **121**, 195 (2005).
33. A. Khalili-Shirazi *et al.*, *J. Gen. Virol.* **86**, 2635 (2005).
34. D. Westaway *et al.*, *Cell* **76**, 117 (1994).
35. Our unpublished data with aged tga20 mice.
36. G. C. Telling *et al.*, *Genes Dev.* **10**, 1736 (1996).
37. K. E. Nazor *et al.*, *EMBO J.* **24**, 2472 (2005).
38. In these experiments, 30 μl of PrP (0.5 mg/ml) was inoculated, which equates to $>10^{14}$ molecules. An infectious unit of bona fide prion material approximates to $10^4$ to $10^5$ PrP molecules. Therefore, if composed primarily of infectious material, such a synthetic prion inoculum would contain $10^9$ to $10^{10}$ infectious units. If dilution of the synthetic prion inoculum 10-fold resulted in no transmissions, this would imply <10 infectious units per undiluted inoculum and therefore that prions composed <1 in $10^{-8}$ of the material.
39. R. B. Wickner *et al.*, *Annu. Rev. Genet* **38**, 681 (2004).
40. C. Y. King, R. Diaz-Avalos, *Nature* **428**, 319 (2004).
41. M. Tanaka, P. Chien, N. Naber, R. Cooke, J. S. Weissman, *Nature* **428**, 323 (2004).
42. R. Krishnan, S. L. Lindquist, *Nature* **435**, 765 (2005).
43. R. Diaz-Avalos, C. Y. King, J. Wall, M. Simon, D. L. Caspar, *Proc. Natl. Acad. Sci. U.S.A.* **102**, 10165 (2005).
44. M. Tanaka, P. Chien, K. Yonekura, J. S. Weissman, *Cell* **121**, 49 (2005).
45. A. Brachmann, U. Baxa, R. B. Wickner, *EMBO J.* **24**, 3082 (2005).
46. K. Wuthrich, R. Riek, *Adv. Protein Chem.* **57**, 55 (2001).
47. M. Tanaka, S. R. Collins, B. H. Toyama, J. S. Weissman, *Nature* **442**, 585 (2006).
48. D. M. Taylor *et al.*, *Arch. Virol.* **139**, 313 (1994).
49. J. D. Wadsworth *et al.*, *Science* **306**, 1793 (2004).
50. M. E. Bruce, *Br. Med. Bull.* **49**, 822 (1993).
51. L. L. Hosszu *et al.*, *J. Biol. Chem.* **279**, 28515 (2004).
52. E. A. Asante *et al.*, *EMBO J.* **21**, 6358 (2002).
53. S. E. Lloyd *et al.*, *J. Gen. Virol.* **85**, 2471 (2004).
54. R. H. Kimberlin, C. A. Walker, *J. Gen. Virol.* **39**, 487 (1978).
55. M. Polymenidou *et al.*, *Lancet Neurol.* **4**, 805 (2005).
56. H. M. Yull *et al.*, *Am. J. Pathol.* **168**, 151 (2006).
57. D. M. Taylor, K. Fernie, I. McConnell, P. J. Steele, *Vet. Microbiol.* **64**, 33 (1998).
58. H. Fraser, M. E. Bruce, D. Davies, C. F. Farguhar, P. A. McBride, in *Prion Diseases of Humans and Animals*, S. B. Prusiner, J. Collinge, J. Powell, B. Anderton, Eds. (Horwood, London, 1992), chap. 22.
59. D. A. Hilton, E. Fathers, P. Edwards, J. W. Ironside, J. Zajicek, *Lancet* **352**, 703 (1998).
60. A. F. Hill *et al.*, *Lancet* **353**, 183 (1999).
61. J. D. F. Wadsworth *et al.*, *Lancet* **358**, 171 (2001).
62. H. Bueler *et al.*, *Nature* **356**, 577 (1992).
63. G. R. Mallucci *et al.*, *EMBO J.* **21**, 202 (2002).
64. H. Bueler *et al.*, *Cell* **73**, 1339 (1993).
65. J. C. Manson, A. R. Clarke, P. A. McBride, I. McConnell, J. Hope, *Neurodegeneration* **3**, 331 (1994).
66. G. Forloni *et al.*, *Nature* **362**, 543 (1993).
67. C. Hetz, M. Russelakis-Carneiro, K. Maundrell, J. Castilla, C. Soto, *EMBO J.* **22**, 5435 (2003).
68. J. Collinge *et al.*, *Lancet* **346**, 569 (1995).
69. R. Medori *et al.*, *Neurology* **42**, 669 (1992).
70. K. K. Hsiao *et al.*, *Science* **250**, 1587 (1990).
71. C. I. Lasmézas *et al.*, *Science* **275**, 402 (1997).
72. A. Sailer, H. Bueler, M. Fischer, A. Aguzzi, C. Weissmann, *Cell* **77**, 967 (1994).
73. S. Brandner *et al.*, *Nature* **379**, 339 (1996).
74. G. Mallucci *et al.*, *Science* **302**, 871 (2003).
75. G. R. Mallucci *et al.*, *Neuron* **53**, 325 (2007).
76. L. Solforosi *et al.*, *Science* **313**, 1514 (2004).
77. R. S. Hegde *et al.*, *Science* **279**, 827 (1998).
78. J. Ma, R. Wollmann, S. Lindquist, *Science* **298**, 1781 (2002).
79. B. Chesebro *et al.*, *Science* **308**, 1435 (2005).
80. A. F. Hill *et al.*, *Proc. Natl. Acad. Sci. U.S.A.* **97**, 10248 (2000).
81. R. Race, A. Raines, G. J. Raymond, B. Caughey, B. Chesebro, *J. Virol.* **75**, 10106 (2001).
82. A. F. Hill, J. Collinge, *Trends Microbiol.* **11**, 578 (2003).
83. M. Fischer *et al.*, *EMBO J.* **15**, 1255 (1996).
84. C. Haass, D. J. Selkoe, *Nat. Rev. Mol. Cell Biol.* **8**, 101 (2007).
85. M. Meyer-Luehmann *et al.*, *Science* **313**, 1781 (2006).
86. Prion titer curves shown with exponential rise and no plateau phase are illustrative only. However, the model is not dependent on specific kinetics. $PrP^*$ remains hypothetical and cannot yet be assayed directly.


87. We are grateful to J. Wadsworth for discussion and to R. Young for preparation of figures. J.C. is a director of, and both J.C. and A.R.C. are shareholders in, D-Gen Ltd., a research-based biomedical company that identifies, develops, and exploits proprietary diagnostic and therapeutic targets and technologies for prion-related diseases.


### Supporting Online Material

www.sciencemag.org/cgi/content/full/318/5852/930/DC1
Table S1

10.1126/science.1138718

# A Cretaceous Hoofed Mammal from India

G. V. R. Prasad,[1]* O. Verma,[1] A. Sahni,[2] V. Parmar,[1] A. Khosla[2]

Ungulate or hoofed mammals represent the most important herbivores of Cenozoic land mammal communities. Condylarths or archaic ungulates are a paraphyletic group regarded as an ancestral or sister taxon to living ungulate mammals (*1*) and are known by fossils from the Early Paleocene of North America and South America, the Late Paleocene and Eocene of Europe, and the Eocene of Africa and possibly Australia. The earliest definitive ungulates represented by *Protungulatum*, *Oxyprimus*, *Baioconodon*, and *Mimatuta* (*1*, *2*) come from the Early Paleocene (Puercan) of northeastern Montana. No Cretaceous condylarth has yet been documented. Here, we describe an isolated lower molar ($m_1$ or $m_2$) of a condylarth mammal from the Late Cretaceous (Maastrichtian) lacustrine rocks interbedded with Deccan volcanic flows of Central India [Supporting Online Material (SOM) text and fig. S1]. The tooth is cataloged as VPL/JU/IM/31 and deposited in the Vertebrate Paleontology Laboratory of Jammu University.

**Class:** Mammalia Linnaeus, 1758. **Order:** Condylarthra Cope, 1881. **Family:** Incertae Sedis. *Kharmerungulatum vanvaleni* genus et species nova.

**Holotype.** VPL/JU/IM/31, isolated right lower molar.

**Generic Diagnosis.** Asymmetrical trigonid wider and longer than talonid, bulbous cusps, paraconid slightly labial to the lingual margin, voluminous protoconid twice as large as metaconid and closely appressed to it, metaconid slightly posterior to protoconid with the posterior trigonid wall slightly oblique to the long axis, entoconid smaller than hypoconulid and basally conjoined to it forming an oblique posterolingual crest, hypoconid is the most voluminous talonid cusp, talonid basin partially closed lingually, obliquely transverse talonid groove, size smaller as compared to other archaic ungulates (SOM text).

**Etymology.** Genus named after the nearby Kharmer River; species named in honor of Leigh Van Valen.

**Specific Diagnosis.** As for genus.

Basal expansion and sidewall convexity of the lower molars are conspicuous differences between archaic ungulates and Cretaceous eutherians such as *Cimolestes*, *Procerberus*, *Batodon*, *Gypsonictops*, and *Deccanolestes*. Archaic ungulates developed the ability to crush and grind food through reduced height difference between the trigonid and talonid, cusp bunodonty, the possession of a large hypoconid, and characteristic abrasion causing beveling of cusp apices (*1*). The morphology of *Kharmerungulatum* (Fig. 1, A to F) is like that of the lower molar morphology of archaic ungulates, but the latter are relatively larger and have more bunodont cusps. *Kharmerungulatum* retains many plesiomorphic characters that occur variably in *Protungulatum*, *Oxyprimus*, *Baioconodon*, and *Mimatuta*. These include trigonid moderately taller than the talonid; paraconid slightly labial to the lingual margin and well separated from the metaconid, as in *Mimatuta*, *Protungulatum gorgun*, and *Baioconodon middletoni*; obliquely oriented paracristid, as in *Protungulatum* and *Oxyprimus*; obliquely oriented posterior trigonid wall with a slightly posteriorly developed metaconid and asymmetrical trigonid, as in *Protungulatum donnae*; short entocristid partially closing the talonid lingually, as in *Protungulatum*, *Oxyprimus*, and *Baiconodon*; and a cristid obliqua joining the posterior trigonid wall below the posterolabial base of the metaconid. However, in relative dimensions of talonid cusps and closely appressed entoconid and hypoconulid forming a posterolingual crest, *Kharmerungulatum* is also comparable to South American *Molinodus* (*3*).

Among all species of archaic ungulates, *Kharmerungulatum* is closest to *P. gorgun* in cusp morphology except that it lacks cingulids [figure 3F of (*4*)] and to *Baioconodon* in having a talonid shorter and narrower than the trigonid (SOM text). We consider *Kharmerungulatum* to represent an early stage in the evolution of ungulates.

The presence of an archaic ungulate in the latest Cretaceous of India may reflect that (i) archaic ungulates had a pan-Gondwanan distribution, and their absence in other landmasses may be an artifact of limited field investigations; (ii) *Kharmerungulatum* immigrated to India from Western Asia, which had a diversified assemblage of zhelestids (85 million years ago) regarded by some as ancestral to archaic ungulates (*5*), although any connection is disputed (*6*); and (iii) the drifting Indian subcontinent may have served as a center of origin for many mammalian orders and other vertebrate and plant groups.

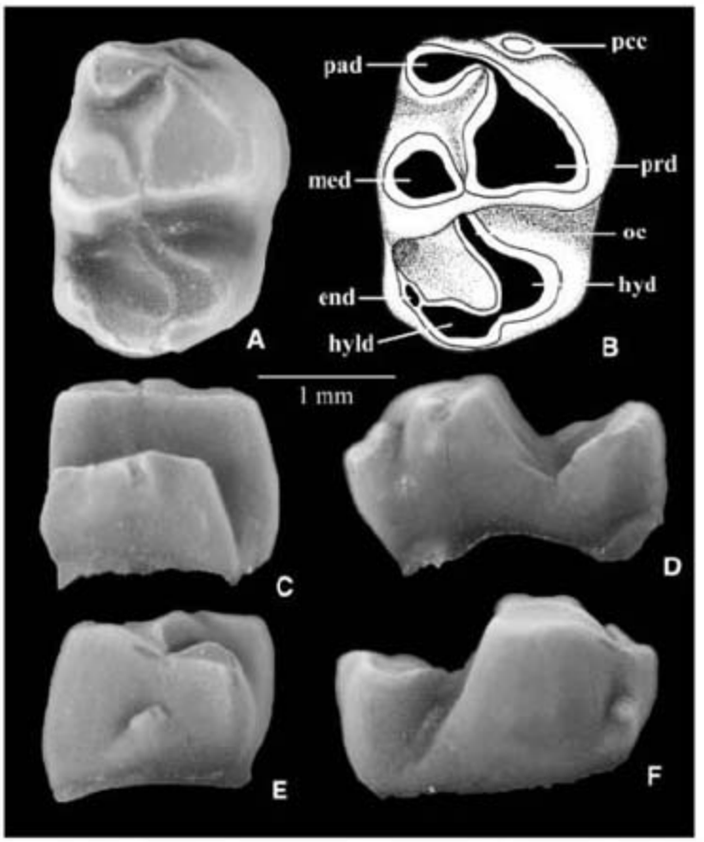


**Fig. 1.** Holotype of *Kharmerungulatum vanvaleni* genus et species nova, isolated right lower molar ($m_1$ or $m_2$, VPL/JU/IM/31). End, entoconid; hyd, hypoconid; hyld, hypoconulid; med, metaconid; oc, cristid obliqua; pad, paraconid; pcc, precingulid cuspule; and prd, protoconid. **(A)** Occlusal view. **(B)** Line drawing of (A). **(C)** Posterior view. **(D)** Lingual view. **(E)** Anterior view. **(F)** Labial view.


## References and Notes

1. J. D. Archibald, *Univ. Calif. Publ. Geol. Sci.* **122**, 1 (1982).
2. L. Van Valen, *Evol. Theory* **4**, 45 (1978).
3. C. de Muizon, R. L. Cifelli, *Geodiversitas* **22**, 47 (2000).
4. J. J. Eberle, J. A. Lillegraven, *Rocky Mount. Geol.* **33**, 49 (1998).
5. J. D. Archibald, *Science* **272**, 1150 (1996).
6. J. R. Wible, G. W. Rougier, M. J. Novacek, R. J. Asher, *Nature* **447**, 1003 (2007).


7. G.V.R.P. acknowledges support from the Department of Science and Technology (DST), New Delhi (grant no. SR/S4/ES/24/2002). A.S. thanks the Indian National Science Academy for grant no. SP/SS/2006/2841, and O.V. and A.K. are thankful to the Council of Scientific and Industrial Research, New Delhi and DST, respectively.

## Supporting Online Material

www.sciencemag.org/cgi/content/full/318/5852/937/DC1
SOM Text
Fig. S1
References

15 August 2007; accepted 27 September 2007
10.1126/science.1149267

[1]Department of Geology, University of Jammu, Jammu 180 006, India. [2]Centre of Advanced Study in Geology, Panjab University, Chandigarh 160 014, India.

*To whom correspondence should be addressed. E-mail: guntupalli.vrprasad@gmail.com

# Correlation of the Highest-Energy Cosmic Rays with Nearby Extragalactic Objects

The Pierre Auger Collaboration*

## AUTHORS' SUMMARY

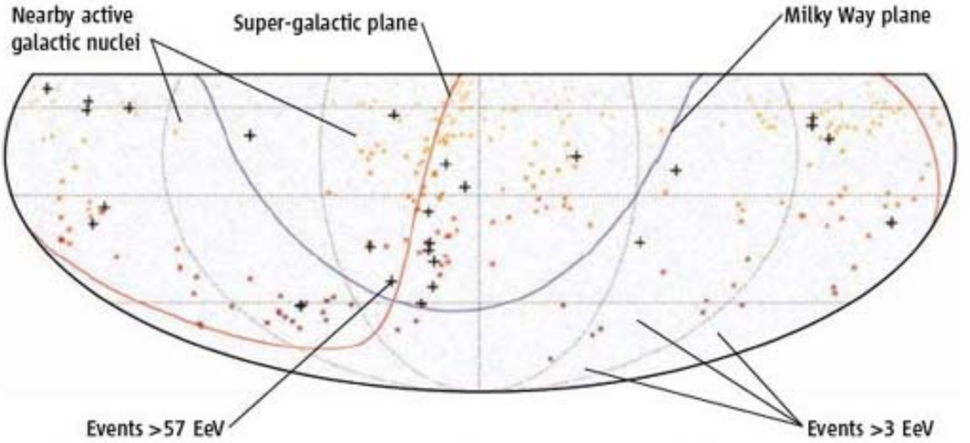


Sky map (*2*) showing cosmic rays detected by the Pierre Auger Observatory. Low-energy cosmic rays appear to originate from evenly distributed sources (blue dots), but the origins of the highest-energy events (crosses) correlate with the distribution of local matter as represented by nearby active galactic nuclei (red stars). Thus, active galactic nuclei are a likely source of these rare high-energy cosmic rays.

Cosmic rays are particles and nuclei that bombard the Earth from space in all directions (*1*). A few have astounding energies—beyond 100 EeV (1 EeV = 1 exa-electron volt = $10^{18}$ eV)—orders of magnitude beyond even the future capabilities of any earthly particle accelerator. Such energies are so extreme that they could arise in only the most violent places in the universe. One possible location is within active galactic nuclei (AGN), galaxies hosting central black holes that feed on gas and stars and may eject vast plasma jets into intergalactic space.

As cosmic rays propagate, the highest-energy particles interact strongly with the ubiquitous cosmic background radiation and lose some energy. Thus, they can only travel limited distances and, consequently, their flux is suppressed (the "GZK effect"). So the survival of the highest-energy cosmic rays as they traverse space is in itself a puzzle. Simply stated, we don't know what they are, where they came from, or how they got here from there.

The highest-energy cosmic rays are so rare that in the last 50 years, only a handful of 100-EeV particles have been detected. The low flux (only a few per $km^2$ on Earth per millennium) renders their direct detection infeasible. Instead, instruments with extremely large collecting areas are deployed and sample the shower of secondary particles produced when the primary cosmic ray collides with Earth's atmosphere. The Pierre Auger Observatory stretches over 3000 $km^2$ in western Argentina, an area similar to that of Rhode Island. It measures extensive air showers both on the ground with 1600 detectors spaced 1.5 km apart and in the air, viewing the brief flash of nitrogen molecules de-exciting after the shower passes by (the same radiation is seen from a different stimulus and over longer time scales as the Aurora Borealis). The Pierre Auger Observatory uses these two detection techniques routinely at the same time. The size of the data set now exceeds that from all earlier experiments.

The direction of the primary cosmic ray can be reconstructed with good precision—to within 1° or so—by the ground detectors. Most cosmic-ray particles are charged and so their trajectories are bent by the magnetic fields in space. For particles with energies above a few tens of EeV, the deflection is, however, small enough that the prospect of identifying possible sources becomes a reality.

Since 2004, the Auger Observatory has collected a million cosmic-ray events, and about 80 had energies exceeding 40 EeV, the energy at which we expect to begin to see the flux suppression of the GZK effect. First, we examined the data gathered before June 2006. We explored the amount of correlation between the arrival directions and the positions of known AGN by tuning several factors: a cutoff for the maximum distance of an AGN, a cutoff for the minimum energy of cosmic rays, and the angular separation of an event from some AGN.

We found a strong association between the cosmic-ray directions and nearby AGN. Of 15 events with energies greater than about 60 EeV, 12 were located within 3.1° of AGN closer than 75 Mpc from Earth (about 250 million light-years). The likelihood of a random isotropic set of arrival directions conspiring to fool us this much was small. We fixed the values of the correlation parameters and applied them to new data collected after June 2006. Data collected more recently, until August 2007 (see the figure), confirmed the correlation.

Interpretation of these results merits some caution. We used a catalog of AGN that is known to be incomplete, especially in directions in which we peer through the dusty plane of our Galaxy and beyond 300 million light-years away from Earth. (It is notable that most of the few events that do not appear to be near AGN are indeed somewhat near the Galactic plane.) The AGN themselves tend to be distributed among the nearby galaxies, and so based on the statistics of our present data we can only declare that the cosmic-ray sources are correlated with the distribution of nearby matter, including AGN. However, because of the energetic processes within them, AGN have long been considered as likely sources of cosmic rays. Our data suggest that they remain the prime candidates.

### Summary References

1. J. W. Cronin, T. K. Gaisser, S. Swordy, *Sci. Am.* **276**, 44 (January 1997).
2. Equal areas on this plot represent equal exposure on the sky. The declination is on the vertical axis. Declinations 0°, −30°, and −60° are marked (from the top) (the observatory zenith is close to dec = −30°). The observatory has more exposure to the AGN indicated by darker stars than those shown in lighter shades of red.

CREDIT: C. BICKEL/*SCIENCE*

FULL-LENGTH ARTICLE

**Using data collected at the Pierre Auger Observatory during the past 3.7 years, we demonstrated a correlation between the arrival directions of cosmic rays with energy above $6 \times 10^{19}$ electron volts and the positions of active galactic nuclei (AGN) lying within ~75 megaparsecs. We rejected the hypothesis of an isotropic distribution of these cosmic rays with at least a 99% confidence level from a prescribed a priori test. The correlation we observed is compatible with the hypothesis that the highest-energy particles originate from nearby extragalactic sources whose flux has not been substantially reduced by interaction with the cosmic background radiation. AGN or objects having a similar spatial distribution are possible sources.**

Cosmic rays are energetic particles and nuclei from space that strike the Earth's atmosphere. Their energies vary from a few $10^8$ eV to beyond $10^{20}$ eV. The flux of cosmic rays at Earth decreases very rapidly with energy, from a few particles per square centimeter per second in the low-energy region to less than one particle per square kilometer per century above $10^{20}$ eV. The identification of the sources of ultrahigh-energy cosmic rays (UHECR) with energies ~$10^{20}$ eV has been a great challenge since they were first observed in 1962 (*1*). Because cosmic rays at these energies are not expected to be confined by magnetic fields in the disk of our galaxy, and indeed no significant excess from the direction of the Milky Way has been observed, it is likely that they originate outside the Galaxy. Until now, there has been no experimental confirmation of this hypothesis.

Because of their very low flux, UHECR can only be detected through their interaction with the Earth's atmosphere, producing a cascade of billions of particles that excite nitrogen molecules in the air along their path and spread over a large area when they reach the ground. The Pierre Auger Southern Observatory (*2*), now nearing completion in Argentina, was designed to simultaneously observe the shower particles at ground level and the associated fluorescence light generated in the atmosphere. A large array of 1600 surface detectors (SDs), laid out as an equilateral triangular grid with 1500-m spacing, covers an area of 3000 km$^2$ and detects the particles at ground level by means of the Cherenkov radiation they produce in water. At each of four sites on the periphery of the instrumented area, six inward-facing optical telescopes observe the sky on clear moonless nights. These devices measure the atmospheric fluorescence light produced as an extensive air shower passes through the field of view. The two techniques—the SDs and the fluorescence detectors (FDs)—are complementary, and also provide cross-checks and redundancy in the measurement of air-shower parameters. The SD measures the two-dimensional lateral structure of the shower at ground level, whereas the FD records the longitudinal profile of the shower during its development through the atmosphere. In Fig. 1, we present the layout of the Observatory as of 30 September 2007.

The Pierre Auger Southern Observatory has been taking data stably since January 2004. The large exposure of its ground array, combined with accurate energy and arrival-direction measurements, calibrated and verified from the hybrid operation with the fluorescence detectors, provides an opportunity to explore the spatial correlation between cosmic rays and their sources in the sky.

If cosmic rays with the highest energies are predominantly protons or nuclei, only sources closer than about 200 Mpc from Earth can contribute appreciably to the observed flux above 60 EeV (1 EeV = $10^{18}$ eV). Protons or nuclei with energies above 60 EeV interact with the cosmic microwave background (*3*–*5*), leading to a strong attenuation of their flux from distant sources. This attenuation is known as the Greisen, Zatsepin, and Kuzmin (GZK) effect, from the names of the three physicists that predicted it. If the sources of the most energetic cosmic rays are relatively nearby and are not uniformly distributed, then an anisotropic arrival distribution is expected, provided the particles have a sufficiently small charge and a sufficiently high energy for their directions to be minimally perturbed by intervening magnetic fields.

Anisotropy of the cosmic rays with the highest energies could manifest as clustering of events from individual point sources or through the correlation of arrival directions with a collection of astronomical objects. The Akeno Giant Air Shower Array (AGASA) Collaboration claimed some excess of clustering at small angular scales compared to isotropic expectations (*6*), but this was not supported by data recorded by the HiRes experiment (*7*). Analyses of data recorded by several air-shower experiments revealed a general correlation with the direction of the supergalactic plane (*8*, *9*), where several nearby galaxies cluster, but with limited statistical significance.

AGN have long been considered sites where energetic-particle production might take place and where protons and heavier nuclei could be accelerated up to the highest energies yet measured (*10*, *11*). Here, we report the observation of a correlation between the arrival directions of the cosmic rays with highest energies measured by the Pierre Auger Observatory and the positions of nearby AGN from the 12th edition of the catalog of quasars and active nuclei by Véron-Cetty and Véron (V-C catalog) (*12*).

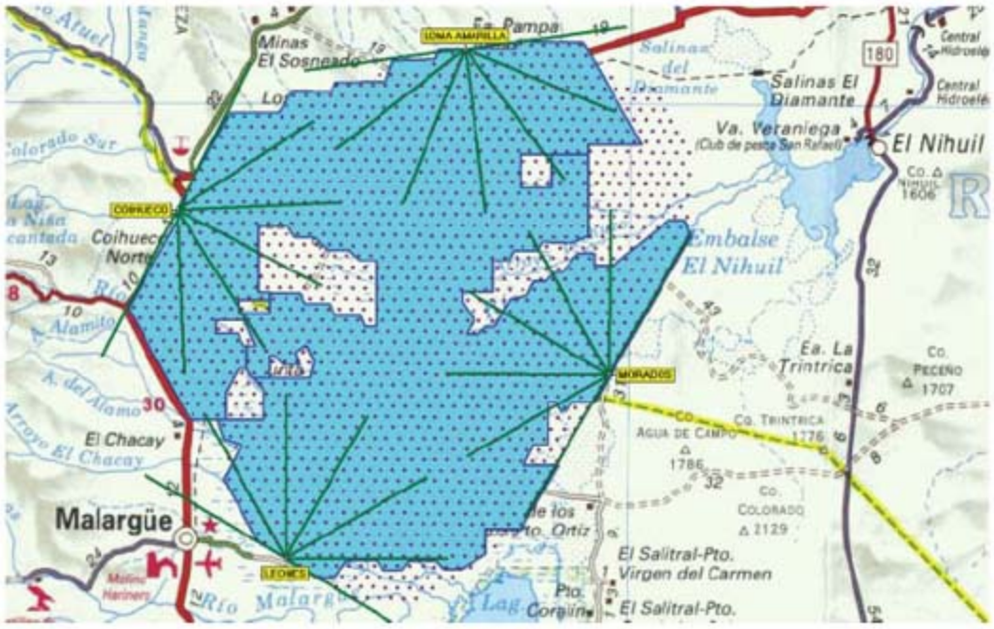


**Fig. 1.** Layout of the Pierre Auger Southern Observatory. The dots represent the position of each of the 1600 SD stations. The 1430 SD stations deployed and activated as of 30 September 2007 lie in the area shaded blue. The 4 FD sites are labeled in yellow, with green lines indicating the field of view of the six telescopes at each site. To give the scale of the Observatory, the lengths of the green line correspond to 20 km.

Observatorio Pierre Auger, Avenida San Martín Norte 304, (5613) Malargüe, Mendoza, Argentina. E-mail: auger_collaboration2@fnal.gov

*The full list of authors and their affiliations appears at the end of this paper.

**Data set and method.** The data set analyzed here consists of the cosmic-ray events recorded by the surface array of the Observatory from 1 January 2004 to 31 August 2007. It contains 81 events with reconstructed energies above 40 EeV and zenith angles smaller than 60°. The integrated exposure is $9.0 \times 10^3$ km$^2$ sr year.

We only use recorded events if they meet strict criteria with regard to the quality of the reconstruction of their energy and direction. The selection of those events is done via a quality trigger (*13*), which is only a function of the topology of the footprint of the event on the ground. This trigger requires that the detector with the highest signal must be surrounded by five active nearest neighbors, and that the reconstructed shower core be inside an active equilateral triangle of detectors. This represents an efficient quality cut while guaranteeing that no crucial information is missed for the shower reconstruction.

The arrival direction of a cosmic ray is a crucial ingredient in our study. The event direction is determined by a fit of the arrival times of the shower front at the SD. The precision achieved in the arrival direction depends on the clock resolution of each detector and on the fluctuations in the time of arrival of the first particle (*14*). The angular resolution is defined as the angular aperture around an arrival direction of cosmic rays within which 68% of the showers are reconstructed. This resolution has been verified experimentally with events for which two independent geometrical reconstructions can be performed. The first test uses hybrid events, which are measured simultaneously by the SD and the FD; the second one uses events falling in a special region of our array where two surface stations are laid in pairs 11 m apart at each position. Events that triggered at least six surface stations have energies above 10 EeV and an angular resolution better than 1° (*15*, *16*).

The energy of each event is determined in a two-step procedure. The shower size $S$, at a reference distance and zenith angle, is calculated from the signal detected in each surface station and then converted to energy with a linear calibration curve based on the fluorescence telescope measurements (*17*). The uncertainty resulting from the adjustment of the shower size, the conversion to a reference angle, the fluctuation from shower to shower, and the calibration curve amounts to about 18%. The absolute energy scale is given by the fluorescence measurements and has a systematic uncertainty of 22% (*18*). The largest systematic uncertainty arises primarily from an incomplete knowledge of the yield of photons from the fluorescence of atmospheric nitrogen (14%), the telescope calibration (9.5%), and the reconstruction procedure (10%). Additional uncertainty in the energy scale for the set of high-energy events used in the present analysis is due to the relatively low statistics available for calibration in this energy range.

Events with energy above 3 EeV are recorded with nearly 100% efficiency over the area covered by the surface array. The nonuniformity of the exposure in right ascension is below 1%, negligible in the context of the present analysis. The dependence of the exposure on declination is calculated from the latitude of the detector and the full acceptance for showers up to 60° zenith angle.

A key element of our study is the probability $P$ for a set of $N$ events from an isotropic flux to contain $k$ or more events at a maximum angular distance $\psi$ from any member of a collection of candidate point sources. $P$ is given by the cumulative binomial distribution $\sum_{j=k}^{N} C_j^N p^j (1-p)^{N-j}$, where the parameter $p$ is the fraction of the sky (weighted by the exposure) defined by the regions at angular separation less than $\psi$ from the selected sources.

We analyze the degree of correlation of our data with the directions of AGN referenced in the V-C catalog (*12*). This catalog does not contain all existing AGN and is not an unbiased statistical sample of them. This is not an obstacle to demonstrating the existence of anisotropies but may affect our ability to identify the cosmic-ray sources unambiguously. The catalog contains 694 active galaxies with redshifts $z \leq 0.024$, corresponding to distances $D$ smaller than 100 Mpc (*19*). At larger distances, and around the Galactic plane, the catalog is increasingly incomplete.

**Exploration and confirmation.** Using data acquired between 1 January 2004 and 26 May 2006, we scanned for the minimum of $P$ in the three-dimensional parameter space defined by maximum angular separations $\psi$, maximum redshifts $z_{\max}$, and energy thresholds $E_{\text{th}}$. The lower limit for the scan in $\psi$ corresponds to the angular resolution of the surface array. Our scan in energy threshold and maximum distance was motivated by the assumption that cosmic rays with the highest energies are the ones that are least deflected by intervening magnetic fields and that have the smallest probability of arrival from very distant sources due to the GZK effect (*3*, *4*).

We found a minimum of $P$ for the parameters $\psi = 3.1°$, $z_{\max} = 0.018$ ($D_{\max} \leq 75$ Mpc), and $E_{\text{th}} = 56$ EeV. For these values, 12 events among 15 correlate with the selected AGN, whereas only 3.2 were expected by chance if the flux were isotropic. This observation motivated the definition of a test to validate the result with an independent data set, with parameters specified a priori, as is required by the Auger source and anisotropy search methodology (*20*, *21*).

The Auger search protocol was designed as a sequence of tests to be applied after the observation of each new event with energy above 56 EeV. The total probability of incorrectly rejecting the isotropy hypothesis along the sequence was set to a maximum of 1%. The parameters for the prescribed test were chosen as those, given above, that led to the minimum of $P$ in the exploratory scan. The probability of a chance correlation at the chosen angular scale of a single cosmic ray with the selected astronomical objects is $p = 0.21$ if the flux were isotropic. The test was applied to data collected between 27 May

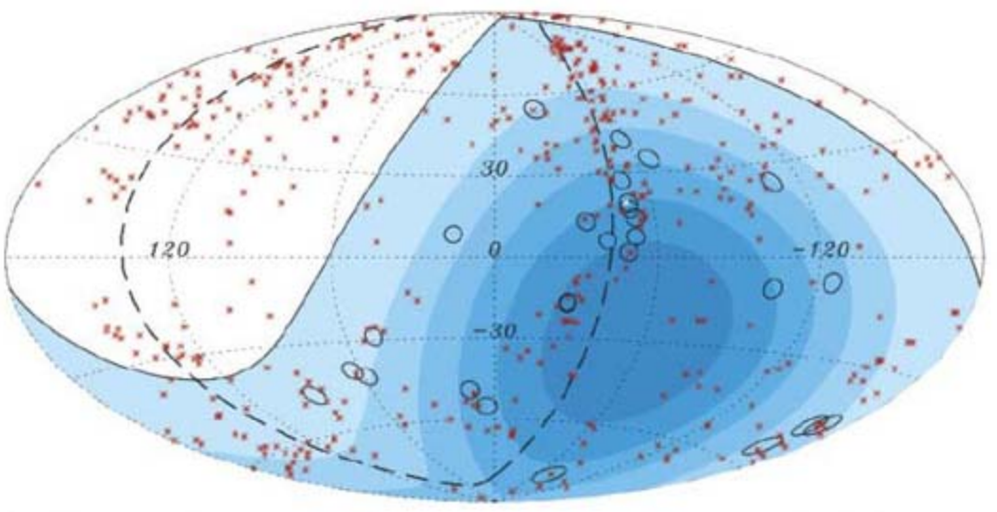


**Fig. 2.** Aitoff projection of the celestial sphere in galactic coordinates with circles of radius 3.1° centered at the arrival directions of the 27 cosmic rays with highest energy detected by the Pierre Auger Observatory. The positions of the 472 AGN (318 in the field of view of the Observatory) with redshift $z \leq 0.018$ ($D < 75$ Mpc) from the 12th edition of the catalog of quasars and active nuclei (*12*) are indicated by red asterisks. The solid line represents the border of the field of view (zenith angles smaller than 60°). Darker color indicates larger relative exposure. Each colored band has equal integrated exposure. The dashed line is the supergalactic plane. Centaurus A, one of our closest AGN, is marked in white.

2006 and 31 August 2007, with exactly the same reconstruction algorithms, energy calibration, and quality cuts for event selection as in the exploratory scan. In these independent data, there are 13 events with energy above 56 EeV, of which 8 have arrival directions closer than 3.1° from the positions of AGN less than 75 Mpc away, with 2.7 expected on average. The probability that this configuration would occur by chance if the flux were isotropic is $1.7 \times 10^{-3}$. Following our search protocol and based on the independent data set alone, we reject the hypothesis of isotropy in the distribution of the arrival directions of cosmic rays with the highest energies with at least a 99% confidence level.

**Results.** Having determined that an anisotropy exists, based on the a priori prescription, we rescanned the full data set from 1 January 2004 to 31 August 2007, using the method described above to substantiate the observed correlation. We used steps of 0.1° in $\psi$, in the range $1° \leq \psi \leq 8°$, and 0.001 in $z_{max}$, in the range $0 \leq z_{max} \leq 0.024$. We also used a newer version of our reconstruction and calibration algorithm that gives slightly different reconstructed directions and energies. These small differences, well within our reconstruction uncertainty, modify the final event selection, but this has minor consequences on the value of the parameters $\psi$, $z_{max}$, and $E_{th}$ that maximize the correlation signal. We start the scan with the event of highest energy and add events one by one in order of decreasing energy, down to $E_{th} = 40$ EeV.

Strong correlation signals occur for energy thresholds around 60 EeV and several combinations of the other parameters in the range $\psi \leq 6°$, and $z_{max} \leq 0.024$ ($D_{max} < 100$ Mpc). The absolute minimum value of $P$ occurs for the 27 events with the highest energies (above 57 EeV in the new analysis). We generated simulated sets of directions, drawn from an isotropic distribution in proportion to the relative exposure of the observatory. Performing an identical scan on those simulated samples to that applied to the real data, we obtain smaller or equal values of $P$ in $\sim 10^{-5}$ of the simulated direction sets.

We present (Fig. 2) a sky map in Galactic coordinates of our 27 highest-energy events ($E > 57$ EeV), as determined by our most recent version of the reconstruction code. The anisotropy is clearly visible. We note the proximity of several events close to the supergalactic plane, and also that two events arrive within 3° of Centaurus A, one of the closest AGN, marked in white on the figure.

**Discussion.** With the statistics of our present data set, the observed correlation is significant for maximum distances to AGN of up to 100 Mpc, for maximum angular separations of up to 6°, and for energy thresholds around 60 EeV. Those numbers are to be taken as indicative because the minimization of $P$ is not totally exempt from biases. Accidental correlation with foreground AGN different from the actual sources may induce bias toward smaller maximum source distances, while accidental correlation with distant background ones may reduce the optimal maximum angular separation by a few degrees.

Under the simplifying assumptions of a uniform distribution of sources with equal intrinsic luminosity and continuous energy loss in the cosmic microwave background due to the GZK effect (*3*, *4*), 90% of the protons arriving at Earth with energy exceeding 60 EeV originate from sources closer than 200 Mpc. This (somewhat arbitrarily defined) "GZK horizon" decreases rapidly with increasing energy and drops to 90 Mpc for energies exceeding 80 EeV. The relation between the horizon distance and the value of $D_{max}$ that minimizes $P$ is not a simple one, given the possible biases in the method, which has nonuniform sensitivity over the range of parameters scanned. Increasing catalog incompleteness also prevents confidently scanning over sources at distances much larger than 100 Mpc. Moreover, the local density and luminosities of sources could have significant departures from the uniformity assumed in the GZK horizon scale for a given energy threshold. Taking into consideration these caveats, in addition to the uncertainty in the reconstructed energies, the range of $D_{max}$ and $E_{th}$ over which we observe a significant correlation is compatible with the frequently made assumption that the highest-energy cosmic rays are protons experiencing predicted GZK energy losses. We note that the correlation increases abruptly at the energy threshold of 57 EeV, which coincides with the point on the energy spectrum recently reported from the observatory at which the flux is reduced by ~50% with respect to a power-law extrapolation of lower-energy observations (*17*).

If the regular component of the galactic magnetic field is coherent over scales of 1 kpc with a strength of a few μG, as indicated by data from studies of pulsars (*22*), the observed correlation over an angular scale of only a few degrees for $E \sim 60$ EeV is indicative that most of the primaries are not heavy nuclei.

These features are compatible with the interpretation that the correlation we observe is evidence for the GZK effect and the hypothesis that the highest-energy cosmic rays reaching Earth are mostly protons from nearby sources.

The catalog of AGN that we use is increasingly incomplete near the galactic plane, where extinction from dust in the Milky Way reduces the sensitivity of observations. Deflections from the galactic magnetic field are also expected to be significantly larger than average for cosmic rays that arrive at equatorial Galactic latitudes, because they traverse a longer distance across any regular Galactic magnetic component. These effects are likely to have some impact upon the estimate of the strength of the correlation. Six out of the eight events that do not correlate with AGN positions within our prescribed parameters and reconstruction code lie less than 12° away from the Galactic plane.

Despite its strength, the correlation that we observe with nearby AGN from the V-C catalog cannot be used alone as a proof that AGN are the sources. Other sources, as long as their distribution within the GZK horizon is sufficiently similar to that of the AGN, could lead to a significant correlation between the arrival directions of cosmic rays and the AGN positions. Such correlations are under investigation in particular for the Infra-Red Astronomical Satellite (IRAS) galaxies. The autocorrelation signal of the highest-energy events is also being investigated. It shows departures from isotropic expectations at angular scales between 5° and 20° (*23*) and serves as an additional tool to identify the spatial distribution of the sources.

**Conclusion.** We have demonstrated the anisotropy of the arrival directions of the highest-energy cosmic rays and their extragalactic origin. Our observations are consistent with the hypothesis that the rapid decrease of flux measured by the Pierre Auger Observatory above 60 EeV is due to the GZK effect and that most of the cosmic rays reaching Earth in that energy range are protons from nearby astrophysical sources, either AGN or other objects with a similar spatial distribution.

The number of high-energy cosmic-ray events recorded so far by the Pierre Auger Observatory and analyzed in this work corresponds to 1.2 years of operation of the complete southern array. The data set that the observatory will gather in just a few more years should offer a better chance to unambiguously identify the sources. The pattern of correlations of cosmic-ray events with their sources could also assist in determining the properties of the intervening magnetic-field structures and in particle physics explorations at the largest energies. Astronomy based on cosmic rays with the highest energies opens a new window on the nearby universe.

### References and Notes


1. J. Linsley, *Phys. Rev. Lett.* **10**, 146 (1963).
2. J. Abraham *et al.* (Pierre Auger Collaboration), *Nucl. Instrum. Methods A* **523**, 50 (2004).
3. K. Greisen, *Phys. Rev. Lett.* **16**, 748 (1966).
4. G. T. Zatsepin, V. A. Kuzmin, *Sov. Phys. JETP Lett.* **4**, 78 (1966).
5. V. S. Berezinsky, S. I. Grigorieva, *Astron. Astrophys.* **199**, 1 (1988).
6. N. Hayashida *et al.*, *Phys. Rev. Lett.* **77**, 1000 (1996).

7. R. U. Abbasi *et al.*, The HiRes collaboration. *Astrophys. J.* **610**, L73 (2004).
8. T. Stanev, P. L. Biermann, J. Lloyd-Evans, J. P. Rachen, A. A. Watson, *Phys. Rev. Lett.* **75**, 3056 (1995).
9. Y. Uchihori, M. Nagano, M. Takeda, M. Teshima, J. Lloyd-Evans and A.A. Watson, *Astropart. Phys.* **13**, 151 (2000).
10. V. L. Ginzburg, S. I. Syrovatskii, *The Origin of Cosmic Rays* (Pergamon, Oxford, 1964).
11. A. M. Hillas, *Annu. Rev. Astron. Astrophys.* **22**, 425 (1984).
12. M.-P. Véron-Cetty, P. Véron, *Astron. Astrophys.* **455**, 773 (2006).
13. D. Allard *et al.* (Pierre Auger Collaboration), *Astrophysics*, available at http://arxiv.org/abs/astro-ph/0511104.
14. C. Bonifazi, A. Letessier-Selvon, E. M. Santos, *Astrophysics*, available at http://arxiv.org/abs/0705.1856.
15. C. Bonifazi (Pierre Auger Collaboration), in *Proceedings of the 29th International Cosmic Ray Conference*, Pune, India (Tata Institute of Fundamental Research, India, 2005), vol. 17, pp. 17–20.
16. M. Ave (Auger Collaboration), *Astrophysics*, available at http://arxiv.org/abs/0709.2125.
17. M. Roth (Pierre Auger Collaboration), *Astrophysics*, available at http://arxiv.org/abs/0706.2096.
18. B. R. Dawson (Pierre Auger Collaboration), *Astrophysics*, available at http://arxiv.org/abs/0706.1105.
19. A redshift $z$ corresponds to a distance 42 Mpc × ($z$/0.01) for a Hubble constant $H_0$ = 71 km $s^{-1}$ $Mpc^{-1}$.
20. R. W. Clay (Pierre Auger Collaboration), in *Proceedings of the 28th International Cosmic Ray Conference*, Tsukuba, Japan (Universal Academic Press, Tokyo, Japan, 2003), vol. 1, pp. 421–424
21. B. Revenu, (Pierre Auger Collaboration), *Proceedings of the 29th International Cosmic Ray Conference* (2005), Pune, India, 75.
22. J. L. Han, R. N. Manchester, A. G. Lyne, G. J. Qiao, W. van Straten, *Astrophys. J.* **642**, 868 (2006).
23. S. Mollerach (Pierre Auger Collaboration), *Astrophysics*, available at http://arxiv.org/abs/0706.1749.


24. We are grateful to the following agencies and organizations for financial support: Gobierno De La Provincia de Mendoza, Comisión Nacional de Energía Atómica, Municipalidad de Malargüe, Fundación Antorchas, Argentina; the Australian Research Council; Conselho Nacional de Desenvolvimento Científico e Tecnológico (CNPq), Financiadora de Estudos e Projetos do Ministerio da Ciencia e Tecnologia (FINEP/MCT), Fundação de Amparo à Pesquisa do Estado de Rio de Janeiro (FAPERJ), Fundação de Amparo à Pesquisa do Estado de São Paulo (FAPESP), Brazil; Ministry of Education, Youth and Sports of the Czech Republic; Centre National de la Recherche Scientifique (CNRS), Conseil Régional Ile-de-France, Département Physique Nucléaire et Corpusculaire (PNC-IN2P3/CNRS), Département Sciences de l'Univers (SDU-INSU/CNRS), France; Bundesministerium für Bildung und Forschung (BMBF), Deutsche Forschungsgemeinschaft (DFG), Finanzministerium Baden-Württemberg, Helmholtz-Gemeinschaft Deutscher Forschungszentren (HGF), Ministerium für Wissenschaft und Forschung, Nordrhein Westfalen, Ministerium für Wissenschaft, Forschung und Kunst, Baden-Württemberg, Germany; Istituto Nazionale di Fisica Nucleare (INFN), Ministero dell'Istruzione, dell'Università e della Ricerca (MIUR), Italy; Consejo Nacional de Ciencia y Tecnología (CONACYT), Mexico; Ministerie van Onderwijs, Cultuur en Wetenschap, Nederlandse Organisatie voor Wetenschappelijk Onderzoek (NWO), Stichting voor Fundamenteel Onderzoek der Materie (FOM), Netherlands; Ministry of Science and Higher Education, Poland; Fundação para a Ciência e a Tecnologia, Portugal; Ministry for Higher Education, Science, and Technology, Slovenian Research Agency, Slovenia; Comunidad de Madrid, Consejería de Educación de la Comunidad de Castilla La Mancha, FEDER funds, Ministerio de Educación y Ciencia, Xunta de Galicia, Spain; Science and TechnologyFacilities Council, UK; Department of Energy, National Science Foundation, The Grainger Foundation, USA; América Latina Formación Académica–European Community/High Energy Physics Latin-American European Network, and UNESCO.



**Full author list and affiliations**

J. Abraham,[1] P. Abreu,[2] M. Aglietta,[3] C. Aguirre,[4] D. Allard,[5] I. Allekotte,[6] J. Allen,[7] P. Allison,[8] C. Alvarez,[9] J. Alvarez-Muñiz,[10] M. Ambrosio,[11] L. Anchordoqui,[12,13] S. Andringa,[2] A. Anzalone,[14] C. Aramo,[11] S. Argirò,[15] K. Arisaka,[16] E. Armengaud,[5] F. Arneodo,[17] F. Arqueros,[18] T. Asch,[19] H. Asorey,[6] P. Assis,[2] B. S. Atulugama,[20] J. Aublin,[21] M. Ave,[22] G. Avila,[1,23] T. Bäcker,[24] D. Badagnani,[25] A. F. Barbosa,[26] D. Barnhill,[16] S. L. C. Barroso,[27] P. Bauleo,[28] J. Beatty,[8] T. Beau,[5] B. R. Becker,[29] K. H. Becker,[30] J. A. Bellido,[20] S. BenZvi,[31] C. Berat,[32] T. Bergmann,[33] P. Bernardini,[34] X. Bertou,[6] P. L. Biermann,[35] P. Billoir,[21] O. Blanch-Bigas,[21] F. Blanco,[18] P. Blasi,[36,37] C. Bleve,[38] H. Blümer,[33,39] M. Boháčová,[40] C. Bonifazi,[21,26] R. Bonino,[3] M. Boratav,[21] J. Brack,[41] P. Brogueira,[2] W. C. Brown,[42] P. Buchholz,[24] A. Bueno,[43] N. G. Busca,[5,22] K. S. Caballero-Mora,[33] B. Cai,[44] D. V. Camin,[45] R. Caruso,[46] W. Carvalho,[47] A. Castellina,[3] O. Catalano,[14] G. Cataldi,[34] L. Cazón-Boado,[22] R. Cester,[15] J. Chauvin,[32] A. Chiavassa,[3] J. A. Chinellato,[48] A. Chou,[7,49] J. Chye,[50] P. D. J. Clark,[51] R. W. Clay,[52] E. Colombo,[53] R. Conceição,[2] B. Connolly,[31] F. Contreras,[23] J. Coppens,[54,55] A. Cordier,[56] U. Cotti,[57] S. Coutu,[20] C. E. Covault,[58] A. Creusot,[59] J. Cronin,[22] S. Dagoret-Campagne,[56] K. Daumiller,[39] B. R. Dawson,[52] R. M. de Almeida,[48] C. De Donato,[45] S. J. de Jong,[54] G. De La Vega,[1] W. J. M. de Mello Junior,[48] J. R. T. de Mello Neto,[60] I. De Mitri,[34] V. de Souza,[33] L. del Peral,[61] O. Deligny,[62] A. Della Selva,[63] C. Delle Fratte,[64] H. Dembinski,[65] C. Di Giulio,[64] J. C. Diaz,[50] C. Dobrigkeit,[48] J. C. D'Olivo,[66] D. Dornic,[62] A. Dorofeev,[67] J. C. dos Anjos,[26] M. T. Dova,[25] D. D'Urso,[63] M. A. DuVernois,[44,68] R. Engel,[39] L. Epele,[25] M. Erdmann,[65] C. O. Escobar,[48] A. Etchegoyen,[53] P. Facal San Luis,[10] H. Falcke,[69] G. Farrar,[7] A. C. Fauth,[48] N. Fazzini,[49] A. Fernández,[9] F. Ferrer,[58] S. Ferry,[59] B. Fick,[50] A. Filevich,[53] A. Filipčič,[59] I. Fleck,[24] R. Fonte,[46] C. E. Fracchiolla,[70] W. Fulgione,[3] B. García,[1] D. García Gámez,[43] D. Garcia-Pinto,[18] X. Garrido,[56] H. Geenen,[30] G. Gelmini,[16] H. Gemmeke,[19] P. L. Ghia,[3] M. Giller,[71] H. Glass,[49] M. S. Gold,[29] G. Golup,[6] F. Gomez Albarracin,[25] M. Gómez Berisso,[6] R. Gómez Herrero,[61] P. Gonçalves,[2] M. Gonçalves do Amaral,[72] D. Gonzalez,[33] J. G. Gonzalez,[67] M. González,[73] D. Góra,[33,74] A. Gorgi,[3] P. Gouffon,[47] V. Grassi,[45] A. Grillo,[17] C. Grunfeld,[25] Y. Guardincerri,[25] F. Guarino,[63] G. P. Guedes,[75] J. Gutiérrez,[61] J. D. Hague,[29] J. C. Hamilton,[5] P. Hansen,[30] D. Harari,[6] S. Harmsma,[76] J. L. Harton,[28,62] A. Haungs,[39] T. Hauschildt,[3] M. D. Healy,[16] T. Hebbeker,[65] D. Heck,[39] C. Hojvat,[49] V. C. Holmes,[52] P. Homola,[74] J. Hörandel,[54] A. Horneffer,[54] M. Horvat,[59] M. Hrabovský,[40] T. Huege,[39] M. Iarlori,[36] A. Insolia,[46] F. Ionita,[22] A. Italiano,[46] M. Kaducak,[49] K. H. Kampert,[30] B. Keilhauer,[33] E. Kemp,[48] R. M. Kieckhafer,[50] H. O. Klages,[39] M. Kleifges,[19] J. Kleinfeller,[39] R. Knapik,[28] J. Knapp,[38] D. -H. Koang,[32] A. Kopmann,[19] A. Krieger,[53] O. Krömer,[19] D. Kümpel,[30] N. Kunka,[19] A. Kusenko,[16] G. La Rosa,[14] C. Lachaud,[5] B. L. Lago,[60] D. Lebrun,[32] P. LeBrun,[49] J. Lee,[16] M. A. Leigui de Oliveira,[77] A. Letessier-Selvon,[21] M. Leuthold,[65] I. Lhenry-Yvon,[62] R. López,[9] A. Lopez Agüera,[10] J. Lozano Bahilo,[43] M. C. Maccarone,[14] C. Macolino,[36] S. Maldera,[3] M. Malek,[49] G. Mancarella,[34] M. E. Manceñido,[25] D. Mandat,[40] P. Mantsch,[49] A. G. Mariazzi,[25] I. C. Maris,[33] D. Martello,[34] J. Martínez,[73] O. Martínez Bravo,[9] H. J. Mathes,[39] J. Matthews,[67,78] J. A. J. Matthews,[29] G. Matthiae,[64] D. Maurizio,[15] P. O. Mazur,[49] T. McCauley,[32] M. McEwen,[67] R. R. McNeil,[67] M. C. Medina,[53] G. Medina-Tanco,[66] A. Meli,[35] D. Melo,[53] E. Menichetti,[15] A. Menschikov,[19] Chr. Meurer,[39] R. Meyhandan,[76] M. I. Micheletti,[53] G. Miele,[63] W. Miller,[29] S. Mollerach,[6] M. Monasor,[18,61] D. Monnier Ragaigne,[56] F. Montanet,[32] B. Morales,[66] C. Morello,[3] E. Moreno,[9] J. C. Moreno,[25] C. Morris,[8] M. Mostafá,[79] M. A. Muller,[48] R. Mussa,[15] G. Navarra,[3] J. L. Navarro,[43] S. Navas,[43] L. Nellen,[66] C. Newman-Holmes,[49] D. Newton,[10,38] T. Nguyen Thi,[80] N. Nierstenhöfer,[30] D. Nitz,[50] D. Nosek,[81] L. Nožka,[40] J. Oehlschläger,[39] T. Ohnuki,[16] A. Olinto,[5,22] V. M. Olmos-Gilbaja,[10] M. Ortiz,[18] S. Ostapchenko,[33] L. Otero,[1] D. Pakk Selmi-Dei,[48] M. Palatka,[40] J. Pallotta,[1] G. Parente,[10] E. Parizot,[5] S. Parlati,[17] S. Pastor,[82] M. Patel,[38] T. Paul,[12] V. Pavlidou,[22] K. Payet,[32] M. Pech,[40] J. Pękala,[74] R. Pelayo,[73] I. M. Pepe,[83] L. Perrone,[34] S. Petrera,[36] P. Petrinca,[64] Y. Petrov,[28] DiepPham Ngoc,[80] DongPham Ngoc,[80] T. N. Pham Thi,[80] A. Pichel,[84] R. Piegaia,[25] T. Pierog,[39] M. Pimenta,[2] T. Pinto,[82] V. Pirronello,[46] O. Pisanti,[63] M. Platino,[53] J. Pochon,[6] T. A. Porter,[67] P. Privitera,[64] M. Prouza,[31] E. J. Quel,[1] J. Rautenberg,[30] S. Reucroft,[12] B. Revenu,[5] F. A. S. Rezende,[26] J. Řídký,[40] S. Riggi,[46] M. Risse,[30] C. Rivière,[32] V. Rizi,[36] M. Roberts,[20] C. Robledo,[9] G. Rodriguez,[10] D. Rodríguez Frías,[61] J. Rodriguez Martino,[64] J. Rodriguez Rojo,[23] I. Rodriguez-Cabo,[10] G. Ros,[18,61] J. Rosado,[18] M. Roth,[39] B. Rouillé-d'Orfeuil,[5] E. Roulet,[6] A. C. Rovero,[84] F. Salamida,[36] H. Salazar,[9] G. Salina,[64] F. Sánchez,[66] M. Santander,[23] C. E. Santo,[2] E. M. Santos,[21,26] F. Sarazin,[85] S. Sarkar,[86] R. Sato,[23] V. Scherini,[30] H. Schieler,[39] F. Schmidt,[22] T. Schmidt,[33] O. Scholten,[76] P. Schovánek,[40] F. Schüssler,[39] S. J. Sciutto,[25] M. Scuderi,[46] A. Segreto,[14] D. Semikoz,[5] M. Settimo,[34] R. C. Shellard,[26,70] I. Sidelnik,[53] B. B. Siffert,[60] G. Sigl,[5] N. Smetniansky De Grande,[53] A. Smiałkowski,[71] R. Šmída,[40] A. G. K. Smith,[52] B. E. Smith,[38] G. R. Snow,[87] P. Sokolsky,[79] P. Sommers,[20] J. Sorokin,[52] H. Spinka,[49,88] R. Squartini,[23] E. Strazzeri,[64] A. Stutz,[32] F. Suarez,[3] T. Suomijärvi,[62] A. D. Supanitsky,[66] M. S. Sutherland,[8] J. Swain,[12] Z. Szadkowski,[71] J. Takahashi,[48] A. Tamashiro,[84] A. Tamburro,[33] O. Taşcău,[30] R. Tcaciuc,[24] D. Thomas,[79] R. Ticona,[89] J. Tiffenberg,[25] C. Timmermans,[54,55] W. Tkaczyk,[71] C. J. Todero Peixoto,[48] B. Tomé,[2] A. Tonachini,[15] D. Torresi,[14] P. Travnicek,[40] A. Tripathi,[16] G. Tristram,[5] D. Tschemiakhovski,[19] M. Tueros,[25] V. Tunnicliffe,[51] R. Ulrich,[39] M. Unger,[39] M. Urban,[56] J. F. Valdés Galicia,[66] I. Valiño,[10] L. Valore,[63] A. M. van den Berg,[76] V. van Elewyck,[62] R. A. Vázquez,[10] D. Veberič,[59] A. Veiga,[25] A. Velarde,[89] T. Venters,[5,22] V. Verzi,[64] M. Videla,[1] L. Villaseñor,[57] S. Vorobiov,[59] L. Voyvodic,[49] H. Wahlberg,[25] O. Wainberg,[53] T. Waldenmaier,[33] P. Walker,[51] D. Warner,[28] A. A. Watson,[38] S. Westerhoff,[90] G. Wieczorek,[71] L. Wiencke,[85] B. Wilczyńska,[74] H. Wilczyński,[74] C. Wileman,[38] M. G. Winnick,[52] H. Wu,[56] B. Wundheiler,[53] J. Xu,[19] T. Yamamoto,[22] P. Younk,[79] E. Zas,[10] D. Zavrtanik,[59] M. Zavrtanik,[59] A. Zech,[21] A. Zepeda,[73] M. Ziolkowski,[24]

[1]Universidad Tecnológica Nacional, Regionales Mendoza y San Rafael, 5500Mendoza, Argentina. [2]Laboratório de Instrumentação e Física Experimental de Partículas and Instituto Superior Técnico, P-1000-149 Lisboa, Portugal. [3]Istituto di Fisica dello Spazio Interplanetario (INAF), Università di Torino and Sezione INFN, 10125 Torino, Italy. [4]Universidad Catolica de Bolivia, POB 5829 La Paz, Bolivia. [5]Laboratoire AstroParticule et Cosmologie, Université Paris 7, IN2P3/CNRS, F-75231 Paris CEDEX 05, France. [6]Centro Atómico Bariloche (CNEA); Instituto Balseiro (UNCuyo), 8400 Río Negro, Argentina. [7]New York University, New York, NY 10027, USA. [8]Ohio State University, Columbus, OH 43210–1061, USA. [9]Benemérita Universidad Autónoma de Puebla, 72500 Puebla, Mexico. [10]Universidad de Santiago de Compostela, E-15782 Santiago de Compostela, Spain. [11]Sezione INFN di Napoli, I-80126 Napoli, Italy. [12]Northeastern University, Boston, MA 02115–5096, USA. [13]University of Wisconsin, Milwaukee, WI 53201, USA. [14]Istituto di Astrofisica Spaziale e Fisica Cosmica di Palermo (INAF), I-90146 Palermo, Italy. [15]Università di Torino and Sezione INFN, I-10125 Torino, Italy. [16]University of California, Los Angeles, CA 90095, USA. [17]INFN, Laboratori Nazionali del Gran Sasso, I-67010 Assergi (L'Aquila), Italy. [18]Universidad Complutense de Madrid, E-28040 Madrid, Spain. [19]Forschungszentrum Karlsruhe, Institut für Prozessdatenverarbeitung und Elektronik, D-76021 Karlsruhe, Germany. [20]Pennsylvania State University, University Park, PA 16802–6300, USA. [21]Laboratoire de Physique Nucléaire et de Hautes Energies, Université Paris 6 and 7, 75252 Paris Cedex 05, France. [22]University of Chicago, Enrico Fermi Institute, Chicago, IL 60637, USA. [23]Pierre Auger Southern Observatory, (5613) Malargüe, Prov. De Mendoza, Argentina. [24]Universität Siegen, D–57068 Siegen, Germany. [25]Universidad Nacional de la Plata, Instituto de Física La Plata/Consejo Nacional de Investigaciones Científicas y Técnicas, (1900) La Plata, Argentina. [26]Centro Brasileiro de Pesquisas Físicas, CEP 22290-180 Rio de Janeiro, RJ, Brazil. [27]Universidade Estadual do Sudoeste da Bahia, 45083-900 Vitoria da Conquista, BA, Brazil. [28]Colorado State University, Fort Collins, CO 80523, USA. [29]University of New Mexico, Albuquerque, NM 87131, USA. [30]Bergische Universität Wuppertal, D–42097 Wuppertal, Germany. [31]Columbia University, New York, NY 10027, USA. [32]Laboratoire de Physique Subatomique et de Cosmologie, IN2P3/CNRS, F-

# IRE1 Signaling Affects Cell Fate During the Unfolded Protein Response

Jonathan H. Lin,[1,2,3]* Han Li,[1,2] Douglas Yasumura,[4] Hannah R. Cohen,[2] Chao Zhang,[1,5] Barbara Panning,[2] Kevan M. Shokat,[1,5] Matthew M. LaVail,[4] Peter Walter[1,2]

## AUTHORS' SUMMARY

Organism health depends on the accuracy of the signals sent and received by constituent cells. Proteins, either secreted from the cell or embedded in the plasma membrane to monitor the environment, transmit much of this information. On the basis of these signals, cells make vital decisions—when and where to divide, migrate or change shape, differentiate, or die.

Cells have evolved elaborate mechanisms to ensure the accuracy with which proteins are folded and assembled before export or transport to the cell surface. Stringent quality control is imposed by the endoplasmic reticulum (ER), a membrane-bound labyrinth of tubes and sacs, where virtually all plasma membrane and secreted proteins begin their journey to the surface. Only properly folded proteins are allowed to leave the ER; misfolded proteins are degraded. In this way, cells display or release only high-quality, functional proteins.

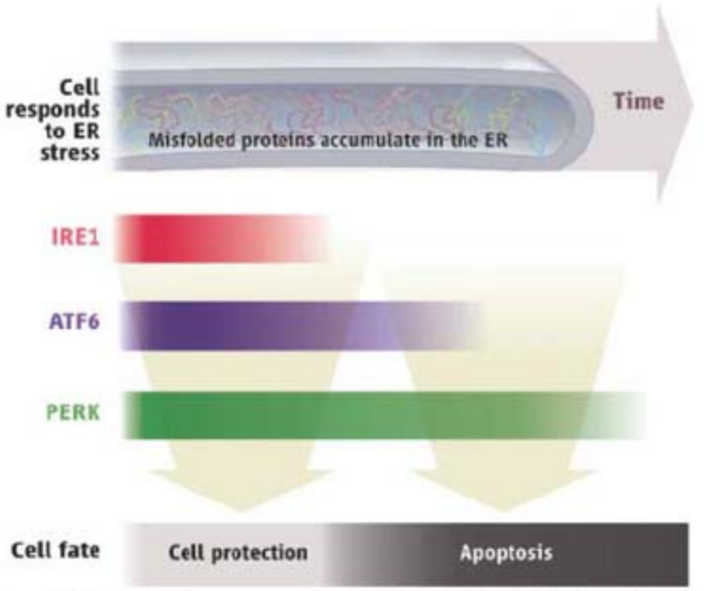


The unfolded protein response. Accumulation of misfolded proteins (ER stress) triggers both cell protective and cell death responses, but with different time courses.

To maintain fidelity, the cell needs to fold proteins as they are made, and this system needs to adapt to changing conditions. This feat is achieved by a set of intracellular signaling pathways, collectively termed the "unfolded protein response" (UPR), which senses when the ER has accumulated too many unfolded proteins. The UPR then activates transcription of certain genes that serve to increase the ER's protein folding capacity as needed. UPR signaling can protect cells from such ER stress by expanding the amount of ER in the cell, enhancing the degradation of misfolded proteins, and reducing the synthesis of new proteins. If homeostasis cannot be reestablished, however, UPR signaling eventually induces cell death by apoptosis, an effective means of protecting the organism from rogue cells expressing dysfunctional signaling molecules. How does the UPR switch between these mutually incompatible life and death fates for the cell?

No trigger for ER stress has been identified that selectively elicits only protective responses or only apoptosis. Instead, ER stress activates all UPR signaling pathways, thereby simultaneously producing antagonistic outputs. To address this paradox, we developed assays to examine the molecular behavior of three parallel branches of the UPR—governed by the ER-stress sensors IRE1, PERK, and ATF6, respectively—in human cells exposed to persistent, pharmacologically induced ER stress. As expected, all three branches were activated upon induction of ER stress but, unexpectedly, the behavior of individual signaling pathways varied markedly with time after the onset of stress. The responses set in motion via IRE1 quickly attenuated within 8 hours despite the persistence of the stress; the ATF6 responses showed somewhat delayed attenuation (see figure). By contrast, the responses mediated by PERK persisted under prolonged ER stress and were still evident 30 hours after stress onset.

These findings suggested that the varied time courses of the individual UPR branches influence the cell's ultimate fate in response to ER stress. To test this, we developed a chemical-genetic strategy to control IRE1 and its downstream targets, independent of ER stress. We created isogenic human cells that expressed an artificial, drug-inducible mutant IRE1, which allowed us to sustain prolonged IRE1 signaling in the face of persistent ER stress. Cell survival was significantly enhanced under these conditions, demonstrating that the termination of IRE1 activity is an important factor in allowing cell death after UPR activation.

Last, we found similar time-related switches in the endpoint of the UPR (from cell protection to apoptosis) in animal models of a heritable degenerative proteinopathy—retinitis pigmentosa—where photoreceptor cells die as a result of the expression of misfolded rhodopsin molecules, leading to blindness. Our findings thus provide a molecular rationale for how cells control whether to live or die when confronted with ER stress.

Pressing next questions include identifying the mechanisms by which different UPR branches can be selectively controlled. Phosphatases modulate PERK branch activity (*1*) and could also influence IRE1 signaling. Other transcriptional, translational, and posttranslational regulatory mechanisms may also contribute. Furthermore, different cell types may tailor the UPR for their own needs. Which parts of the model apply to all cells and which are tailored to allow different cell types to "dial-in" physiologically appropriate tolerance levels to ER stress? Do tissues with inherently different IRE1, ATF6, or PERK activities display greater or lesser resistance to cell death upon induction of ER stress? In addition to transcriptional output of the UPR branches, direct protein-protein interactions may also contribute to the control of apoptosis. Mammalian IRE1, for example, associates with the apoptosis-regulating BCL-2 protein family members BAK and BAX (*2*). IRE1 signaling activates the JNK pathway, possibly by directly phosphorylating downstream targets (*3*). Finally, the association of ER stress with diverse human diseases—cancer, diabetes, proteinopathies, and viral infections—raises the possibility of altering pathogenesis by manipulating the UPR.

**Summary References**

1. I. Novoa, H. Zeng, H. P. Harding, D. Ron, *J. Cell Biol.* **153**, 1011 (2001).
2. C. Hetz *et al.*, *Science* **312**, 572 (2006).
3. F. Urano *et al.*, *Science* **287**, 664 (2000).

FULL-LENGTH ARTICLE

**Endoplasmic reticulum (ER) stress activates a set of signaling pathways, collectively termed the unfolded protein response (UPR). The three UPR branches (IRE1, PERK, and ATF6) promote cell survival by reducing misfolded protein levels. UPR signaling also promotes apoptotic cell death if ER stress is not alleviated. How the UPR integrates its cytoprotective and proapoptotic outputs to select between life or death cell fates is unknown. We found that IRE1 and ATF6 activities were attenuated by persistent ER stress in human cells. By contrast, PERK signaling, including translational inhibition and proapoptotic transcription regulator *Chop* induction, was maintained. When IRE1 activity was sustained artificially, cell survival was enhanced, suggesting a causal link between the duration of UPR branch signaling and life or death cell fate after ER stress. Key findings from our studies in cell culture were recapitulated in photoreceptors expressing mutant rhodopsin in animal models of retinitis pigmentosa.**

The UPR comprises a set of signaling pathways that collectively adjust the cell's ER protein folding capacity according to need. As such, UPR signaling reestablishes homeostasis in the face of changing developmental and environmental conditions, thereby preserving ER protein folding fidelity. Upon unmitigated ER stress, the UPR also triggers apoptosis. Thus, rather than produce misfolded or malfunctioning proteins, cells are eliminated, perhaps to protect the organism from rogue cells that do not receive or relay signals properly.

Physiologic or pathologic processes that create an imbalance between protein folding load and capacity induce the UPR through ER-resident transmembrane proteins—IRE1, PERK, and ATF6—that act as sensors in the ER lumen and transmit the information to the rest of the cell (*1*). IRE1 is a transmembrane kinase/endoribonuclease (RNAse) that, upon activation, initiates the nonconventional splicing of *Xbp-1* mRNA (*2*, *3*). Spliced *Xbp-1* mRNA encodes a transcription activator that drives transcription of genes such as ER chaperones, whose products directly participate in ER protein folding (*4*). PERK is a transmembrane kinase that phosphorylates the eukaryotic translation initiation factor 2 subunit α (eIF2α), thereby reducing protein synthesis and counteracting ER protein overload (*5*). eIF2α phosphorylation also allows the selective translation of some mRNAs that contain small open reading frames in their 5′ untranslated regions, thereby leading to the production of transcription activators such as ATF4 (*6*). ATF6 is a transcription factor that is made initially as an ER-resident transmembrane protein. Upon protein misfolding, the ATF6 cytoplasmic domain (ATF6f) is liberated from its membrane anchor by regulated proteolysis (*7*, *8*). The transcription factors thus produced (i.e., XBP1, ATF4, and ATF6f) collaborate to activate UPR target genes, thereby controlling the cell's response to ER stress.

Genetic studies have begun to assign cytoprotective or proapoptotic functions to individual UPR target genes. For instance, expression of the ER chaperone BiP protects cells from ER stress (*9*), whereas CHOP, a B-ZIP transcription factor induced by the PERK branch of the UPR, promotes cell death (*10*). Paradoxically, all known ER stresses simultaneously elicit protective and toxic outputs from the UPR, and it has remained unclear how the UPR integrates these opposing outputs to arrive at a life or death decision.

**IRE1 signaling is attenuated during persistent ER stress.** To determine the activation status of IRE1 after ER stress, we examined *Xbp-1* mRNA splicing by reverse transcription polymerase chain reaction (RT-PCR) in human embryonic kidney (HEK) 293 cells (Fig. 1A). We observed the appearance of spliced *Xbp-1* mRNA after treating the cells with tunicamycin or thapsigargin: agents that elicit ER stress by blocking N-linked glycosylation or inhibiting the ER $Ca^{2+}$ pump, respectively (Fig. 1B). Unexpectedly, we found a strong diminution in *Xbp-1* mRNA splicing with prolonged exposure to either drug (Fig. 1B). Consistent with the mRNA splicing data, XBP-1$^s$ protein levels (the form of XBP-1 derived from its spliced mRNA) also decreased with prolonged drug treatment (Fig. 1B). Other human cell lines showed qualitatively similar effects, although they differed in the observed timing of onset and shutoff, as well as in the degree of *Xbp-1* mRNA splicing (fig. S1).

To ascertain that loss of *Xbp-1* mRNA splicing at the late time points was not due to inactivation of the ER stress–inducing agents, we transferred media from HEK293 cells that had been treated with tunicamycin or thapsigargin for 24 hours (a time when little *Xbp-1* mRNA splicing was seen) to plates of fresh, untreated cells. After 4 hours of incubation in conditioned media, *Xbp-1* mRNA splicing was induced to a degree indistinguishable to that seen in cells treated with fresh agents (Fig. 1C).

We next tested if, at late time points, cells continued to accumulate misfolded proteins in their ER or had acquired means of neutralizing the effects of the ER stress–inducing agents. To this end, we examined the glycosylation status of vascular cell adhesion molecule–1 (VCAM-1), a transmembrane protein that is cotranslationally inserted into the ER membrane where it becomes N-glycosylated (*11*). We transfected HEK293 cells with VCAM-1, added tunicamycin, and compared IRE1 activity with the glycosylation status of VCAM-1 (Fig. 1D). HEK293 cells expressing VCAM-1 spliced *Xbp-1* mRNA in a manner indistinguishable from that of wild-type (WT) cells after tunicamycin treatment, and, as in untransfected cells, *Xbp-1* mRNA splicing progressively decayed back to baseline levels with prolonged treatment (Fig. 1D). VCAM-1 was fully glycosylated before tunicamycin addition and first became partially glycosylated and then unglycosylated (Fig. 1D). Not only the steady-state pool but also all newly synthesized VCAM-1 was unglycosylated at later time points (Fig. 1E).

To determine if other IRE1-dependent functions were attenuated in a manner akin to *Xbp-1* mRNA splicing, we examined the activation status of c-Jun N-terminal kinase (JNK). In response to ER stress, IRE1 initiates a signal transduction pathway that activates JNK (*12*). In HEK293 cells, JNK was rapidly phosphorylated with ER stress (Fig. 1F). The initial burst in phosphorylation was followed by a progressive decrease in phospho-JNK levels, a trend that paralleled *Xbp-1* mRNA splicing (compare the time points from 4 hours to 20 hours in Fig. 1F with the equivalent time points in Fig. 1B). Thus, cells responded to unmitigated ER stress by first activating and then attenuating IRE1 activity.

**Behavior of ATF6 and PERK signaling with persistent ER stress.** To assess whether other branches of the UPR elicit kinetic behavior similar to that elicited by IRE1, we monitored ATF6 and PERK activities over time (after UPR induction). To measure ATF6 activation, we followed the liberation of its cleaved cytosolic fragment, ATF6f, using a FLAG-tagged ATF6 reporter that recapitulated ATF6 processing upon induction of ER stress (*13*). We saw rapid production of ATF6f after exposure of HEK293 cells to ER stress (Fig. 2A). With prolonged ER stress, ATF6f levels diminished and ultimately disappeared (Fig. 2A). Thus, like IRE1 signaling, ATF6 activation also diminished after prolonged ER stress, albeit with different kinetics: Although IRE1 signaling decayed within 8 hours, cessation of ATF6f production was not apparent until after at least 20 hours of continuous stress.

The dynamics of the transcriptional targets of IRE1 and ATF6 were consistent with the induction kinetics of these ER-proximal UPR signal transducers. Induction of *BiP* mRNA, encoding an HSP70-class ER chaperone that is transcriptionally regulated by both ATF6f and XBP-1$^s$ (*4*, *7*), peaked at 8 hours after drug treatment and then declined to near preinduction levels (Fig. 2C).

[1]Howard Hughes Medical Institute, University of California at San Francisco, San Francisco, CA 94158, USA. [2]Department of Biochemistry and Biophysics, University of California at San Francisco, San Francisco, CA 94158, USA. [3]Departments of Pathology and Ophthalmology, University of California at San Francisco, San Francisco, CA 94158, USA. [4]Departments of Anatomy and Ophthalmology, University of California at San Francisco, San Francisco, CA 94158, USA. [5]Department of Cellular and Molecular Pharmacology, University of California at San Francisco, San Francisco, CA 94158, USA.

*To whom correspondence should be addressed. E-mail: Jonathan.Lin@ucsf.edu

To assess the activation kinetics of the PERK branch of the UPR, we monitored the accumulation of phosphorylated PERK and its downstream product: phosphorylated eIF2α. PERK activation did not diminish even after prolonged ER stress (Fig. 2B). Consistent with this finding, the translational capacity of cells remained attenuated at all times after the imposition of ER stress (Fig. 2B). Similarly, we observed continuous production of ATF4 (Fig. 2B) and its transcriptional target *Chop* after ER stress (Fig. 2C), although there was some gradual diminution at the later time points. Thus, by contrast to IRE1 and ATF6, PERK branch activation is largely sustained with unmitigated ER stress.

**Chemical-genetic control of IRE1 signaling in human cells.** To ask whether the attenuation of IRE1 activity had physiological consequences, we sought to selectively control IRE1 activity. We followed a strategy that permitted chemical regulation of IRE1's RNase activity using the adenosine triphosphate (ATP) analog 4-amino-1-*tert*-butyl-3-(1′-naphthylmethyl)pyrazolo[3,4-*d*] pyrimidine (1NM-PP1) (Fig. 3A), which binds selectively to the kinase domain of IRE1 mutants bearing an enlarged ATP-binding site (*14*). A leucine-to-glycine [Leu$^{745}$→Gly$^{745}$ (L745G)] mutation rendered yeast IRE1 sensitive to 1NM-PP1. We therefore constructed an allele of human IRE1 in which the orthologous amino acid [isoleucine 642 (Ile$^{642}$)] was changed to glycine [Fig. 3A, "IRE1(I642G)"]. Because conventional transfection or transduction gene expression activated the UPR constitutively and caused cell death (*15*, *16*), we used flippase-mediated, site-specific DNA recombination to introduce the drug-sensitized IRE1(I642G) mutant allele directly into the genome of HEK293 cells bearing a defined *frt* site (*17*). No deleterious growth defects were observed in the transgenic cells expressing the IRE1(I642G) allele. The UPR was not constitutively induced in these cells, as indicated by the absence of spliced *Xbp-1* mRNA (Fig. 3B, 0-hours time point). Application of 1NM-PP1 alone induced robust splicing of *Xbp-1* mRNA in IRE1(I642G)-expressing cells but had no effect on *Xbp-1* mRNA in the parental cells (Fig. 3B). By contrast, the corresponding 1NM-PP1–sensitized allele in yeast required both ER protein misfolding and 1NM-PP1 to activate *HAC1* mRNA splicing. The human allele, thus, provided a molecular switch that could be toggled by 1NM-PP1 regardless of ER protein folding status.

We used IRE1(I642G)-expressing cells to test if we could manipulate *Xbp-1* mRNA splicing during prolonged ER stress. As in WT cells, in the absence of 1NM-PP1, robust *Xbp-1* mRNA splicing occurred in the transgenic cells after drug treatment at early time points and then diminished at later time points (Fig. 3, C and D; compare top panels to Fig. 1A). Thus, the expression of the mutant allele had no deleterious effects on IRE1 activation or attenuation by prolonged ER stress. By contrast, in the presence of 1NM-PP1, *Xbp-1* mRNA splicing in transgenic cells was induced and remained elevated (Fig. 3, C and D). Thus, artificial activation of IRE1(I642G) by 1NM-PP1 overcame the attenuation of IRE1 activity seen upon prolonged ER stress, sustaining *Xbp-1* mRNA splicing at levels approaching those seen at early time points (Fig. 3, C and D, bottom panels). Although 1NM-PP1 activated IRE1(I642G)'s RNAse activity, we detected no comparable activation of JNK signaling (fig. S2), indicating that the mRNA splicing function of IRE1(I642G) is selectively activated by 1NM-PP1.

**IRE1 activity enhances cell viability.** 1NM-PP1 control of IRE1 allowed us to assess the physiological consequences of IRE1 activation and attenuation during the UPR. In particular, we asked whether extended IRE1 activation would have a beneficial effect on cell viability upon prolonged ER stress. ER stress induced by both tunicamycin and thapsigargin is toxic to HEK293 cells. Forty-eight hours after treatment, less than 2% of the WT cells survived (Fig. 4 and fig. S3). The addition of 1NM-PP1 had no substantial effect, although it diminished the viability of WT cells slightly (~25% reduction in viable cell number).

By contrast, 1NM-PP1 treatment of HEK293 cells expressing IRE1(I642G) significantly improved their survival. At the 48-hours time point, cell numbers after thapsigargin and tunicamycin

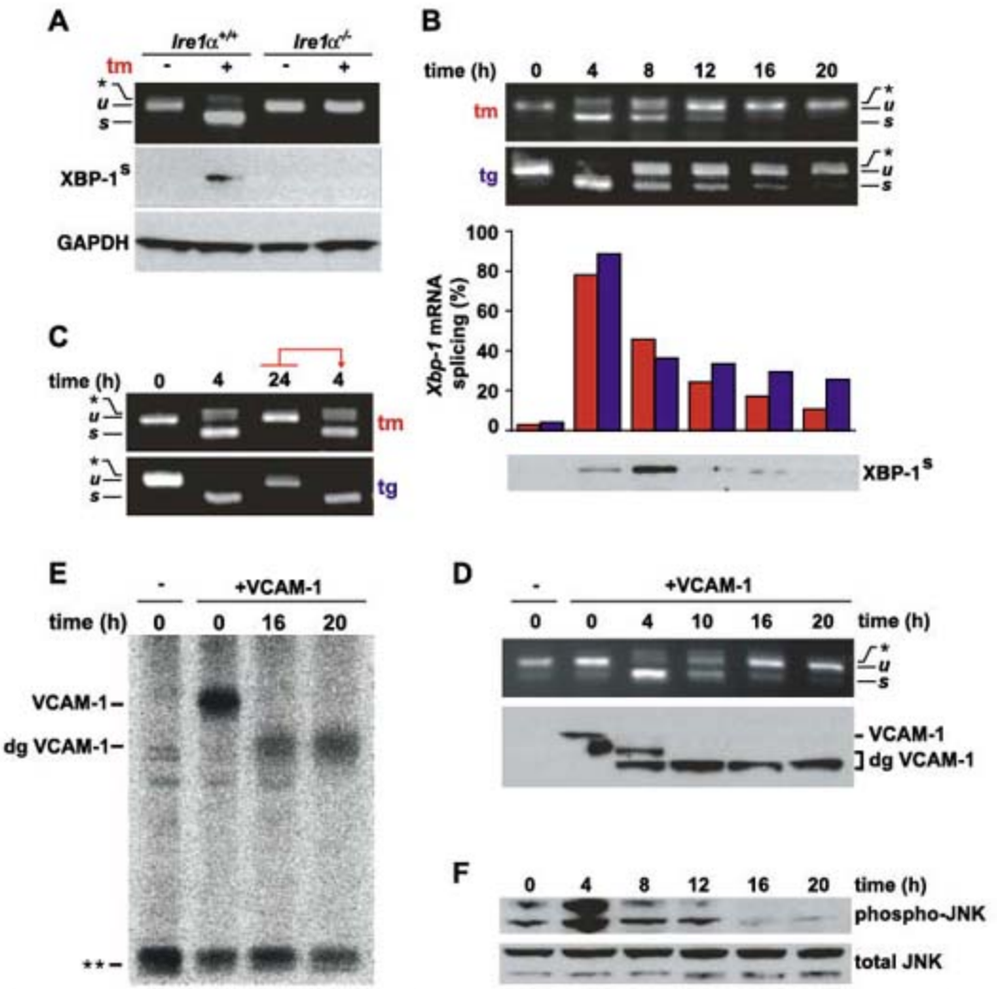


**Fig. 1.** Kinetics of IRE1 signaling with persistent ER stress. (**A**) WT *Ire1α*$^{+/+}$ or *Ire1α*$^{-/-}$ mouse embryo fibroblasts were treated with tunicamycin (tm) (5 μg/ml), and *Xbp-1* mRNA splicing was determined by RT-PCR. Unspliced (*u*) and spliced (*s*) *Xbp-1* mRNA products are indicated. The asterisk indicates the position of a hybrid amplicon (*27*). XBP-1$^{S}$ was detected by immunoblotting. Glyceraldehyde-3-phosphate dehydrogenase (GAPDH) levels served as a protein loading control. (**B**) HEK293 cells were treated with tm (5 μg/ml) or thapsigargin (tg) (500 nM) for the indicated times. tm, red bars; tg, blue bars. Results are representative of five independent experiments. (**C**) HEK293 cells were treated with agents for the indicated times. At 24 hours, media containing drug were transferred to fresh cells. After 4 additional hours, *Xbp-1* mRNA splicing was determined by RT-PCR. (**D**) HEK293 cells, transfected with VCAM-1, were treated with tm (5 μg/ml) for the indicated times. *Xbp-1* mRNA splicing was determined by RT-PCR. Mature and deglycosylated (dg) VCAM-1 species were determined by immunoblotting. (**E**) HEK293 cells, transfected with VCAM-1, were treated with tm for the indicated times and were pulse-labeled, and radiolabeled VCAM-1 was detected after immunoprecipitation. The double asterisk indicates the position of a nonspecific band used as a loading control. (**F**) HEK293 cells were treated with tg for the indicated times, and phospho-JNK protein levels were assessed by immunoblotting. Total JNK protein levels served as a loading control.

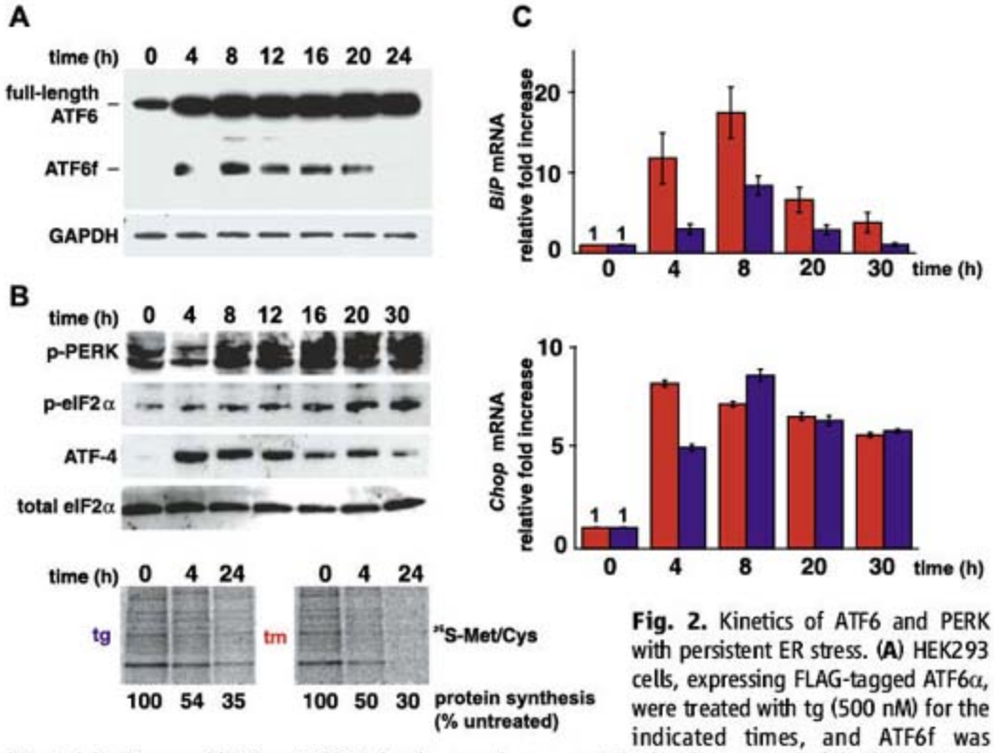


**Fig. 2.** Kinetics of ATF6 and PERK with persistent ER stress. **(A)** HEK293 cells, expressing FLAG-tagged ATF6α, were treated with tg (500 nM) for the indicated times, and ATF6f was detected by immunoblotting. GAPDH levels served as a protein loading control. **(B)** HEK293 cells were treated with tg, and phospho-PERK, phospho-eIF2α, and ATF-4 levels were determined by immunoblotting. Total eIF2α levels served as a protein loading control. In the bottom panels, cells were treated with drug for the indicated times and were pulse-labeled, and radioisotope incorporation was measured via phosphoimaging. $^{35}$S-Met/Cys, $^{35}$S-labeled methionine/cysteine. **(C)** Cells were treated with agents (tm, red bars; tg, blue bars) for the indicated hours, and normalized *BiP* (top panel) and *Chop* (bottom panel) mRNA levels were measured by quantitative PCR and shown relative to levels in untreated cells. Error bars represent SDs from five independent experiments.

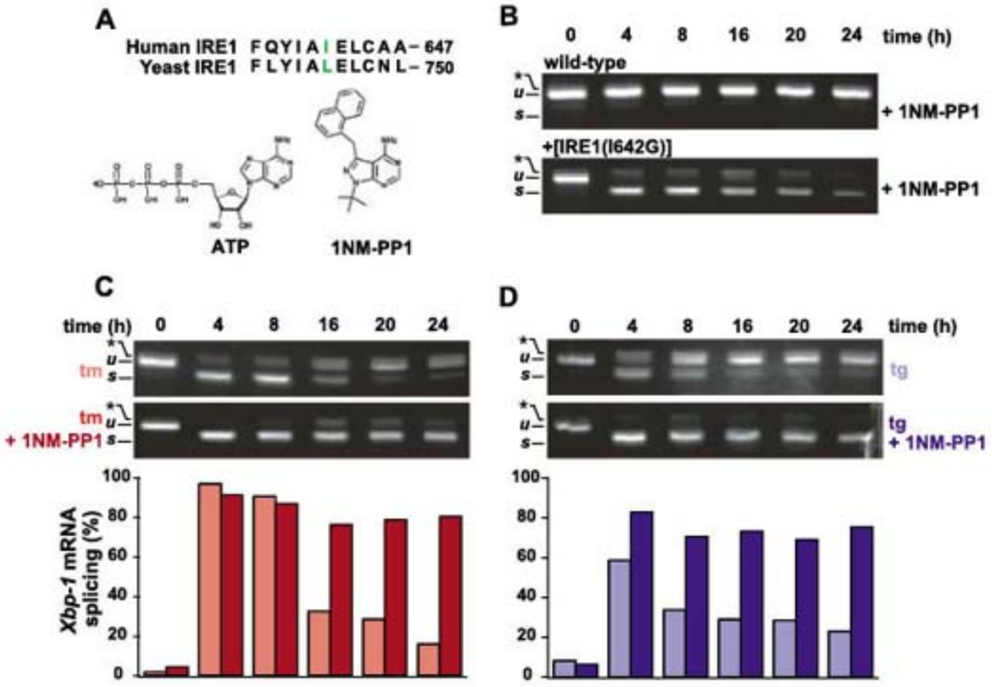


**Fig. 3.** Chemical-genetic control of human IRE1. **(A)** Alignments of a portion of the ATP-binding domains of yeast and human IRE1 are shown. The residue mutated to glycine is shown in color (*28*). The structure of the ATP analog, 1NM-PP1, is shown below. **(B)** Parental WT and transgenic HEK293 cells expressing 1NM-PP1–sensitized IRE1 were treated for the indicated times with 1NM-PP1 (5 μM), and *Xbp-1* mRNA splicing was determined by RT-PCR. **(C)** Transgenic HEK293 cells were treated with tm (5 μg/ml) ± 1NM-PP1 (5 μM). *Xbp-1* mRNA splicing was assessed by RT-PCR and quantified. Results are representative of five independent experiments. **(D)** Transgenic HEK293 cells were treated with tg (300 nM) ± 1NM-PP1 (5 μM). *Xbp-1* mRNA splicing was assessed by RT-PCR and quantified. Results are representative of five independent experiments.

treatment were 5 and 20 times higher, respectively, in the presence of 1NM-PP1 than in its absence (Fig. 4). Even in the absence of experimental induction of ER stress, 1NM-PP1 proved beneficial in cells expressing IRE1(I642G), affording a ~30% enhancement of cell growth (Fig. 4 and fig. S3). Thus, IRE1 signaling directly enhanced cell viability in the face of ER stress.

**UPR behavior in models of retinitis pigmentosa.** The UPR has been postulated to play a role in the pathogenesis of protein misfolding diseases (*18*). Autosomal dominant retinitis pigmentosa (adRP) is a human protein misfolding disease most commonly caused by a proline-to-histidine mutation at position 23 of rhodopsin (P23H rhodopsin) that leads to its retention within the ER (*19*–*21*). Retinal photoreceptors expressing P23H rhodopsin ultimately die, leading to blindness, but the molecular pathways linking rhodopsin misfolding in the ER to cell death are unclear (*22*). To explore whether the UPR is instrumental in retinal cell death, we examined its activation status in cells expressing P23H rhodopsin.

We assessed P23H rhodopsin's ability to induce ER stress in transfected HEK293 cells. Increased *BiP* mRNA levels were detected in cells expressing two control ER-targeted proteins, VCAM-1 and WT rhodopsin (Fig. 5A), but not in cells expressing cytosolic green fluorescent protein (GFP), indicating that increasing the protein folding load of the ER induced the UPR. *BiP* mRNA expression was significantly higher in cells expressing P23H rhodopsin as compared with cells expressing WT rhodopsin (Fig. 5A). The rhodopsin mRNA levels were identical in cells expressing WT and mutant forms of the protein. Thus, P23H rhodopsin is a more potent UPR inducer than WT rhodopsin, presumably because of its folding defect.

We next examined *BiP* and *Chop* mRNA levels in retinas from transgenic rat models of adRP that express mouse P23H rhodopsin at low (P23H-3 Rho Tg) or high (P23H-1 Rho Tg) levels (*23*, *24*). In WT Sprague-Dawley rats and those expressing the P23H rhodopsin transgene at either level, *BiP* mRNA increased after the birth of photoreceptor neurons [postnatal day 6 (PND 6)] and increased up to PND 10 or 12 (Fig. 5B). Thereafter, *BiP* mRNA levels selectively dropped in both transgenic lines expressing P23H rhodopsin (Fig. 5B, top panel). By contrast, *Chop* mRNA levels concomitantly increased in animals expressing P23H rhodopsin but remained low in WT animals (Fig. 5B, bottom panel). The time course of *BiP* mRNA decline and *Chop* mRNA rise tightly matched the rate of retinal degeneration in P23H rhodopsin transgenic animals (Fig. 5, C and D). Furthermore, the changes in *BiP* and *Chop* mRNA levels in retinas expressing misfolded rhodopsin mirrored the results seen in cell culture after prolonged ER stress (compare Figs. 5B and 2C). Thus, selective attenuation of cytoprotective UPR output coupled with sustained CHOP production—seen

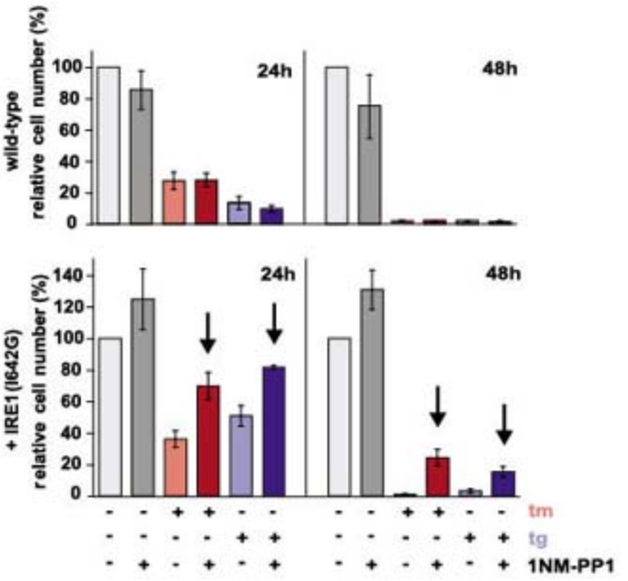


**Fig. 4.** IRE1 signaling enhances cell viability. Parental WT and transgenic HEK293 cells were treated with the indicated agents, and adherent, cresyl violet–stained positive cells were counted at the indicated times and are shown relative to counts of mock-treated cells. Error bars represent SDs from three independent experiments. The arrows indicate $P$ value < 0.01 when the corresponding samples ± 1NM-PP1 were compared (Student's $t$ test).

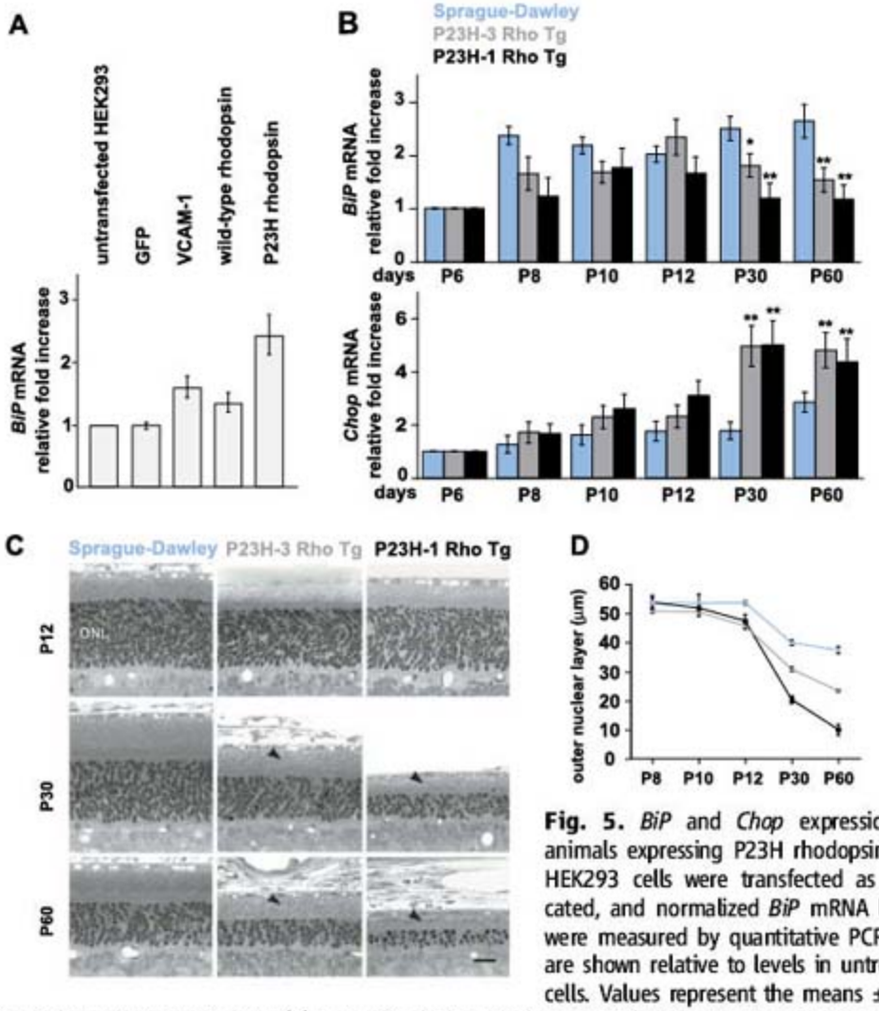


**Fig. 5.** *BiP* and *Chop* expression in animals expressing P23H rhodopsin. **(A)** HEK293 cells were transfected as indicated, and normalized *BiP* mRNA levels were measured by quantitative PCR and are shown relative to levels in untreated cells. Values represent the means ± SDs from five independent experiments. **(B)** Normalized *BiP* and *Chop* mRNA levels were measured in retinas [from WT Sprague-Dawley or transgenic rats expressing P23H rhodopsin at high (P23H-1 Rho Tg) or low (P23H-3 Rho Tg) levels] by quantitative PCR and are shown relative to levels at PND 6 (P6): a time when >95% of the mature complement of retinal photoreceptors has been generated. Error bars represent SDs from three animals at each age. *, $P = 0.003$; **, $P < 0.001$ [as compared with age-matched WT animals (Student's $t$ test)]. **(C)** Light micrographs of representative retinal sections from the inferior posterior retinas of WT, P23H-1, and P23H-3 rats at the indicated ages. The outer nuclear layer (ONL), which is proportional to photoreceptor nuclei numbers, thins as photoreceptors degenerate, and rhodopsin-containing outer segments (arrowheads) shorten. Scale bar, 25 µm. **(D)** The mean ONL thickness was measured in retinal cross sections from transgenic and WT rats at the indicated ages. Error bars represent SDs of ONL thickness from three to six animals at each age. The onset of ONL thinning in both transgenes was at P12 ($P < 0.05$), with progressive thinning at later ages ($P < 0.0001$) (Student's $t$ test).

after drug-induced protein misfolding in vitro or, in the case of P23H rhodopsin, constitutive misfolded protein production in vivo—contributed to cell death.

**Discussion.** The UPR elicits paradoxical outputs, inducing cytoprotective functions that reestablish homeostasis and cell destructive functions that promote apoptosis. We found that the switch between cytoprotective and proapoptotic output lies in part in the duration of individual UPR branch activity. After rapid initial activation of all UPR branches by ER stress, IRE1 signaling was selectively attenuated in human cells, even though stress persisted. ATF6 signaling also declined with slower kinetics, yet PERK signaling persisted much longer in the presence of unmitigated ER stress. We observed enhanced cell survival after experimentally prolonging IRE1 signaling, thereby demonstrating a causal link between IRE1 activity and cell survival. Thus, IRE1 signaling attenuation by persistent ER stress emerges as a key step in making the life or death decision after UPR induction.

Our results suggest a model by which distinct combinations of individual UPR signaling pathways determine a cell's fate after ER stress. The initial combined activation of IRE1, PERK, and ATF6 produces cytoprotective outputs such as reduced translation, enhanced ER protein folding capacity, and clearance of misfolded ER proteins, along with proapoptotic outputs such as CHOP production. Cytoprotective outputs would outweigh proapoptotic factors at this point, which would be helped by the relatively longer mRNA and protein half-lives of factors such as BiP (*25*). This phase of predominantly beneficial UPR output would thus provide a "window of opportunity" for cells to readjust their ER to cope with stress. If these steps fail to reestablish homeostasis, IRE1 signaling and then ATF6 signaling are attenuated, creating an imbalance in which unchecked proapoptotic output guides the cell toward its demise. The variation in IRE1 signaling kinetics across different human cell types (fig. S1) may reflect differential susceptibility to ER stress–induced cell death among different cells and organs, reinforcing growing evidence that the metazoan UPR is tailored toward the physiologic functions of particular organs and cell types (*26*).

The experimental conditions used in our cell culture studies induce irreparable protein misfolding and resemble pathological processes in which inherited mutations produce misfolded proteins. It was unexpected that in retinal degeneration models, rhodopsin molecules bearing the causative mutation of the disease induced changes in UPR activity that resembled those observed with unmitigated stress after drug treatment. Whereas WT retinal cells induced BiP concomitant with the developmental need to fold large amounts of rhodopsin, retinal cells expressing mutant rhodopsin selectively shut down BiP production and increased CHOP production, suggesting that down-regulation of IRE1, coupled with maintenance of PERK signaling, may drive

the cell death seen with the P23H rhodopsin mutation. Similarly, insufficient or imbalanced UPR output could also trigger cell loss in other diseases that arise from persistent ER stress.


**References and Notes**

1. D. Ron, P. Walter, *Nat. Rev. Mol. Cell Biol.* **8**, 519 (2007).
2. M. Calfon *et al.*, *Nature* **415**, 92 (2002).
3. H. Yoshida, T. Matsui, A. Yamamoto, T. Okada, K. Mori, *Cell* **107**, 881 (2001).
4. A. H. Lee, N. N. Iwakoshi, L. H. Glimcher, *Mol. Cell. Biol.* **23**, 7448 (2003).
5. H. P. Harding, Y. Zhang, D. Ron, *Nature* **397**, 271 (1999).
6. H. P. Harding *et al.*, *Mol. Cell* **6**, 1099 (2000).
7. K. Haze, H. Yoshida, H. Yanagi, T. Yura, K. Mori, *Mol. Biol. Cell* **10**, 3787 (1999).
8. J. Ye *et al.*, *Mol. Cell* **6**, 1355 (2000).
9. J. A. Morris, A. J. Dorner, C. A. Edwards, L. M. Hendershot, R. J. Kaufman, *J. Biol. Chem.* **272**, 4327 (1997).
10. H. Zinszner *et al.*, *Genes Dev.* **12**, 982 (1998).
11. J. L. Garrison, E. J. Kunkel, R. S. Hegde, J. Taunton, *Nature* **436**, 285 (2005).
12. F. Urano *et al.*, *Science* **287**, 664 (2000).
13. J. Shen, R. Prywes, *Methods* **35**, 382 (2005).
14. F. R. Papa, C. Zhang, K. Shokat, P. Walter, *Science* **302**, 1533 (2003).
15. W. Tirasophon, K. Lee, B. Callaghan, A. Welihinda, R. J. Kaufman, *Genes Dev.* **14**, 2725 (2000).
16. X. Z. Wang *et al.*, *EMBO J.* **17**, 5708 (1998).
17. H. R. Cohen, B. Panning, *Chromosoma* **116**, 373 (2007).
18. M. Schroder, R. J. Kaufman, *Annu. Rev. Biochem.* **74**, 739 (2005).
19. M. M. Sohocki *et al.*, *Hum. Mutat.* **17**, 42 (2001).
20. C. H. Sung, C. M. Davenport, J. Nathans, *J. Biol. Chem.* **268**, 26645 (1993).
21. S. Kaushal, H. G. Khorana, *Biochemistry* **33**, 6121 (1994).
22. H. F. Mendes, J. van der Spuy, J. P. Chapple, M. E. Cheetham, *Trends Mol. Med.* **11**, 177 (2005).
23. R. H. Steinberg *et al.*, *Invest. Ophthalmol. Visual Sci.* **37**, Association for Research in Vision and Ophthalmology (ARVO) Abstract 3190, S698 (1996).
24. S. Machida *et al.*, *Invest. Ophthalmol. Visual Sci.* **41**, 3200 (2000).
25. D. T. Rutkowski *et al.*, *PLoS Biol.* **4**, 374 (2006).
26. D. Acosta-Alvear *et al.*, *Mol. Cell* **27**, 53 (2007).
27. S. H. Back, M. Schroder, K. Lee, K. Zhang, R. J. Kaufman, *Methods* **35**, 395 (2005).
28. Single-letter abbreviations for the amino acid residues are as follows: A, Ala; C, Cys; D, Asp; E, Glu; F, Phe; G, Gly; H, His; I, Ile; K, Lys; L, Leu; M, Met; N, Asn; P, Pro; Q, Gln; R, Arg; S, Ser; T, Thr; V, Val; W, Trp; and Y, Tyr.


29. We thank the Walter lab, B. Farese, J. L. Garrison, R. J. Kaufman, R. Locksley, M. Matthes, D. Morgan, J. Nathans, R. Prywes, F. Sanchez, and B. Yen for comments, provision of reagents, or technical advice. This work was supported by the Amyotrophic Lateral Sclerosis Association, U.S. Department of Defense, Foundation Fighting Blindness, John Douglas French Alzheimer's Foundation, National Eye Institute, NIH, and Research to Prevent Blindness. P.W. and K.M.S. are Howard Hughes Medical Institute Investigators.


**Supporting Online Material**

www.sciencemag.org/cgi/content/full/318/5852/944/DC1
Materials and Methods
Figs. S1 to S3
References


12 June 2007; accepted 7 September 2007
10.1126/science.1146361


REPORTS

# The Simplest Double Slit: Interference and Entanglement in Double Photoionization of $H_2$


**D. Akoury,[1,2] K. Kreidi,[1] T. Jahnke,[1] Th. Weber,[1,2] A. Staudte,[1] M. Schöffler,[1] N. Neumann,[1] J. Titze,[1] L. Ph. H. Schmidt,[1] A. Czasch,[1] O. Jagutzki,[1] R. A. Costa Fraga,[1] R. E. Grisenti,[1] R. Díez Muiño,[3] N. A. Cherepkov,[4] S. K. Semenov,[4] P. Ranitovic,[5] C. L. Cocke,[5] T. Osipov,[2] H. Adaniya,[2] J. C. Thompson,[6] M. H. Prior,[2] A. Belkacem,[2] A. L. Landers,[6] H. Schmidt-Böcking,[1] R. Dörner[1]***



The wave nature of particles is rarely observed, in part because of their very short de Broglie wavelengths in most situations. However, even with wavelengths close to the size of their surroundings, the particles couple to their environment (for example, by gravity, Coulomb interaction, or thermal radiation). These couplings shift the wave phases, often in an uncontrolled way, and the resulting decoherence, or loss of phase integrity, is thought to be a main cause of the transition from quantum to classical behavior. How much interaction is needed to induce this transition? Here we show that a photoelectron and two protons form a minimum particle/slit system and that a single additional electron constitutes a minimum environment. Interference fringes observed in the angular distribution of a single electron are lost through its Coulomb interaction with a second electron, though the correlated momenta of the entangled electron pair continue to exhibit quantum interference.


One of the most powerful paradigms in the exploration of quantum mechanics is the double-slit experiment. Thomas Young was the first to perform such an experiment, as early as 1801, with light. It took until the late 1950s (*1*), long after the experimental proof of the wave nature of particles was revealed, for a similar experiment to be carried out with electrons. Today, such experiments have been demonstrated for particles as heavy as $C_{60}$ (*2*) and for bound electrons inside a highly excited atom (*3*). All of these experiments were aimed at a demonstration of double-slit self interference for a single particle fully isolated from the environment. If, however, this ideal laboratory situation is relaxed and the quantum particles are put in contact with the environment in a controlled manner, the quantum interference may be diminished so that the particles start behaving in an increasingly classical way (*4*–*6*). Recently, Hackermüller *et al.* (*7*) have demonstrated this phenomenon by sending heated $C_{60}$ clusters through a double slit. The hot molecules couple via the emission of thermal photons to the environment, and a loss of interference as a function of their temperature is observed. The emission of the photons alters the relative phase between different pathways of the particle toward the detector, an effect referred to as decoherence. Such decoherence of a quantum system can be caused by single or multiple interactions with an external system (*6*). Limiting cases are one single hard interaction causing the decoherence by entanglement with the external system and multiple weak couplings to external perturbers (for instance, a bath) at the other extreme. A gradual transition between these two extremes has been demonstrated for photon scattering (*6*).

We experimentally demonstrated that a system of two electrons is already sufficient to observe the transition from a quantum interference pattern to a classical particle-like intensity distribution for an individual electron. The quantum coherence is not destroyed, however, but remains in the entangled two-electron system. By measuring the correlated momenta of both particles, we illustrate this interference pattern, which is otherwise concealed in the two-body wave function.

The idea of using a homonuclear molecule as the slit-scattering center of a photoelectron goes back to a paper published in 1966 by Cohen and Fano (*8*). Because of the coherence in the initial molecular state, the absorption of one


[1]Institut für Kernphysik, University Frankfurt, Max von Laue Str 1, D-60438 Frankfurt, Germany. [2]Lawrence Berkeley National Laboratory, Berkeley, CA 94720, USA. [3]Centro de Física de Materiales and Donostia International Physics Center, 20018 San Sebastián, Spain. [4]State University of Aerospace Instrumentation, 190000 St. Petersburg, Russia. [5]Department of Physics, Kansas State University, Cardwell Hall, Manhattan, KS 66506, USA. [6]Department of Physics, Auburn University, Auburn, AL 36849, USA.

*To whom correspondence should be addressed. E-mail: doerner@atom.uni-frankfurt.de

photon by the homonuclear molecule launches two coherent electron waves at each of the protons of the molecule (Fig. 1, A and B). The interference pattern of these waves should be visible in the angular distribution of the electron, with respect to the molecular axis. In K shell ionization of heavy diatomics (e.g., $N_2$ and $O_2$, as discussed by Cohen and Fano), interference is visible only if the symmetry (gerade or ungerade) of the molecule with a single 1s hole is resolved (*9*, *10*). For ground-state $H_2^+$ and $H_2$ molecules, only gerade orbitals are populated, and thus these systems constitute clean cases where slitlike behavior is expected (*11*). Still, the originally proposed experiment on $H_2$ (*11*) has not been carried out, because it requires knowledge of the direction of the molecular axis (*12*, *13*). A signature of the interference effect has nonetheless been observed in the wavelength dependence of electrons emitted from a randomly oriented sample of $H_2$ molecules by ion impact ionization (*14*, *15*).

We extended the idea of Cohen and Fano from single photoionization to double photoionization to study the two-body interference of an electron pair. This electron pair is emitted by absorption of a single circularly polarized photon from the $H_2$ molecule (Eq. 1)

$$h\nu + H_2 \rightarrow 2p^+ + 2e^- \qquad (1)$$

$h\nu$ symbolizes a photon of frequency $\nu$. The two electrons are distinguishable by their energy, which allows us to study the interference pattern as a function of the interaction strength or momentum exchanged between the two particles.

Single photons from beamlines 4.0 or 11.0 at the Advanced Light Source at Lawrence Berkeley National Laboratory were used to photoeject both electrons of each $H_2$ molecule. A supersonic $H_2$ gas jet was crossed with the photon beam. For each ionized molecule, the vector momenta of all fragment particles—both ions and both electrons—were determined in coincidence. The orientation of the $H_2$ molecule, or molecular double slit, was measured for each fragmentation by detecting the emission direction of the two protons. Once the two electrons are ejected, the protons rapidly fly apart along the molecular axis, driven by their mutual Coulomb repulsion. A multiparticle imaging technique (cold target recoil ion momentum spectroscopy) (*16*, *17*) was used to detect all particles. The ions and electrons created in the intersection volume of the photon and gas beams were guided by weak electric (50 V/cm) and magnetic fields (8 G) toward two separate multichannel plate detectors with delayline readouts (*18*). From the position of impact and the time of flight, the initial vector momentum of each particle can be determined. Only three particles (two protons and one electron) need to be detected. The momentum of the second electron (in the present case the more energetic of the two) is deduced through momentum conservation of the total system. The Coulomb explosion of the two protons at the equilibrium distance of $H_2$ of 1.4 atomic units (au) yields a kinetic energy of about 10 eV per proton (*19*), and the total electronic binding energy of $H_2$ is about 30 eV. The experiment has been performed at two different photon energies of $E_\gamma = 240$ and 160 eV, leaving about 190 and 110 eV of energy to be shared among the two electrons, respectively. At the high photon energies under consideration here, double photoionization of $H_2$ leads in most cases to one fast electron and one slow electron (*20*).

Figure 1D shows, for ionization by 240-eV photons, the measured angular distribution for a highly energetic electron (called "1" here) of energy $E_1$: 185 eV $< E_1 <$ 190 eV. The second electron, unobserved here, acquires an energy of only $E_2 < 5$ eV. The angular distribution is in the plane perpendicular to the photon propagation vector, and the molecular axis is oriented horizontally in that plane. (The data plotted include events where electron 1 and the molecular axis lie within 10 degrees of the ideal plane perpendicular to the photon propagation direction)

The experimental data show a strong interference pattern that qualitatively resembles the pattern induced by a double slit. For the optical double-slit experiment in which the interference results from a superposition of two coherent spherical waves, the intensity distribution I is given by Eq. 2

$$I(\Phi_{e-mol}) = C\cos^2\left[\frac{k_e \times R \times \cos(\Phi_{e-mol})}{2}\right] \qquad (2)$$

In our case, $R$ is the internuclear distance (1.4 au for $H_2$), $\Phi_{e-mol}$ is the angle of electron emission with respect to the internuclear axis (*12*), $k_e$ is the momentum of the electron, and $C$ is a proportionality constant. An electron energy of 190 eV (as in Fig. 1) corresponds to $k_e = 3.75$ au. The double-slit prediction of Eq. 2 is shown by the blue line in Fig. 1E.

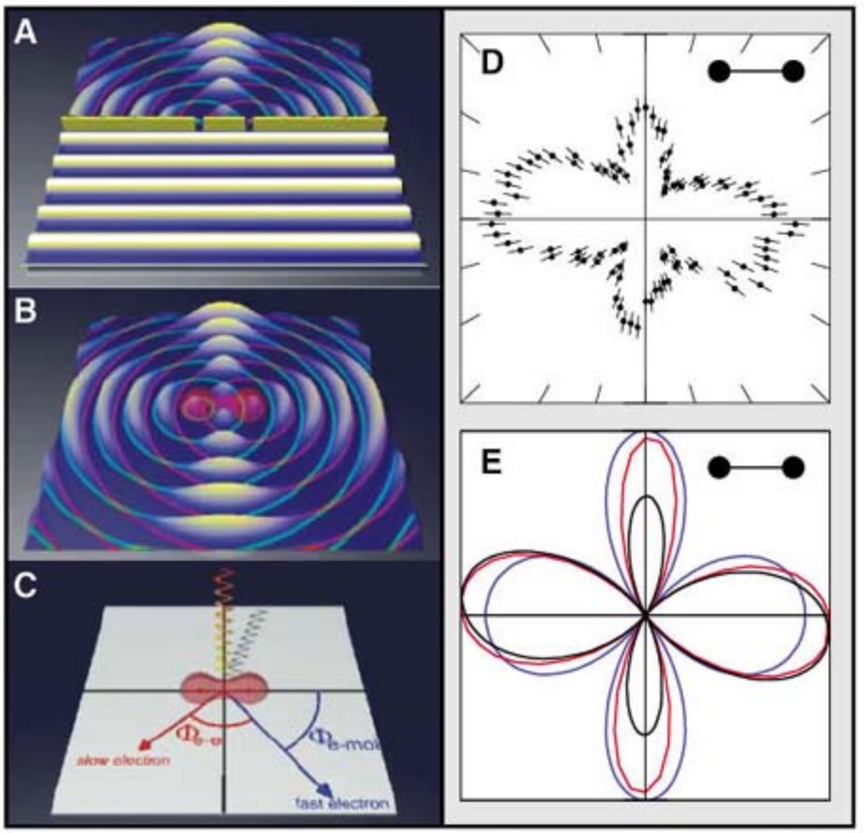


**Fig. 1.** (**A**) Schematic view of a double-slit arrangement. A plane wave approaches the slit from the front. The slit separation is 1.4 au (the internuclear distance in $H_2$), and the wavelength is 3.75 au, which corresponds to an electron energy of 190 eV. (**B**) Photoionization by circularly polarized light launches a coherent spherical photoelectron wave at each nucleus of the molecule; the light propagates into the plane. (**C**) Geometry of the present experiment; circularly polarized light comes from the top. All angular distributions shown in this paper are in the plane perpendicular to the photon propagation vector, $\Phi_{e-mol}$ is the angle of the fast electron's trajectory to the molecular axis, and $\Phi_{e-e}$ is the angle between both electron trajectories. (**D**) Measured electron angular distribution ($\Phi_{e-mol}$) of the faster electron from double photoionization of $H_2$ by circularly polarized light. The orientation of the molecule is horizontal. Light propagates into the plane of the figure, the molecule is fixed ±10° within the plane shown, $E_\gamma = 240$ eV, and the energy of the slow electron $E_2 = 0$ to 5 eV, resulting in $E_1 = 185$ to 190 eV. (**E**) Angular probability distributions derived from Eq. 2 (blue line), RPA calculation (red), and multiple scattering calculation (black).

The deviations from the double-slit prediction can be understood from the somewhat more elaborate theoretical treatment shown in Fig. 1E. By treating the electrons as spherical waves, the simple approximation in Eq. 2 neglects the fact that the electrons are ejected by circularly polarized light and further that they must escape from the two-center Coulomb potential of the two nuclei. The helicity of the light leads to a slight clockwise rotation of the angular distribution, as seen in the experiment and the more elaborate calculations. The Coulomb interaction with the nuclei has two major effects. First, the wavelength of the electron in the vicinity of the protons is shorter than the asymptotic value. This property modifies, in particular, the emission probability along the molecular axis due to a phase shift in the nearfield (*21*). Second, the original partial wave emerging from one of the nuclei is scattered at the neighboring nucleus, thereby launching another partial wave. Thus, the final diffraction pattern is the superposition of four (or more) coherent contributions: the primary waves from the left and right nuclei and the singly or multiply scattered waves created subsequently in the molecular potential. We performed two calculations to take the helicity of the photon, as well as multiple scattering effects, into account. The first calculation (red line in Fig. 1E) was based on the random phase approximation (RPA) (*22*), and the second (black line in Fig. 1E) entailed a multiple scattering calculation, wherein a spherical wave is launched at one proton (*23*). This wave is then multiply scattered in the two-center potential of two protons, which is terminated at a boundary. The direct and multiple scattered waves are then coherently added and symmetrized. Although conceptually very different, both calculations account for all of the relevant physical features: the two-center interference determining the position of minima and maxima, the molecular potential altering the relative height of the peaks, and the helicity of the ionizing photon inducing a rotation. The details of the molecular potential differ in the calculations. The RPA uses a Hartree-Fock potential, whereas the multiple scattering calculation assumes two bare protons.

The full calculations treat the emission of a single electron. Therefore, their good agreement with the experimental data (Fig. 1D) obtained from double ionization might be surprising. This suggests that the additional emission of a slow electron does not substantially alter the wave of the fast particle. For the particular case in which the electron pair consists of a fast and a very slow electron, the diffraction of a coherent electron pair can be treated by simply neglecting the slow electron.

This simple one-particle picture completely fails in scenarios where lower primary and higher scattered electron energies result in stronger coupling between the electrons. Figure 2, A and B, shows the results for different energy partitions of the first and second electron after ionization by 160-eV photons. Whereas for $E_1 \approx 110$ eV and $E_2 < 1$ eV the interference is still visible (Fig. 2A), it completely disappears when $E_1 \approx 95$ eV and 5 eV $< E_2 <$ 25 eV (Fig. 2B). In the latter case, the distribution approaches the isotropic result without two-center interference. By comparing these data to the corresponding theoretical estimates (Fig. 2, C and D), we can now show that the observed loss of interference contrast is a result of decoherence and not of the changing electron wavelength.

Coulomb interaction between two quantum mechanical systems (electrons 1 and 2 in our case) does not destroy phases. Rather, it entangles the wave functions of the two subsystems (*24*, *5*). In our experiment, we observed both electrons in coincidence. Therefore we can investigate this entangled two-particle system to search for the origin of the apparent loss of coherence in a single-particle subsystem. Figure 3 shows the correlation in this two-body system. The horizontal axis is the angle of the fast-electron momentum, with respect to the molecular axis (i.e., the angle that is plotted in all other figures). The vertical axis is the angle between the two electron's momenta. It may be helpful to think of the horizontal axis as the scattering of electron 1 by the double slit and the vertical axis as the scattering angle between the electrons. Marked interference patterns emerge in this display of the two-particle wave function. No vestige of these patterns remains, however, if the distribution is integrated over the vertical axis.

When subsets of the data with restricted angular ranges of $\Phi_{e-e} = +70 \pm 20°$ (Fig. 3, B and C) and $\Phi_{e-e} = -70 \pm 20°$ (Fig. 3, D and E) are examined, then the interference pattern is resurrected (here, $\Phi_{e-e}$ is the angle between both electron trajectories). However, depending on the angle between the electrons in the selected subset of the data, the interference pattern is tilted to the right (Fig. 3C) or left (Fig. 3E). Without the restriction of this relative angle, the shifted minima and maxima cancel each other out, leading to the almost isotropic distribution of Fig. 2B.

The interference maxima are concentrated along two horizontal lines. These lines of highest intensity lie at a relative angle of about 100° between the two electrons. This distribution is a well-known indication of the mechanism whereby the absorption of a single photon by one electron can induce its ejection, as well as that of the other electron, after their binary collision

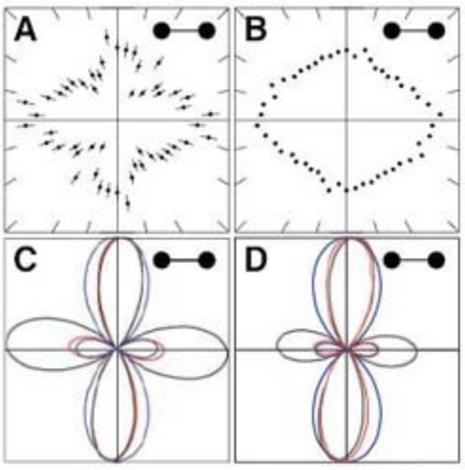


**Fig. 2.** (**A**) Electron angular distribution as in Fig. 1D but for $E_\gamma = 160$ eV, $E_2 < 1$ eV, and $E_1 \approx 110$ eV. (**B**) $E_\gamma = 160$ eV and 5 eV $< E_2 <$ 25 eV, resulting in $E_1 \approx 85$ to 105 eV. (**C** and **D**) Angular distribution of a single electron of energy $E_e$ for the energy distributions in (A) and (B), respectively. Red, Eq. 2; blue, RPA calculation; black, multiple scattering calculation.

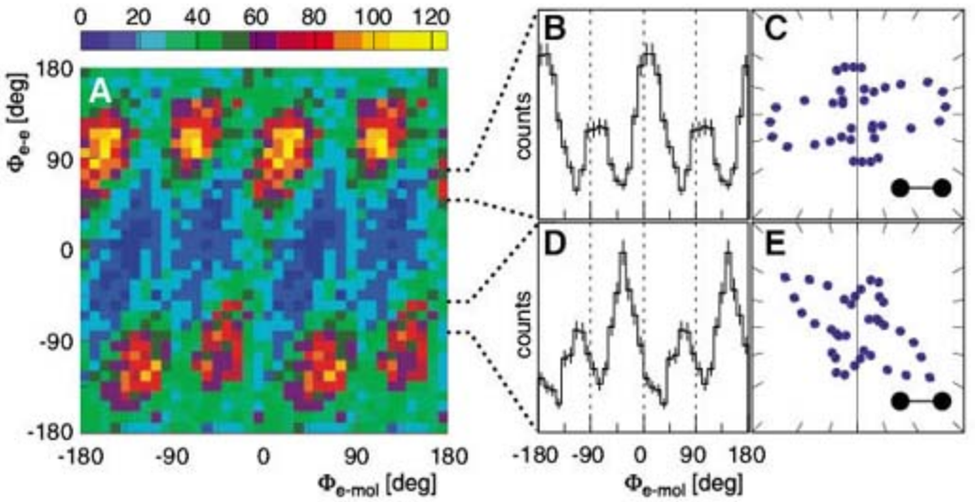


**Fig. 3.** Correlation between both electrons for double photoionization of $H_2$ at $E_\gamma = 160$ eV and 5 eV $< E_2 <$ 25 eV, corresponding to $E_1 \approx 85$ to 105 eV. (**A**) *x* axis: angle of fast electron to the molecular axis ($\Phi_{e-mol}$) (see Fig. 1C), and *y* axis: angle $\Phi_{e-e}$ between the two electrons. Both electrons and the molecule are selected to lie within ±30° of the polarization plane. Thus, Fig. 2B is a projection of this figure onto the horizontal axis. (**B**) Projection of (A) onto the horizontal axis for $50° < \Phi_{e-e} < 80°$. (**C**) Polar presentation of the data shown in (B). (**D**) Projection analogous to (B) for $-80° < \Phi_{e-e} < -50°$. (**E**) Polar presentation of data shown in (D).

(*20*, *25*). The angles $\Phi_{e-e} = 90°$ and $\Phi_{e-e} = -90°$ correspond to a kick of the second electron, either to the left or the right. This strong electron-electron Coulomb interaction mediates the double ionization and creates an entanglement between the two electrons. Electron collisions of this sort in bound systems have been demonstrated directly in pump-probe experiments (*26*).

This situation is an intramolecular version of a scattering event downstream of a double slit (*27*, *6*). When either photons (*6*) or particles (*27*) are scattered from a beam after passage through a double slit, the scattering induces a phase shift, which then leads to a shift of the interference pattern. If the momentum transfer is not measured in coincidence (*6*), the fringe visibility is lost. In this experiment, both electrons are initially delocalized inside the molecule in a completely coherent single quantum state. Before photoabsorption, both electrons are confined in the hydrogen ground state, which is symmetric with respect to its two atomic centers. Thus, we observed not a scattering between classical localized particles but a coherent entanglement of the wave function of the two electrons.

It is instructive to think of the electronic two-body system as split into its subsystems and to consider one subsystem as the environment of the other. The strong Coulomb interaction entangles the two subsystems and leads to a position-dependent modification of phase of the single-particle wave function inside each of the two subsystems. The entanglement of the electrons in the pair is directly visible in their mutual angular distribution and is further evidenced by the observation that selecting the momentum of one electron makes the interference pattern of its partner reappear. In the spirit of discussions dating from the early history of quantum mechanics, one particle can be considered an observer that carries partial information about the other particle and its path through the double slit. The amount of which-way information exchanged between the particles is limited by the observer particle's de Broglie wavelength (*28*). The key difference between the situation depicted in Fig. 2A (which shows interference) and Fig. 2B (which shows no interference) is that the wavelength of the second, unobserved electron is much shorter in the latter case.

Our experiment thus reveals that a very small number of particles suffices to induce the emergence of classical properties, such as the loss of coherence. A four-body system, such as fragmented molecular hydrogen, acts as a double slit in the sense that coherence is lost in a subsystem of entangled electrons. Such a fundamental system facilitates the study of the influence of interelectronic Coulomb interactions on the coherence properties of a single electron. In solid-state–based quantum computing devices, such electron-electron interaction represents a key challenge. One advantageous aspect of the finite system investigated here is that, theoretically, it is fully tractable at present (*29*–*32*).

### References and Notes


1. C. Jönnson, *Z. Phys. A* **161**, 454 (1961).
2. M. Arndt *et al.*, *Nature* **401**, 680 (1999).
3. M. Noel, C. Stroud, *Phys. Rev. Lett.* **75**, 1252 (1995).
4. E. Joos, H. Zeh, *Z. Phys. B* **59**, 223 (1985).
5. W. Zurek, *Rev. Mod. Phys.* **75**, 715 (2003).
6. D. A. Kokorowski, A. D. Cronin, T. D. Roberts, D. E. Pritchard, *Phys. Rev. Lett.* **86**, 2191 (2001).
7. L. Hackermüller, K. Hornberger, B. Brezger, A. Zeilinger, M. Arndt, *Nature* **427**, 711 (2004).
8. H. Cohen, U. Fano, *Phys. Rev.* **150**, 30 (1966).
9. D. Rolles *et al.*, *Nature* **7059**, 711 (2005).
10. X. Liu *et al.*, *J. Phys. B* **39**, 4801 (2006).
11. I. Kaplan, A. Markin, *Sov. Phys. Dokl.* **14**, 36 (1969).
12. M. Walter, J. Briggs, *J. Phys. B* **32**, 2487 (1999).
13. J. Fernandez, O. Fojon, A. Palacios, F. Martín, *Phys. Rev. Lett.* **98**, 043005 (2007).
14. N. Stolterfoht *et al.*, *Phys. Rev. Lett.* **87**, 023201 (2001).
15. D. Misra *et al.*, *Phys. Rev. Lett.* **92**, 153201 (2004).
16. J. Ullrich *et al.*, *Rep. Prog. Phys.* **66**, 1463 (2003).
17. R. Dörner *et al.*, *Phys. Rep.* **330**, 95 (2000).
18. O. Jagutzki *et al.*, *Nucl. Instrum. Methods A* **477**, 244 (2002).
19. T. Weber *et al.*, *Nature* **431**, 437 (2004).
20. A. Knapp *et al.*, *Phys. Rev. Lett.* **89**, 033004 (2002).
21. G. L. Yudin, S. Chelkowski, A. D. Bandrauk, *J. Phys. B* **39**, L17 (2006).
22. S. K. Semenov, N. A. Cherepkov, *J. Phys. B* **36**, 1409 (2003).
23. R. Díez Muiño, D. Rolles, F. J. García de Abajo, C. S. Fadley, M. A. Van Hove, *J. Phys. B* **35**, L359 (2002).
24. T. Opatrny, G. Kurizki, *Phys. Rev. Lett.* **86**, 3180 (2001).
25. M. Pont, R. Shakeshaft, *Phys. Rev. A* **51**, R2676 (1995).
26. S. N. Pisharody, R. R. Jones, *Science* **303**, 813 (2004).
27. K. Hornberger *et al.*, *Phys. Rev. Lett.* **90**, 160401 (2003).
28. W. Wootters, W. Zurek, *Phys. Rev. D* **19**, 473 (1979).
29. W. Vanroose, F. Martín, T. Rescigno, C. W. McCurdy, *Science* **310**, 1787 (2005).
30. F. Martín *et al.*, *Science* **315**, 629 (2007).
31. J. Colgan, M. S. Pindzola, F. Robicheaux, *J. Phys. B* **37**, L377 (2004).
32. D. Dundas, *J. Phys. B* **37**, 2883 (2004).


33. We thank M. Walter, J. Briggs, A. Kheifets, U. Becker, D. Rolles, E. Joos, K. Ueda, M. Arndt, and M. Aspelmeyer for enlightening discussions. We acknowledge outstanding support by the staff of the Advanced Light Source, in particular by E. Arenholz, T. Young, H. Bluhm, and T. Tyliszczak. This work was supported by the Deutsche Forschungsgemeinschaft and by the Office of Basic Energy Sciences, Division of Chemical Sciences of the U. S. Department of Energy under contract DE-AC03-76SF00098.

10 May 2007; accepted 18 September 2007
10.1126/science.1144959


# Accelerated Uplift and Magmatic Intrusion of the Yellowstone Caldera, 2004 to 2006


**Wu-Lung Chang,[1]* Robert B. Smith,[1]* Charles Wicks,[2] Jamie M. Farrell,[1] Christine M. Puskas[1]**



The Yellowstone caldera began a rapid episode of ground uplift in mid-2004, revealed by Global Positioning System and interferometric synthetic aperture radar measurements, at rates up to 7 centimeters per year, which is over three times faster than previously observed inflation rates. Source modeling of the deformation data suggests an expanding volcanic sill of ~1200 square kilometers at a 10-kilometer depth beneath the caldera, coincident with the top of a seismically imaged crustal magma chamber. The modeled rate of source volume increase is 0.1 cubic kilometer per year, similar to the amount of magma intrusion required to supply the observed high heat flow of the caldera. This evidence suggests magma recharge as the main mechanism for the accelerated uplift, although pressurization of magmatic fluids cannot be ruled out.


The Yellowstone volcanic field is the largest in North America (Fig. 1A). The youngest of three giant eruptions that formed the field occurred 640,000 years ago, creating the 40-km-wide by 60-km-long Yellowstone caldera. This eruption was followed by 30 smaller eruptions of dominantly rhyolite flows, the youngest 70,000 years ago (*1*). Earthquakes, ground deformation, very high heat flow, and the world's largest distribution of hydrothermal features characterize Yellowstone (*2*, *3*), similar to those of other silicic volcanic fields such as Long Valley, California, and Phlegrean Fields, Italy (*4*, *5*).

Geodetic measurements of Yellowstone from 1923 to 2004 using precise leveling, GPS (Global Positioning System), and InSAR (interferometric synthetic aperture radar) have revealed multiple episodes of caldera uplift and subsidence, with maximum average rates of ~1 to 2 cm/year generally centered at its two resurgent domes, Sour Creek and Mallard Lake (*6*–*8*). In addition, an area northwest of the caldera near Norris Geyser Basin experienced periods of substantial ground deformation (*8*, *9*). These spatial and temporal variations of the Yellowstone unrest also correlated with pronounced changes in seismic and hydrothermal activity (*9*, *10*) (Fig. 1B).


[1]Department of Geology and Geophysics, University of Utah, Salt Lake City, UT 84112, USA. [2]U.S. Geological Survey, MS 977, Menlo Park, CA 94025, USA.

*To whom correspondence should be addressed. E-mail: wchang@earth.utah.edu (W.-L.C.); R.Smith@earth.utah.edu (R.B.S.)

The University of Utah and the Plate Boundary Observatory (PBO) operate twelve continuous-recording GPS stations in Yellowstone to monitor ground movement (*11*) (Fig. 1A). Temporal variations of the vertical deformation (Fig. 2A) show 1 to 2 cm of subsidence in the caldera (e.g., at station LKWY) and uplift in the Norris area (at station NRWY) during the first 6 months of 2004. The caldera motion then suddenly reversed to uplift in July 2004 at unexpected high rates, ~7 cm/year at station WLWY, whereas the Norris area began to subside about 3 months later. Accelerated horizontal movements correlated in time with the changes in vertical motions (fig. S1). The GPS data also reveal a near-simultaneous inception of uplift across the entire caldera (Fig. 2A), in contrast to the previous observations that deformation shifted laterally from the Sour Creek dome toward the Mallard Lake dome in 1 to 2 years (*7*).

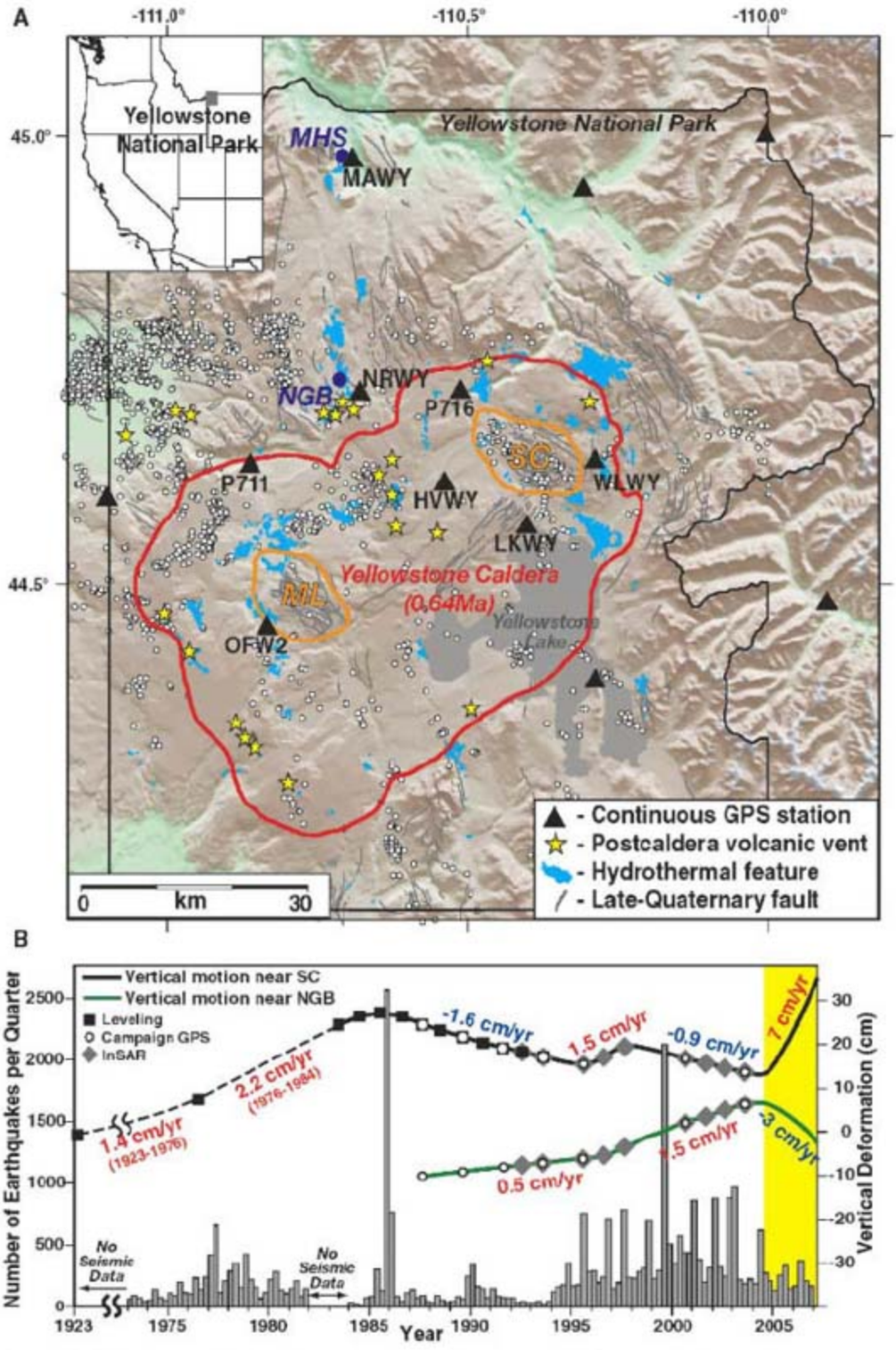


**Fig. 1.** (**A**) Volcano tectonic setting and GPS station locations of the Yellowstone volcanic field. White circles are earthquake epicenters from October 2004 to March 2007. SC indicates Sour Creek resurgent dome; ML, Mallard Lake resurgent dome; NGB, Norris Geyser Basin; and MHS, Mammoth Hot Springs. GPS station names are abbreviated to four-character codes. Ma, million years ago. (**B**) Time sequence of Yellowstone vertical ground motions and quarterly earthquake counts. Different symbols represent early geodetic measurements (*6*–*9*). The yellow shaded area highlights the period of accelerated deformation reported in this study. Note that the 1923–1976 and 1976–1984 rates were each determined from only two measurements.

InSAR measurements (ENVISAT IS1 and IS2 modes) from 2004 to 2006 (*11*), with a spatial resolution of ~30 m, reveal ground motions that are consistent with the GPS observations (Fig. 2B and fig. S2). The inflation increases symmetrically toward the caldera center about the long axis (northeast-southwest), with the highest rate of ~7 cm/year at the Sour Creek dome being three to five times faster than uplift rates in 1923–1984 and 1995–1997 (Fig. 1B). The Norris subsidence is ~3 cm/year, more than two times greater than the 1996–2002 uplift rate in this area. The GPS horizontal velocities, in addition, indicate ground motions directed outward from the caldera at 0.8 to 2.2 cm/year and inward to the Norris area at 0.7 to 2.0 cm/year.

To evaluate the causes of the observed rapid deformation, we jointly inverted the GPS and InSAR data (*12*) for the geometry and expansion or contraction of rectangular dislocations in a homogeneous elastic half-space to simulate inflating and deflating volcanic volumes. A nonlinear optimization method was used to determine the source model that minimizes the difference between the observed and predicted ground motions (*13*). Uncertainties of model parameters were evaluated by a $\chi^2$ method (*11*).

The best-fitting sources for the GPS and IS2 InSAR data include an expanding sill-like volume dipping 5°SE (5°NW to 15°SE) at a depth of 10 km (6 to 14 km) beneath the Yellowstone caldera and a contracting volume dipping 12°SE (7°NW to 18°SE) at a depth of 8 km (6 to 16 km) under the Norris area (Fig. 3). The average rates of volumetric change are 0.11 km$^3$/year (0.10 to 0.12 km$^3$/year) and –0.01 km$^3$/year (–0.005 to –0.015 km$^3$/year) for the inflating and deflating sources, respectively. A joint inversion of the GPS and IS1 InSAR data also resulted in similar source parameters, indicating the robust nature of the modeling results (fig. S3). Our models, assuming uniform constitutive properties, predict ~90% of the observed ground motion within the data confidence limits. We also tested the effects of crustal heterogeneity by including layers with different elastic constants and showed that they would not notably affect our modeling results (*11*).

Episodic intrusion or recharge of magma into the upper crust has been proposed as a mechanism for previous Yellowstone caldera uplift (*1*, *2*). In this conceptual model, basaltic

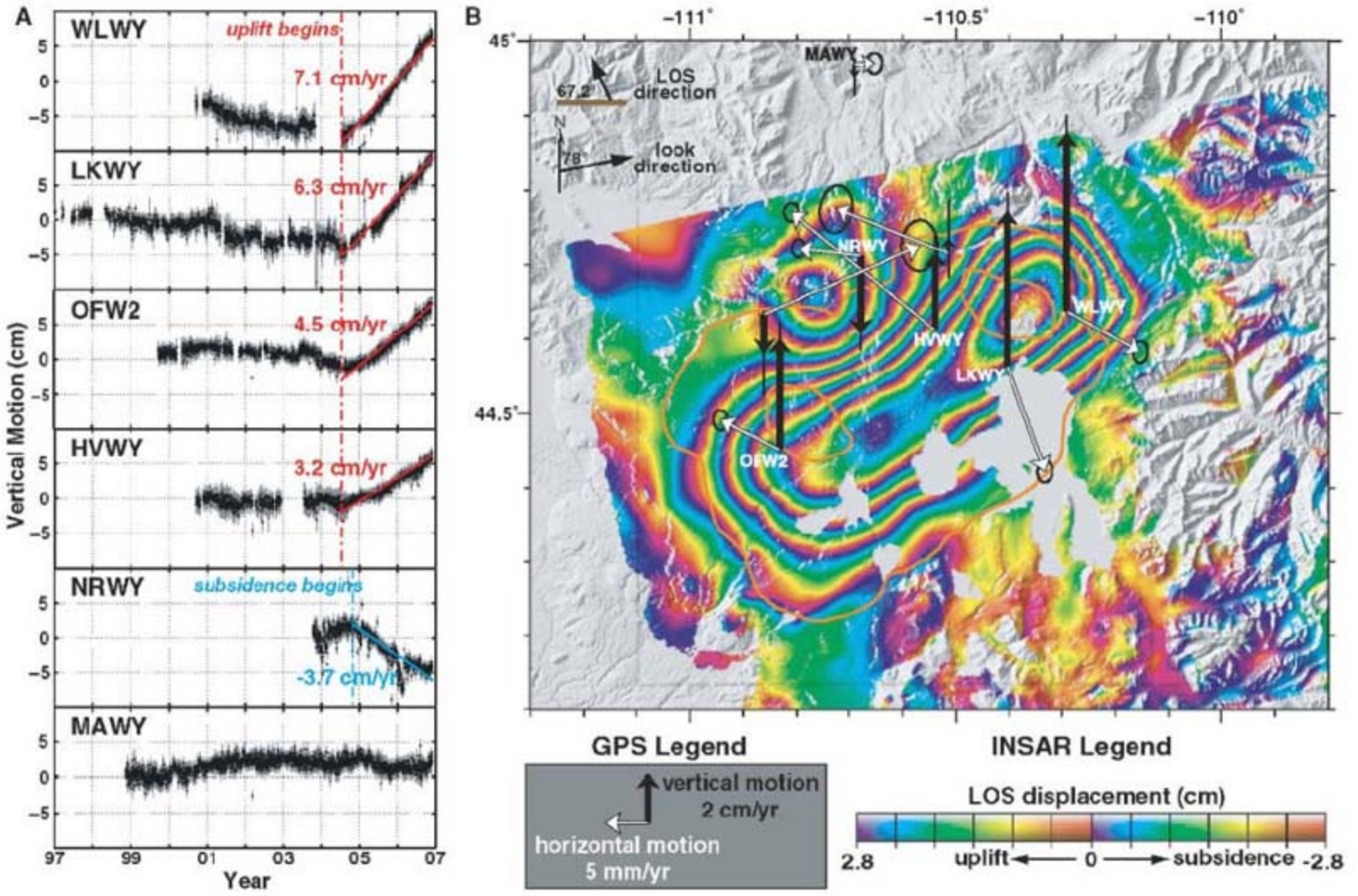


**Fig. 2.** **(A)** Temporal variation of vertical ground motions of labeled Yellowstone GPS stations. Each dot represents a daily position determination. Light gray bars are 1-σ errors. Red and blue dot-dash lines mark the inceptions of the uplift and the subsidence, respectively. Deformation rates are the slopes of the interpolated lines. **(B)** A stacked InSAR interferogram (ENVISAT IS2 mode) from 22 September 2004 to 23 August 2006 overlain with averaged GPS velocities from 07 October 2004 and 07 October 2006. The line-of-sight (LOS) displacement of Earth's surface toward the satellite from the interferogram infers a total uplift of about 11 cm in the west part of the caldera and as large as 15 cm at the Sour Creek resurgent dome and a subsidence of 6.6 cm near the Norris Geyser Basin. White and black arrows represent horizontal and vertical velocity vectors, respectively. Black ellipses and bars are scaled 2-σ errors (*11*).

magma originating from a mantle plume at depths of ~50 km ascends buoyantly through the crust, providing thermal energy to partially melt crustal rocks and create the rhyolitic magma component that characterizes the silicic volcanism. The basaltic and rhyolitic magmas then crystallize and cool, releasing energy responsible for Yellowstone's extraordinarily high heat flow of ~2000 mW/m$^2$ measured from Yellowstone Lake (*14*) and geochemical evidence (*3*).

Seismic tomographic imaging provided direct evidence for the partially molten crustal magma chamber beneath the caldera (*15*). Anomalies of low P-wave velocity, up to 6%, at depths of 8 to 16 km were interpreted as a body of crystallized magma of ~4000 km$^3$ directly underlying the caldera. The top of this body and our modeled sill overlap (Fig. 3E), implying that the accelerated uplift is caused by inflation from the shallow part of the magma chamber. Moreover, to maintain the observed caldera heat flux requires a magma crystallization rate of ~0.1 km$^3$/year (*3*), which is comparable to our modeled source expansion rate.

We thus suggest that the 2004–2006 episode of accelerated inflation occurred in response to a caldera-wide magma recharge of the Yellowstone volcanic system. Such a high rate of intrusion may have occurred during past uplift episodes, for example between the first two leveling surveys in 1923 and 1976, when the caldera rose a total of ~75 cm but the rate of 1.4 cm/year was linearly interpolated between observations (Fig. 1B).

An alternate interpretation for the caldera uplift is that magmatic fluids (water and gases) exsolved from magma crystallization were trapped beneath impermeable rocks, causing pressurization of the deep hydrothermal system and in turn inflating the ground surface (Fig. 4). Crystallizing 0.1 km$^3$/year of rhyolitic magma, which is required to provide the observed thermal heat flow, and trapping all the released water would result in a volumetric expansion of ~0.013 km$^3$/year (*3*, *16*). This value, however, is about 10 times smaller than the source inflation rate of 0.11 km$^3$/year responsible for the current uplift. Although the volumetric expansion could be greater if gas discharge is taken into account, this mechanism requires a rapid increase in fluid exsolution from magma crystallization to account for the accelerated caldera uplift and is thus a less viable cause for the observed deformation.

Source modeling of early episodes of caldera inflation (*7*, *17*) imply geometries and depths similar to those from our model but much lower rates of volumetric increase, 0.01 to 0.03 km$^3$/year, which are comparable to the rates from the above magmatic fluid model. This evidence suggests that pressurizing fluid systems near the top of the crustal magma reservoir is a plausible source mechanism for the previous uplift episodes. Therefore, magma intrusion and fluid pressurization should be considered as jointly operating processes to explain the accelerated caldera uplift reported here, although our estimate of large volume increase implies the former as a preferred source model. Further independent observations, such as temporal microgravity changes, capable of resolving mass and density variations of the magmatic reservoir would be useful to discrim-

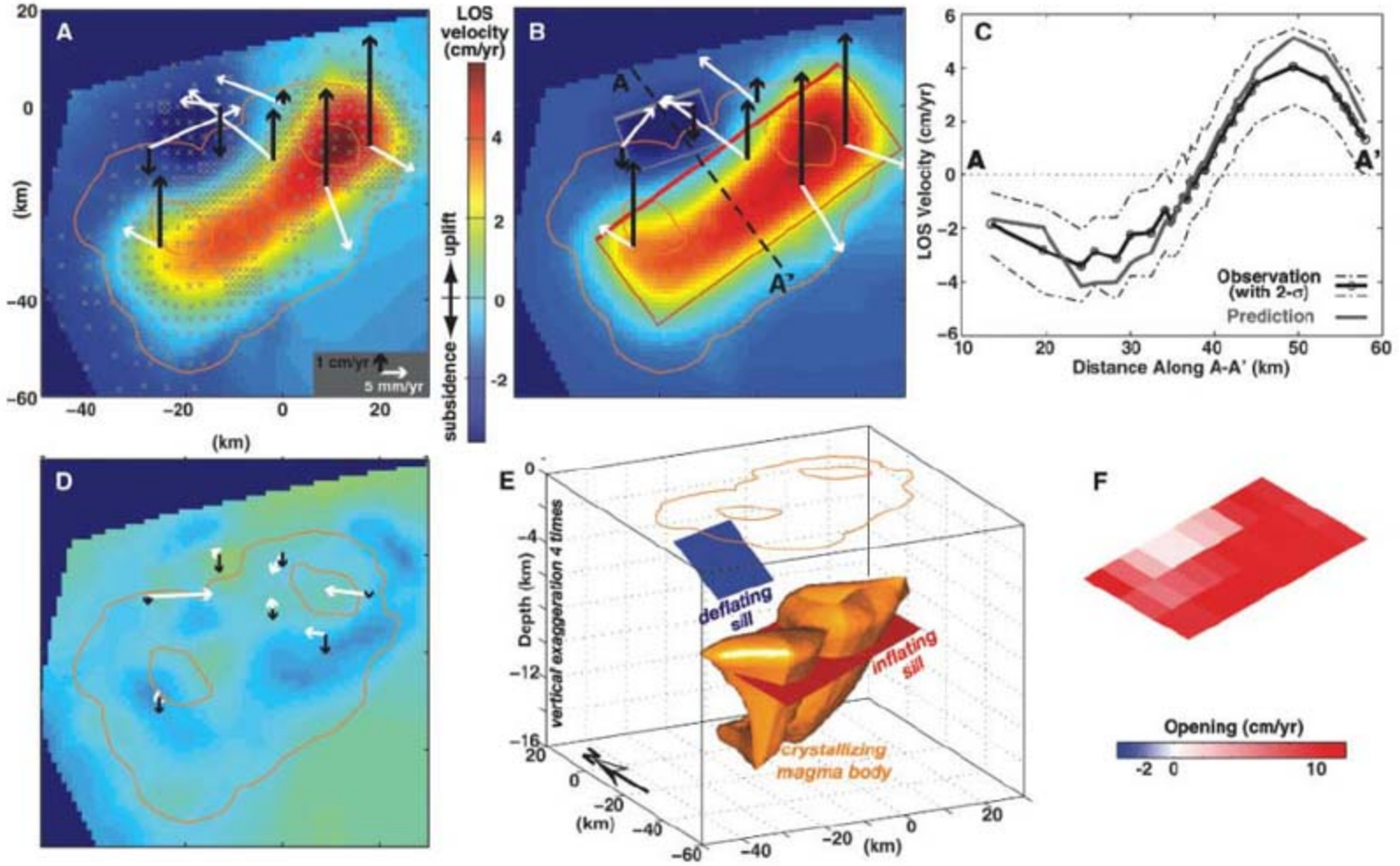


**Fig. 3.** **(A)** Observed Yellowstone ground motion, 2004–2006. Black and white arrows are vertical and horizontal velocity vectors, respectively, measured by GPS. Background colors represent average LOS velocities interpolated by reduced InSAR data points (gray crosses) (*11*). **(B)** Modeled ground motion. Surface projections of the modeled expanding and contracting sills are shown by red and gray rectangles, respectively. Solid lines highlight the tops of the sills. **(C)** Modeled and observed ground motion along the profile A-A′ in (B). **(D)** Residuals between data and model predictions. **(E)** Three-dimensional view (from the southwest) of the modeled volcanic sills superimposed on a seismically imaged magma body (*15*). **(F)** Opening distribution of the modeled inflating sill. We first assumed a uniform dislocation beneath the caldera to solve for the geometry of the sill. The dislocation was then discretized into 30 patches, and the opening of each was estimated to best explain the spatial variation of the caldera uplift (*11*).

inate the contribution between the two different volcanic mechanisms (*18*, *19*).

The inflation of the magmatic sill can induce dilatational strain in the surrounding volcanic rocks (Fig. 4), leading to an increase in permeability and a decrease in pore pressure by opening new or self-sealed fractures. Accordingly, the dilated zone beneath the northern caldera can experience lower pore pressure relative to the hydrothermal reservoirs beneath the Norris area. This induced pressure gradient can thereby drive fluids southeastward into the caldera, depressurizing the Norris hydrothermal systems and causing the ground there to subside. Previous studies also implied that the widespread hydrothermal and volcanic features across the northern caldera boundary indicate highly fractured and permeable crustal rocks, providing pathways for fluid migration (*9*, *16*).

We therefore propose that the 2004–2006 deflation near Norris Geyser Basin was in response to a redistribution of hydrothermal fluids as a consequence of caldera inflation. Moreover, earthquake activity during the deformation period was concentrated near the northern caldera boundary, while the rest of the caldera experienced low rates of seismicity (Fig. 1A). Volumetric expansion of crustal rocks due to the induced dilatation can increase the strain rate and promote brittle fracturing. With fluids migrating from the Norris region into the caldera, earthquakes can be induced within the dilated zone between the inflating and deflating source volumes (Fig. 4).

The caldera-wide accelerated uplift reported here is interpreted as magmatic recharge of the Yellowstone magma body (*20*). Although the geodetic observations and models do not imply an impending volcanic eruption or hydrothermal explosion, they are important evidence of ongoing processes of a large caldera that was produced by a super volcano eruption.

### References and Notes


1. R. L. Christiansen, *U.S. Geol. Surv. Prof. Pap. 729-G* (2001).
2. R. B. Smith, L. W. Braile, *J. Volcanol. Geotherm. Res.* **61**, 121 (1994).
3. R. O. Fournier, *Annu. Rev. Earth Planet. Sci.* **17**, 13 (1989).
4. D. P. Hill, *Geol. Soc. London Spec. Publ.* **269**, 1 (2006).
5. G. De Natale *et al.*, *Geol. Soc. London Spec. Publ.* **269**, 25 (2006).
6. D. Dzurisin, K. M. Yamashita, J. W. Kleinman, *Bull. Volcanol.* **56**, 261 (1994).
7. C. Wicks, W. Thatcher, D. Dzurisin, *Science* **282**, 458 (1998).
8. C. M. Puskas, R. B. Smith, C. M. Meertens, W. L. Chang, *J. Geophys. Res.* **112**, 10.1029/2006JB004325 (2007).
9. C. Wicks, W. Thatcher, D. Dzurisin, J. Svarc, *Nature* **440**, 72 (2006).
10. G. P. Waite, R. B. Smith, *J. Geophys. Res.* **107**, 10.1029/2001JB000586 (2002).
11. Materials and methods are available as supporting material on *Science* Online.
12. After several tests we chose to weigh the GPS velocity measurements by a factor of 5 to equal the contribution of the GPS and InSAR data sets to the inversion.
13. P. Cervelli *et al.*, *J. Geophys. Res.* **107**, 10.1029/2001JB000602 (2002).
14. P. Morgan, D. D. Blackwell, R. E. Spafford, R. B. Smith, *J. Geophys. Res.* **82**, 3719 (1977).
15. S. Husen, R. B. Smith, G. P. Waite, *J. Volcanol. Geotherm. Res.* **131**, 397 (2004).
16. D. Dzurisin, J. C. Savage, R. O. Fournier, *Bull. Volcanol.* **52**, 247 (1990).
17. D. W. Vasco, C. M. Puskas, R. B. Smith, C. M. Meertens, *J. Geophys. Res.* **112**, 10.1029/2006JB004641 (2007).
18. M. Battaglia, C. Roberts, P. Segall, *Science* **285**, 2119 (1999).

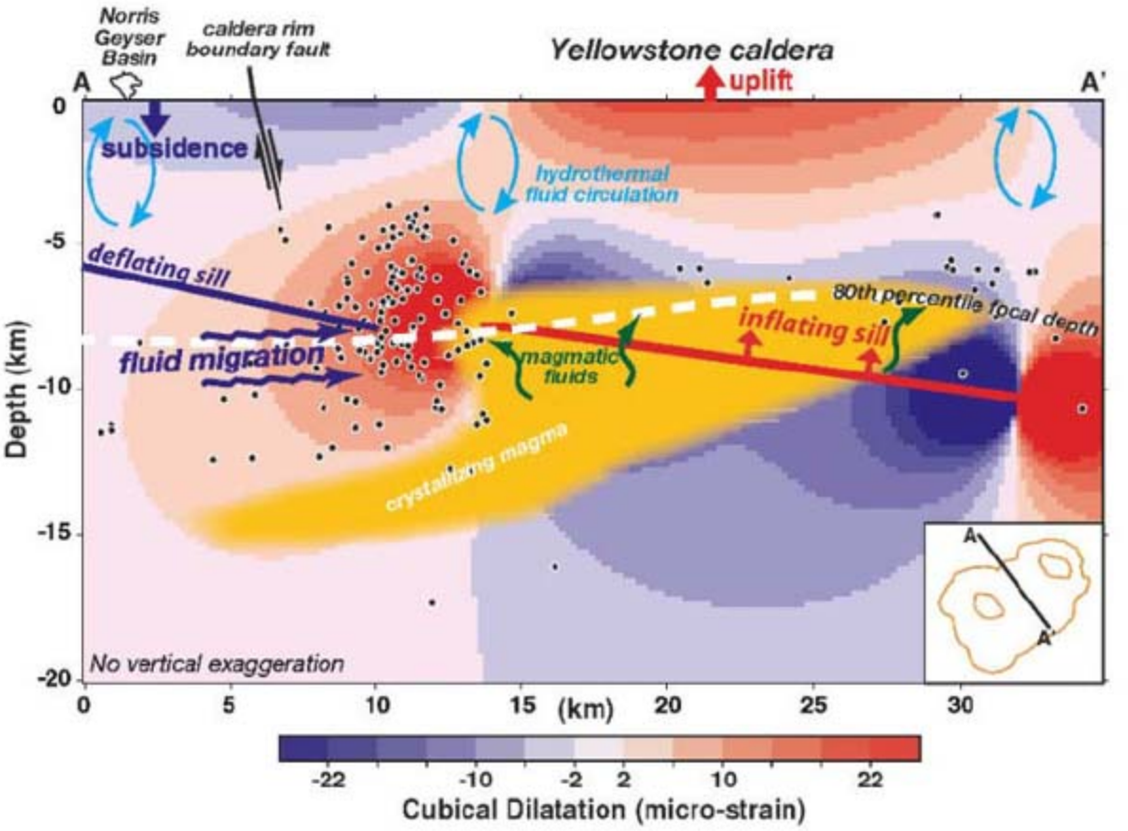


**Fig. 4.** Schematic diagram of plausible magmatic and hydrothermal processes responsible for 2004–2006 accelerated Yellowstone caldera uplift and Norris subsidence. Black dots are earthquake hypocenters from October 2004 to March 2007 (see Fig. 1A for the epicenters). The yellow area shows the seismically imaged magma body in Fig. 3E. Background colors represent cubical dilatation, in unit changes of volume, induced by the modeled inflating sill. Fluids exsolved from magma crystallization can be trapped beneath the nonpermeable rocks near the brittle-ductile transition zone, taken as the 80th percentile focal depth of earthquakes (white dashed line) (*21*, *22*), to produce the caldera uplift.


19. J. Gottsmann, A. Folch, H. Rymer, *J. Geophys. Res.* **111**, 10.1029/2005JB003745 (2006).
20. Updated GPS data show that this episode of Yellowstone caldera uplift is continuing as of September 2007 (fig. S1).
21. R. B. Smith, R. L. Bruhn, *J. Geophys. Res.* **89**, 5733 (1984).
22. S. Husen, R. B. Smith, *Bull. Seismol. Soc. Am.* **94**, 880 (2004).


23. This project has been a cooperative effort of the University of Utah, the Yellowstone Volcano Observatory, and the EarthScope PBO. ENVISAT data were provided by the European Space Agency as part of Cat-1 project 2765. Discussions with R. Fournier, C. Meertens, G. Waite, H. Heasler, and J. Lowenstern greatly benefited the paper. M. Poland, S.-H. Yun, and three anonymous reviewers provided constructive comments. The research was funded by the NSF Continental Dynamics Program, grant no. EAR0314237, and The Brinson Foundation.


**Supporting Online Material**
www.sciencemag.org/cgi/content/full/318/5852/952/DC1
Materials and Methods
Figs. S1 to S3
Tables S1 and S2
References and Notes


21 June 2007; accepted 4 October 2007
10.1126/science.1146842


# Observation of the One-Dimensional Diffusion of Nanometer-Sized Dislocation Loops


K. Arakawa,[1]* K. Ono,[2] M. Isshiki,[3] K. Mimura,[3] M. Uchikoshi,[3] H. Mori[1]



Dislocations are ubiquitous linear defects and are responsible for many of the properties of crystalline materials. Studies on the glide process of dislocations in bulk materials have mostly focused on the response of dislocations with macroscopic lengths to external loading or unloading. Using in situ transmission electron microscopy, we show that nanometer-sized loops with a Burgers vector of ½⟨111⟩ in α-Fe can undergo one-dimensional diffusion even in the absence of stresses that are effective in driving the loops. The loop size dependence of the loop diffusivity obtained is explained by the stochastic thermal fluctuation in the numbers of double kinks.


The hardness and toughness of crystalline materials is often governed by the generation and motion of linear defects termed dislocations (*1*). Previous studies on the glide process of dislocations in bulk materials have focused on the response of dislocations with macroscopic lengths to external loading or unloading (*1*, *2*). On the other hand, it is known that nanoscale dislocations can be formed as loops in bulk materials by the agglomeration of self-interstitial atoms, which are produced upon energetic particle irradiation, in the shape of disks. Recent molecular dynamics (MD) calculations have shown that in metals and alloys, extremely small interstitial-type dislocation loops with diameters of less than a few nanometers can undergo fast one-dimensional (1D) glide diffusion in the direction of their Burgers vector, **b**, even under zero stress (*3*–*7*). This phenomenon has also been examined theoretically (*8*–*10*). Other computational and theoretical studies have shown that the loop diffusion plays a central role in the degradation processes of materials for nuclear fission and nuclear fusion, upon high-energy particle irradiation (*11*, *12*).

One MD study has shown that the highly diffusive loops with **b** values of ½[111] in α-Fe, which are smaller than ~2.4 nm in diameter, can be regarded as bundles of crowdions with [111] axes (*6*). A crowdion is a kind of a self-interstitial atom (*13*); it has a long-range compression-strain field in a close-packed direction, and its center of mass can easily move one-dimensionally along the axis. The crowdion bundles move by the almost independent motions of the constituent crowdions along their


[1]Research Center for Ultra-High Voltage Electron Microscopy, Osaka University, 7-1 Mihogaoka, Ibaraki, Osaka 567-0047, Japan. [2]Department of Material Science, Shimane University, 1060 Nishikawatsu, Matsue 690-8504, Japan. [3]Institute of Multidisciplinary Research for Advanced Materials, Tohoku University, 2-2-1 Katahira, Aoba-ku, Sendai 980-8577, Japan.

*To whom correspondence should be addressed. E-mail: arakawak@uhvem.osaka-u.ac.jp

axes. The manner of the motion of the crowdion bundles seems to differ from that of "conventional dislocations," which move like strings because of the cooperative motion of atoms around the core (*1*). In contrast, loops larger than crowdion bundles are regarded as the simple loops of the "conventional dislocations." However, such loops did not show any significant movement during the span calculated by MD on the order of nanoseconds (*6*); therefore, their diffusion process is difficult to examine by MD.

In contrast, experimental studies using transmission electron microscopy (TEM) have shown that nanometer-sized loops can perform a glide motion (*14*–*16*). However, these results were only qualitative and the origin for the loop motion was not clear.

We used in situ TEM to examine the motion process of nanometer-sized ½⟨111⟩ "conventional" loops (>5.9 nm in diameter) in α-Fe with purity of 99.998 weight % (table S1) upon heating under the application of no external stress and negligible internal stresses. Our study was motivated by the following essential but unresolved questions: Can "conventional" loops undergo diffusion? If they can diffuse, how high is their diffusivity? How do loops undergo the diffusion?

We performed two kinds of experiments: (i) measurement of the dependence of the motion fraction of loops on temperature and time, and (ii) examination of the behavior of almost isolated loops. Figure 1 shows the experimental setup for both experiments (*17*). The surfaces of the TEM thin foils were set at almost (011) so that we could select only loops whose **b** values (½[11$\bar{1}$] and ½[1$\bar{1}$1]) were almost parallel to the surfaces for the examination of the behavior of almost isolated loops. By this procedure, we minimized the force applied onto these loops along their direction of motion from the surfaces. In the examination of the behavior of almost isolated loops, other internal stresses were also reduced to a level at which they could not affect the loop behavior (*17*). Using the specimens that satisfied the above condition, we observed the projection of the loop motion onto the screen at temperatures ranging from 290 to 700 K.

Loops occasionally exhibited 1D motion. The dependence of the motion fraction of the loops on temperature and time is shown in fig. S1 and movie S1. Here, the motion fraction is defined as the ratio of the number of moving loops to that of the visible loops. The "mobile" loops become immobile below ~450 K (the atmosphere formation temperature $T_c$) once the specimen is heated to a temperature above $T_c$. This suggests that the Cottrell atmosphere (*18*) of the interstitial impurity atoms with high diffusivity—such as C and N (*19*)—is formed around the loops when approaching $T_c$, and the atmosphere locks the loops below $T_c$. The equilibrium concentration of the impurity atoms that compose the atmosphere is obtained by the Fermi-Dirac distribution function (*20*). For example, the binding energy between a C atom and an edge dislocation is 0.7 eV at the maximum (*21*). These sites are occupied by C atoms up to 100% at 450 K and 30% at 700 K, although the amount of C atoms in the specimen is only 0.8 ppm by weight (table S1) (*17*). We examined the modes of the motion of almost isolated individual loops above $T_c$, where the motion fraction monotonously increases with temperature.

The behavior of an almost isolated loop is shown in Fig. 2 and movie S2, which show that a loop performs 1D motion in the direction of **b**. Figure 3A shows a temporal variation in the 1D displacement of the position of a loop, obtained by measuring the center of mass of the loop image by a time step of 1/30 s ($\Delta t$) (*17*). Figure 3B shows its wavelet transform (*17*). For comparison, the temporal variation in the 1D displacement of a particle performing a random walk (*13*, *22*) with a unit step of |**b**| without any trapping sites, obtained by kinetic Monte Carlo (kMC) simulation (*17*), is shown in fig. S2A; its wavelet transform is shown in fig. S2B. Comparison of Fig. 3B and fig. S2B reveals that significant defects exist in the high-frequency region in Fig. 3B. These defect periods are attributed to the trapping of the dislocation that composes the loop by dispersed static impurity atoms (*23*).

The motion of a loop detrapped from a trapping site is slow enough to enable its position to be traced continuously, even with a time step of $\Delta t$. Hence, we can examine whether the loop undergoes the diffusion, and we can then measure the loop diffusivity by the following procedure. Figure 3C shows the time ($t$) dependence of the mean-square displacement MSD($t$) of the temporal variation in the 1D displacement $x = x[(i-1)\cdot\Delta t]$ ($i = 1, 2, \ldots, n$) during a single motion period (81.633 to 150.867 s), as shown in Fig. 3A. Here, MSD is calculated by the following equation under the assumption of the realization of ergodicity

$$\mathrm{MSD}(j\cdot\Delta t) = \left\langle [x(j\cdot\Delta t) - x(0)]^2 \right\rangle = \frac{1}{n-j}\sum_{i=1}^{n-j}\{x[(j+i-1)\cdot\Delta t] - x[(i-1)\cdot\Delta t]\}^2 \quad (j = 0, 1, \ldots) \qquad (1)$$

Figure 3C shows that MSD is approximately proportional to $t$; hence, the loop clearly undergoes Brownian motion or normal diffusion (*22*). We estimate $D$ by the equation

$$D = \lim_{t\to 0}[d\ \mathrm{MSD}(t)/2dt] \qquad (2)$$

excluding the period during which a time correlation effect appears. Figure 3D shows the temporal variation in the diffusivity estimated

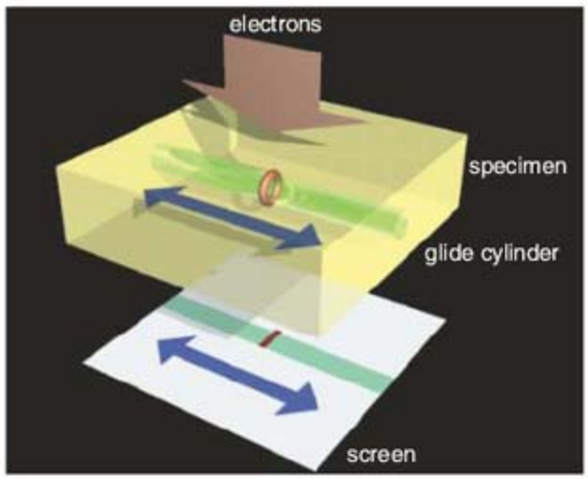


**Fig. 1.** Schematic view of the observation of the 1D glide motion of a nanometer-sized interstitial-type prismatic perfect dislocation loop by TEM. The red ring is a loop. The direction of the motion of the loop is parallel to its Burgers vector.

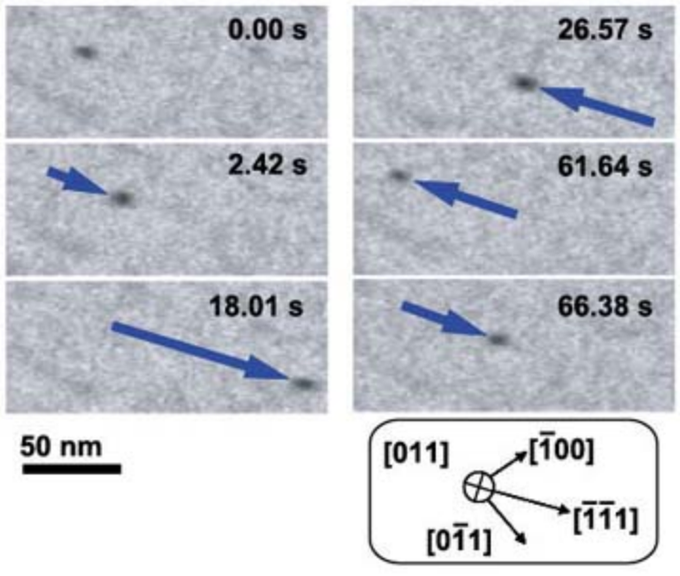


**Fig. 2.** One-dimensional motion of an almost isolated ½[11$\bar{1}$] loop at 575 K. The observation axis is approximately along [011]. The reflection adopted is **g** = 200. The diameter of the loop is 5.9 ± 0.2 nm. A loop almost continuously moves in a direction parallel to its Burgers vector.

by the subtraction, $D_{sub}$, instead of the time differential of MSD. The drop in $D_{sub}$ during the period from 1/30 to 4/30 s is attributed to the afterimage of the current imaging system (*17*). By extrapolating $D_{sub}$ to $t = 0$ s with the exclusion of the effect of the afterimage, we estimate the real value of $D$ to be 50.1 ± 0.4 nm$^2$/s. The appropriateness of this procedure for estimating $D$ is assured: When this procedure is applied to the result obtained by kMC (fig. S2A), it yields a value of $D$ (49.5 ± 0.4 nm$^2$/s) almost equal to that set in kMC (fig. S2, C and D) (*17*).

The temperature dependence of $D$ and its loop size dependence are shown in Fig. 4A. The temperature dependence of $D$ satisfies Arrhenius' law (*24*). From the slope of the lines in Fig. 4A, the values of the activation energy for loop diffusion, $E$, are estimated to be 1.3 eV, independent of the loop size, with statistical dispersions less than 0.03 eV. A simple extrapolation of the size dependence of the $E$ values of the crowdion bundles [which were calculated by MD (*3*–*7*)] to the size range of these "conventional" loops yields $E < 0.1$ eV, independent of the size. One of the origins of the drastic slowdown in "conventional" loop diffusion is attributed to atmosphere dragging, as described below. The dependence of the pre-exponential factor, $D_0$, on the number of self-interstitial atoms that compose a loop, $N$, obtained for $E = 1.3$ eV, is shown in Fig. 4B, where $D_0$ monotonously decreases with increasing $N$. If we assume that a power law on the $N$-dependence of $D_0$ is established, we obtain

$$D_0 = (2.3 \pm 0.3) \times 10^{15} N^{-(0.80 \pm 0.02)} \quad (\mathrm{nm}^2/\mathrm{s}) \tag{3}$$

The loop size independence of $E$ implies that the loop moves not by overcoming the Peierls potential (*1*) hill at once and as a whole, but by forming and moving double kinks (*1*, *2*). The presence of double kinks in a loop has been mentioned in MD studies (*3*, *5*) and a theoretical study (*10*). These studies relate the origin of $E$ to the kink-pair nucleation process. However, in general, the rate-controlling process of dislocation glide under low stress is not double-kink nucleation but the sidewise motion of the double kinks present at thermal equilibrium (*1*, *25*).

In response to low shear stress symmetric with respect to the central axis of the loop, the dislocation velocity $u_d$ is expressed as a function of the kink velocity $u_k$ (*1*) (fig. S4A)

$$u_d \approx \frac{a}{1/c_k} u_k = a c_k u_k \tag{4}$$

where $a$ is the period for the Peierls potential, and $c_k$ is the equilibrium concentration of all (positive and negative) single kinks and is a function of $E_k$, the formation energy of a kink. In the case of the sinusoidal-type Peierls potential, $c_k$ at the high-temperature limit becomes

$$c_k \approx \frac{2}{w_k} \sqrt{\frac{2\pi E_k}{kT}} \exp\left(-\frac{E_k}{kT}\right) \tag{5}$$

where $w_k$ is kink width, $k$ is the Boltzmann constant, and $T$ is absolute temperature (*2*). Equation 4 indicates that a dislocation moves by a distance of $a$ due to the movement of each kink, with average spacing of $1/c_k$ between kinks. Thermal kinks are formed as double kinks. Backward double kinks, which bow out in the direction opposite from the direction of motion of the dislocation, easily undergo mutual annihilation by the stress; hence, they cannot effectively contribute to the dislocation glide. In contrast, under zero stress, both backward double kinks and forward double kinks are present in the same number on average (fig. S4B). In this case, the drift velocity of the dislocation is obviously zero; however, the diffusivity is determined by the stochastic thermal fluctuation in the difference between the numbers of forward double kinks, $n_f$, and backward double kinks, $n_b$

$$\langle (n_f - n_b)^2 \rangle = \langle (2n_f - N_{dk})^2 \rangle = \frac{1}{2^{N_{dk}}} \sum_{n_f=0}^{N_{dk}} \frac{N_{dk}!}{n_f!(N_{dk} - n_f)!} (2n_f - N_{dk})^2 = N_{dk} \tag{6}$$

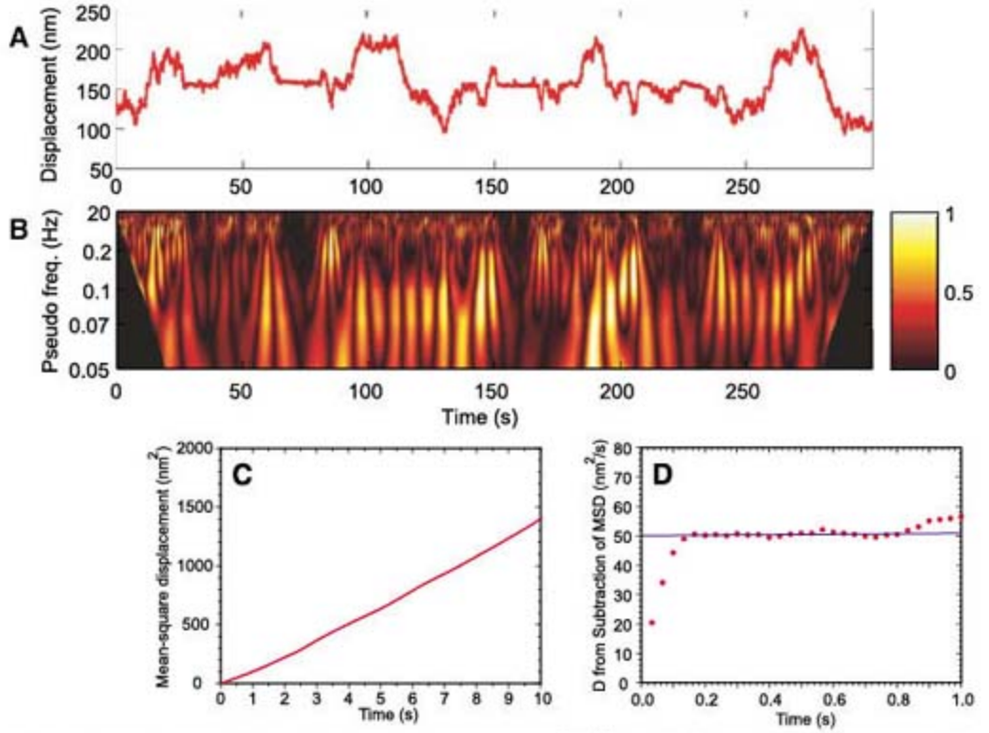


**Fig. 3.** Analysis of the 1D motion of an almost isolated ½[11$\bar{1}$] loop. **(A)** Temporal variation in the 1D displacement of the loop with diameter of 5.9 ± 0.2 nm at 575 K. **(B)** Wavelet transform of the temporal variation of the 1D displacement shown in (A). Color scale is shown in dimension less units. **(C)** Relationship with time of the MSD of an extracted 1D displacement variation corresponding to the motion period from 81.633 to 150.867 s in (A). **(D)** Dependence of the diffusivity, $D$, obtained by the temporal subtraction of the MSD shown in (C).

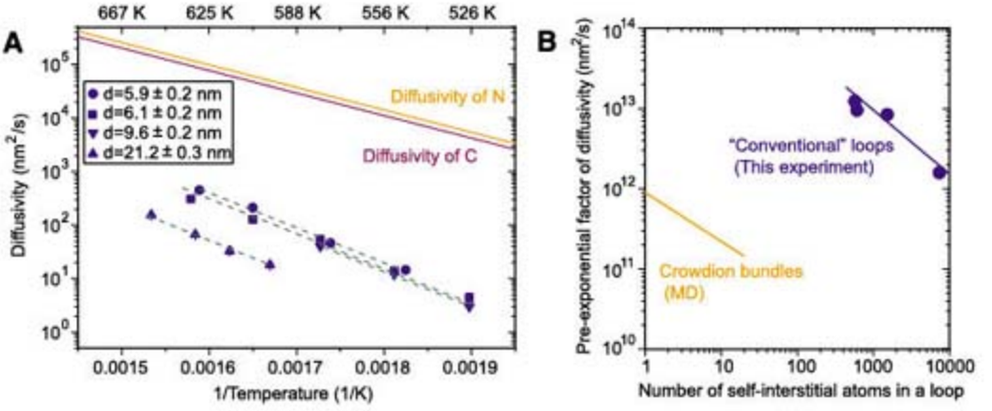


**Fig. 4.** Diffusivity of almost isolated ½⟨111⟩ loops. **(A)** Arrhenius plot of the diffusivity. Matching symbols correspond to the same loop with a diameter $d$. The diffusivities of carbon and nitrogen in the matrix (*19*) are also drawn. **(B)** Relationship between the pre-exponential factor of the diffusivity and the number of self-interstitial atoms that compose each loop. The additional inserted line is a result for crowdion bundles obtained by MD calculations (*5*).

where $N_{dk}$ is the total number of double kinks. By an extension of Eq. 4, $D$ is approximated as

$$D \approx a^2 \left\langle \left[ \frac{2(n_f - n_b)}{L} \right]^2 \right\rangle D_k = \frac{2a^2}{L} c_k D_k \propto N^{-0.5} c_k D_k \quad (7)$$

where $L$ is the loop-line length and $D_k$ is the kink diffusivity. Even when $N_{dk} < 1$, the identical result is obtained (*17*). The power of $N$ reduces for extremely small $N$ because the attractive force is applied on two adjacent kinks of opposite signs (*2*), accelerating the motion of both kinks so that they coalesce. This satisfies the dependence of $D_0$ on $N$, as obtained in the present study. The temperature dependence of $D$ is expressed by the term $c_k D_k$ in Eq. 7. $D_k$ is controlled by the dragged impurity atmosphere surrounding the dislocation. The dragging stress applied onto a dislocation by the atmosphere is generally proportional to the velocity of the dislocation, when the atmosphere can promptly follow the dislocation motion (*1*, *26*, *27*). If we set the proportionality factor to be $B$ (*27*), $D_k$ can be approximated with the use of Einstein's relation (*22*)

$$D_k \approx \frac{kT}{abB} \approx \frac{\alpha D_c (kT)^2}{c_0} \quad (8)$$

where $b$ is the absolute value of $\mathbf{b}$, $\alpha$ is the constant, $c_0$ is the concentration of dragged impurities in the matrix, and $D_c$ [ $= D_{c,0} \exp(-E_c/kT)$, where $E_c$ is the activation energy for the migration of dragged impurities] is the diffusivity of the impurity atoms that compose the atmosphere (*24*). Here, other effects influencing $D_k$—such as phonon dragging, electron dragging, and Peierls potential of the second kind (*1*, *28*)—are neglected. From Eqs. 5, 7, and 8, the apparent activation energy for the diffusion of a loop is expressed as

$$E \equiv -\frac{d \ln D}{d(1/kT)} = E_k + E_c + \frac{3}{2} kT \quad (9)$$

In contrast, if the atmosphere dragging does not occur and the phonon dragging due to the phonon wind (*28*) is dominant, $D_k$ for this "naked" loop becomes constant above the Debye temperature. This yields $E = E_k - \frac{1}{2}kT$. In general, the addition of solutes into pure Fe changes the shear modulus only slightly (*29*); therefore, their atmosphere will not effectively influence the $E_k$ value. Thus, $E$ increases by $E_c + 2kT$ when the loop drags the atmosphere. The most probable elements composing the dragged atmosphere of all the impurity elements are C or N. We do not know the precise values of $E_c$ for C or N around the dislocation. However, if we adopt $E_c$ values for C or N ($E_c = 0.83$ eV for C, $E_c = 0.80$ eV for N) (*19*), both the $E_k$ value and the $E$ value for "naked" loops become ~0.4 eV.

Using in situ TEM, we have shown that nanometer-sized dislocation loops can undergo 1D diffusion even in the absence of stresses that are effective in driving loops. These findings are relevant for the prediction of the lifetime of radiation-resistant materials for nuclear fission and energy systems in which the microstructures are controlled by the motion of loops formed upon high-energy particle irradiation. In addition, this study opens up a pathway for further experimental investigation of the unresolved dynamics of extremely small self-interstitial atom complexes.

### References and Notes


1. J. P. Hirth, J. Lothe, *Theory of Dislocations* (Wiley, New York, 1982).
2. A. Seeger, P. Schiller, in *Physical Acoustics*, W. P. Mason, Ed. (Academic Press, New York, 1966), vol. 3, part A, pp. 361–512.
3. B. D. Wirth, G. R. Odette, D. Maroudas, G. E. Lucas, *J. Nucl. Mater.* **276**, 33 (2000).
4. N. Soneda, T. D. De la Rubia, *Philos. Mag. A* **81**, 331 (2001).
5. J. Marian *et al.*, *Phys. Rev. B* **65**, 144102 (2002).
6. Y. N. Osetsky, D. J. Bacon, A. Serra, B. N. Singh, S. I. Golubov, *Philos. Mag.* **83**, 61 (2003).
7. D. A. Terentyev, L. Malerba, M. Hou, *Phys. Rev. B* **75**, 104108 (2007).
8. A. V. Barashev, Yu. N. Osetsky, D. J. Bacon, *Philos. Mag. A* **80**, 2709 (2000).
9. S. L. Dudarev, *Phys. Rev. B* **65**, 224105 (2002).
10. K. Ohsawa, E. Kuramoto, *Phys. Rev. B* **72**, 054105 (2005).
11. H. Trinkaus, B. N. Singh, S. I. Golubov, *J. Nucl. Mater.* **283–287**, 89 (2000).
12. D. Walgraef, N. M. Ghoniem, *Phys. Rev. B* **67**, 064103 (2003).
13. J. R. Manning, *Diffusion Kinetics for Atoms in Crystals* (Van Nostrand, Princeton, NJ, 1968).
14. M. Kiritani, *J. Nucl. Mater.* **251**, 237 (1997).
15. H. Abe, N. Sekimura, Y. Yang, *J. Nucl. Mater.* **323**, 220 (2003).
16. K. Arakawa, M. Hatanaka, E. Kuramoto, K. Ono, H. Mori, *Phys. Rev. Lett.* **96**, 125506 (2006).
17. See supporting material on *Science* Online.
18. A. H. Cottrell, *Reports on the Strength of Solids* (Physical Society, London, 1948), p. 30.
19. A. E. Lord Jr., D. N. Beshers, *Acta Metall.* **14**, 1659 (1966).
20. N. Louat, *Proc. Phys. Soc. B* **69**, 459 (1956).
21. J. Th. M. de Hosson, *Solid State Commun.* **17**, 747 (1975).
22. S. Chandrasekhar, *Rev. Mod. Phys.* **15**, 1 (1943).
23. G. A. Cottrell, S. L. Dudarev, R. A. Forrest, *J. Nucl. Mater.* **325**, 195 (2004).
24. T. Heumann, *Diffusion in Metallen* (Springer, Berlin, 1992).
25. G. Schoeck, in *Dislocations in Solids*, F. R. N. Nabarro, Ed. (North-Holland, Amsterdam, 1980), vol. 3, pp. 63–163.
26. H. Yoshinaga, S. Morozumi, *Philos. Mag.* **23**, 1367 (1971).
27. A. H. Cottrell, M. A. Jaswon, *Proc. R. Soc. London Ser. A* **199**, 104 (1949).
28. V. I. Alshits, V. L. Indenbom, in *Dislocations in Solids*, F. R. N. Nabarro, Ed. (North Holland, Amsterdam, 1986), vol. 7, pp. 43–111.
29. G. R. Speich, A. J. Schwoeble, W. C. Leslie, *Metall. Trans.* **3**, 2031 (1972).



30. We thank Nippon Mining & Metal Co. Ltd. for the careful heat treatment of the experimental specimens. Supported by the Ministry of Education, Sports, Culture, Science and Technology of Japan (Grant-in-Aid for Scientific Research 17760530) and by Priority Assistance for the Formation of Worldwide Renowned Centers of Research—The Global COE Program (Project: Center of Excellence for Advanced Structural and Functional Materials Design) from the same ministry.


### Supporting Online Material

www.sciencemag.org/cgi/content/full/318/5852/956/DC1
Materials and Methods
SOM Text
Figs. S1 to S4
Table S1
References
Movies S1 and S2


18 May 2007; accepted 3 October 2007
10.1126/science.1145386


# One-Dimensional Fast Migration of Vacancy Clusters in Metals


Yoshitaka Matsukawa[1,2]*† and Steven J. Zinkle[1]



The migration of point defects, for example, crystal lattice vacancies and self-interstitial atoms (SIAs), typically occurs through three-dimensional random walk in crystalline solids. However, when vacancies and SIAs agglomerate to form planar clusters, the migration mode may change. We observed nanometer-sized clusters of vacancies exhibiting one-dimensional (1D) fast migration. The 1D migration transported a vacancy cluster containing several hundred vacancies with a mobility higher than that of a single vacancy random walk and a mobility comparable to a single SIA random walk. Moreover, we found that the 1D migration may be a key physical mechanism for self-organization of nanometer-sized sessile vacancy cluster (stacking fault tetrahedron) arrays. Harnessing this 1D migration mode may enable new control of defect microstructures such as effective defect removal and introduction of ordered nanostructures in materials, including semiconductors.


The one-dimensional (1D) fast migration of nanometer-sized defect clusters is currently of particular interest in nuclear materials research (*1*). Recent molecular dynamics (MD) simulations have indicated that nanometer-sized, sessile clusters of vacancies and glissile clusters of self-interstitial atoms (SIAs) are produced together in collision cascades during energetic ion and neutron irradiation (*2*). In face-centered cubic (fcc) metals, sessile vacancy clusters often form stacking fault tetrahedra (SFTs) having 3D pyramidal structure. The configuration of the glissile SIA clusters is a 2D platelet, 1/2<110>{110} prismatic perfect dislocation loop. Sufficiently small SIA clusters can exhibit 1D fast migration (*3*–*8*), which transports the entire cluster contain-

ing several tens of SIAs with a mobility comparable to that of a single SIA (*4*). This anisotropic migration of SIA clusters is currently considered to have a noticeable impact on the evolution of a material's neutron-irradiation damage microstructure, which determines the material's lifetime in nuclear reactor environments (*1*, *9*).

Although SIA clusters form a dislocation loop, the 1D migration may involve a cooperative atomic diffusion mechanism not described by conventional dislocation theory. Because the line senses of dislocation segments facing each other in a loop are always opposite, it is impossible to glide the whole loop in the same direction simultaneously under shear stress, as shown in fig. S1. In theory, it is possible to induce glide of the entire loop in the same direction by pushing the atoms in the prismatic column from one side. This type of motion, which is traditionally called prismatic punching, proposed by Seitz (*10*), can be induced in specific situations, such as indentation. However, the loop's 1D motion observed in irradiated metals is not one way but reciprocates back and forth, as reported by several researchers (*11*–*14*). Therefore, prismatic punching does not appear to be a viable mechanism. A widely accepted mechanism for the 1D migration has its basis in thermally activated dense fluctuation of its constituent elements, "crowdions," in the dense packed <110> atomic direction along their Burgers vector in the case of fcc metals (*4*), as shown schematically in Figs. 1 and 2. Figure 2 schematically shows the relationship between the loop 1D migration direction, geometry of the loop, and bundled crowdions. Because the 1D migration is induced by collective motion of numerous neighboring crowdions in the loop, this phenomenon is substantial only when the loop size is small: MD simulations have indicated that only nanometer-sized SIA loops exhibit 1D migration (*4*). A previously proposed alternative account for the 1D motion within the scope of dislocation theory is that the loop motion is induced by the thermally activated formation and propagation of a double kink on the loop, which is expressed by a (dislocation) line tension model (*5*, *15*), as shown in fig. S2. However, in 1D motion all of the crowdions inside the prismatic cylinder must be transported, whereas the line tension model only describes the motion of crowdions on the dislocation line. In MD simulations, inner crowdions are often observed to move before the crowdions on the loop perimeter (as schematically shown in fig. S2F). The motion of whole loop is led by the inner crowdions (*16*).

A fundamental question is whether the 1D migration is also possible for vacancy-type prismatic dislocation loops. Osetsky *et al.* examined the possibility of 1D migration for vacancy loops in both body-centered cubic (bcc) and fcc metals by using MD simulations (*17*). They predicted 1D migration of small vacancy loops in bcc iron but not in fcc copper. The prismatic vacancy loop in copper immediately became sessile by developing stacking faults from the loop edges within a picosecond. They attributed the absence of 1D migration in fcc copper to its low stacking fault energy. To date, there have been no observations of 1D migration of vacancy clusters, whereas several experimental studies have reported 1D migration of SIA clusters (*11*–*14*). Thus, based on the MD results, the existing consensus is that the 1D migration of vacancy clusters is not possible, especially in fcc metals (*1*).

In the present study, vacancy loops were introduced into 99.9975% pure fcc gold through plastic deformation or quenching and then examined in a nominally stress-free condition. The stacking fault energy of gold (32 mJ/m$^2$) is even lower than that for copper (45 mJ/m$^2$), which would promote conversion of dislocation loops to SFTs even more strongly in gold than in copper (*18*). Therefore, 1D migration of vacancy clusters is not expected in gold. A very high density of vacancy clusters is produced by plastic deformation in ductile metal thin foils having a specific geometry (*19*). Although the majority of vacancy clusters produced by plastic deformation at room temperature in gold are SFTs (*19*), a few vacancy-type dislocation loops are also produced. Those dislocation loops exhibited 1D oscillating motion, inconsistent with the reported MD simulation results. Figure 3 and movie S1 show an example of the observed behavior at room temperature. A small dislocation loop (diameter about 2 nm, ~174 vacancies) glided intermittently back and forth between two SFTs at an oblique angle along the projection of the <110> direction (oscillating distance of 1 to 2 nm). The loop position changed frame by frame (frame rate of 30 frames/s) for about 4 min and then suddenly transformed to an SFT within a few video frames (<0.1 s). Because SFTs are vacancy-type defects in fcc structures (*20*), Fig. 3 provides evidence that nanometer-sized vacancy loops can exhibit 1D migration. The vacancy loop transformed into an SFT at an intermediate position between two preexisting SFTs, presumably because the stress field on the loop from the two SFTs is balanced at the intermediate position. As a result, a well-aligned SFT array consisting of three SFTs was obtained.

There are many reports showing ordered arrays of nanometer-sized SFTs created through high-energy particle irradiation such as neutron irradiation and ion bombardment (*21*–*23*). Because SFTs are sessile, it has been believed that the self-organized microstructure is created by glissile SIA clusters exhibiting 1D migration; vacancy clusters that are geometrically aligned along close-packed <110> directions in fcc crystals would be preferentially shielded from annihilation by the 1D migrating SIA clusters. However, the present dynamic observation (Fig. 3) suggests that spatial self-organization of sessile SFTs can be achieved through the 1D migration (and conversion to SFTs) of glissile vacancy loops, without the necessity of 1D migration of SIA clusters. Fig. S3 shows previously proposed models of loop-SFT conversion (*24*), and fig. S4 shows the crystallography of various potential loop geometries.

Figure 4 and movies S2 and S3 show the 1D migration of a vacancy loop introduced into gold

[1]Materials Science and Technology Division, Oak Ridge National Laboratory (ORNL), Post Office Box 2008, TN 37831–6138, USA. [2]Center for Materials Processing, University of Tennessee, Knoxville, TN 37996–0750, USA.
*Present address: Department of Materials Science and Engineering, University of Illinois at Urbana-Champaign, Materials Science and Engineering Building 408A, 1304 West Green Street, Urbana, IL 61801, USA.
†To whom correspondence should be addressed. E-mail: ym2@uiuc.edu

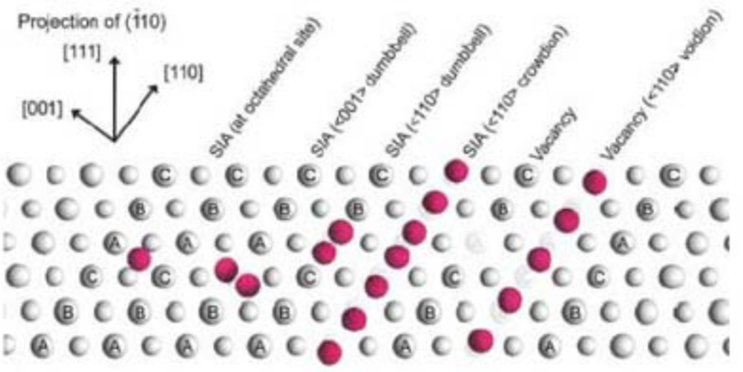


**Fig. 1.** Various atom configurations of SIAs and vacancies projected on $(\bar{1}01)$: small atoms represent atoms on a plane ¼$[\bar{1}01]$ below the large atoms. In the fcc structure, single SIAs are preferentially located at octahedral sites denoted as (1/2, 1/2, 1/2) on the basis of atomic volume considerations; however, it is energetically more favorable to be arranged in a <001> dumbbell structure. The crowdion distributes the localized displacement of the SIA along the <110> close-packed atom direction. Subtracting an atom, i.e., introduction of a vacancy, may create a delocalized dilute atom configuration complementary to the <110> crowdion (<110> voidion). Note that this configuration never occurs for single vacancies.

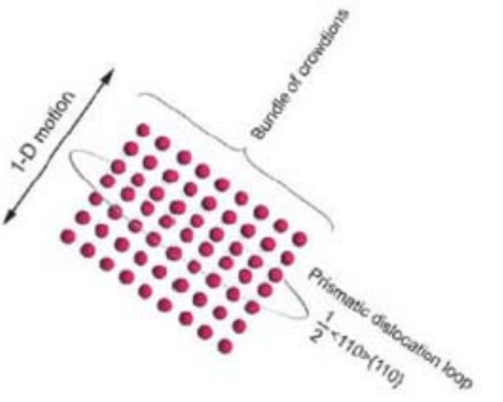


**Fig. 2.** Schematic sketch of the 1D migration of the SIA-type 1/2<110>{110} dislocation loop and its atomic structure.

by quenching that introduces only vacancies. The transmission electron microscopy (TEM) observation was carried out at 113 K. The vacancy loop (diameter about 3.5 nm; ~534 vacancies) exhibited oscillating 1D migration for about 6 min, whereas single vacancies were immobile below ~300 K in gold (*25*). The loop wiggled intermittently, back and forth, along a straight dislocation with a wide variety of migration distances for each oscillation. The maximum observed migration distance per oscillation (within two video frames, i.e., 66 ms) was 15 nm, which corresponds to 52 times the {110} interplanar distance in gold. In general, the number of atomistic jumps per second in a thermally activated process is expressed as $\nu = \nu_0 \exp(S/k)\exp(-E_m/kT)$, where $\nu_0$ is the lattice vibration frequency, $k$ is the Boltzmann constant, $S$ is entropy, and $T$ is absolute temperature. We assume $\exp(S/k) = 1$ for the sake of simplicity. The migration energies of single vacancies and single SIAs in gold are $E_m = 0.85$ eV and $E_m = 0.19$ eV, respectively (*26*). With $\nu_0 = 10^{13}$ s$^{-1}$, $\nu$ at 113 K is $1.3 \times 10^{-25}$ s$^{-1}$ for single vacancies and $3.4 \times 10^{4}$ s$^{-1}$ for single SIAs. The maximum observed migration distance of the vacancy loop (15 nm) corresponds to $\nu = 789$ s$^{-1}$, which gives $E_v$ of 0.22 to about 0.23 eV as the effective migration energy for the vacancy loop 1D motion (*27*). This effective migration energy for the 1D glissile vacancy loop is much less than that for single vacancies. This suggests that the mobility of nanometer-sized dislocation loops via 1D migration is independent of the mobility of the constituent point defects, that is, vacancies in this case.

The diffraction contrast images of the vacancy loops observed in the present study are quite unusual as a dislocation loop image. Seen from the <110> direction, the loop is in an edge-on view, i.e., visible as a line segment (*28*). However, the loop image in Fig. 4 is oval in shape, elongated in the 1D glide direction. The loop image in Fig. 3 is also oval in shape. This may be an artifact due to the high velocity of 1D motion. MD simulations (obtained for SIA loops) have indicated that the loop's oscillation is essentially a sub-picosecond–time scale event (*4*). Such high-speed motion cannot be captured by the present video-recording system, whose time resolution is 33 ms. Instead, a composite image of the loop's motion during ~33 ms is recorded on a single video frame. Note that the loop image remained the same even after the motion became undetectable in Fig. 4. This may be an indication that the loop was still moving one-dimensionally with a very short oscillating distance and high frequency, even after the large motion detectable by the present dynamic TEM observation disappeared.

The size of the vacancy loops observed in the present TEM study (2 to 3.5 nm) is much larger than the loop examined in the 1999 MD simulation (up to 50 vacancies; <1 nm). On the basis of the results on SIA loops obtained through MD simulations, larger loops are less mobile than small loops: The critical size above which the predicted mobility is practically zero is ~100 SIAs (~1.3 nm) in copper and ~300 SIAs (~2.4 nm) in iron (*4*). However, in TEM experiments, much larger SIA loops exhibit 1D migration above 450 K: The critical size in iron may be as large as 20 to ~30 nm (*11*). The present experimental results were obtained in a TEM operated at 200 keV, which is well below the critical voltage to introduce Frenkel pairs (vacancy and an SIA) into gold. The critical electron energy for Frenkel pair creation is ~2 MeV because of the large mass of gold atoms. The temperature increase by the 200-keV electron irradiation is negligible because the specimen was thin (<50 nm) and the electron beam diameter was less than 2 μm, which gives less than a few tens of Kelvin local temperature increase for the electron beam fluxes used in the present study (*29*).

Although vacancy loops cannot have crowdions, we speculate that they may develop an analogous (dilute) atom configuration similar to crowdions (we tentatively call this dilute-packed <110> atomic row "voidions"), as shown in Fig. 1. Such a configuration does not occur for single vacancies; however, in the form of a 1/2<110>{110} prismatic loop, numerous vacancies are neighboring on a {110} plane, potentially favoring this cooperative voidion configuration.

An unresolved question is whether the 1D migration of SIA and vacancy clusters can be effectively harnessed to enable directed assembly of technologically useful nanoscale architectures. The formation of a linear array of SFTs in Fig. 3 implies that it may be possible to create unique nanoscale ordered defect microstructures by particle irradiation. The very high mobility of the 1D glide vacancy clusters may also provide a hint regarding efficient defect removal from not only metals but also semiconductor materials, whose defect clustering behavior is essentially the same as fcc metals because of their similar crystal structures, as well as introduction of nanoscale ordered structures.

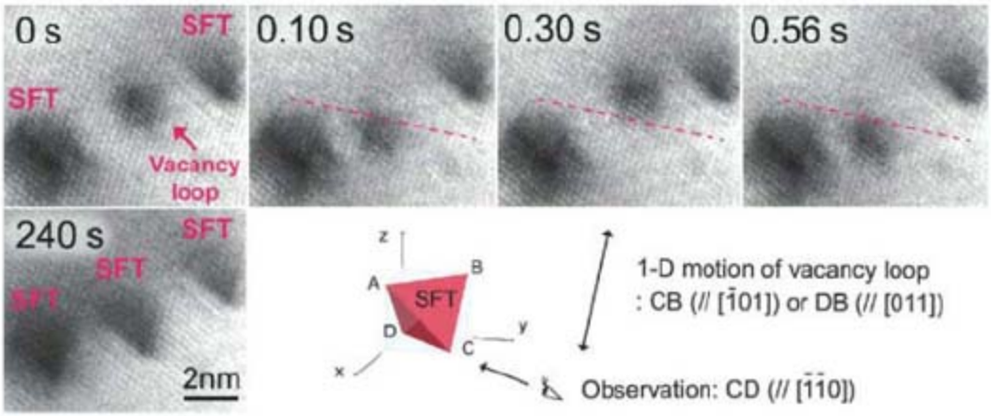


**Fig. 3.** Sequence of snapshots showing the 1D oscillating motion of a vacancy loop and eventual transformation to an SFT (after 240 s) in deformed gold at room temperature.

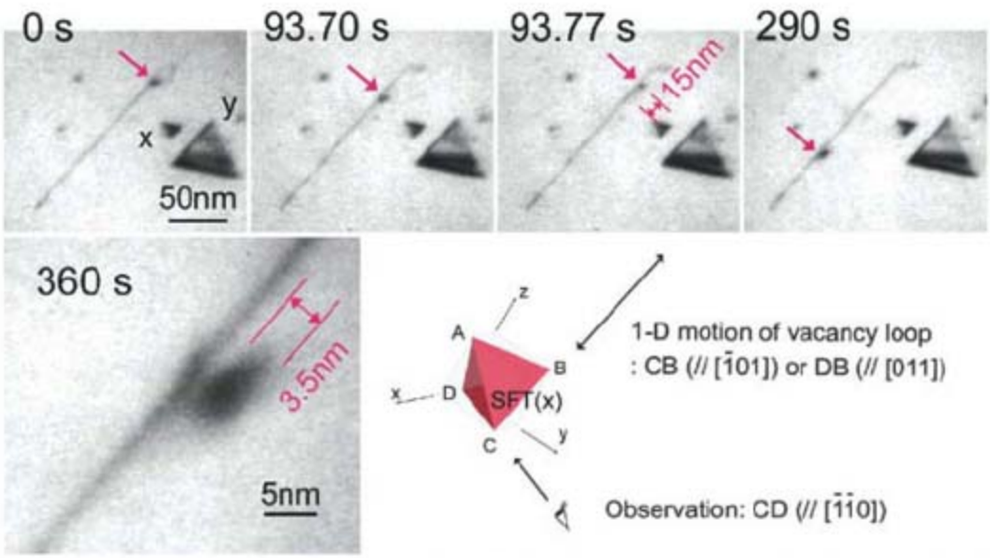


**Fig. 4.** Sequence of snapshots showing the 1D oscillating migration of a vacancy loop in quenched gold at 113 K. The spatial dimension shown in the frame of 93.77 s is the jump distance from the previous observed loop position at 93.70 s. Two types of crystallographically equivalent SFTs (marked by x and y) are involved in the figure.

**References and Notes**

1. B. N. Singh, in *Encyclopedia of Materials: Science and Technology*, K. H. J. Buschow *et al.*, Eds. (Elsevier, New York, 2001), pp. 7957–7972.

2. Yu. N. Osetsky, D. J. Bacon, *Nucl. Instrum. Methods Phys. Res. B* **180**, 85 (2001).
3. A. J. E. Foreman, C. A. English, W. J. Phythian, *Philos. Mag. A* **66**, 655 (1992).
4. Yu. N. Osetsky, D. J. Bacon, A. Serra, B. N. Singh, S. I. Golubov, *Philos. Mag.* **83**, 61 (2003).
5. J. Marian *et al.*, *Phys. Rev. B* **65**, 144102 (2002).
6. E. Kuramoto, *J. Nucl. Mater.* **276**, 143 (2000).
7. B. D. Wirth, G. R. Odette, D. Maroudas, G. E. Lucas, *J. Nucl. Mater.* **276**, 33 (2000).
8. S. L. Dudarev, *Philos. Mag.* **83**, 3577 (2003).
9. H. Trinkaus, B. N. Singh, A. J. E. Foreman, *J. Nucl. Mater.* **206**, 200 (1993).
10. F. Seitz, *Phys. Rev.* **79**, 723 (1950).
11. K. Arakawa, M. Hatanaka, E. Kuramoto, K. Ono, H. Mori, *Phys. Rev. Lett.* **96**, 125506 (2006).
12. M. Kiritani, *J. Nucl. Mater.* **251**, 237 (1997).
13. T. Hayashi, K. Fukumoto, H. Matsui, *J. Nucl. Mater.* **307–311**, 993 (2002).
14. H. Abe, N. Sekimura, Y. Yang, *J. Nucl. Mater.* **323**, 220 (2003).
15. K. Ohsawa, E. Kuramoto, *Phys. Rev. B* **72**, 054105 (2005).
16. The crowdions located at the loop center have a smaller energy barrier for motion than that of the crowdions located on the loop perimeter (*4*). This is because the most stable configuration for single SIAs is the dumbbell: The crowdions on the loop perimeter are more likely to transform to dumbbell configuration. Conversely, Marian (*5*) claimed that crowdion jumps are more likely to occur at the loop perimeter. This is because the interatomic potential used by Marian incorrectly predicts the crowdion configuration to be more stable than the dumbbell configuration.
17. Yu. N. Osetsky, D. J. Bacon, A. Serra, *Philos. Mag. Lett.* **79**, 273 (1999).
18. J. P. Hirth, J. Lothe, *Theory of Dislocations* (McGraw-Hill, New York, ed. 2, 1982).
19. M. Kiritani *et al.*, *Philos. Mag. Lett.* **79**, 797 (1999).
20. S. Kojima *et al.*, *Philos. Mag. A* **59**, 519 (1989).
21. N. M. Ghoniem, D. Walgraef, S. J. Zinkle, *J. Computer-Aided Mater. Des.* **8**, 1 (2002).
22. A. Seeger, N. Y. Jin, F. Phillip, M. Zaiser, *Ultramicroscopy* **39**, 342 (1991).
23. C. Tölg, P. Hähner, M. Zaiser, W. Frank, *Appl. Phys. A* **58**, 3 (1994).
24. D. Kuhlmann-Wilsdorf, *Acta Metall.* **13**, 257 (1965).
25. J. E. Bauerle, J. S. Koehler, *Phys. Rev.* **107**, 1493 (1957).
26. M. Kiritani, *J. Phys. Soc. Jpn.* **40**, 1035 (1976).
27. We did not regard the loop migration of 15 nm as a ballistic jump because of the following context. The 1D migration of dislocation loop is a result of collective motion of numerous atoms whose elementary jump length is $d_{110}$, the interplanar distance between (110) planes. Although the vacancy loop migrated ballistically 15 nm within a few video frames, it seems reasonable to assume that this migration consists of several hundred jumps of a few hundred atoms in the same direction, involving thermally activated atomic jumps in the reverse direction on an atomic scale.
28. The loop shape (triangle or circular) is unidentifiable in the edge-on view.
29. S. B. Fisher, *Radiat. Eff.* **5**, 239 (1970).



30. This research was sponsored by the Office of Fusion Energy Sciences, U.S. Department of Energy. The microscope facility within the SHaRE (Shared Research Equipment User Facility) Collaborative Research Center at ORNL was supported by the Division of Scientific User Facilities, Office of Basic Energy Science. We are grateful to Y. N. Osetsky, S. I. Golubov, B. N. Singh, and P. J. Kamenski for valuable comments.


**Supporting Online Material**

www.sciencemag.org/cgi/content/full/318/5852/959/DC1
Materials and Methods
SOM Text
Figs. S1 to S4
Movies S1 to S3


25 July 2007; accepted 3 October 2007
10.1126/science.1148336


# Widespread Morning Drizzle on Titan


**Máté Ádámkovics,[1,2]* Michael H. Wong,[1] Conor Laver,[1] Imke de Pater[1,2]**



**Precipitation is expected in Titan's atmosphere, yet it has not been directly observed, and the geographical regions where rain occurs are unknown. Here we present near-infrared spectra from the Very Large Telescope and W. M. Keck Observatories that reveal an enhancement of opacity in Titan's troposphere on the morning side of the leading hemisphere. Retrieved extinction profiles are consistent with condensed methane in clouds at an altitude near 30 kilometers and concomitant methane drizzle below. The moisture encompasses the equatorial region over Titan's brightest continent, Xanadu. Diurnal temperature gradients that cause variations in methane relative humidity, winds, and topography may each be a contributing factor to the condensation mechanism. The clouds and precipitation are optically thin at 2.0 micrometers, and models of "subvisible" clouds suggest that the droplets are 0.1 millimeter or larger.**


A zoo of clouds is scattered across Saturn's largest moon, Titan, including convective clouds near the south pole (*1*, *2*), geographically controlled clouds at 40°S latitude (*3*), and a large cloud of ethane near the north pole (*4*). These and other types of clouds have been predicted with the use of combinations of chemical, microphysical, and general circulation models (*5*, *6*). Analysis of the methane relative humidity profile at the Huygens probe entry site suggests that there is a solid-methane cloud from 20 to 30 km altitude and a light drizzle of methane that wets the surface (*7*). However, the fluvial channels seen at the landing site (*8*) are due to heavier rainfall (*9*), which may occur during intense storms that are predicted by dynamical models (*10*). Conditions in the lower troposphere are best constrained where the Huygens probe landed, yet a single weather station cannot characterize Titan's meteorology on a planetwide scale. If widespread, methane condensation could be the dominant pathway for returning methane to the surface and closing the methane cycle.

Because the near-infrared aerosol opacity $\tau$ in Titan's atmosphere is low ($\tau = 0.2$ at 2 μm), light can penetrate to the surface at wavelengths where methane absorption is negligible (*11*). Radiative transfer (RT) models of Titan's spectra have been used to probe the heights of cloud tops and the aerosol vertical structure (*1*, *2*, *12*, *13*). One of the main challenges in accurately retrieving altitudes with these models is that the contribution function for a particular wavelength is dependent on the vertical distribution of aerosol. Variations in surface reflectivity can also be masked by near-surface atmospheric opacity. One way to break these degeneracies is to simultaneously analyze spectra taken along different paths through the atmosphere. Spatially resolved spectra from a new class of instruments, such as the OH-Suppressing InfraRed Imaging Spectrograph (OSIRIS) (*14*) at the W. M. Keck Observatory or the Spectrograph for INtegral Field Observations in the Near Infrared (SINFONI) (*15*) at the Very Large Telescope (VLT), are an ideal source of data for such an analysis. These instruments may be used to create a global picture of Titan's lower atmosphere and surface.

During our campaign to monitor the seasonal changes in the global distribution of Titan's aerosol, we observed Titan on 28 February 2005 universal time (UT) with SINFONI (*13*) and on 17 April 2006 UT with OSIRIS. Together the two instruments provide independent measurements of Titan at different epochs and viewing geometries. Systematic errors that arise from mosaicking and correcting for Earth's atmosphere (fig. S1) are specific to each instrument, and comparison facilitates the rejection of observational artifacts. Here we describe a method for making measurements of condensed-phase opacity from specific altitude regions in Titan's atmosphere using narrow (10- to 15-nm) spectral bandpass difference imaging. We used RT models to quantify the altitude and magnitude of the opacity enhancements, and we report the detection of widespread methane drizzle: precipitation from stratiform clouds of solid methane.

In order to discern the light scattered by clouds, drizzle, and haze in the lower troposphere, the contribution from the surface albedo variation (Fig. 1A) was removed from the images that probed the bottom of the atmosphere (Fig. 1B). We empirically quantified the relative surface flux $f$ in images taken at wavelengths with significant and with negligible methane gas opacity by minimizing the correlation coefficient between the surface-subtracted image of the atmosphere and the image of the surface (fig. S2). The mean surface flux in images probing the lower troposphere is ~72% of the flux in images of the surface, which is confirmed by our RT models. After subtracting the surface contribution from images that probe the lower troposphere, we can identify equatorial opacity changes


[1]Department of Astronomy, University of California, Berkeley, CA 94611, USA. [2]Center for Integrative Planetary Science, University of California, Berkeley, CA 94611, USA.

*To whom correspondence should be addressed. E-mail: mate@berkeley.edu

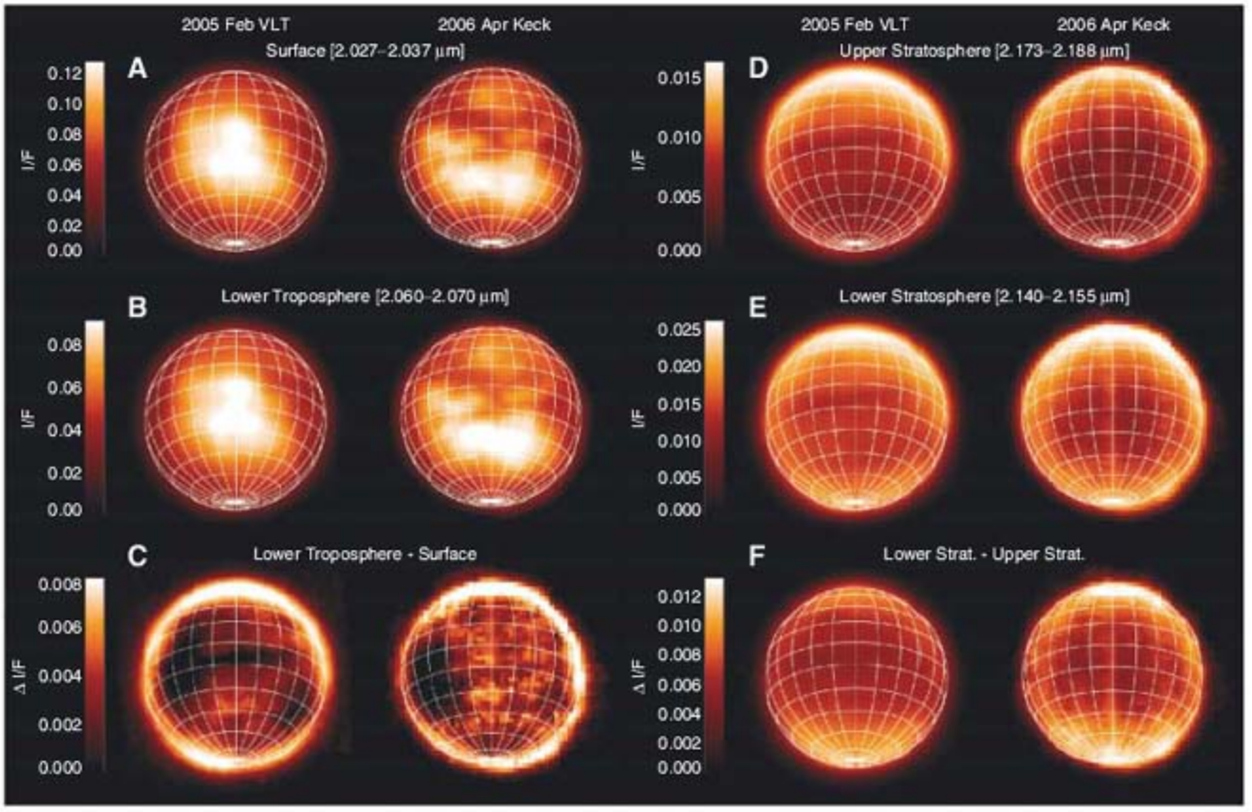


**Fig. 1.** Difference imaging of the condensed-phase scattering at specific altitudes in the atmosphere. The lower troposphere (below 20 km) can be probed by subtracting images at wavelengths sensitive to the variations in surface reflectivity (**A**) from those that probe both the surface and the lower troposphere (**B**). The difference images (**C**) reveal a dark feature in the morning equatorial regions, with sub-observer longitudes of 89°W and 42°W for the VLT and Keck, respectively. Artifacts such as the narrow linear feature in the VLT data are not observed with both instruments. The regions with lower $\Delta I/F$ in the difference images (**C**) have increased atmospheric opacity. The lower stratosphere can be similarly probed by subtracting images of the upper stratosphere (**D**) from images of the lower stratosphere (**E**) to highlight the contrast from the SPH (**F**); in this case, larger $\Delta I/F$ indicates more scattering. Difference images of the troposphere and stratosphere have a ($1\sigma$) pixel-to-pixel noise of $\Delta I/F$ = 0.003 and 0.0005, respectively.

on the morning (left) side of the disk in both observations (Fig. 1C). The dark regions cover slightly different portions of the disk because of different viewing angles during the two observations, yet correspond to the same latitudes on Titan, so the observation of the dark feature in both data sets is a confirmation of the localized change in opacity.

The nature of the increased opacity is determined by creating a model of the observed datacube. A 1.50- to 2.25-μm spectrum, corresponding to each observed spatial pixel, was calculated using a two-stream numerical solution to the RT equation (*16*, *17*). We accounted for the spatial variation in surface albedo by using a Visual and Infrared Mapping Spectrometer (VIMS) map of the 2.018-μm albedo (*18*) as input for the surface reflectivity. The surface spectrum is gray with four Gaussian absorption features (*19*). The aerosol (haze) extinction at the tropopause is 0.0025 $km^{-1}$ at southern latitudes above 45°S and increases toward the north by a factor of 0.0065 per degree of latitude (*13*). Aerosol extinction decreases with altitude above the tropopause, with a scale height of 100 km. The south polar hood (SPH) is included as a doubling of extinction from 50 to 70 km altitude and is located poleward of 45°S. Uniform aerosol extinction (0.001 $km^{-1}$), consistent with results from the Huygens probe, was used throughout the troposphere. Based on the temperature at a particular altitude, condensed-phase methane opacity was included as a layer of liquid or solid methane. The optical depth of condensed methane is the product of the absorption coefficient (*20*) and path length (i.e., column volume). A normalized point spread function from a calibration star was used to convolve the model for comparison with the observations. Images from the model datacube show excellent agreement with the observed data (fig. S1).

**Fig. 2.** Contrast in the difference images (Fig. 1, C and F) is due to localized changes in extinction. In order to understand that the dark region in Fig. 1C is due to a relative increase in opacity, we calculated the expected contrast in the lower troposphere (solid line) and lower stratosphere (dotted line).

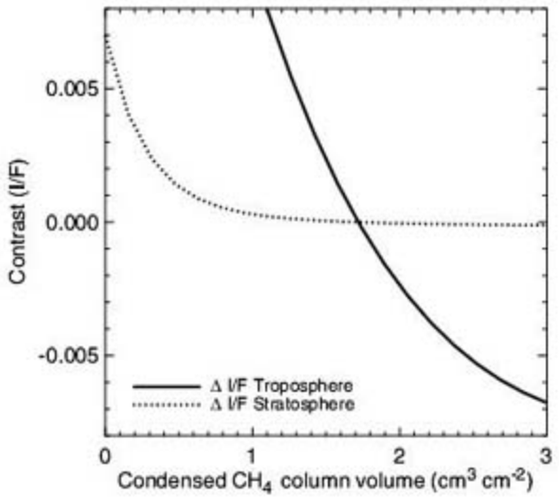


With a model of Titan's atmosphere and surface, various hypotheses for the source of the observed dark contrast feature (Fig. 1C) may be tested. We calculated a characteristic spectrum and determined the mean flux in the wavelength regions corresponding to images in Fig. 1 to obtain a nominal subtracted image flux ($\Delta I/F_0$) for both the lower troposphere and the lower stratosphere. The contrast was then defined as the difference between $\Delta I/F_0$ and the $\Delta I/F$ from a new spectrum in which a model parameter was changed. In Fig. 2, we plot the contrast expected in images of the lower troposphere and lower stratosphere when the column of condensed-phase methane is varied. Changes in aerosol haze density have been systematically ruled out by inadequately reproducing the observed contrast. If the observed opacity enhancement were attributed to small tropospheric haze particles (<0.001 mm), then the steep wavelength dependence of the extinction efficiency would extrapolate to unit optical depth at 0.938 μm (fig. S3), yet there have not been reports of aerosol enhancements over Xanadu or near the morning hemisphere. On the other hand, a mist

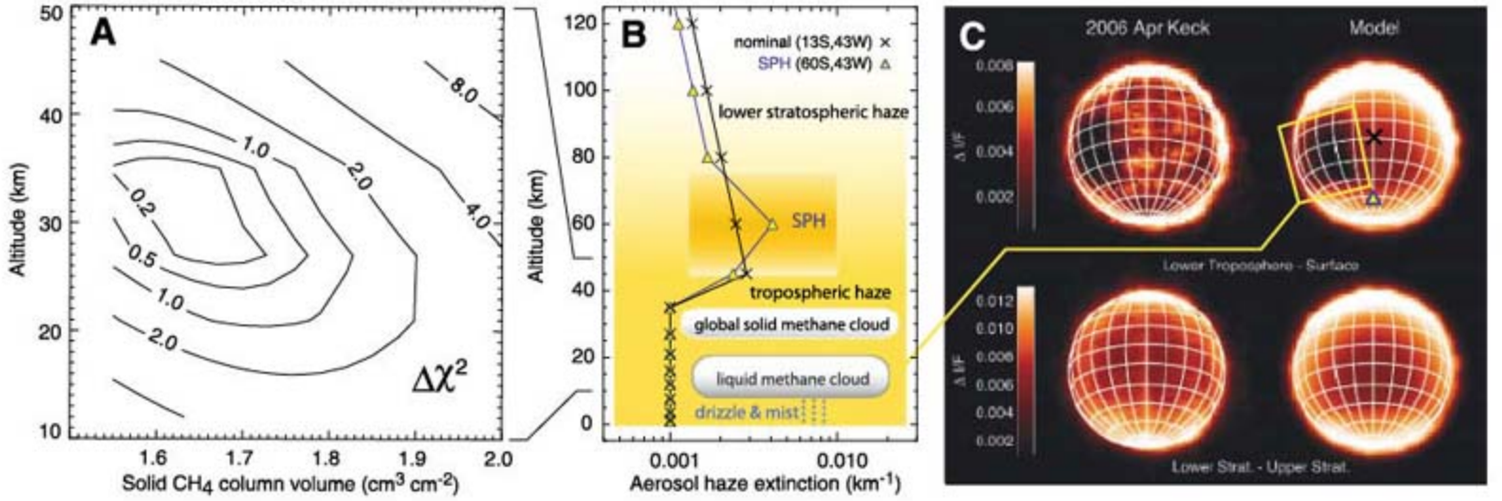


**Fig. 3.** A disk-encompassing cloud of condensed-phase methane is revealed by goodness-of-fit ($\Delta\chi^2$) contours for several altitudes and column volumes of methane (**A**). Vertical profiles of 2-μm aerosol extinction at two locations on the disk along with altitudes of condensed methane clouds show the altitudes of large-scale atmospheric features (**B**). Difference images extracted from the RT model of the observed OSIRIS datacube quantitatively reproduce the contrast caused by the enhancement in lower tropospheric opacity and the south polar hood (SPH) (**C**). Extinction profiles from the center of the disk (black crosses) and from the SPH (blue triangles) show the characteristic differences in the aerosol densities at south and equatorial latitudes.

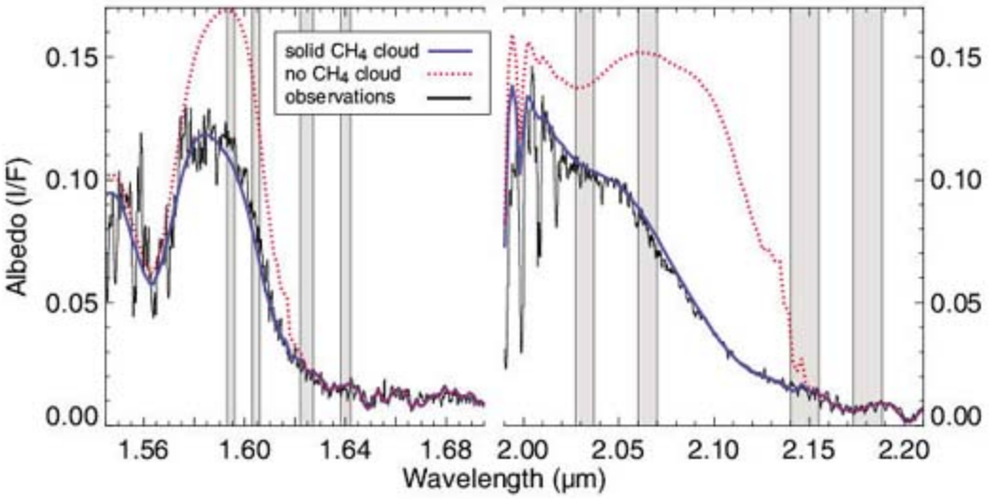


**Fig. 4.** Opacity caused by a cloud of solid methane provides a significantly improved fit of spectra at all locations on the disk. A representative Keck/OSIRIS spectrum from the center of the disk (black) is compared against model spectra with (blue) and without (red) a cloud of solid methane in the 25- to 30-km layer of the model. Shaded vertical regions indicate spectral bandpasses used for difference imaging in Fig. 1 and fig. S5.

or drizzle of methane droplets (>0.01 mm) that is optically thin at 2.0 μm would be optically thin at visible wavelengths as well and could more easily elude detection.

The altitude and total column of condensed methane were fit to observations by minimizing the root mean square deviation between a model datacube and observations. The cloud of methane was indeed found to be globally widespread, with a column volume of 1.65 $cm^3\ cm^{-2}$ in the altitude range of 25 to 35 km (Fig. 3A). Temperatures at these altitudes indicate that methane must be a solid (*7*). The morning enhancement of opacity is consistent with an additional column volume of 0.25 $cm^3\ cm^{-2}$ below 20 km, where methane is a liquid (Fig. 3B). The difference images are a sensitive test of the vertical profile of the tropospheric extinction, and the calculated datacubes with condensed methane opacity reproduce the observations (Fig. 3C). Artifacts or variations in surface absorption were are excluded by performing analogous (fig. S4) difference imaging at 1.5 μm. The difference images in the H band (fig. S5) can be used to independently reach all the qualitative conclusions arising from the K-band analysis (fig. S6). The improvement in spectral fit across both bands, when condensed methane is included, is illustrated in Fig. 4.

Depending on size and composition, drizzle will either reach the surface or form a near-surface mist. Although no direct detection of drizzle has been reported by Huygens (*8*), the uniform methane mixing ratio below 6 km (*21*) is consistent with the evaporation of methane from droplets (*22*). We detected both the solid methane cloud at 25 to 35 km and morning drizzle below. It had been suggested that precipitation from subvisible clouds would reach the surface and close the methane cycle and that the drizzle could be occurring over nearly 60% of the globe (*7*). By measuring the global extent of methane cloud, we see here that the methane drizzle is indeed precipitation related to stratiform clouds and does cover a substantial fraction of Titan.

Drizzle is observed in the morning hemisphere, and we first consider a diurnal mechanism that facilitates condensation. Because the methane is saturated around 15 km (*7*) in the morning [Huygens landed at local true solar time (LTST) of 9:47 a.m.], a small overnight drop in temperature at this altitude could initiate droplet formation that would then lead to drizzle in the lower troposphere. During our observations, it seems it was drizzling on Titan until approximately 10:40 a.m. LTST (roughly 3 Earth days after sunrise), which is consistent with the Huygens results.

Geographic factors may affect circulation and control localized condensation. One possibility is that the observed drizzle is due to the cooling of air caused by advection. Large-scale winds may push a moist airmass upslope, thus cooling it and driving condensation. Observations of sand dunes have shown that prevailing easterlies blow toward the bright continent of Xanadu (*23*). If the bright region is indeed a topographical high, then a "coastal" drizzle may form and cover the landmass. The relationship between the drizzle and the bright reflectivity of Xanadu is unclear (*24*), and it is possible that the drizzle contributes to rinsing the bright surface of the dark deposited aerosol. Perhaps the combination of nighttime cooling and local microclimates together make for consistently misty mornings in Xanadu.

### References and Notes

1. M. E. Brown, A. H. Bouchez, C. A. Griffith, *Nature* **420**, 795 (2002).
2. C. A. Griffith *et al.*, *Science* **310**, 474 (2005).

3. H. G. Roe, M. E. Brown, E. L. Schaller, A. H. Bouchez, C. A. Trujillo, *Science* **310**, 477 (2005).
4. C. A. Griffith *et al.*, *Science* **313**, 1620 (2006).
5. E. L. Barth, O. B. Toon, *Icarus* **182**, 230 (2006).
6. P. Rannou, F. Montmessin, F. Hourdin, S. Lebonnois, *Science* **311**, 201 (2006).
7. T. Tokano *et al.*, *Nature* **442**, 432 (2006).
8. M. G. Tomasko *et al.*, *Nature* **438**, 765 (2005).
9. J. T. Perron *et al.*, *J. Geophys. Res. (Planets)* **111**, 11001 (2006).
10. R. Hueso, A. Sánchez-Lavega, *Nature* **442**, 428 (2006).
11. C. A. Griffith, T. Owen, R. Wagener, *Icarus* **93**, 362 (1991).
12. M. Ádámkovics, I. de Pater, H. G. Roe, S. G. Gibbard, C. A. Griffith, *Geophys. Res. Lett.* **31**, L17S05 (2004).
13. M. Ádámkovics *et al.*, *J. Geophys. Res. (Planets)* **111**, 7 (2006).
14. J. E. Larkin *et al.*, *Proc. SPIE* **4841**, 1600 (2003).
15. F. Eisenhauer *et al.*, *Proc. SPIE* **4841**, 1548 (2003).
16. O. B. Toon, C. P. McKay, T. P. Ackerman, K. Santhanam, *J. Geophys. Res.* **94**, 16287 (1989).
17. C. P. McKay, J. B. Pollack, R. Courtin, *Icarus* **80**, 23 (1989).
18. J. W. Barnes *et al.*, *Icarus* **186**, 242 (2007).
19. Gaussian absorptions are fit to the entire disk by minimizing the sum squared residuals over the entire cube. The best-fit absorptions have central wavelengths of 1.505, 1.563, 1.614, and 2.028 μm; full width at half maximum of 0.052, 0.012, 0.010, and 0.021 μm; and peak absorptions of 99, 85, 80, and 16% of the surface reflectivity, respectively.
20. W. M. Grundy, B. Schmitt, E. Quirico, *Icarus* **155**, 486 (2002).
21. S. K. Atreya *et al.*, *Planet. Space Sci.* **54**, 1177 (2006).
22. T. Tokano, F. Ferri, G. Colombatti, T. Mäkinen, M. Fulchignoni, *J. Geophys. Res. (Planets)* **111**, 8007 (2006).
23. R. D. Lorenz *et al.*, *Science* **312**, 724 (2006).
24. C. A. Griffith, *Nature* **364**, 511 (1993).



25. This work was supported by NSF and the Technology Center for Adaptive Optics, managed by the University of California at Santa Cruz under cooperative agreement AST-9876783, NASA grant NNG05GH63G, and the Center for Integrative Planetary Science at the University of California at Berkeley. Data presented here were obtained at the W. M. Keck Observatory atop the sacred mountain of Mauna Kea and at the VLT operated by the European Southern Observatory.


**Supporting Online Material**

www.sciencemag.org/cgi/content/full/1146244/DC1
Observations and Methods
Figs. S1 to S6
References


8 June 2007; accepted 5 October 2007
Published online 11 October 2007;
10.1126/science.1146244
Include this information when citing this paper.


# Facultative Mate Choice Drives Adaptive Hybridization


**Karin S. Pfennig**



Mating with another species (hybridization) is often maladaptive. Consequently, females typically avoid heterospecifics as mates. Contrary to these expectations, female spadefoot toads were more likely to choose heterospecific males when exposed to environmental conditions that favor hybridization. Indeed, those females with phenotypic characteristics for which hybridization is most favorable were most likely to switch from choosing conspecifics to heterospecifics. Moreover, environmentally dependent mate choice has evolved only in populations and species that risk engaging in, and can potentially benefit from, hybridization. Thus, when the benefits of mate choice vary, females may radically alter their mate selection in response to their own phenotype and their environment, even to the point of choosing males of other species.


Mating between species typically results in no, few, or poor-quality offspring (*1*). Consequently, females generally prefer to mate with males of their own species (*1*–*3*). When hybridization does occur, it is often ascribed to mistakes during, or constraints on, female mate choice (*4*–*7*). Yet, hybridization can sometimes be beneficial (*8*), and females might facultatively adjust their choice of conspecific versus heterospecific mates depending on the fitness consequences of hybridization (*9*–*12*). Such facultative switches in female mate choice may thereby mediate adaptive hybridization and could explain patterns of hybridization observed in many species (*8*).

Spadefoot toads, *Spea bombifrons* and *Spea multiplicata*, risk hybridizing where they cooccur in the southwestern United States across ~20% of *S. bombifrons'* range (*13*, *14*). Hybrid offspring are viable and can reproduce, albeit with reduced fertility: Hybrid males can be sterile (*15*) [although the frequency of sterility among hybrid males is unknown (*16*)], and female hybrids produce fewer eggs than pure-species females (*15*). Hybridization between these species has historically been spatially variable, with hybrid frequency ranging from 0 to 40% across populations (*14*). Hybridization is most common in small ponds that tend to be shallow and highly ephemeral, with *S. bombifrons* females hybridizing more often than *S. multiplicata* females (*14*).

These observed patterns of hybridization may be explained if *S. bombifrons* females can benefit from hybridization. Spadefoots breed in ephemeral pools (Fig. 1, A and B), and their tadpoles often fail to metamorphose before ponds dry (*17*). *S. multiplicata* develop more rapidly than *S. bombifrons*, and hybrid tadpoles metamorphose sooner than pure *S. bombifrons* tadpoles (*14*). Thus, for *S. bombifrons* females, hybridization may enhance offspring survival.

As further evidence that hybridization may be beneficial for *S. bombifrons* females, hybrid offspring of *S. bombifrons* females ("BM" tadpoles) developed significantly faster than did pure *S. bombifrons* tadpoles ("BB" tadpoles) when reared in the lab for 16 days (*18*) [mean difference in Gosner developmental stage, BB – BM = –0.75 ± 0.28 (SEM), $t_{97} = -2.67$, $P = 0.009$]. Additionally, for tadpoles reared in naturally drying artificial pools in the field (*14*, *18*), the likelihood that all tadpoles metamorphosed in a given replicate was higher for BM tadpoles (likelihood ratio $\chi_1^2 = 8.15$, $P = 0.004$) and increased with maternal condition ($\chi_1^2 = 4.70$, $P = 0.03$). Similarly, the proportion of tadpoles in a replicate that metamorphosed (*18*) was higher for BM tadpoles ($F_{1,53} = 11.76$, $P = 0.001$) and increased with maternal condition ($F_{1,53} = 3.98$, $P = 0.05$).

Hybridization by *S. bombifrons* females therefore results in a trade-off: Hybrid offspring may have lower fertility and fecundity, but they can develop faster than pure *S. bombifrons* offspring and may therefore be more likely to escape a drying pool. Consequently, the fitness effects of hybridization depend on the habitat in which offspring develop. Because pond duration depends largely on initial pond size and depth [deeper ponds generally outlast shallow ones (*17*)], in deep (long-lasting) ponds, pure *S. bombifrons* offspring can metamorphose before the ponds dry (*14*). Thus, in such ponds, *S. bombifrons* females would have higher fitness by mating with conspecifics. In contrast, in shallow (rapidly drying) ponds, hybridization may be beneficial for *S. bombifrons* females because hybrids are more likely than pure *S. bombifrons* offspring to escape and therefore to survive. Furthermore, a given pond's depth (and longevity) can vary dramatically with the amount of yearly rainfall (Fig. 1, A and B). Thus, because *S. bombifrons* females may encounter year-to-year variation in pond longevity, they may facultatively adjust their choice for conspecific versus heterospecific mates, depending on the depth of their breeding pond.

To evaluate this hypothesis, I tested two predictions by performing controlled mate-choice tests in the lab (*18*). First, I predicted that *S. bombifrons* females would more likely choose *S. multiplicata* males in shallow ponds than in deep ponds. Second, because maternal condition predicts the likelihood that offspring will metamorphose, I predicted that *S. bombifrons* females in relatively poor condition would be more apt than those in good condition to alter their choice for conspecifics depending on water level.

*S. bombifrons* females were presented with calls of conspecific versus heterospecific (*S. multiplicata*) males under conditions simulating a deep (long-duration) pond versus a shallow (short-duration) pond (*18*). When females were tested three times in a deep pool (*18*), they showed a significant preference for conspecific calls versus heterospecific calls (Wilcoxon signed rank = 245,


Department of Biology, Campus Box 3280, Coker Hall, University of North Carolina, Chapel Hill, NC 27599, USA. E-mail: kpfennig@email.unc.edu

$n = 52$ females, $P = 0.009$) (Fig. 1C). In these deep water trials, individual females were significantly consistent in their choice: females chose the same stimulus, on average, 87.5 ± 2.5% (SEM) of the time (Wilcoxon signed rank = 345.5, $n = 52$, $P < 0.001$; 34 out of 52 females chose the same stimulus in all three trials). When these same females were tested four times in a shallow pool (*18*), as a group, they showed no preference for conspecific calls (Wilcoxon signed rank = –84, $n = 52$, $P = 0.24$) (Fig. 1C). Indeed, the frequency with which females chose conspecifics was higher in deep versus shallow water ($t_{51} = 3.16$, $P = 0.003$) (Fig. 1C). Although females as a group were not significantly more likely to choose one stimulus over the other in shallow water, individual females were significantly consistent in their preference: females chose the same stimulus, on average, 76.4 ± 2.8% (SEM) of the time (Wilcoxon signed rank = 390, $n = 52$, $P < 0.001$; 19 out of 52 females chose the same stimulus in all four trials, and 30 out of 52 females chose the same stimulus in at least three of the four trials). Thus, *S. bombifrons* females, as a group, were more likely to choose *S. multiplicata* males in shallow ponds than in deep ponds, as predicted.

Also as predicted, whether an individual female switched from choosing conspecifics in deep water to heterospecifics in shallow water depended on the female's condition. Females in relatively poor condition were most likely to make such a switch (Fig. 2A). Poor-condition females may be more prone to switch because, as noted above, they can potentially benefit more by hybridizing. Indeed, when bred with conspecific males (*18*), females with a higher propensity to switch their choice from conspecifics in deep water to heterospecifics in shallow water produced tadpoles that developed more slowly than those produced by females with a lower propensity to switch (Fig. 2B). Thus, females' responses to changes in the water level depended on their condition and the developmental rate of their offspring in pure-species pairings, suggesting that female mate choice results from an interplay of a female's own phenotype and the specific ecological circumstances in which her offspring develop.

The tendency to switch patterns of mate choice in response to water level appears to have evolved only in populations and species that risk engaging in, and can potentially benefit from, hybridization. In three mate-choice trials [two in deep water and one in shallow water (*18*)], allopatric females (females from populations where *S. multiplicata* does not occur) did not discriminate between conspecific and heterospecific calls (first deep water trial: 9 chose conspecific calls, 16 chose heterospecific calls, $\chi_1^2 = 1.99$, $P = 0.16$; second deep water trial: 17 chose conspecific calls, 12 chose heterospecific calls, $\chi_1^2 = 0.87$, $P = 0.35$; shallow water trial: 14 chose conspecific calls, 12 chose heterospecific calls, $\chi_1^2 = 0.15$, $P = 0.69$). These responses were not significantly different among the three trials ($\chi_1^2 = 3.01$, $P = 0.22$). Thus, contrary to sympatric *S. bombifrons* females, allopatric *S. bombifrons* females did not vary their choice depending on water level.

Moreover, switches in patterns of mate choice are not generalized responses of sympatric *Spea* females to shallow water: Sympatric *S. multiplicata* from the same populations as the sympatric *S. bombifrons* used in the experiments above significantly preferred conspecific calls, regardless of water level (deep water: 43 chose conspecific calls, 22 chose heterospecific calls, $\chi_1^2 = 6.91$, $P = 0.009$; shallow water: 47 chose conspecific calls, 29 chose heterospecific calls,

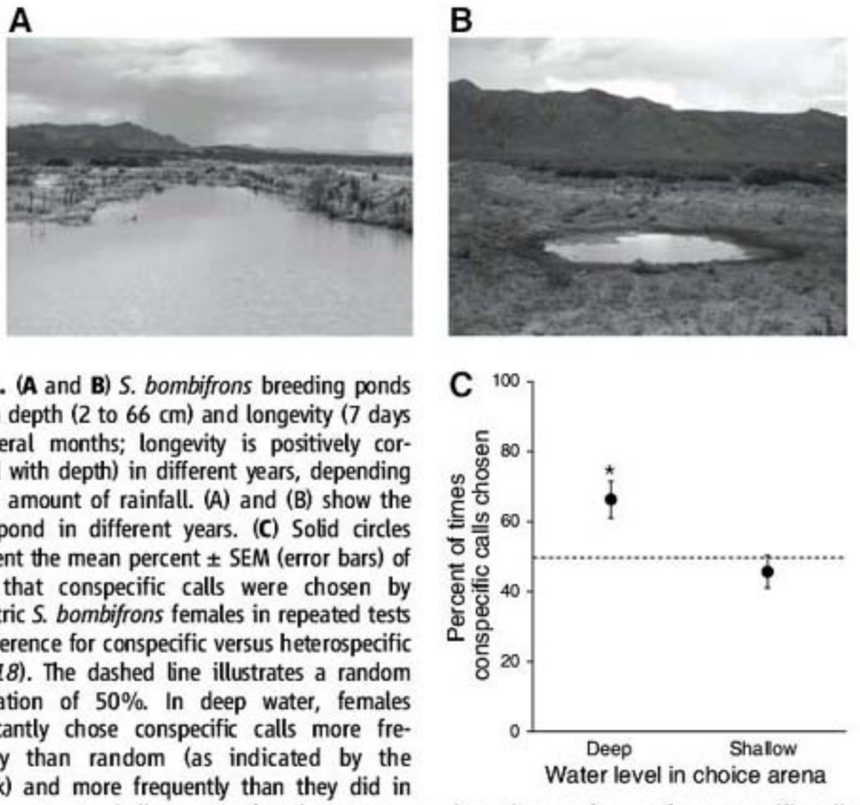


**Fig. 1.** (**A** and **B**) *S. bombifrons* breeding ponds vary in depth (2 to 66 cm) and longevity (7 days to several months; longevity is positively correlated with depth) in different years, depending on the amount of rainfall. (**A**) and (**B**) show the same pond in different years. (**C**) Solid circles represent the mean percent ± SEM (error bars) of times that conspecific calls were chosen by sympatric *S. bombifrons* females in repeated tests of preference for conspecific versus heterospecific calls (*18*). The dashed line illustrates a random expectation of 50%. In deep water, females significantly chose conspecific calls more frequently than random (as indicated by the asterisk) and more frequently than they did in shallow water. In shallow water, females as a group showed no preference for conspecific calls.

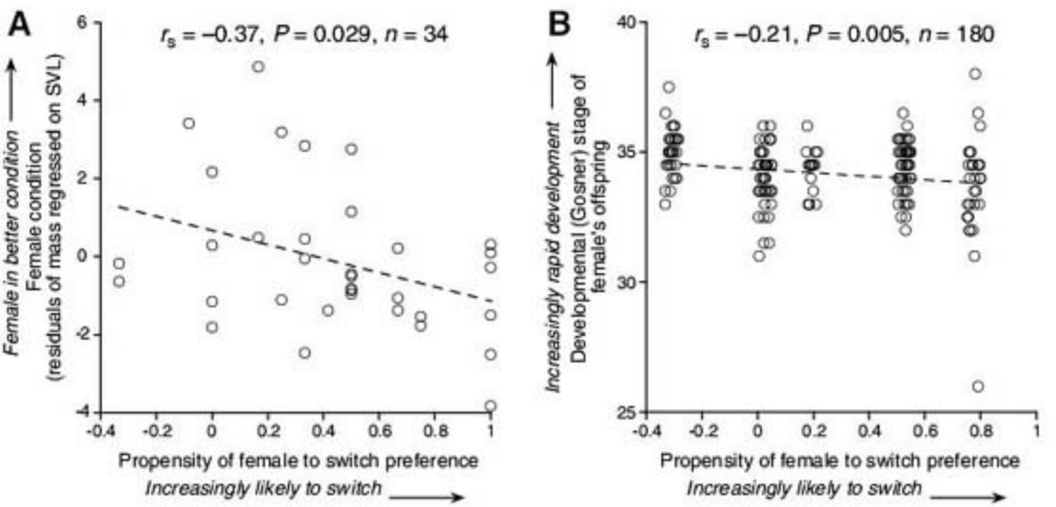


**Fig. 2.** (**A**) Female condition as a function of female propensity to switch from choosing conspecific calls in deep water to choosing heterospecific calls in shallow water (*18*). (**B**) Development rate of a female's offspring (from pure *S. bombifrons* pairings) as a function of that female's propensity to switch from choosing conspecific calls in deep water to choosing heterospecific calls in shallow water (*18*). Each point represents the mean of two tadpoles from a given replicate; there were 15 replicates for each of the 12 females (*18*). Data are jittered (by adding small random values to the original data along the *x* axis for presentation only). Each panel shows the results of a nonparametric Spearman rank-order correlation analysis that is not sensitive to outliers (*18*). Least-squares regression (dashed) lines are shown for illustration only. $r_s$, Spearman rank correlation coefficient; SVL, snout-to-vent length.

$\chi_1^2 = 4.30$, $P = 0.038$). Mate choice of *S. multiplicata* females did not differ significantly between water-depth treatments ($\chi_1^2 = 0.28$, $P = 0.60$). Thus, because *S. multiplicata* females do not benefit by hybridizing with *S. bombifrons* males (*14*), the fact that they chose conspecific mates regardless of water level supports the hypothesis that switches in mate choice should evolve only when hybridization is potentially adaptive.

In deep-water trials, sympatric *S. bombifrons* chose conspecific calls significantly more often than did allopatric females (Wilcoxon normal approximation: $z$ score= –2.15, $P = 0.03$, $n = 81$). The fact that sympatric *S. bombifrons* females discriminated against heterospecifics when hybridization was not favorable (i.e., in deep water) suggests that behaviors that minimize hybridization have evolved in sympatry. Such differences between allopatry and sympatry are expected if selection favors mating behaviors that promote reproductive isolation between species (*1*, *2*, *19*–*22*). Thus, sympatric females have apparently evolved the ability to modify their discrimination against heterospecifics, depending on the fitness consequences of hybridization.

These findings suggest that facultative switches in female mate-choice behavior contribute to adaptive hybridization and explain localized hybridization in habitats where hybrids may have higher fitness (*8*, *14*). In addition, these results suggest how hybrids may persist in the face of a general pattern of selection against them. Generally, when hybrids are disfavored, selection should promote the evolution of behaviors in sympatry that preclude hybridization (i.e., reinforcement) (*1*, *2*, *19*–*22*). As expected, *S. bombifrons* females in sympatry, but not allopatry, discriminate against heterospecifics when hybridization is costly. If, however, females facultatively hybridize when it is beneficial, hybridization may persist locally in the face of a global pattern of reinforcement. The presence of hybrids in systems that have seemingly undergone reinforcement is often attributed to mistakes in mate choice, constraints on female choice, or forced copulation by males (*4*–*7*). However, facultative adaptive hybridization potentially explains the persistence of hybrids despite the prediction that reinforcement should eventually eliminate hybridization (*19*, *23*–*25*).

Generally, whenever fitness is reversed in different habitats, facultative switches in mating behavior may evolve if females routinely experience different habitats and can assess environmental cues that reliably predict offspring fitness (*26*, *27*). Because the fitness consequences of mate choice may often depend on the females' own phenotype or the habitat in which their offspring develop (*10*, *12*, *28*), context-dependent female mate choice may be common (*9*–*12*). Explaining such variation in mate choice is important, because it can dramatically affect the outcome of sexual selection and, ultimately, speciation.


**References and Notes**

1. J. A. Coyne, H. A. Orr, *Speciation* (Sinauer Associates, Sunderland, MA, 2004).
2. D. J. Howard, in *Hybrid Zones and the Evolutionary Process*, R. G. Harrison, Ed. (Oxford Univ. Press, New York, 1993), pp. 46–69.
3. M. Andersson, *Sexual Selection* (Princeton Univ. Press, Princeton, NJ, 1994).
4. T. Lamb, J. C. Avise, *Proc. Natl. Acad. Sci. U.S.A.* **83**, 2526 (1986).
5. P. Wirtz, *Anim. Behav.* **58**, 1 (1999).
6. K. B. Malmos, B. K. Sullivan, T. Lamb, *Evol. Int. J. Org. Evol.* **55**, 626 (2001).
7. T. Veen *et al.*, *Nature* **411**, 45 (2001).
8. M. L. Arnold, *Natural Hybridization and Evolution* (Oxford Univ. Press, Oxford, 1997).
9. M. D. Jennions, M. Petrie, *Biol. Rev. Camb. Philos. Soc.* **72**, 283 (1997).
10. I. Lesna, M. W. Sabelis, *Nature* **401**, 581 (1999).
11. F. Widemo, S. A. Sæther, *Trends Ecol. Evol.* **14**, 26 (1999).
12. S. Cotton, J. Small, A. Pomiankowski, *Curr. Biol.* **16**, R755 (2006).
13. P. W. Sattler, *Copeia* **1985**, 324 (1985).
14. K. S. Pfennig, M. A. Simovich, *Evol. Int. J. Org. Evol.* **56**, 1840 (2002).
15. M. A. Simovich, C. A. Sassaman, A. Chovnick, *Proc. San Diego Soc. Nat. Hist.* **1991**, 1 (1991).
16. D. C. Forester, *Herpetologica* **31**, 282 (1975).
17. D. W. Pfennig, *Evol. Int. J. Org. Evol.* **46**, 1408 (1992).
18. See supporting material on *Science* Online.
19. T. Dobzhansky, *Am. Nat.* **74**, 312 (1940).
20. M. A. Noor, *Nature* **375**, 674 (1995).
21. G. P. Sætre *et al.*, *Nature* **387**, 589 (1997).
22. M. R. Servedio, M. A. F. Noor, *Annu. Rev. Ecol. Evol. Syst.* **34**, 339 (2003).
23. J. M. Jones, *Evol. Int. J. Org. Evol.* **27**, 435 (1973).
24. S. C. Britch, M. L. Cain, D. J. Howard, *Mol. Ecol.* **10**, 627 (2001).
25. K. S. Pfennig, *Evol. Int. J. Org. Evol.* **57**, 2842 (2003).
26. R. Levins, *Evolution in Changing Environments: Some Theoretical Explorations* (Princeton Univ. Press, Princeton, NJ, 1968).
27. N. A. Moran, *Am. Nat.* **139**, 971 (1992).
28. A. M. Welch, *Evol. Int. J. Org. Evol.* **57**, 883 (2003).


29. I thank D. Pfennig, R. Martin, C. Bookhout, M. McGee, M. Scott, G. Zimmerman, K. Reynolds, W. Harcombe, M. Landstrom, A. Stewart, and A. Nagel for lab and field assistance; D. Pfennig, M. Noor, R. Martin, C. Gerhardt, A. Rice, A. Chunco, C. Ledon-Rettig, M. Servedio, S. Dhole, C. Kight, and E. Wojtowicz for comments; and the state agencies of Arizona, Colorado, New Mexico, and Texas for permits. This work was supported by NSF grant DEB-0542566.


**Supporting Online Material**

www.sciencemag.org/cgi/content/full/318/5852/965/DC1
Materials and Methods
Fig. S1
Audio S1 and S2
References


4 June 2007; accepted 9 October 2007
10.1126/science.1146035


# Bypass of DNA Lesions Generated During Anticancer Treatment with Cisplatin by DNA Polymerase η


**Aaron Alt,[1]* Katja Lammens,[1,2]* Claudia Chiocchini,[1] Alfred Lammens,[1,2] J. Carsten Pieck,[1] David Kuch,[1] Karl-Peter Hopfner,[1,2]† Thomas Carell[1]†**



DNA polymerase η (Pol η) is a eukaryotic lesion bypass polymerase that helps organisms to survive exposure to ultraviolet (UV) radiation, and tumor cells to gain resistance against cisplatin-based chemotherapy. It allows cells to replicate across cross-link lesions such as 1,2-d(GpG) cisplatin adducts (Pt-GG) and UV-induced *cis–syn* thymine dimers. We present structural and biochemical analysis of how Pol η copies Pt-GG–containing DNA. The damaged DNA is bound in an open DNA binding rim. Nucleotidyl transfer requires the DNA to rotate into an active conformation, driven by hydrogen bonding of the templating base to the dNTP. For the 3′dG of the Pt-GG, this step is accomplished by a Watson-Crick base pair to dCTP and is biochemically efficient and accurate. In contrast, bypass of the 5′dG of the Pt-GG is less efficient and promiscuous for dCTP and dATP as a result of the presence of the rigid Pt cross-link. Our analysis reveals the set of structural features that enable Pol η to replicate across strongly distorting DNA lesions.


All three kingdoms of life possess special Y-family DNA polymerases (*1*, *2*). These enzymes share with high-fidelity DNA polymerases the basic nucleotidyl transfer mechanism and the right-hand–like structure, but the potential DNA duplex binding surface is increased by a polymerase-associated domain (PAD, also denoted "little finger" for its role in template binding) found only in Y-family polymerases (*3*). DNA polymerase η (Pol η) in eukaryotes is able to replicate through UV-induced cyclobutane pyrimidine dimers (CPDs) (*4*–*6*), or cisplatin-induced 1,2-d(GpG) adducts (Pt-GGs) (*7*) formed in a typical anticancer therapy with cisplatin (*8*). Bypass of such cross-links is particularly difficult because two adjacent coding bases are simultaneously damaged. To reveal the mechanism for this poorly understood lesion


[1]Munich Center for Integrated Protein Science (CiPS[M]), Ludwig Maximilians University, D-81377 Munich, Germany. [2]Gene Center at the Department of Chemistry and Biochemistry, Ludwig Maximilians University, D-81377 Munich, Germany.

*These authors contributed equally to this work.
†To whom correspondence should be addressed. E-mail: hopfner@lmb.uni-muenchen.de (K.-P.H.); thomas.carell@cup.uni-muenchen.de (T.C.)

bypass capability, we crystallized the large fragment of yeast Pol η as ternary complexes with incoming dNTP and two different 16-bp templates containing a site-specific Pt-GG, annealed to two different 9-bp primers (*CP1* and *CP2*).

The first crystals analyzed featured two different complexes (Fig. 1, A and C, and Fig. 2A) in the asymmetric unit. Their structures were determined at 3.1 Å resolution. The crystals were obtained by co-crystallizing Pol η with the DNA template-primer construct *CP1*. In both complexes, the Pt-GG cross-link is well defined in the electron density, and the bases forming the Pt-GG lesion are positioned at a ~90° angle with respect to each other (Fig. 1B). The first complex (Fig. 1, A to D) (3′dG elongation step) contains the Pt-GG lesion partially situated in the active site, with the 3′dG of the lesion forming a standard Watson-Crick base pair with the incoming dCTP (Fig. 1C), representing a model for the efficient bypass of the 3′dG of the lesion. The second complex shows the Pt-GG lesion outside the active site in front of the DNA binding rim (Fig. 1D, 2A). We suggest that this complex resembles the "pre-elongation" state. In both structures, the template primer complex is bound in a wide DNA binding rim between the opposing thumb and PAD domains (Fig. 1A).

The structures reported here and the structure of the apoenzyme (*9*) share the same space groups and similar unit cell dimensions. A comparison of the 3′dG elongation complex with the apoenzyme reveals small but important changes. The thumb domain moves toward the DNA (fig. S1), and the loop 306-312 (Fig. 1D) contacts the DNA backbone. Loop 353-363 moves toward the minor groove, and β-sheet $\beta_{14}$ of the PAD domain shifts by 4 Å toward the DNA backbone. The reorientation of the DNA from the pre-elongation into the 3′dG elongation state (Fig. 2, B and C) is accompanied by small motions of the thumb and PAD domains, relative to the palm and finger domains (fig. S2). The DNA contacts to the PAD domain are shifted by one base pair (fig. S3). In the pre-elongation complex (Fig. 2A), the Pt-GG lesion is positioned outside the active site and the 3′dG of the lesion is held 6 Å away from the dCTP (3′dG-O6•••4$NH_2$-dCTP). Still, the dCTP is positioned in the active site even in the absence of any templating base. Two metal ions are seen in the active site, coordinated by the catalytically essential residues $Asp^{30}$, $Asp^{155}$ and $Glu^{156}$ (Fig. 2A). The 3′OH group, which was modeled into the structure because the primer features a dideoxy terminus, is located ~8.5 Å away from the dCTP's α-phosphate and hence is unable to perform primer elongation. This situation is substantially changed when the template-primer complex rotates into the 3′dG elongation state (Fig. 2, B and C). Here, the 3′dG of the lesion establishes a standard Watson-Crick base pair with the pre-orientated dCTP (Fig. 1C). $Arg^{73}$ coordinates the dCTP's α-phosphate and stacks on the base moiety. In this complex, the distance between the putative 3′OH nucleophile and the α-phosphate is only ~5.0 Å, well aligned for nucleotidyl transfer, explaining why the first step of lesion bypass is relatively efficient. Correct positioning of the dCTP for the 3′dG translesion synthesis is guided by a H-bond between the 3′OH group of dCTP and the backbone of Pol η at $Phe^{35}$, as well as by hydrophobic interactions with $Phe^{35}$ (fig. S4). $Phe^{35}$ is the steric gate, needed to exclude ribonucleoside triphosphates from entering the catalytic center (*10*).

We next crystallized Pol η together with the template-primer construct *CP2* in which the 5′dG of the lesion is the first unpaired base. Again crystals were obtained with two different complexes in the asymmetric unit (complex 1b and 2b) determined at 3.3 Å resolution, (Complex 1b) (Fig. 3, A and B). The obtained structures, which are very similar, provide insight into the second lesion bypass step (5′dG elongation). Biochemically, we observed that bypass of the 3′dG by Pol η is efficient and mostly error free (Fig. 3C). Bypass of the 5′dG, however, is slower and promiscuous for dCTP and dATP (Fig. 3D). In the 5′dG elongation complex, the 3′dG of the lesion remains Watson-

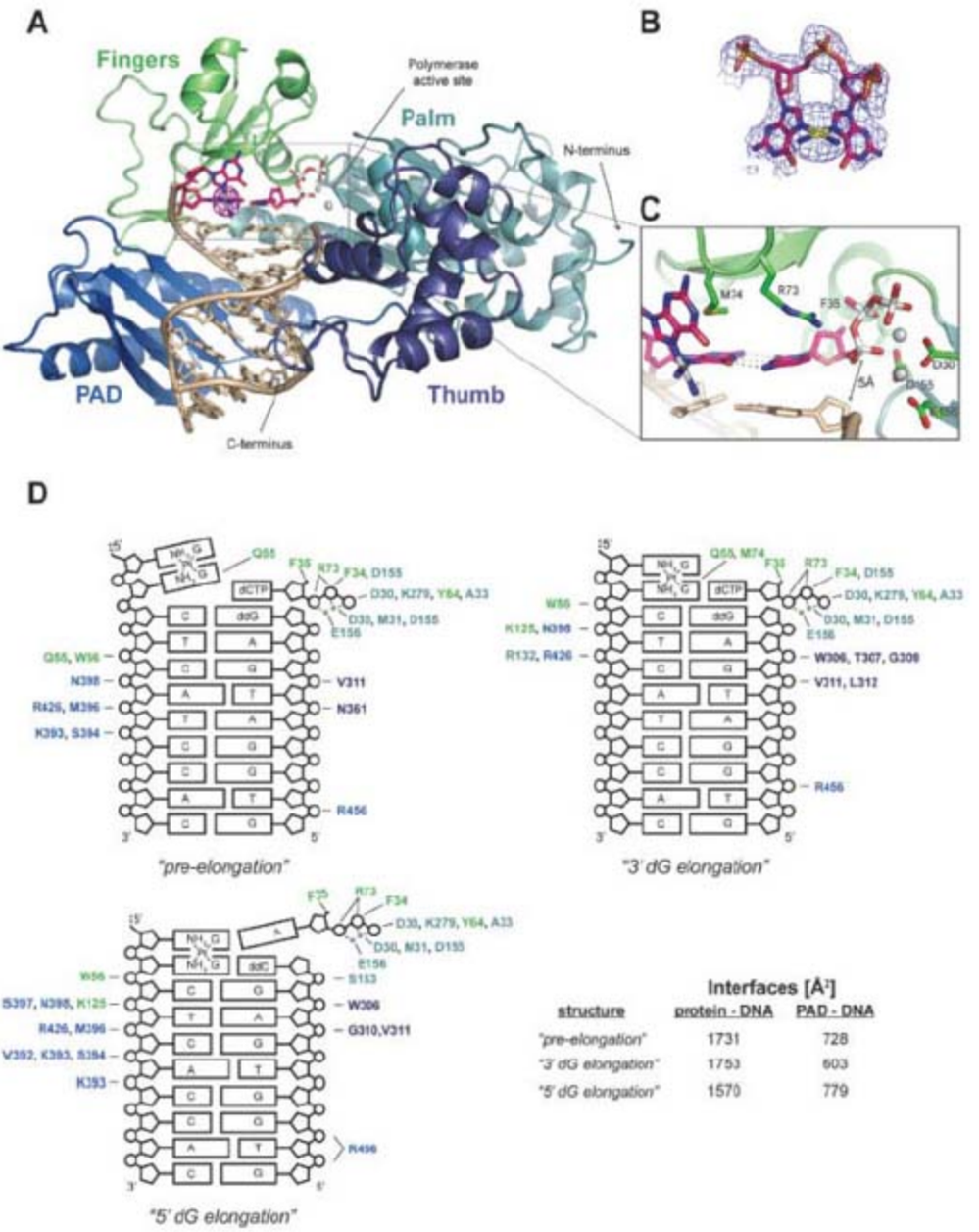


**Fig. 1.** Pol η structure in ternary complex with lesion containing DNA. **(A)** In the 3′dG elongation complex, the cisplatin (magenta) is shown with the platinum anomalous electron density contoured at 10 σ. The primer and template strands of the DNA (brown) and the Watson-Crick H-bonded dCTP (magenta) are depicted as sticks. The two metal ions are shown as gray spheres. **(B)** View of the 1,2-d(GpG) cisplatin lesion superimposed with the simulated annealed composit-omit density map contoured at 1.0 sigma. **(C)** The catalytic residues in the active site. R73 orients the dCTP for H-bonding with the 3′desoxyguanine of the lesion. **(D)** Schematics of protein-DNA contacts representing the pre-elongation, 3′dG elongation, and 5′dG elongation complex. Direct hydrogen-bonds are indicated by solid lines. DNA contacts with the symmetry-related molecule are not shown.

Crick base-paired to the primer dC base. The incoming dNTP stacks on top of this base pair. The 5′dG of the moved into the active site, but the cross-linking Pt-bond to the 3′-dG forces this stay perpendicular relative to the incoming dATP (Fig. 3B). Only one H-bond is established between the exocyclic C(6)-$NH_2$ amino group of dATP and the C(6)=O carbonyl oxygen of the 5′dG. In this structure, the modeled primer 3′OH is 7.5 Å away from the dATP, a distance that is significantly larger compared with the first elongation complex (5 Å), providing a rationale for the slower second bypass step. In complex 2b, the 5′dG is even 9.5 Å away from the α-phosphate, and no hydrogen bond is formed to the incoming dATP (fig. S5). Thus, the single H-bond formed between the two perpendicularly oriented heterocycles pulls the primer strand and the dATP together. Such an H-bond is only possible with dATP and dCTP, which explains the promiscuity for dCTP and dATP during the second bypass step. To obtain further support for this hypothesis, primer extension studies were performed with Pt-GG containing templates and 6-deaminocytidinetriphosphate (dZTP), which cannot form the critical H-bond. As predicted, bypass of the 5′dG with dZTP is indeed reduced (fig. S6).

We have constructed a model of how Pol η effects bypass of Pt-GG lesions [despite the limited resolution (~3 Å) and bearing in mind that crystal packing forces might influence aspects of the structure remote from the active site]. The enzyme binds the template-primer complex nonproductively in the "pre-elongation" state, which is in equilibrium with the productive 3′dG elongation state (*11*). We suppose that the dNTPs are bound and presumably rapidly exchanged in the active site. If a dNTP is bound, and able to interact with the templating base, it shifts the primer-template equilibrium toward the 3′dG elongation state, in which nucleotidyl transfer occurs. In the second step of lesion bypass, the primer template moves forward, with one H-bond apparently being the minimum requirement to pull the template primer complex toward the incoming dNTP in order to allow the 5′dG nucleotidyl transfer. This happens at much reduced efficiency and accuracy. The proposed rotation step would be mechanistically quite distinct from the dNTP-directed induced fit observed in high-fidelity polymerases (*3*) and could be a specific adaptation for replication of templates containing intrastrand cross-

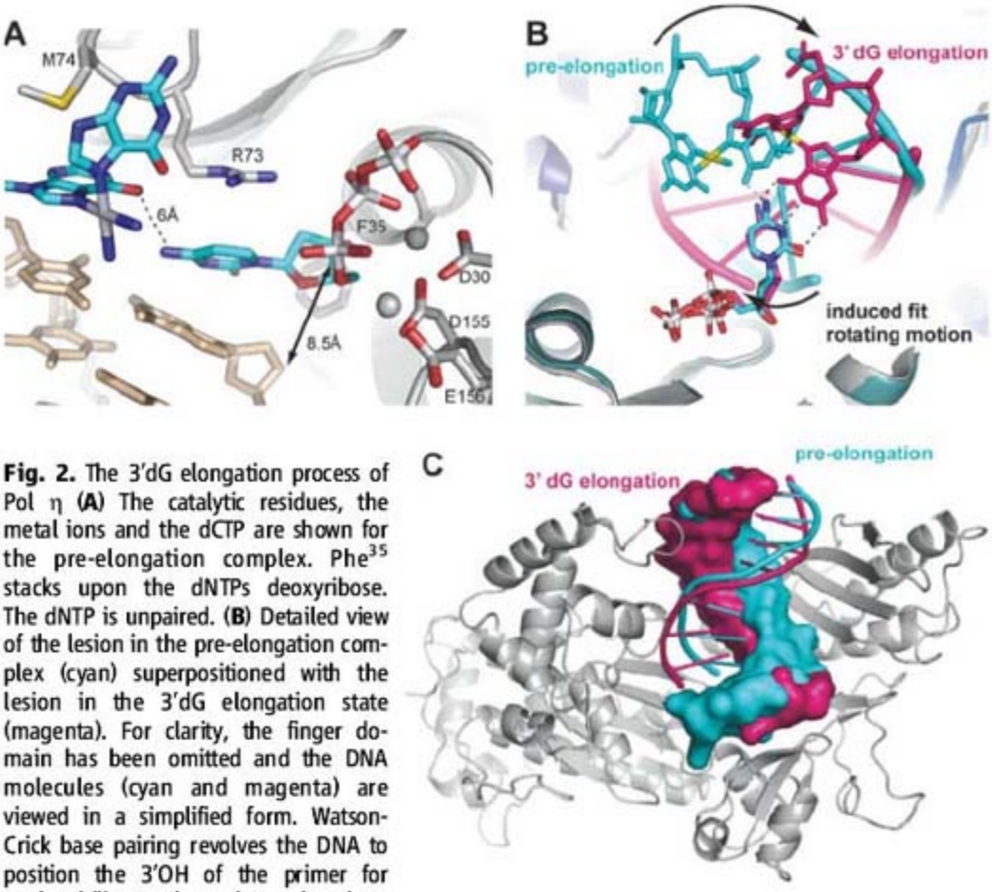


**Fig. 2.** The 3′dG elongation process of Pol η **(A)** The catalytic residues, the metal ions and the dCTP are shown for the pre-elongation complex. $Phe^{35}$ stacks upon the dNTPs deoxyribose. The dNTP is unpaired. **(B)** Detailed view of the lesion in the pre-elongation complex (cyan) superpositioned with the lesion in the 3′dG elongation state (magenta). For clarity, the finger domain has been omitted and the DNA molecules (cyan and magenta) are viewed in a simplified form. Watson-Crick base pairing revolves the DNA to position the 3′OH of the primer for nucleophilic attack on the α-phosphate of the dNTP. **(C)** The DNA revolves from the pre-elongation state into the first elongation state, forming a Watson-Crick base pair. This aligns the 3′OH of the primer for nucleotidyl transfer. The protein of the pre-elongation complex is omitted for clarity, and the protein of the 3′dG elongation state is depicted in gray. The DNA molecules are color coded as in Fig. 2B.

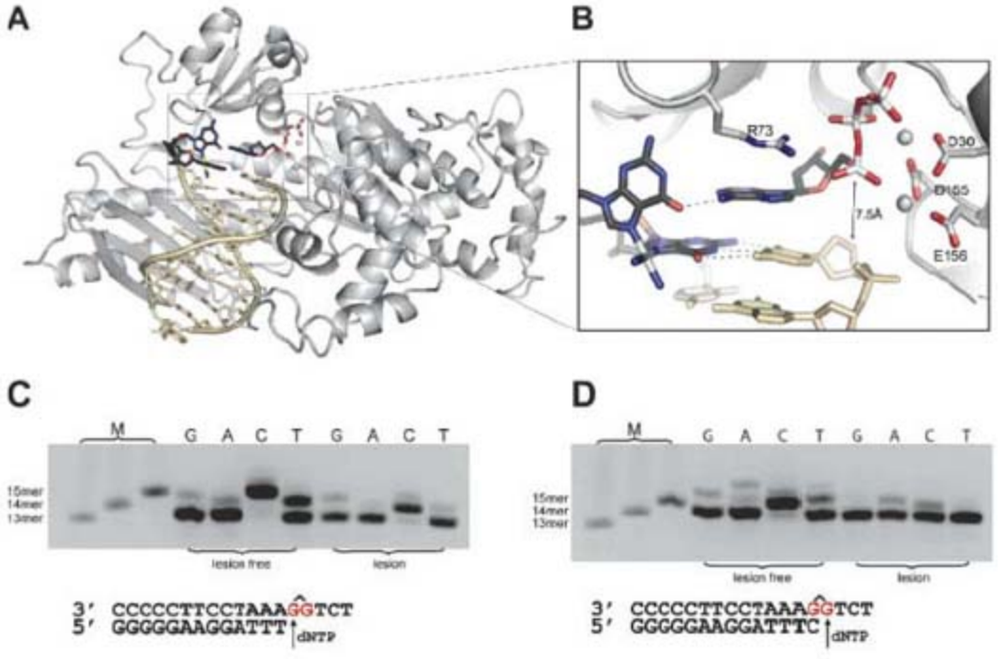


**Fig. 3.** The 5′dG elongation process of Pol η **(A)** The 5′dG elongation complex is shown in gray, and the primer and template strands are depicted as sticks (brown). The lesion and the dNTP are depicted as sticks in color. **(B)** The catalytic residues together with the metal ions bound to dATP are shown. The nucleotide forms one H-bond with the 5′desoxyguanine of the lesion. **(C)** Nucleotide insertion studies opposite the 3′G of the lesion using a fluorescein-labeled 13mer hybridized to an 18mer DNA template either with a site-specific cisplatin lesion (lesion) or without (lesion free). The dNTP used in each experiment is noted at the top of the lanes. The markers (M) represent an insertion opposite the 3′G (14mer) and the 5′G (15mer). **(D)** Nucleotide insertion studies opposite the lesions 5′G using the same reaction conditions as in (C), with a fluorescein-labeled 14mer hybridized to a 18mer DNA template with either a site specific cisplatin lesion (lesion) or without (lesion free).

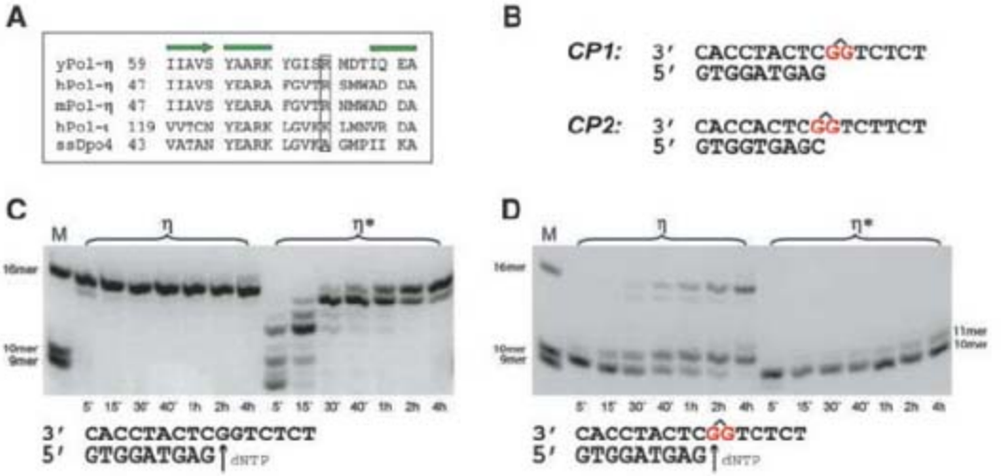


**Fig. 4.** Structure-based point mutation of Arg[73] **(A)** Sequence alignment of *S. cerevisae*, human and mouse Pol η, DPO4, and human Pol ι showing that R73 is conserved in Pol η homologs. Secondary structure elements are a rectangle for α helix and arrows for β strands. **(B)** DNA sequences used for primer extension studies and for the crystallization of the first bypass step (CP1) and the second bypass step (CP2). The sites of the lesions are indicated in red. **(C)** Time-dependent primer extension studies with Pol η (η) and Pol ηR73L (η*), using the same template and primer strands used for crystallization but without the site-specific cisplatin lesion. **(D)** Time-dependent primer extension studies with Pol η (η) and Pol ηR73L (η*) with the same template and primer strands as in 4C but with a site-specific cisplatin lesion.

link lesions (*12*, *13*). The proposed mechanism argues that Pol η selects correct dNTPs not by shape but by hydrogen bond complementarity, which is consistent with previous biochemical observations (*14*).

To gain further insight into the biochemistry of the bypass reaction we analyzed a site-directed mutant of Pol η. Arg73 seems to activate and stabilize the dNTP for the lesion bypass steps. The guanidinium group stacks on top of the base moiety of the incoming dNTP (*15*), which is important for the correct positioning of the dNTP (Fig. 3B). Arg73 is highly conserved among Pol η homologs but not among other Y-family polymerases (Fig. 4A). We mutated Arg73 to leucine (fig. S8) and found that Pol ηR73L (Pol η*) still can replicate undamaged templates (Fig. 4C, η*), although the polymerization efficiency is substantially reduced. Pol ηR73L is able to perform the first bypass step slowly, in comparison with the wild-type enzyme (Fig. 4D, η*), whereas the second step of lesion bypass is strongly compromised. The same biochemical properties are observed with CPD lesions (fig. S7), showing that the function of R73 is generally required for the replication through intrastrand cross-links (*16*).

These four crystallographically analyzed complexes, together with the biochemical data, provide a step-by-step picture of the lesion bypass process. This information may lead to new cisplatin derivatives able to escape translesion replication in order to overcome tumor resistance in cisplatin chemotherapy.

### References and Notes


1. W. Yang, *Curr. Opin. Struct. Biol.* **13**, 23 (2003).
2. E. C. Friedberg, R. Wagner, M. Radman, *Science* **296**, 1627 (2002).
3. T. A. Steitz, *J. Biol. Chem.* **274**, 17395 (1999).
4. C. Masutani *et al.*, *Nature* **399**, 700 (1999).
5. R. E. Johnson, C. M. Kondratick, S. Prakash, L. Prakash, *Science* **285**, 263 (1999).
6. R. E. Johnson, S. Prakash, L. Prakash, *Science* **283**, 1001 (1999).
7. M. R. Albertella, C. M. Green, A. R. Lehmann, M. J. O'Connor, *Cancer Res.* **65**, 9799 (2005).
8. D. Wang, S. J. Lippard, *Nat. Rev. Drug Discov.* **4**, 307 (2005).
9. J. Trincao *et al.*, *Mol. Cell* **8**, 417 (2001).
10. A. M. DeLucia, N. D. Grindley, C. M. Joyce, *Nucleic Acids Res.* **31**, 4129 (2003).
11. P. J. Rothwell, G. Waksman, *J. Biol. Chem.* **282**, 28884 (2007).
12. R. E. Johnson, M. T. Washington, S. Prakash, L. Prakash, *J. Biol. Chem.* **275**, 7447 (2000).
13. M. T. Washington, L. Prakash, S. Prakash, *Cell* **107**, 917 (2001).
14. M. T. Washington, S. A. Helquist, E. T. Kool, L. Prakash, S. Prakash, *Mol. Cell. Biol.* **23**, 5107 (2003).
15. E. A. Meyer, R. K. Castellano, F. Diederich, *Angew. Chem. Int. Ed.* **42**, 1210 (2003).
16. M. T. Washington, R. E. Johnson, S. Prakash, L. Prakash, *Proc. Natl. Acad. Sci. U.S.A.* **97**, 3094 (2000).


17. We thank the staff of the PX-1 beamline at Swiss Light Source (Villingen, Switzerland) and ID23-2 at European Synchrotron Radiation Facility (Grenoble, France).

Supported by European Union Integrated Project "DNA Repair," the Deutsche Forschungsgemeinschaft (CiPS[M] and SFB646), Volkswagen Foundation, Fonds der Chemischen Industrie, and Novartis. A.A. is grateful for a EU Marie Curie Training and Mobility fellowship (CLUSTOXDNA). Coordinates and structure factors have been deposited in the Protein Data Bank under accession code 2R8J and 2R8K. The authors declare no competing financial interests.


**Supporting Online Material**

www.sciencemag.org/cgi/content/full/318/5852/967/DC1
Figs. S1 to S9
Table S1
References


23 July 2007; accepted 10 October 2007
10.1126/science.1148242


# GNAT-Like Strategy for Polyketide Chain Initiation


Liangcai Gu,[1,2*] Todd W. Geders,[1,6*] Bo Wang,[4] William H. Gerwick,[7] Kristina Håkansson,[4] Janet L. Smith,[1,3]† David H. Sherman[1,2,4,5]†



An unexpected biochemical strategy for chain initiation is described for the loading module of the polyketide synthase of curacin A, an anticancer lead derived from the marine cyanobacterium *Lyngbya majuscula*. A central GCN5-related *N*-acetyltransferase (GNAT) domain bears bifunctional decarboxylase/*S*-acetyltransferase activity, both unprecedented for the GNAT superfamily. A CurA loading tridomain, consisting of an adaptor domain, the GNAT domain, and an acyl carrier protein, was assessed biochemically, revealing that a domain showing homology to GNAT ($GNAT_L$) catalyzes (i) decarboxylation of malonyl-coenzyme A (malonyl-CoA) to acetyl-CoA and (ii) direct *S*-acetyl transfer from acetyl-CoA to load an adjacent acyl carrier protein domain ($ACP_L$). Moreover, the N-terminal adapter domain was shown to facilitate acetyl-group transfer. Crystal structures of $GNAT_L$ were solved at 1.95 angstroms (ligand-free form) and 2.75 angstroms (acyl-CoA complex), showing distinct substrate tunnels for acyl-CoA and holo-$ACP_L$ binding. Modeling and site-directed mutagenesis experiments demonstrated that histidine-389 and threonine-355, at the convergence of the CoA and ACP tunnels, participate in malonyl-CoA decarboxylation but not in acetyl-group transfer. Decarboxylation precedes acetyl-group transfer, leading to acetyl-$ACP_L$ as the key curacin A starter unit.


Modular polyketide synthases (PKSs) are large biosynthetic machines that assemble structurally diverse secondary metabolites with a broad spectrum of biological activities. Multifunctional enzymes catalyze programmed metabolic pathways to assemble short-chain acyl-CoA building blocks into complex polyketide products by one step of chain initiation, followed by multiple steps of chain elongation and processing. Polyketide chain elongation steps are catalyzed by extension modules that are minimally composed of

three essential domains—ketosynthase (KS), acyltransferase (AT), and acyl carrier protein (ACP)—plus auxiliary processing domains (e.g., ketoreductase, dehydratase, and enoyl reductase). As in fatty acid synthases (FASs), PKSs catalyze chain extension by a decarboxylative condensation reaction. Polyketide chain initiation is catalyzed by a "loading module" that, in all characterized PKSs, consists of domains homologous with domains of the minimal extension module. A loading acyltransferase domain ($AT_L$) uses an acyl-CoA substrate to load an adjacent ACP domain ($ACP_L$). Typically, the $AT_L$ substrate is an α-carboxylated acyl-CoA, like the substrate for chain extension, and acyl transfer is followed by decarboxylation by a "$KS^{Q*}$" domain within the loading module (*1*, *2*). Alternatively, in the well-studied erythromycin PKS, a trans-acting methylmalonyl-CoA decarboxylase acts on α-carboxylated acyl-CoA before acyl transfer by $AT_L$ (*3*, *4*).

Curacin A, a marine cyanobacterial metabolite from *L. majuscula*, is a mixed-polyketide nonribosomal-peptide natural product with potent antiproliferative and cytotoxic activity against colon-, renal-, and breast-cancer–derived cell lines (*5*). The recent identification and partial characterization of the biosynthetic pathway for curacin A (*6*) revealed an atypical loading module, in which only the $ACP_L$ resembled typical PKS domains. Similar loading modules also occur in the biosynthetic pathways for pederin (*7*), its structural analogs onnamide and theopederin (*8*), myxovirescin A (*9*), and rhizoxin (*10*). In these natural product biosynthetic gene clusters, the chain initiation modules are structured as an N-terminal ~180–amino acid region of unknown function [adapter (AR) domain, not present in OnnB for onnamide], a variable-length linker region, $GNAT_L$, and $ACP_L$ (Fig. 1). The predicted function of all of these $GNAT_L$-containing modules was to load an acetyl group onto the PKS assembly line (*6*–*10*), but the mechanism of this process remained unclear.

GNAT is a superfamily of *N*-acyltransferase enzymes that catalyze acyl transfer to a primary amine and function in diverse pathways in prokaryotes and eukaryotes, including antibiotic resistance, gene regulation, and hormone synthesis (*11*, *12*). Typically, prokaryotic and eukaryotic GNATs have separate binding sites for the acyl donor and acceptor substrates and catalyze direct acyl transfer in the absence of a covalent intermediate on the enzyme (*11*). GNATs are mechanistically and structurally distinguished from the PKS and FAS AT domains that function as *S*-acyltransferases, use a covalent enzyme intermediate, and belong to the α/β hydrolase superfamily (*13*–*16*). Thus, acyl transfer to an ACP thiol group represents an unprecedented reaction for GNAT enzymes.

To investigate the atypical PKS chain initiation process, we cloned and overexpressed fragments of *curA* encoding the N-terminal tridomain, AR-$GNAT_L$-$ACP_L$. Several expression constructs were made to include the three components in various combinations (Fig. 2A and fig. S1, A and B). Constructs containing $ACP_L$ were generated in holo form by coexpression with a plasmid encoding phosphopantetheinyl transferase (Sfp) from *Bacillus subtilis* (*17*); without this plasmid, *Escherichia coli* produced $ACP_L$ in the apo form. All constructs lacking the AR domain were readily produced as soluble polypeptides, but those including AR (AR-$GNAT_L$ and AR-$GNAT_L$-$ACP_L$) had substantially decreased solubility, and the excised AR domain was not obtained in soluble form under any conditions tested. Solubility was substantially greater for the AR-$GNAT_L$-$ACP_L$ (holo) tridomain than for the apo counterpart (fig. S1A), suggesting that the phosphopantetheine (PPant) arm of $ACP_L$ (holo) stabilizes the AR domain. The 63.3-kD AR-$GNAT_L$-$ACP_L$ polypeptide is monomeric (fig. S1C).

To assess the initiation behavior of the CurA starter unit, we treated the apo and holo forms of the CurA tridomain (AR-$GNAT_L$-$ACP_L$) and didomain ($GNAT_L$-$ACP_L$) with radiolabeled acyl-CoAs and analyzed protein radiolabeling by SDS–polyacrylamide gel electrophoresis (PAGE) (Fig. 2B). The holo forms of both the tridomain and didomain incorporated the radiolabel, whereas the apo forms were not labeled, indicating transthioesterification of the acyl group from CoA to the PPant arm of ACP. Thus, the N-terminal domains of CurA catalyze acyl loading, and additional proteins are not required. Lack of radiolabeling of the apo forms also indicates that loading does not proceed through a covalent enzyme intermediate, which is consistent with the direct-transfer mechanism established for other GNAT family members (*3*, *11*). This is in contrast to the "canonical" PKS loading module, typified by 6-deoxyerythronolide B synthase (DEBS) $AT_L$-$ACP_L$ (*3*), in which a covalent intermediate is observed for the apo form (Fig. 2B). The ability of the $GNAT_L$-$ACP_L$ (holo) didomain to load an acyl group demonstrated that the catalytic machinery for chain initiation resides within the $GNAT_L$ domain and not within the AR domain, which is also supported by the fact that selected mutations within $GNAT_L$ affected the loading behavior of AR-$GNAT_L$-$ACP_L$ both in cis (fig. S2) and in trans (fig. S6). However, the increased level of acyl-group loading activity by the AR-$GNAT_L$-$ACP_L$ (holo) tridomain (Fig. 2B and fig. S3) suggests that AR is required for efficient acyl transfer. Unexpectedly, both malonyl-CoA and acetyl-CoA functioned as substrates for the AR-$GNAT_L$-$ACP_L$ (holo) tridomain with similar efficiency (fig. S2).

To further investigate the CurA AR-$GNAT_L$-$ACP_L$ tridomain components, we analyzed the products that were covalently tethered to the PPant arm of $ACP_L$. We interrogated mass changes on AR-$GNAT_L$-$ACP_L$ for in cis acyl-group transfer

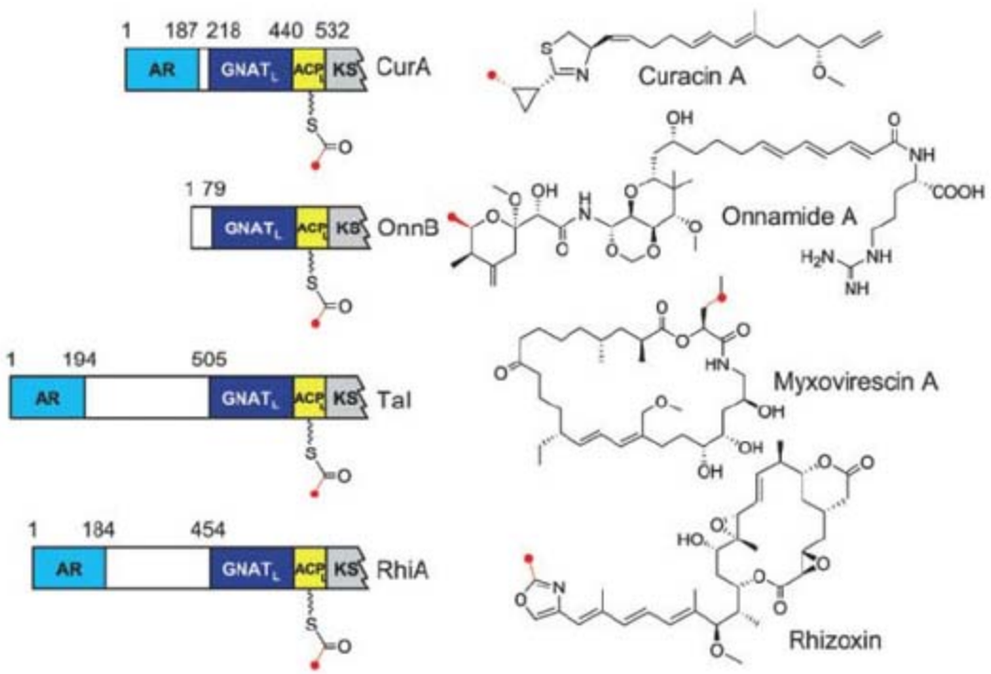


**Fig. 1.** Initiation modules containing $GNAT_L$ and compounds produced by the PKS pathways. All $GNAT_L$-containing modules are predicted to catalyze the loading of an acetyl group. Because of the high similarity of pederin, onnamides, and theopederin, only onnamide A is shown as the prototype example.

[1]Life Sciences Institute, University of Michigan, Ann Arbor, MI 48109, USA. [2]Department of Medicinal Chemistry, University of Michigan, Ann Arbor, MI 48109, USA. [3]Department of Biological Chemistry, University of Michigan, Ann Arbor, MI 48109, USA. [4]Department of Chemistry, University of Michigan, Ann Arbor, MI 48109, USA. [5]Department of Microbiology and Immunology, University of Michigan, Ann Arbor, MI 48109, USA. [6]Department of Biological Sciences, Purdue University, West Lafayette, IN 47907, USA. [7]Scripps Institution of Oceanography, University of California at San Diego, La Jolla, CA 92093, USA.

*These authors contributed equally to this work.
†To whom correspondence should be addressed. E-mail: davidhs@umich.edu (D.H.S.); JanetSmith@umich.edu (J.L.S.)

or by using the excised $ACP_L$ as the in trans acyl-group acceptor (Fig. 2C). Excised $ACP_L$ and trypsin-digested AR-$GNAT_L$-$ACP_L$ samples were examined by Fourier transform ion cyclotron resonance mass spectrometry (FTICR-MS) and infrared multiphoton dissociation (IRMPD) methods (*18*). First, the $ACP_L$ phosphopantetheinylation site was established as $Ser^{477}$ by MS analysis of the trypsin-digested AR-$GNAT_L$-$ACP_L$ (fig. S3) and by generating the corresponding $Ser^{477}\rightarrow Ala^{477}$ (S477A) $ACP_L$ mutant protein (*19*). Notably, for both malonyl-CoA and acetyl-CoA substrates, only an acetyl group was detected on the PPant arm of AR-$GNAT_L$-$ACP_L$ (holo) (Fig. 2C and fig. S3) or $ACP_L$ (holo) (Fig. 2D and fig. S4A). Thus, the CurA $GNAT_L$ loading module catalyzes both decarboxylation and acyl transfer of carboxyl-acyl-CoA substrates. These data reveal a gain-of-function for a GNAT-type polypeptide, as well as a divergence from all other characterized PKS loading modules, in which the acyl transfer and decarboxylation are catalyzed by separate domains (*1*, *4*). Further analysis by high-performance liquid chromatography (HPLC) and FTICR-MS demonstrated that all constructs containing $GNAT_L$ ($GNAT_L$, $GNAT_L$-$ACP_L$, and AR-$GNAT_L$-$ACP_L$) catalyzed decarboxylation of malonyl-CoA, methylmalonyl-CoA, and malonyl-$ACP_L$ to generate acetyl-CoA, propionyl-CoA (fig. S5), and acetyl-$ACP_L$ (fig. S4B), respectively.

Next, kinetic parameters for decarboxylation were measured by HPLC for malonyl-CoA and methylmalonyl-CoA and by radioassay for [1,3-$^{14}$C]malonyl-$ACP_L$ (table S1). The steady-state analysis indicated that malonyl-CoA is the preferred substrate. The catalytic rate constant ($k_{cat}$) for malonyl-CoA was ~1.8 $s^{-1}$, which is about sixfold and ~49-fold higher than those values for methylmalonyl-CoA and malonyl-$ACP_L$, respectively. Similarly, the catalytic efficiency, $k_{cat}/K_M$ (where $K_M$ is the Michaelis-Menton constant), for malonyl-CoA was ~5.25 $mM^{-1}$ $s^{-1}$, which is about threefold and about sixfold higher than those values of methylmalonyl-CoA and malonyl-$ACP_L$, respectively.

With clear evidence for a relatively rapid decarboxylation step catalyzed by $GNAT_L$, we sought to measure the rate of acyl loading by AR-$GNAT_L$-$ACP_L$. We determined the in cis acetyl-group transfer rate of AR-$GNAT_L$-$ACP_L$ (holo) by using [1-$^{14}$C]acetyl-CoA and [2-$^{14}$C]malonyl-CoA substrates. The $k_{cat}$ and $K_M$ values were derived by measuring the intramolecular acyl transfer rate at a series of acyl-CoA concentrations (table S1). The $k_{cat}$ or $K_M$ values for acetyl-group transfer were similar for acetyl-CoA and malonyl-CoA substrates. In contrast, the $k_{cat}$ for acetyl-group transfer was ~780-fold slower than the $k_{cat}$ for decarboxylation of malonyl-CoA, suggesting that decarboxylation and acetyl-group transfer are separated by a slow tridomain conformational change that leads to effective binding of the $ACP_L$ PPant arm in the active site ($k_2$ in fig. S7). Taken together with the decarboxylation kinetic data, these results confirm that malonyl-CoA decarboxylation precedes acetyl-group transfer to $ACP_L$ (holo). In addition, the apparent $K_M$ of acetyl-CoA or malonyl-CoA for acyl transfer is 80- to 90-fold lower than the $K_M$ of malonyl-CoA for decarboxylation and is dependent on the ratio of rate constants ($k_1$ to $k_6$ in fig. S7).

Because previously described GNAT enzymes catalyze various *N*-acetylation reactions,

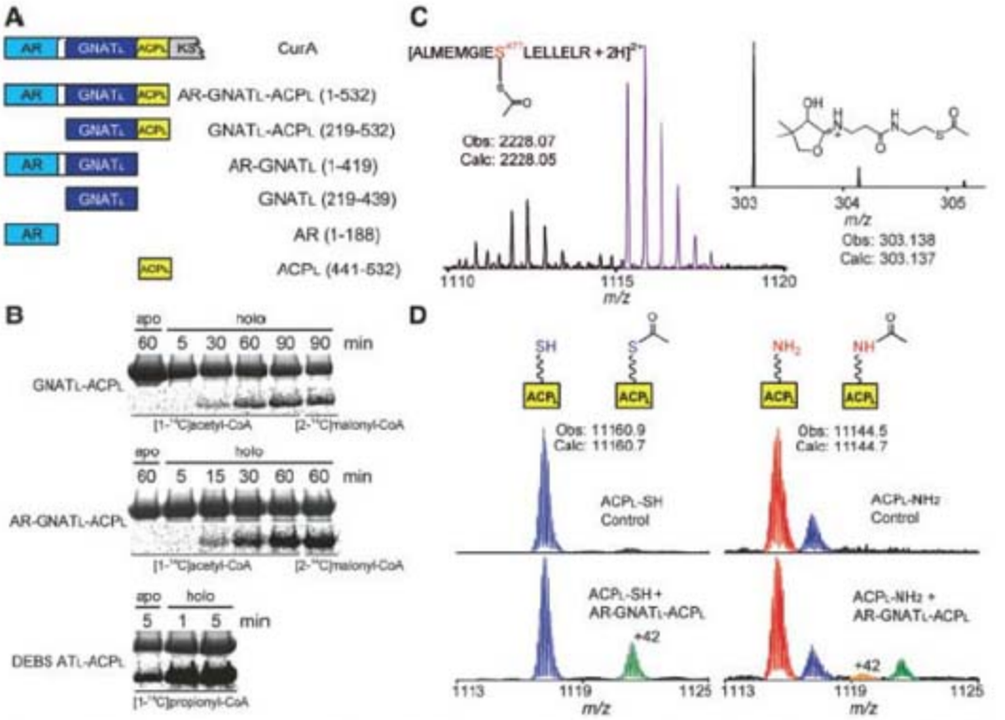


**Fig. 2.** (**A**) Expression constructs for *curA* initiation module. (**B**) Substrate loading of (apo and holo) $GNAT_L$-$ACP_L$, AR-$GNAT_L$-$ACP_L$, and DEBS $AT_L$-$ACP_L$. Proteins (30 μM) were incubated with 90 μM CoA substrates, in 50 mM Mops, pH 7.0, at room temperature. The SDS-PAGE gel images for Coomassie blue staining (top) and autoradiography (bottom) are shown. (**C**) FTICR mass spectrum (left) showing the ACP Ser-containing peptide from the trypsin-digested (holo) AR-$GNAT_L$-$ACP_L$ loaded with malonyl-CoA, and partial IRMPD spectrum (right) showing the PPant ejection product with a covalently linked acetyl group. *m/z*, mass/charge ratio. (**D**) Partial FTICR mass spectra showing (holo) $ACP_L$-SH (left) and (holo) $ACP_L$-$NH_2$ (right) loaded with acetyl-CoA. The N-terminal His tag of $ACP_L$ was removed. 10 μM (holo) $ACP_L$-SH [or ~1.5 μM (holo) $ACP_L$-$NH_2$] and 2 μM AR-$GNAT_L$-$ACP_L$ were incubated with 50 μM acetyl-CoA at room temperature for 30 min.

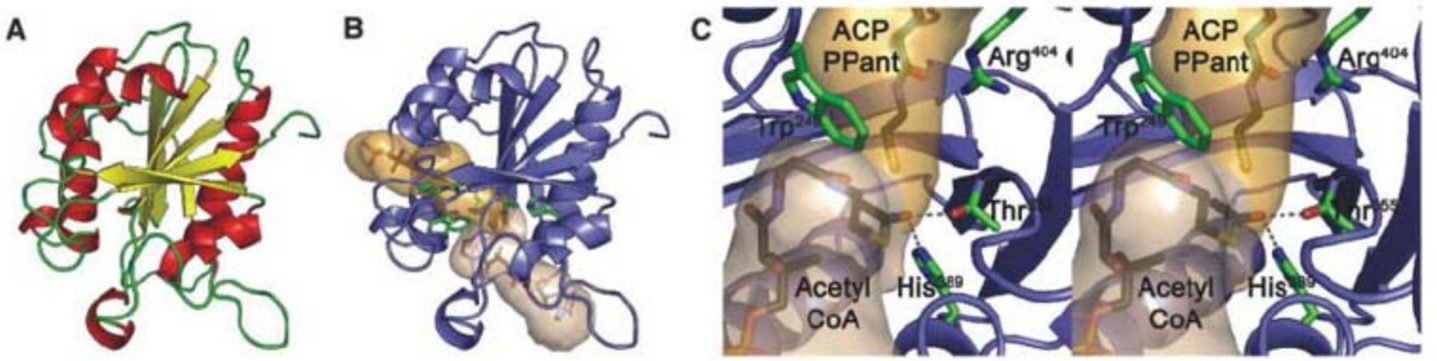


**Fig. 3.** (**A**) Structure of $GNAT_L$ domain. (**B**) Substrate tunnels with models (black-colored carbons) of acetyl-CoA (wheat-colored) and PPant arm of holo-$ACP_L$ (orange-colored). Residues $Trp^{249}$, $His^{389}$, $Thr^{355}$, and $Arg^{404}$ are shown (green-colored carbons). (**C**) Stereo diagram of modeling results overlaid with the observed structure, showing interaction of $His^{389}$ and $Thr^{355}$ with thioester carbonyl of acetyl-CoA. Coloring is identical to that in (B).

we tested whether CurA $GNAT_L$ retained a similar residual activity. We synthesized a CurA $ACP_L$-PPant analog bearing a terminal $NH_2$ in place of native (holo) $ACP_L$-SH (refer to the supporting online material) and tested it for in trans acetyl-group transfer catalyzed by AR-$GNAT_L$-$ACP_L$ (apo) to excised CurA (holo) $ACP_L$-$NH_2$ (monitored by FTICR-MS). A convenient internal standard was supplied by low levels of $ACP_L$-SH in the $ACP_L$-$NH_2$ preparation (Fig. 2D), likely resulting from the activity of endogenous *E. coli* ACP synthase or EntD (*20*). In contrast to the significant level of acetyl loading on $ACP_L$-SH (Fig. 2D), only a trace amount of acetyl-NH-$ACP_L$ was detected. In addition, simple alkyl amines (e.g., ethylenediamine and butylamine) were tested as substrates for acetyl-group transfer by CurA $GNAT_L$, but no *N*-acetyltransferase activity was detected for any of them. Thus, the *N*-acetyltransferase activity typically associated with GNAT enzymes is almost completely attenuated in the CurA AR-$GNAT_L$-$ACP_L$ chain initiation module.

To advance our understanding of $GNAT_L$ function and to identify active site residues, we determined the crystal structures of the excised CurA apo $GNAT_L$ (ligand-free) domain and of the corresponding $GNAT_L$ with added malonyl-CoA (table S2). $GNAT_L$ (CurA residues 219 to 439) has the GNAT superfamily fold, consisting of a central, mostly antiparallel β sheet flanked by α helices (Fig. 3A) (*11*, *12*), and is most similar to serotonin *N*-acetyltransferase (root mean square deviation = 1.9 Å for 160 Cα atoms) (*21*).

The crystal structures of CurA $GNAT_L$ provide key insights into the function of this distinctive member of a large and ubiquitous protein family. Two tunnels from opposite faces of the protein converge at a position corresponding to the active sites of homologous GNATs (Fig. 3B). Presumably, these tunnels are the binding sites for the PPant arms of the CoA and $ACP_L$ substrates. To distinguish the two tunnels, we soaked crystals of $GNAT_L$ with malonyl-CoA (table S2). New electron density was observed in only one tunnel: the CoA-binding tunnel (fig. S8). The location of this tunnel and the mode of CoA binding, in which the nucleotide lies in a surface cleft and the PPant arm extends into the tunnel, are consistent with structures of other members of the GNAT superfamily (*11*, *12*). In CurA $GNAT_L$, selectivity for CoA over $ACP_L$ is imparted by a 5′-diphosphate–binding loop (residues 327 to 332) and by $Arg^{387}$ recognition of the 3′-phosphate. Neither of these recognition features exists in FeeM, a GNAT superfamily member that uses an acyl-ACP donor substrate (*22*). Compared with the strong density for the CoA nucleotide, density for the PPant arm was weaker and indicative of multiple conformations, perhaps as a result of the presence of both the malonyl-CoA substrate and the acetyl-CoA decarboxylation product in the crystal. No new electron density was observed in the second tunnel, which we designate the $ACP_L$-binding tunnel. The side chain of conserved $Arg^{404}$ forms one wall of the putative $ACP_L$-binding tunnel (Fig. 3C and fig. S9), and a series of water molecules extending to the protein exterior forms the opposite wall. The designated ACP-binding tunnel overlays well with the acetyl-group acceptor site in other GNATs, is well-matched in length to the fully extended PPant arm of holo-$ACP_L$ (~15 Å), and likely forms the $ACP_L$ PPant arm–binding site (Fig. 3B). The two tunnels meet at conserved $Trp^{249}$, just as many other GNAT family members have their two binding sites separated by an aromatic residue (Fig. 3B and fig. S9).

We searched for potential catalytic residues for decarboxylation and found $His^{389}$ and $Thr^{355}$ at the junction of the two tunnels (fig. S9 and Fig. 3C). These residues are precisely positioned by hydrogen bonds of $His^{389}$ to $Tyr^{419}$ and of the $Thr^{355}$ backbone to the $Arg^{404}$ side chain. All four of these residues are invariant among $GNAT_L$-containing PKS loading modules (fig. S9). To test the role of $His^{389}$ and $Thr^{355}$, we assayed H389A, H389N, and T355V variant proteins for decarboxylase and acetyltransferase activity (table S1). Decarboxylation was severely impaired by substitutions at either site. Specifically, the $His^{389}$ and $Thr^{355}$ variants resulted in at least 100-fold reduction in $k_{cat}$ for decarboxylation of malonyl-CoA to acetyl-CoA and in relatively modest changes to $K_M$ values. In contrast, substitutions at $His^{389}$ and $Thr^{355}$ had only modest effects on acetyl-group transfer activity, demonstrating that these residues do not play a critical role in acetyl-group transfer.

Based on mutagenesis results and on modeling the PPant arms of acetyl-CoA and $ACP_L$ (Fig. 3C and fig. S8), $His^{389}$ and $Thr^{355}$ are proposed to stabilize an enolate anion intermediate of the decarboxylation reaction. We further propose that the isoenergetic transfer of an acetyl group from acetyl-CoA to $ACP_L$-SH (holo) is catalyzed by direct attack of the deprotonated thiolate of $ACP_L$ upon acetyl-CoA at the junction of the $GNAT_L$ CoA- and $ACP_L$-binding tunnels. The buried $Arg^{404}$ residue at the base of the $ACP_L$-binding tunnel may facilitate binding of the deprotonated thiol of the acceptor PPant arm of $ACP_L$. The N-terminal AR domain, which was stabilized by the PPant arm of $ACP_L$, may also assist in delivering (holo) $ACP_L$ to $GNAT_L$. AR is likely to have a common function in $GNAT_L$-containing modules based on its highly conserved sequence.

Based on the studies described above, the mechanism of CurA AR-$GNAT_L$-$ACP_L$ is proposed to involve a series of acyl-CoA–protein, protein-protein, and protein–PPant arm interactions (Fig. 4 and fig. S7) that mediate the distinctive bifunctional decarboxylase/*S*-acetyltransferase activity. It is likely that other presently unrecognized GNAT members will be found with unexpected biochemical properties or that previously identified proteins will be grouped within this large family. For example, the *eryM*-encoded methylmalonyl-CoA decarboxylase (*4*) has not been the subject of structural analysis, but comparative amino acid sequence analysis now predicts that it contains the GNAT scaffold.

An important outcome of the current work is the realization that $GNAT_L$-containing modules are not uncommon among previously characterized natural product biosynthetic gene clusters and are well-represented within bacterial genome sequences. This metabolic strategy thus represents an additional widely used chain initiation process for assembly of important biologically active small molecules. At a comparative level, the CurA $GNAT_L$ has a significantly slower *S*-acetyltransferase activity than the erythromycin PKS $AT_L$. However, *L. majuscula* has a relatively slow growth rate in the marine environment as well as in culture (i.e., doubling time of ~10 days) (*23*) and a correspondingly low production of curacin A per unit biomass as compared with yields of other microbial natural products [e.g., erythromycin via the DEBS aglycone intermediate by *Saccharopolyspora erythraea* (*24*)]. Thus, the curacin A PKS assembly line has evolved under environmental constraints and organismic needs that reflect its reduced efficiency.

The work described in this report provides clear evidence for an unprecedented bifunctional decarboxylase/*S*-acetyltransferase role for the CurA GNAT scaffold, which substantially broadens the chemical reaction inventory of this well-known protein superfamily. The method of PKS chain initiation described here enables malonyl-CoA to serve as the sole precursor to both initiate and extend the carbon chain of curacin A. Moreover, by virtue of the greater rate of acetate versus propionate transfer to $ACP_L$

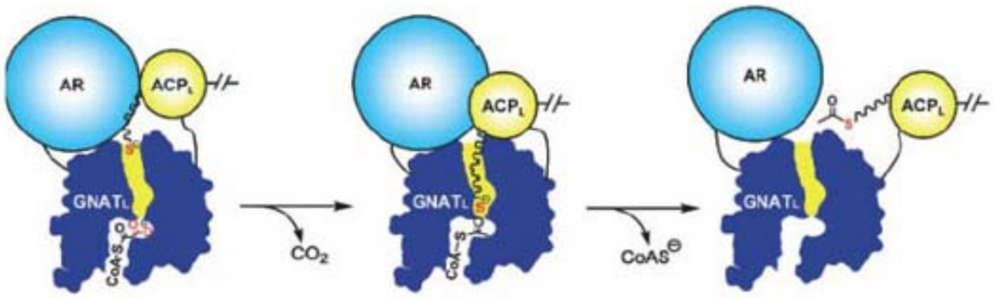


**Fig. 4.** Proposed mechanism of the CurA AR-$GNAT_L$-$ACP_L$ chain initiation module. Malonyl-CoA enters the CoA-binding tunnel (white tunnel) of the $GNAT_L$ domain (dark blue region) and $GNAT_L$ catalyzes decarboxylation to acetyl-CoA. The AR domain (light blue circle) directs the PPant arm of $ACP_L$ (yellow circle) into the ACP tunnel (yellow tunnel) for subsequent acetyl-group transfer via transthioesterification.

after decarboxylation, the $GNAT_L$ strategy for chain initiation provides an additional mechanism to ensure fidelity of curacin A chain length.


**References and Notes**

1. C. Bisang *et al.*, *Nature* **401**, 502 (1999).
2. Y. Xue, L. Zhao, H. W. Liu, D. H. Sherman, *Proc. Natl. Acad. Sci. U.S.A.* **95**, 12111 (1998).
3. J. Lau, D. E. Cane, C. Khosla, *Biochemistry* **39**, 10514 (2000).
4. Y. J. Hsieh, P. E. Kolattukudy, *J. Bacteriol.* **176**, 714 (1994).
5. P. Verdier-Pinard *et al.*, *Mol. Pharmacol.* **53**, 62 (1998).
6. Z. Chang *et al.*, *J. Nat. Prod.* **67**, 1356 (2004).
7. J. Piel, *Proc. Natl. Acad. Sci. U.S.A.* **99**, 14002 (2002).
8. J. Piel *et al.*, *Proc. Natl. Acad. Sci. U.S.A* **101**, 16222 (2004).
9. V. Simunovic *et al.*, *ChemBioChem* **7**, 1206 (2006).
10. L. P. Partida-Martinez, C. Hertweck, *ChemBioChem* **8**, 41 (2007).
11. F. Dyda, D. C. Klein, A. B. Hickman, *Annu. Rev. Biophys. Biomol. Struct.* **29**, 81 (2000).
12. M. W. Vetting *et al.*, *Arch. Biochem. Biophys.* **433**, 212 (2005).
13. C. Khosla, Y. Tang, A. Y. Chen, N. A. Schnarr, D. E. Cane, *Annu. Rev. Biochem.* **76**, 195 (2007).
14. S. Smith, A. Witkowski, A. K. Joshi, *Prog. Lipid Res.* **42**, 289 (2003).
15. T. Maier, S. Jenni, N. Ban, *Science* **311**, 1258 (2006).
16. Y. Tang, C.-Y. Kim, I. I. Mathews, D. E. Cane, C. Khosla, *Proc. Natl. Acad. Sci. U.S.A.* **103**, 11124 (2006).
17. L. E. N. Quadri *et al.*, *Biochemistry* **37**, 1585 (1998).
18. P. C. Dorrestein *et al.*, *Biochemistry* **45**, 12756 (2006).
19. Single-letter abbreviations for the amino acid residues are as follows: A, Ala; C, Cys; D, Asp; E, Glu; F, Phe; G, Gly; H, His; I, Ile; K, Lys; L, Leu; M, Met; N, Asn; P, Pro; Q, Gln; R, Arg; S, Ser; T, Thr; V, Val; W, Trp; and Y, Tyr.
20. R. H. Lambalot *et al.*, *Chem. Biol.* **3**, 923 (1996).
21. A. B. Hickman, D. C. Klein, F. Dyda, *Mol. Cell* **3**, 23 (1999).
22. R. M. Van Wagoner, J. Clardy, *Structure* **14**, 1425 (2006).
23. J. V. Rossi, M. A. Roberts, H. D. Yoo, W. H. Gerwick, *J. Appl. Phycol.* **9**, 195 (1997).
24. W. Minas, P. Brunker, P. T. Kallio, J. E. Bailey, *Biotechnol. Prog.* **14**, 561 (1998).



25. We thank M. D. Burkart for the expression plasmids for CoAA and PPant adenylyltransferase-dephosphoCoA kinase (PPAT-DPCK) and for the pantetheine analog bearing a terminal $NH_2$, R. G. Matthews for the analysis of kinetic data, and H. Liu for FTICR-MS technical assistance. This work was supported by NIH grants GM076477 (to D.H.S.) and DK42303 (to J.L.S.). L.G. is supported by an Eli Lilly graduate fellowship. The GM/CA Collaborative Access Team facility at the Advanced Photon Source (APS) is supported by the NIH National Institute of General Medical Sciences (GM) and National Cancer Institute (CA). Use of the APS was supported by the U.S. Department of Energy. We thank Curaçao and the Caribbean Research and Management of Biodiversity (CARMABI) research station for permission and assistance and in making collections of the curacin-producing cyanobacterium. Coordinates and structure factors have been deposited in the Protein Data Bank (www.rcsb.org) with accession codes 2REE and 2REF.


**Supporting Online Material**

www.sciencemag.org/cgi/content/full/318/5852/970/DC1
Materials and Methods
Figs. S1 to S9
Tables S1 to S4
References


6 August 2007; accepted 10 October 2007
10.1126/science.1148790


# A Bifunctional Bacterial Protein Links GDI Displacement to Rab1 Activation


**Matthias P. Machner[1] and Ralph R. Isberg[1,2]***



**Rab guanosine triphosphatases (GTPases) regulate vesicle trafficking in eukaryotic cells by reversibly associating with lipid membranes. Inactive Rab GTPases are maintained in the cytosol by binding to GDP-dissociation inhibitor (GDI). It is believed that specialized proteins are required to displace GDI from Rab GTPases before Rab activation by guanosine diphosphate–guanosine 5′-triphosphate (GDP-GTP) exchange factors (GEFs). Here, we found that SidM from *Legionella pneumophila* could act as both GEF and GDI-displacement factor (GDF) for Rab1. Rab1 released from GDI was inserted into liposomal membranes and was used as a substrate for SidM-mediated nucleotide exchange. During host cell infection, recruitment of Rab1 to *Legionella*-containing vacuoles depended on the GDF activity of SidM. Thus, GDF and GEF activity can be promoted by a single protein, and GDF activity can coordinate Rab1 recruitment from the GDI-bound pool.**


Vesicle trafficking between membrane-bound organelles in eukaryotic cells is regulated by the highly conserved Rab family of small guanosine triphosphatases (GTPases) (*1*). Rab proteins activated by guanosine diphosphate–guanosine 5′-triphosphate (GDP-GTP) exchange factors (GEFs) are associated with membranes by means of two hydrophobic prenyl groups covalently attached to their C terminus (*2*–*6*). Inactivated GDP-Rabs are extracted from membranes and maintained in the cytosol by GDP-dissociation inhibitor (GDI) (*7*–*11*). GDI binding prevents spontaneous GDP-GTP exchange on Rab proteins, and, therefore, their inappropriate activation (*12*).

Delivery of Rab GTPases to sites of activation involves their release from GDI, a process thought to require GDI-displacement factors (GDFs) (*13*, *14*). PRA-1 (the human homolog of Yip3) facilitates dissociation of endosomal Rab proteins from GDI and represents a protein with GDF activity discrete from a GEF (*15*). The identity and function of other proteins with GDF activity has remained elusive.

The human pathogen *Legionella pneumophila* establishes a replication vacuole within alveolar macrophages by recruiting material from the host cell endoplasmic reticulum (ER) (*16*–*18*). The bacterium translocates a large cohort of effector proteins into the host cell cytosol by means of its Dot-Icm protein type IV secretion system (T4SS) (*19*). Two of these translocated proteins, SidM (DrrA) and LidA, target mammalian Rab1 (*20*, *21*), the key regulator of endoplasmic reticulum (ER) to Golgi vesicle transport (*22*, *23*). SidM was necessary for the recruitment of Rab1 to the *Legionella*-containing vacuole (LCV) and had GEF activity specifically toward Rab1 (*20*, *21*). In vitro, surface-immobilized SidM and LidA could collaborate to tether ER-derived vesicles dependent on activated Rab1 (*20*), which suggests that both *L. pneumophila* effectors are crucial for intercepting Rab1-controlled secretory vesicle transport during infection.

Although recruitment of host cell Rab1 to the LCV required SidM (*20*, *21*), the Rab1-GEF activity of SidM was unlikely to be responsible for this capturing event, because Rab1 must be released from GDI before nucleotide exchange can occur. The *L. pneumophila* genome does not encode any obvious PRA1 homologs that could trigger GDI dissociation from Rab1. Thus, we tested whether SidM and/or LidA had GDF activity toward the Rab1-GDI complex. Because GDI preferentially binds prenylated Rab proteins (*24*), and bacteria lack the enzymatic machinery for Rab prenylation, *Saccharomyces cerevisiae* was used for the production of prenylated hexahistidine ($His_6$)-tagged human Rab1B (ScRab1) and FLAG-tagged human GDI2 (ScGDI2) (fig. S1). Double prenylation of purified ScRab1 was confirmed (*25*), and purified ScRab1 and ScGDI2 formed a heterodimeric 1:1 complex (fig. S2). When ScRab1-ScGDI2 was incubated with bead-immobilized recombinant SidM or LidA, ScRab1 only bound to SidM-coated beads but not to LidA-coated beads or uncoated control beads (Fig. 1A). ScGDI2 did not coprecipitate with SidM-bound ScRab1, which indicated that it was displaced from the complex. Nonprenylated GDI-free human Rab1 purified from *Escherichia coli* (EcRab1) was bound equally by SidM- and LidA-coated beads (Fig. 1A) (*20*). Thus, the Rab1-GEF SidM exhibited GDF activity and promoted dissociation of the ScRab1-ScGDI2 complex during ScRab1 binding, whereas LidA binding was restricted to the GDI-free form of Rab1.

Because SidM dissociated Rab1 from GDI (Fig. 1A), we tested whether SidM could catalyze exchange of GDP against radiolabeled [γ-$^{35}$S]GTP-γ-S [guanosine 5′-*O*-(3′-thiotriphosphate, a nonhydrolyzable GTP analog] in ScRab1 in complex with ScGDI2. In the absence of SidM, ScRab1-ScGDI2 showed only minimal sponta-


[1]Department of Molecular Biology and Microbiology, Tufts University School of Medicine, Boston, MA 02111, USA. [2]Howard Hughes Medical Institute, Tufts University School of Medicine, Boston, MA 02111, USA.

*To whom correspondence should be addressed. E-mail: ralph.isberg@tufts.edu

neous [γ-$^{35}$S]GTP uptake (Fig. 1B). In contrast, addition of SidM led to the rapid incorporation of [γ-$^{35}$S]GTP into ScRab1. However, the amount of [γ-$^{35}$S]GTP incorporated into ScRab1 in complex with ScGDI2 (Fig. 1B) was consistently lower than that observed for EcRab1 (Fig. 1C). Because active Rab GTPases associate with the membrane by means of their C-terminal prenyl groups in vivo (*5*, *6*, *14*, *26*–*28*), the lack of a lipid bilayer during the in vitro GDP–[γ-$^{35}$S]GTP–exchange studies (Fig. 1B) may explain the attenuated activation of prenylated ScRab1. Consistent with this, we found that SidM-promoted [γ-$^{35}$S]GTP incorporation into ScRab1 in the presence of phosphatidylcholine (PC) liposomes was more than four times that seen in the absence of lipid vesicles (Fig. 1D). Thus, ScRab1 activation by SidM was kinetically enhanced in the presence of a lipid bilayer, presumably because the bilayer provided a hydrophobic environment into which GDI-free ScRab1 could be incorporated by SidM.

Next, we performed vesicle floating experiments to monitor protein association with liposomes during the different stages of nucleotide exchange. Incubation of SidM with a molar excess of ScRab1-ScGDI2 revealed that accumulation of ScRab1 on PC vesicles occurred only in the presence of both SidM and GTP-γ-S (Fig. 1E). Without GTP-γ-S, only a fraction of ScRab1 was integrated into PC vesicles and remained bound by SidM, which showed that nucleotide exchange was required to allow release of membrane-bound ScRab1 by SidM before another ScRab1-ScGDI2 complex was targeted. When LidA was added to PC liposomes, the protein specifically interacted with vesicles enriched in GTP-γ-S-ScRab1 (Fig. 1F). Membrane-bound ScRab1 activated and released by SidM was thus available to bind downstream acceptors such as LidA. The SidM-mediated Rab1 activation process can therefore be divided into three stages: (i) GDI release from Rab1 accompanied by membrane insertion of SidM-bound Rab1, (ii) catalysis of nucleotide exchange in Rab1, and (iii) release of activated Rab1 by SidM to allow downstream ligand binding to GTP-Rab1. Alternatively, SidM could have indirectly accelerated the dissociation of ScGDI by catalyzing nucleotide exchange in ScRab1 while bound to ScGDI, thereby generating GTP-charged ScRab1 that is released by ScGDI.

The discovery of both GEF and GDF activity within the same polypeptide chain was surprising. Thus, we wanted to map the regions of SidM contributing to each of these activities. Purified SidM variants with N- or C-terminal truncations (Fig. 2A and fig. S3) were analyzed for their ability to interact with EcRab1. Deletions exceeding amino acids 1 to 316 at the N terminus or residues 545 to 647 at the C terminus disrupted binding of SidM variants to EcRab1 (Fig. 2B). In contrast, fragments containing amino acids 317 to 545 bound EcRab1 as efficiently as full-length SidM. Similar results were obtained in pull-down studies using EcRab1(S25N) (Fig. 2A), a GDP-locked mutant (*29*). Thus, the central region of SidM containing amino acids 317 to 545 was required for EcRab1 binding.

Similarly, we found that only SidM variants containing amino acid residues 317 to 545 associated with ScRab1 (Fig. 2C). ScGDI2 did not precipitate with ScRab1 on the beads and remained in the supernatant (Fig. 2C), consistent with its exclusion from the complex of ScRab1 bound to SidM variants.

To identify the GEF domain, SidM variants with N- or C-terminal truncations were analyzed for their ability to mediate incorporation of [γ-$^{35}$S]GTP into EcRab1. Only SidM fragments containing the entire region required for Rab1 binding (residues 317 to 545) showed GEF activity equivalent to full-length SidM (Fig. 2D). Likewise, only those SidM variants that had GEF activity toward EcRab1 catalyzed GDP–[γ-$^{35}$S]GTP exchange when incubated with ScRab1-ScGDI2, with efficiencies comparable to full-length SidM (Fig. 2E). Thus, GDI displacement, Rab1 binding, and nucleotide exchange activity required the same central region within SidM (Fig. 2A).

We also characterized a SidM variant consisting of only amino acid residues 317 to 545. Purified recombinant SidM(317–545) efficiently bound to immobilized nonprenylated glutathione *S*-transferase (GST)–tagged EcRab1 (Fig. 3A). Similarly, SidM(317–545) was capable of dissociating ScGDI2 from ScRab1 and displayed ScRab1-binding activity comparable to that of full-length SidM (Fig. 3B). Furthermore, SidM(317–545) efficiently catalyzed GDP–[γ-$^{35}$S]GTP exchange in both EcRab1 (Fig. 3C) and ScRab1-ScGDI2 (Fig. 3D). Thus, the central region of SidM comprising amino acid residues 317 to 545 was sufficient to mediate the activities of GDI displacement, Rab1 binding, and nucleotide exchange.

Both SidM and LidA efficiently interacted with Rab1 and localized to the cytoplasmic surface of the LCV (*20*, *30*). Nevertheless, only SidM was required for the recruitment of endogenous Rab1 to LCVs (fig. S4) (*20*, *21*). Because SidM dissociated the ScRab1-ScGDI2 complex in vitro (Fig. 1A), we asked whether GDF activity allowed SidM to target the cytoplasmic pool of GDI-bound host cell Rab1, and whether the lack of GDF activity in LidA prevented this effector from recruiting Rab1 complexed by GDI. Thus, we tested whether the requirement for SidM

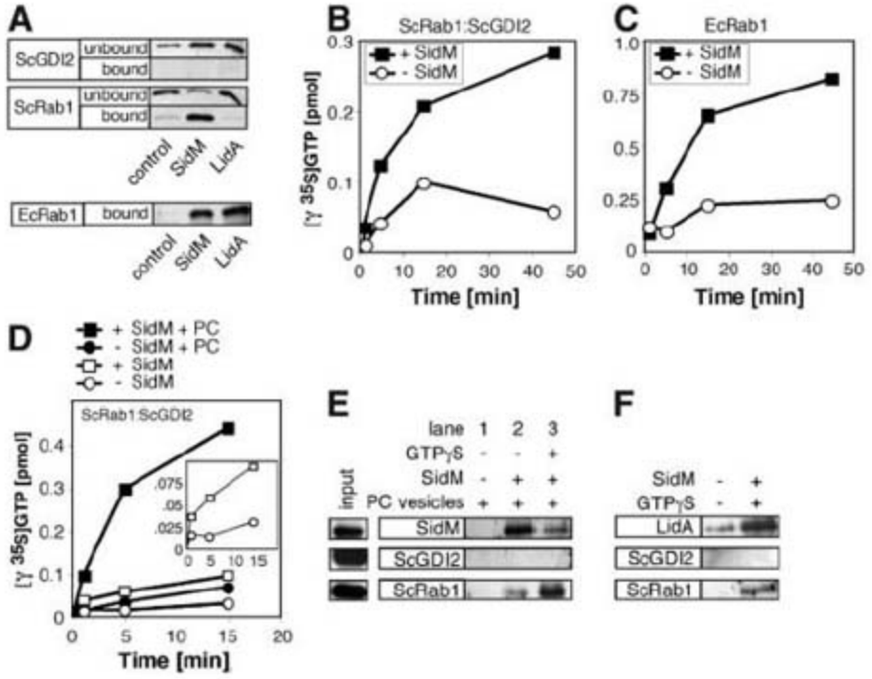


**Fig. 1.** Rab1 activation by SidM involves GDI displacement and membrane insertion of ScRab1. **(A)** ScRab1 pull-down assay shows activity by SidM but not LidA. Bead-immobilized SidM or LidA or uncoated control beads were incubated with ScRab1-ScGDI2 (top panel) or EcRab1 (bottom panel), and proteins on the beads (bound) or in the supernatant (unbound) were detected by immunoblot analysis using antibody against GDI2 or Rab1B. **(B** and **C)** For a [γ-$^{35}$S]GTP incorporation experiment, we used 2 pmol SidM and either 40 pmol ScRab1-ScGDI2 (B) or 20 pmol EcRab1 (C). [γ-$^{35}$S]GTP incorporation was detected as the increase in radioactivity over time. **(D)** [γ-$^{35}$S]GTP incorporation by SidM (1.6 pmol) into a molar excess of ScRab1-ScGDI2 (10 pmol) is accelerated in the presence of phosphatidylcholine (PC) liposomes. The curves of nucleotide-exchange studies in the absence of PC vesicles are shown with another scale in the inset. **(E)** Protein association with PC vesicles during nucleotide exchange. ScRab1-ScGDI2 was incubated with PC liposomes in the presence or absence of SidM or GTP-γ-S (as indicated). Liposomes were separated from soluble proteins by sucrose-gradient centrifugation, and proteins in the vesicle fraction were detected by immunoblot analysis. **(F)** Analysis of LidA association with PC vesicles previously incubated with ScRab1-ScGDI2 in the presence or absence of SidM and GTP-γ-S (as indicated). (A) to (F) represent at least two repetitions.

during Rab1 recruitment to LCVs could be bypassed by LidA in the presence of Rab1(D44N) (fig. S5), a Rab1 mutant in which Asn (N) replaces Arg (D) at residue 44 and that shares all features described for wild-type Rab1 but that is unable to bind GDI (*31*). The D44N substitution in Rab1 did not interfere with LidA binding, as GST-Rab1(D44N) and GST-Rab1 purified from *E. coli* were bound equally by recombinant LidA (Fig. 4A). When COS-1 cells producing green fluorescent protein (GFP)-tagged Rab1(D44N) were infected with *L. pneumophila* (Fig. 4, B and C), GFP-Rab1(D44N) was efficiently recruited to LCVs containing wild-type (44 ± 8%) but not the type IV secretion–defective (T4SS$^-$) strain Lp03 (12 ± 3%), which indicated that GFP-Rab1(D44N) recruitment was dependent on a functional Dot-Icm transporter. *L. pneumophila ΔsidM*, which was defective for the recruitment of wild-type Rab1 (*20*, *21*), showed robust colocalization with GFP-Rab1(D44N) (51 ± 10%). This SidM-independent recruitment of GFP-Rab1(D44N) was mediated by LidA, as deletion of both *sidM* and *lidA* in *L. pneumophila* abrogated recruitment of GFP-Rab1(D44N) to LCVs (17 ± 7%). Thus, LidA binding in vivo was restricted to GDI-free Rab1, which explains why release of GDI and recruitment of Rab1 from the cytoplasmic pool required the GDF activity of SidM. The inability of LidA to extract Rab1 from GDI indicated a hierarchy between these two *L. pneumophila* effectors, presumably to ensure that Rab1 recruited to the LCV was activated by SidM before its association with LidA, which assists in accumulating activated

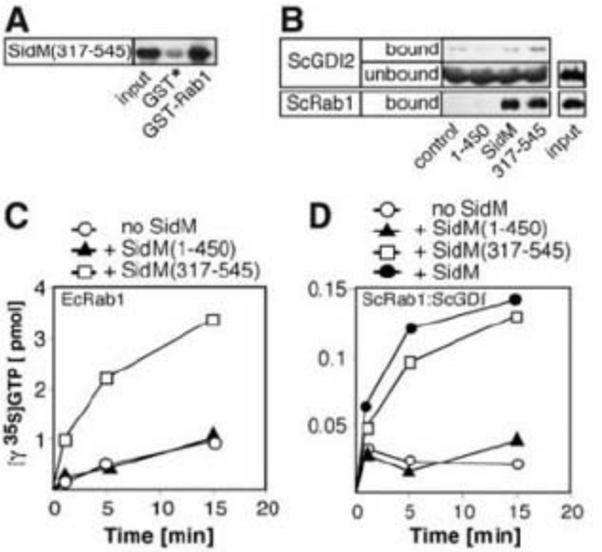


**Fig. 3.** The central region of SidM is sufficient for GDI displacement, Rab1 binding, and GEF activity. (**A**) Immunoblot showing precipitation of SidM(317–545) by GST-Rab1–coated beads but not by GST-bound control beads. Lane marked with an asterisk shows a protein of 25 kD (corresponding to the bait protein GST) cross-reacting with the antibody. (**B**) ScGDI2 displacement and ScRab1 binding by SidM (317–545). ScRab1-ScGDI2 was incubated with bead-immobilized SidM variants (numbers indicate amino acid residues) or uncoated control beads, and proteins on the beads (bound) or in the supernatant (unbound) were detected by immunoblot analysis. (**C** and **D**) SidM(317–545) has GEF activity. EcRab1 (10 pmol) (C) or ScRab1-ScGDI2 (12.5 pmol) (D) were incubated with SidM variants (3 pmol), and uptake of [γ-$^{35}$S]GTP by Rab1 protein was determined over time. All figure parts represent at least two repetitions.

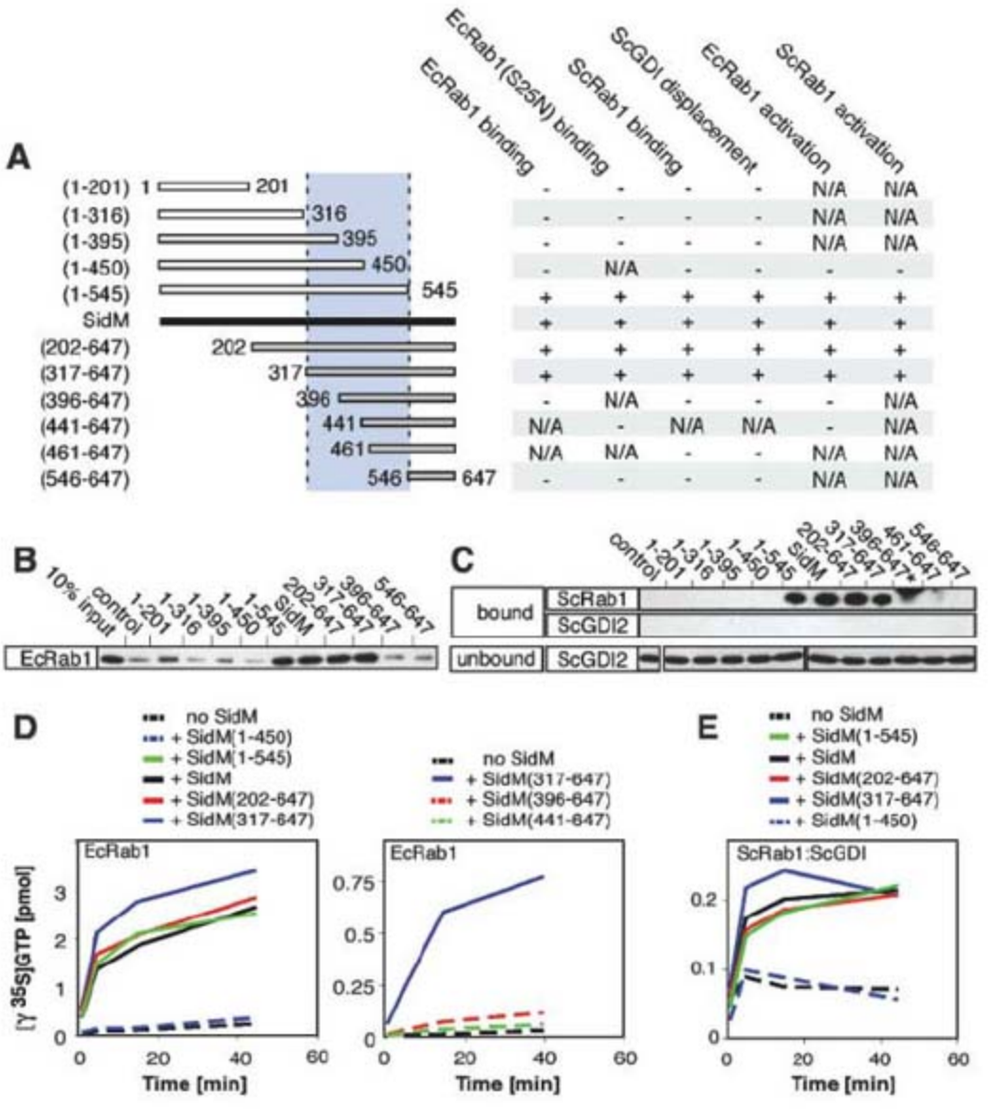


**Fig. 2.** Domain mapping of SidM. (**A**) (Left) Schematic representation of SidM variants used in this study (numbers indicate amino acid residues). (Right) Summary of the experiments shown below in (B to E) indicating positive (+) or negative (–) outcomes. The central region between amino acid residues 317 and 545 (shaded blue) was found to be essential for all in vitro activities of SidM. (**B** and **C**) Pull-down of EcRab1 (B) or ScRab1-ScGDI2 (C) by bead-immobilized SidM variants. Proteins bound to the beads or unbound in the supernatant were detected by immunoblot analysis (using FLAG-specific or Rab1B-specific antibody). The lane marked with an asterisk shows a 28.1-kD protein cross-reacting with an antibody [corresponding to the bait protein SidM(396–647)]. (**D** and **E**) [γ-$^{35}$S]GTP incorporation into (D) EcRab1 [(left) 20 pmol, (right) 10 pmol] or (E) ScRab1-ScGDI2 (10 pmol) by SidM variants (2 pmol). Rab1 proteins and SidM variants were incubated, and [γ-$^{35}$S]GTP uptake by Rab1 proteins was determined as the increase in radioactivity over time. (B) to (E) represent at least two repetitions.

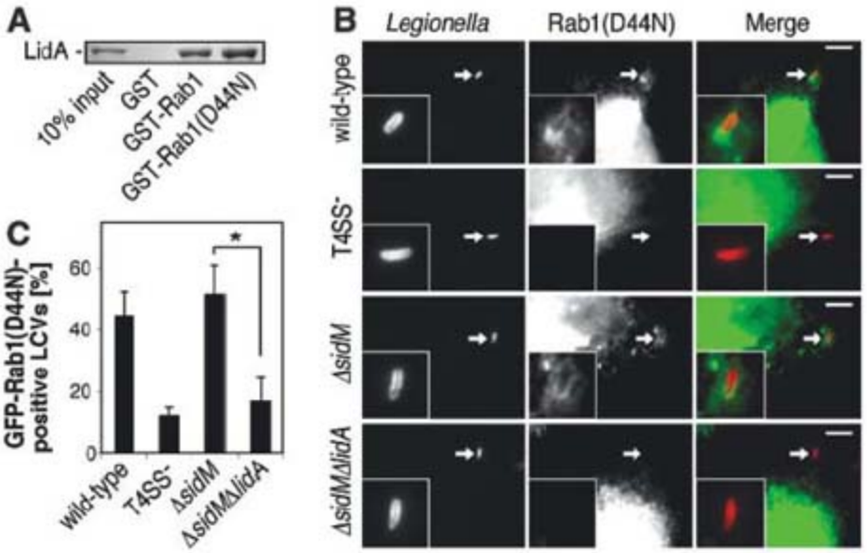


**Fig. 4.** LidA can recruit GDI-free Rab1(D44N) in the absence of SidM. **(A)** LidA can bind Rab1(D44N). Binding of LidA to bead-immobilized GST-Rab1 or GST-Rab1(D44N) but not GST was determined by SDS–polyacrylamide electrophoresis and Coomassie staining. The figure represents two repetitions. **(B)** Recruitment of GFP-Rab1(D44N) during *L. pneumophila* infection. Transiently transfected COS-1 cells producing GFP-Rab1(D44N) were infected for 30 min as indicated. Cells were fixed and stained for intracellular bacteria (left). (Middle) GFP-Rab1(D44N), (right) merged images with bacteria (red) and GFP-Rab1(D44N) (green). Arrows indicate the location of the LCV magnified threefold in the insets of each panel. Scale bar, 5 μm. Contrast was equally changed by linear adjustment. **(C)** Quantification of (B) showing that recruitment of GFP-Rab1(D44N) in the absence of SidM requires LidA. The graph represents pooled data (mean ± SD) from four independent experiments. $*P = 0.0001$ (Student's $t$ test).

Rab1 about the LCV. Indeed, vacuoles containing *L. pneumophila* Δ*lidA* showed delayed Rab1 recruitment compared with wild-type LCVs (*20*).

SidM is a protein that has both GEF and GDF activity toward a Rab GTPase. This unique ability of SidM to link GDI displacement to Rab1 activation explains how the intravacuolar pathogen *L. pneumophila* can efficiently exploit host cell Rab1 even in the presence of GDI that naturally interferes with this process. The discovery of both GEF and GDF activity within SidM raises the intriguing possibility that eukaryotic GEF proteins may possess similar abilities to mediate membrane delivery and activation of Rab GTPases during intracellular vesicle transport.


**References and Notes**

1. M. Zerial, H. McBride, *Nat. Rev. Mol. Cell Biol.* **2**, 107 (2001).
2. C. C. Farnsworth *et al.*, *Proc. Natl. Acad. Sci. U.S.A.* **88**, 6196 (1991).
3. P. Chavrier, R. G. Parton, H. P. Hauri, K. Simons, M. Zerial, *Cell* **62**, 317 (1990).
4. R. Khosravi-Far *et al.*, *Proc. Natl. Acad. Sci. U.S.A.* **88**, 6264 (1991).
5. M. Peter, P. Chavrier, E. A. Nigg, M. Zerial, *J. Cell Sci.* **102**, 857 (1992).
6. B. T. Kinsella, W. A. Maltese, *J. Biol. Chem.* **267**, 3940 (1992).
7. T. Sasaki *et al.*, *J. Biol. Chem.* **265**, 2333 (1990).
8. T. Soldati, M. A. Riederer, S. R. Pfeffer, *Mol. Biol. Cell* **4**, 425 (1993).
9. O. Ullrich *et al.*, *J. Biol. Chem.* **268**, 18143 (1993).
10. M. D. Garrett, J. E. Zahner, C. M. Cheney, P. J. Novick, *EMBO J.* **13**, 1718 (1994).
11. S. Araki, A. Kikuchi, Y. Hata, M. Isomura, Y. Takai, *J. Biol. Chem.* **265**, 13007 (1990).
12. S. R. Pfeffer, A. B. Dirac-Svejstrup, T. Soldati, *J. Biol. Chem.* **270**, 17057 (1995).
13. A. B. Dirac-Svejstrup, T. Sumizawa, S. R. Pfeffer, *EMBO J.* **16**, 465 (1997).
14. T. Soldati, A. D. Shapiro, A. B. Svejstrup, S. R. Pfeffer, *Nature* **369**, 76 (1994).
15. U. Sivars, D. Aivazian, S. R. Pfeffer, *Nature* **425**, 856 (2003).
16. M. A. Horwitz, *J. Exp. Med.* **158**, 1319 (1983).
17. M. S. Swanson, R. R. Isberg, *Infect. Immun.* **63**, 3609 (1995).
18. L. G. Tilney, O. S. Harb, P. S. Connelly, C. G. Robinson, C. R. Roy, *J. Cell Sci.* **114**, 4637 (2001).
19. S. Ninio, C. R. Roy, *Trends Microbiol.* **15**, 372 (2007).
20. M. P. Machner, R. R. Isberg, *Dev. Cell* **11**, 47 (2006).
21. T. Murata *et al.*, *Nat. Cell Biol.* **8**, 971 (2006).
22. H. Plutner *et al.*, *J. Cell Biol.* **115**, 31 (1991).
23. E. J. Tisdale, J. R. Bourne, R. Khosravi-Far, C. J. Der, W. E. Balch, *J. Cell Biol.* **119**, 749 (1992).
24. O. Pylypenko *et al.*, *EMBO J.* **25**, 13 (2006).
25. Materials and methods are available as supporting material on *Science* Online.
26. S. Araki, K. Kaibuchi, T. Sasaki, Y. Hata, Y. Takai, *Mol. Cell. Biol.* **11**, 1438 (1991).
27. T. Musha, M. Kawata, Y. Takai, *J. Biol. Chem.* **267**, 9821 (1992).
28. P. Chavrier *et al.*, *Nature* **353**, 769 (1991).
29. C. Nuoffer, H. W. Davidson, J. Matteson, J. Meinkoth, W. E. Balch, *J. Cell Biol.* **125**, 225 (1994).
30. G. M. Conover, I. Derre, J. P. Vogel, R. R. Isberg, *Mol. Microbiol.* **48**, 305 (2003).
31. A. L. Wilson, R. A. Erdman, W. A. Maltese, *J. Biol. Chem.* **271**, 10932 (1996).


32. We thank C. Kumamoto, L. Feig, and D. Raychaudhuri for reviewing the manuscript; M. Barzik, V. Auerbuch, M. Bergman, E. Creasey, K.-L. Sheahan, Z. Li, T. O'Connor, A. Ensminger, M. Heidtman, and S. Mohammadi for critical comments and scientific advice; and A. Wandinger-Ness for providing reagents. This work was supported by the Howard Hughes Medical Institute and by National Institute of Diabetes and Digestive and Kidney Diseases, NIH, program grant P30DK34928. R.R.I is a Howard Hughes Medical Institute Investigator.


**Supporting Online Material**

www.sciencemag.org/cgi/content/full/1149121/DC1
Materials and Methods
Figs. S1 to S5
Table S1
References


13 August 2007; accepted 9 October 2007
Published online 18 October 2007;
10.1126/science.1149121
Include this information when citing this paper.


# Rheb Activates mTOR by Antagonizing Its Endogenous Inhibitor, FKBP38


**Xiaochun Bai,[1,3] Dongzhu Ma,[1] Anling Liu,[1] Xiaoyun Shen,[1] Qiming J. Wang,[1] Yongjian Liu,[2] Yu Jiang[1]***



The mammalian target of rapamycin, mTOR, is a central regulator of cell growth. Its activity is regulated by Rheb, a Ras-like small guanosine triphosphatase (GTPase), in response to growth factor stimulation and nutrient availability. We show that Rheb regulates mTOR through FKBP38, a member of the FK506-binding protein (FKBP) family that is structurally related to FKBP12. FKBP38 binds to mTOR and inhibits its activity in a manner similar to that of the FKBP12-rapamycin complex. Rheb interacts directly with FKBP38 and prevents its association with mTOR in a guanosine 5′-triphosphate (GTP)–dependent manner. Our findings suggest that FKBP38 is an endogenous inhibitor of mTOR, whose inhibitory activity is antagonized by Rheb in response to growth factor stimulation and nutrient availability.


The mammalian target of rapamycin, mTOR, is a serine-threonine protein kinase that controls a wide spectrum of cellular events in response to various environmental cues, including stimulation by growth factors, changes in nutrient conditions, and fluctuations in energy levels (*1*, *2*). mTOR elicits its pleiotropic function in the context of two distinct multiprotein complexes termed mTOR complex 1 (mTORC1) and mTOR complex 2 (mTORC2) (*3*). Rapamycin, in complex with FKBP12 (an FK506-binding protein), specifically interferes with mTORC1 function, and consequently, inhibits cell growth (*4*, *5*).

The major upstream regulators of mTORC1 are the TSC1 and TSC2 tumor suppressors. The two TSC proteins form a complex that displays

a guanosine triphosphatase (GTPase)–activating protein (GAP) activity toward Rheb, a Ras-like small GTPase (*6*–*8*). Like other small GTPases, the activity of Rheb is dictated by its guanine nucleotide binding states: it is active in its GTP-bound form and inactive in the guanosine diphosphate (GDP)–bound form (*9*). The TSC1-TSC2 complex stimulates the intrinsic GTPase activity of Rheb and, thus, negatively regulates Rheb function. Conversely, inactivation of the TSC1-TSC2 complex results in accumulation of GTP-bound Rheb, which activates mTORC1 (*10*, *11*).

FKBP38 (also known as FKBP8) belongs to the peptidyl prolyl cis/trans isomerase (PPIase) family of FKBPs. It contains a region, referred to as the FKBP-C domain, that is highly related to FKBP12 (*12*). FKBP38 also has a transmembrane domain at the very C terminus, which is unique among all the FKBP proteins and is required for targeting it to mitochondria (*13*, *14*). We isolated FKBP38 in a yeast two-hybrid screen designated to identify Rheb-interacting proteins (fig. S1) (*15*). The potential interaction between Rheb and FKBP38 in mammalian cells was confirmed by coimmunoprecipitation of endogenous Rheb with FKBP38 from human embryonic kidney (HEK293) cell lysates (Fig. 1A). Furthermore, purified bacterially expressed recombinant Rheb and FKBP38 interacted with each other in an in vitro binding assay (Fig. 1B). The interaction of Rheb with FKBP38 appeared to be dependent on its nucleotide binding states, because Rheb loaded with GTP-γ-S, a nonhydrolyzable GTP analog, guanosine 5′-*O*-(3′-thiotriphosphate), exhibited much higher binding affinity toward FKBP38 than did GDP-bound or untreated Rheb (Fig. 1C).

In cells overexpressing FKBP38, insulin-stimulated phosphorylation was largely prevented for several downstream targets of mTORC1, including ribosomal protein S6 kinase (S6K), ribosomal S6 protein (S6) and the eukaryotic initiation factor 4E–binding protein 1 (4E-BP1) (Fig. 2A and fig. S2). In contrast, FKBP38 overproduction had no detectable effect on phosphorylation of protein kinase Akt (Fig. 2A). The inhibitory effect of FKBP38 on mTORC1 activity was reversed if Rheb was overexpressed, which suggested that Rheb antagonizes FKBP38. Similar effects of FKBP38 overproduction on mTORC1 activity were observed when cells deprived of amino acids were exposed to amino acids (Fig. 2B and fig. S2).

In cells transiently transfected with FKBP38-specific small interfering RNA (siRNA) oligonucleotides, the amounts of FKBP38 were reduced by ~80% (Fig. 2C). Accompanying the decreased abundance of FKBP38 was an increase in mTOR-dependent phosphorylation in both S6K and 4E-BP1 but not of extracellular signal–regulated kinase (ERK) 1 or 2 (Fig. 2C). This effect on mTORC1 activity appeared to be specific, because a different FKBP38-specific siRNA oligonucleotide produced a similar effect (fig. S3). In addition to the enhancement in mTORC1 activity under normal growth conditions, decreased abundance of FKBP38 also reduced the rate of mTORC1 inactivation in response to serum or amino acid deprivation (fig. S4), which indicated that the affected cells were less sensitive to growth factor or nutrient limitation. The partial response of mTORC1 to changes in serum and nutrient conditions may result from the remaining FKBP38 in the cells. Alternatively, it may indicate the existence of FKBP38-independent mechanisms that regulate mTORC1. Collective-

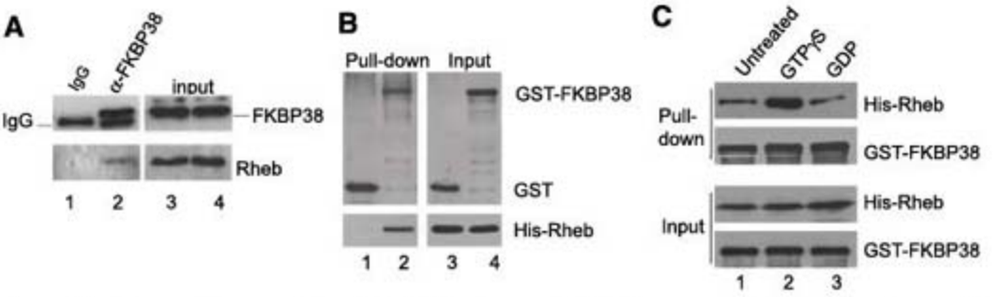


**Fig. 1.** GTP-dependent interaction of Rheb with FKBP38. (**A**) Coimmunoprecipitation of FKBP38 with Rheb. Lysates from HEK293 cells were immunoprecipitated with antibody to FKBP38 (lanes 2 and 4) or control IgG (lanes 1 and 3). FKBP38 (top) and Rheb (bottom) in the precipitates were detected by immunoblotting. (**B**) Direct binding between Rheb and FKBP38 in vitro. Histidine-tagged Rheb (His-Rheb) was incubated with glutathione *S*-transferase (GST) or GST-tagged FKBP38 (GST-FKP38) followed by precipitation with glutathione beads. The precipitates were immunoblotted for His-Rheb (bottom), GST, and GST-FKBP38 (top). (**C**) GTP-dependent binding of Rheb with FKBP38. Untreated His-Rheb (lane 1) GTP-γ-S–loaded His-Rheb (lane 2), and GDP-loaded His-Rheb (lane 3) were all incubated with GST-FKBP38 followed by precipitation with glutathione beads. The precipitates were immunoblotted for GST-FKBP38 and His-Rheb.

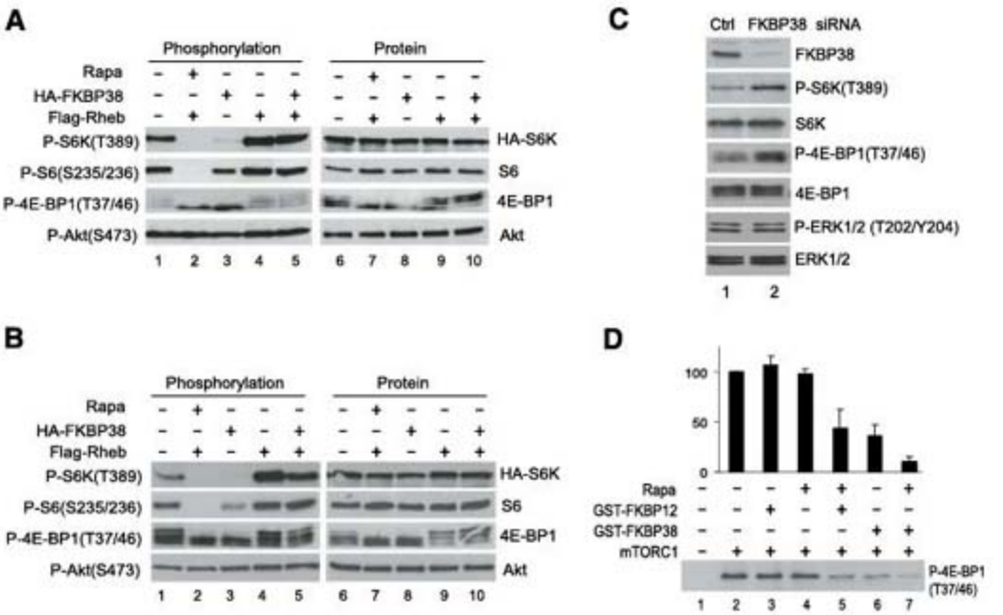


**Fig. 2.** Inhibition of mTORC1 activity by FKBP38. HEK293 cells were transfected with hemagglutinin (HA)–tagged S6K along with (+) or without (–) Flag-tagged Rheb and HA-tagged FKBP38 as indicated. (**A**) Effect of FKBP38 on insulin-stimulated phosphorylation. Cells were collected after being deprived of serum (0.5%) for 16 hours and treated with 100 nM insulin for 30 min. (**B**) Effect of FKBP38 on amino acid–stimulated phosphorylation. Cells were collected after being deprived of amino acids for 1 hour and then incubated with amino acids for 30 min. Rapamycin (20 nM) was added to the indicated samples 30 min before the addition of insulin or amino acids. (**C**) Effect of FKBP38 depletion on mTORC1 activity. HEK293 cells were transfected with FKBP38-specific (lane 2) or control (lane 1) siRNA. Cells were harvested and lysed 60 hours after the transfection. The indicated proteins (right panels) and their phosphorylation (left panels) were detected by immunoblotting. (**D**) In vitro kinase assay of mTORC1. Endogenously expressed mTOR was immunopurified from HEK293 cell lysates with antibody to mTOR and assayed for activity toward recombinant GST–4E-BP1 in the presence (+) or absence (–) of the indicated agents. Phosphorylation was detected by immunoblotting using antibody to phospho–4E-BP1(T37/46), and quantified by densitometry from three independent experiments (top).

[1]Department of Pharmacology, University of Pittsburgh School of Medicine, E1357 Biomedical Science Tower, 200 Lothrop Street, Pittsburgh, PA 15213, USA. [2]Department of Neurology, University of Pittsburgh School of Medicine, Pittsburgh, PA 15213, USA. [3]Department of Cell Biology, School of Basic Medical Science, Southern Medical University, Guangzhou 510515, China.

*To whom correspondence should be addressed. E-mail: jiang@server.pharm.pitt.edu

ly, the above findings demonstrate that FKBP38 is a negative regulator of mTORC1.

FKBP38 inhibited the kinase activity of mTOR in a dose-dependent manner in vitro (Fig. 2D and fig. S5), and the extent of maximal inhibition was similar to that induced by the FKBP12-rapamycin complex (Fig. 2D). Although rapamycin alone had no effect on kinase activity of mTOR, it augmented the inhibitory effect of FKBP38, which suggests that rapamycin may interact with FKBP38 and may increase its inhibitory activity toward mTORC1.

Coimmunoprecipitation revealed that FKBP38 associated with the components of mTORC1, including mTOR itself, the GβL protein and raptor, but not rictor, a unique component of mTORC2 (Fig. 3A), which suggests that FKBP38 targets mTORC1 but not mTORC2. In addition, the association of FKBP38 with mTORC1 appeared to be regulated by nutrient conditions, because the association was increased in cells deprived of amino acids.

Rheb associates with mTOR through a region (amino acids 1967 to 2191) that overlaps with the FKBP12-rapamycin binding (FRB) domain (amino acids 2015 to 2114) (*16*). We tested the possibility that the association was mediated through FKBP38. Indeed, a recombinant peptide containing amino acids 1967 to 2191 of mTOR interacted directly with FKBP38 in an in vitro assay (Fig. 3B). On the other hand, no direct interaction was detected between Rheb and this FKBP38 binding (FKB) domain of mTOR (fig. S6). Deletion analysis of FKBP38 further revealed that its FKBP-C domain, a region highly similar to FKBP12, was sufficient for mTOR binding, which suggested that FKBP38 may bind to mTOR in a manner similar to that of the FKBP12-rapamycin complex (fig. S7B). In support of this, we found that the FKBP12-rapamycin complex competed with FKBP38 for mTOR binding in vitro (fig. S8), and rapamycin reduced the association of FKBP38 with mTOR in cells (Fig. 3C).

The interaction of FKBP38 with the FKB domain of mTOR appeared to be regulated by Rheb in a GTP-dependent manner, because the interaction was unaffected by the presence of GDP-bound Rheb but was abolished by the presence of the same amount of GTP-bound Rheb (Fig. 3D). The dissociation of FKBP38 from the FKB domain of mTOR was also accompanied by its binding to Rheb, which suggested that the interaction with Rheb interfered with FKBP38 binding to mTOR.

Because Rheb activity is regulated by growth factor and nutrient conditions (*6*, *17*, *18*), we examined whether Rheb controlled the interaction between endogenous FKBP38 and mTOR in a growth factor– and nutrient-dependent manner. FKBP38 interacted with mTOR in cells deprived of amino acids, and the interaction was reduced when amino acids were restored (Fig. 4A). Overexpression of wild-type Rheb also reduced the interaction of FKBP38 with mTOR in cells deprived of amino acids, and the interaction was further diminished when amino acids were restored. Accompanying the amino acid–induced decrease in the interaction of FKBP38 with mTOR was an increase in the binding of Rheb with FKBP38, which suggested that Rheb prevented FKBP38 from binding to mTOR in response to amino acid availability.

Rheb mutants, including an active allele, Q64L, in which leucine replaces glutamine at residue 64, and two inactive alleles, S20N and D60K (in which asparagine replaces serine at residue 20 and lysine is substituted for aspartic acid at residue 60), are defective for nucleotide binding, which renders the mutants largely insensitive to the GAP activity of the TSC1/TSC2 complex (*19*, *20*). In cells expressing the Q64L mutant, the interaction of FKBP38 with mTOR was barely detectable, regardless of the availability

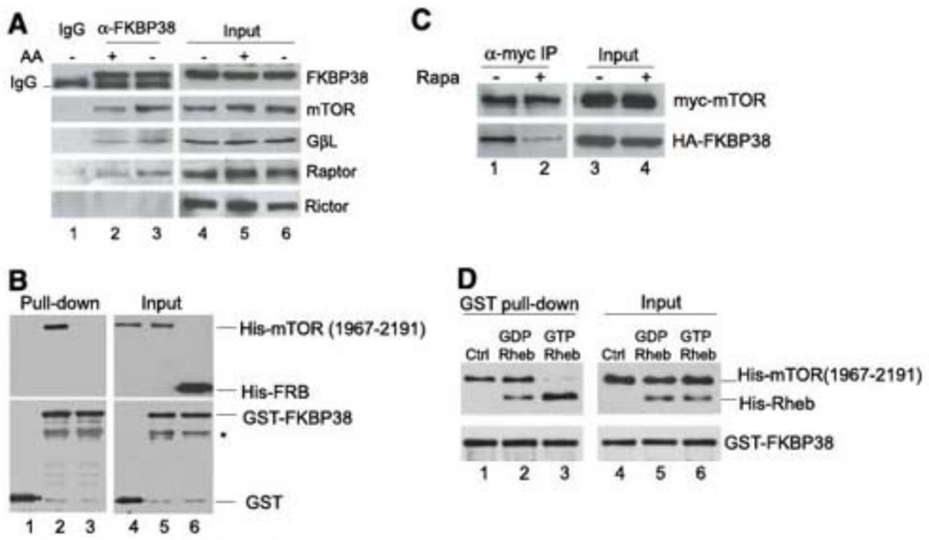


**Fig. 3.** Control of the interaction between FKBP38 and mTOR by Rheb. (**A**) Association of FKBP38 with mTORC1. HEK293 cells were deprived of amino acids for 1 hour and then incubated with amino acids for 30 min. Lysates were precipitated with antibody to FKBP38 or control IgG, and precipitates were blotted for the components of mTORC1 and mTORC2. (**B**) The FKBP38 binding domain in mTOR. Recombinant His-mTOR(1967–2191) or His-FRB domain of mTOR was incubated with GST or GST-FKBP38 followed by precipitation with glutathione beads. The precipitates were immunoblotted for GST (bottom, lane 1), GST-FKBP38 (bottom, lanes 2 and 3), His-mTOR (1967–2191) and His-FRB (top, lanes 1 to 3). Asterisk denotes a breakdown product of FKBP38. (**C**) Effect of rapamycin on the association of FKBP38 with mTOR. HEK293 cells expressing both myc-mTOR and HA-FKBP38 were treated with 20 nM rapamycin (lanes 2 and 4) or drug vehicle (lanes 1 and 3) for 1 hour. Lysates were precipitated with antibody to myc epitope. HA-FKBP38 and myc-mTOR in the precipitates were detected by immunoblotting. (**D**) Effect of Rheb on the interaction of FKBP38 with mTOR. Recombinant His-mTOR (1967–2191) and GST-FKBP38 were incubated together in the absence (lane 4) or presence of GDP-loaded His-Rheb (lane 5) or GTP-loaded His-Rheb (lane 6), followed by precipitation with glutathione beads. The precipitates were immunoblotted for GST-FKBP38 (bottom), His-mTOR(1967–2191) (top, top bands), and His-Rheb (top, lower bands).

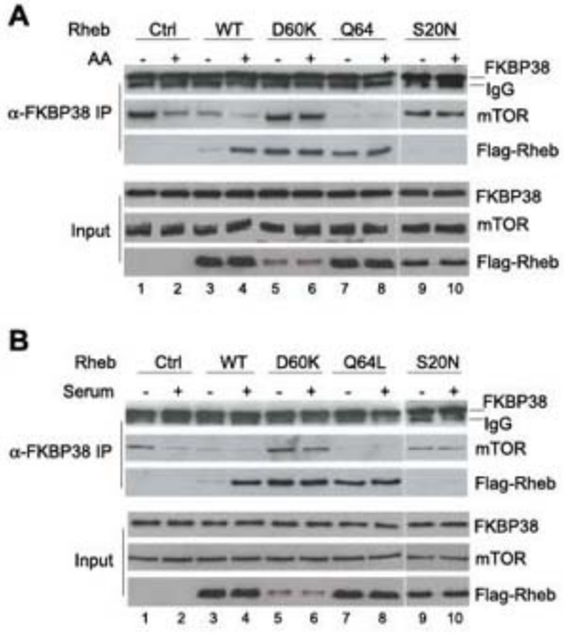


**Fig. 4.** Controlling interaction of FKBP38 with mTOR by Rheb in response to serum stimulation and nutrient availability. HEK293 cells were transfected with control vector or the indicated Rheb mutants and incubated for 24 hours. (**A**) Effect of amino acid conditions on the interaction of FKBP38 with mTOR. Cells were deprived of amino acids (AA) for 1 hour (–) followed by readdition of amino acids for 30 min (+). (**B**) Effect of serum conditions on the interaction of FKBP38 with mTOR. Cells were serum deprived (0.5% serum) for 16 hours, followed by treatment with 20% serum for 30 min (+) or no treatment (–). Lysates (input) were precipitated with antibody to FKBP38. The presence of endogenous FKBP38, mTOR, and ectopically expressed Rheb in the precipitates was detected by immunoblotting.

of amino acids, whereas the interaction of the expressed Rheb mutant with FKBP38 was strong (Fig. 4A and fig. S9). Despite this, the latter interaction was partially sensitive to amino acid starvation, consistent with a previous finding that the Q64L mutant retains a limited response to the GAP activity of the TSC1/TSC2 complex (*20*). In contrast, in cells expressing the S20N mutant, little Rheb was bound to FKBP38, and the interaction of FKBP38 with mTOR was strong and largely insensitive to changes in amino acid conditions. These observations indicate that these Rheb mutants block the amino acid–dependent regulation of the interaction between FKBP38 and mTOR, which suggests that amino acid conditions control the interaction of FKBP38 with mTOR through Rheb.

The effect of D60K on the interaction of FKBP38 with mTOR was similar to that of S20N. However, despite its failure to bind nucleotide and a low expression level (*19*), the D60K mutant interacted with FKBP38 more strongly than did wild-type Rheb, and the interaction was insensitive to changes in amino acid conditions. This observation suggests that the Asp to Lys (D to K) substitution at position 60 confers to Rheb a higher affinity for FKBP38 but impedes its action to release mTOR from FKBP38. The fact that the D60K mutant binds strongly to FKBP38 but does not displace it from mTOR interaction suggests that the binding of FKBP38 with Rheb and that with mTOR are not mutually exclusive.

Cells deprived of serum also showed increased interaction between FKBP38 and mTOR that was prevented by serum repletion or overexpression of wild-type Rheb (Fig. 4B). Similarly, overexpression of active Rheb mutant (Q64L) or inactive Rheb mutants (S20N and D60K) rendered the interaction of FKBP38 with mTOR insensitive to changes in serum conditions, which suggests that the interaction was regulated by Rheb in response to serum conditions.

The ability to bind and inhibit mTOR activity in the absence of rapamycin establishes FKBP38 as an endogenous inhibitor of mTOR. Under amino acid or serum starvation this mTOR inhibitor binds and interferes with mTORC1 function in a manner similar to that of the FKBP12-rapamycin complex. In response to growth factors or amino acid availability, Rheb prevents the interaction of FKBP38 with mTOR in a GTP-dependent manner, which leads to mTORC1 activation. This mechanism for the action of Rheb on mTOR is consistent with evidence that active Rheb associates less with mTOR than does the inactive form (*16*). In addition to mTOR, FKBP38 associates with Bcl-2 and calcineurin (*14*, *21*). It is thus possible that Rheb may also control Bcl-2–dependent apoptosis and calcineurin-dependent transcription through FKBP38.

### References and Notes


1. D. E. Martin, M. N. Hall, *Curr. Opin. Cell Biol.* **17**, 158 (2005).
2. S. Wullschleger, R. Loewith, M. N. Hall, *Cell* **124**, 471 (2006).
3. R. Loewith *et al.*, *Mol. Cell* **10**, 457 (2002).
4. K. Hara *et al.*, *Cell* **110**, 177 (2002).
5. D. H. Kim *et al.*, *Cell* **110**, 163 (2002).
6. A. Garami *et al.*, *Mol. Cell* **11**, 1457 (2003).
7. K. Inoki, Y. Li, T. Xu, K. L. Guan, *Genes Dev.* **17**, 1829 (2003).
8. Y. Zhang *et al.*, *Nat. Cell Biol.* **5**, 578 (2003).
9. P. J. Aspuria, F. Tamanoi, *Cell. Signal.* **16**, 1105 (2004).
10. B. D. Manning, L. C. Cantley, *Trends Biochem. Sci.* **28**, 573 (2003).
11. Y. Li, M. N. Corradetti, K. Inoki, K. L. Guan, *Trends Biochem. Sci.* **29**, 32 (2004).
12. G. Fischer, T. Tradler, T. Zarnt, *FEBS Lett.* **426**, 17 (1998).
13. F. Edlich *et al.*, *EMBO J.* **24**, 2688 (2005).
14. M. Shirane, K. I. Nakayama, *Nat. Cell Biol.* **5**, 28 (2003).
15. Materials and methods are available as supporting material on *Science* Online.
16. X. Long, Y. Lin, S. Ortiz-Vega, K. Yonezawa, J. Avruch, *Curr. Biol.* **15**, 702 (2005).
17. X. Long, S. Ortiz-Vega, Y. Lin, J. Avruch, *J. Biol. Chem.* **280**, 23433 (2005).
18. M. Roccio, J. L. Bos, F. J. Zwartkruis, *Oncogene* **25**, 657 (2006).
19. A. P. Tabancay Jr. *et al.*, *J. Biol. Chem.* **278**, 39921 (2003).
20. Y. Li, K. Inoki, K. L. Guan, *Mol. Cell. Biol.* **24**, 7965 (2004).
21. F. Edlich *et al.*, *J. Biol. Chem.* **281**, 14961 (2006).



22. We thank K. Nakayama, K.-L. Guan, F. Tamanoi, N. Sonenberg, and J. Chen for plasmids and reagents; D. Alschuler for suggestions; and P. Houghton for critical reading of this manuscript. Supported by grants to Y.L. from the U.S. Department of Defense (W81XWH-06-1-0047) and to Y.J. from American Cancer Society (RSG-03-169-TBE) and NIH (GM068832).


### Supporting Online Material

www.sciencemag.org/cgi/content/full/318/5852/977/DC1
Materials and Methods
Figs. S1 to S9
References


5 July 2007; accepted 14 September 2007
10.1126/science.1147379


# Magnetic Resonance Spectroscopy Identifies Neural Progenitor Cells in the Live Human Brain


**Louis N. Manganas,[1,3] Xueying Zhang,[1] Yao Li,[1] Raphael D. Hazel,[1,2] S. David Smith,[2] Mark E. Wagshul,[1] Fritz Henn,[2] Helene Benveniste,[1,2] Petar M. Djurić,[1] Grigori Enikolopov,[3]* Mirjana Maletić-Savatić[1,3]***



The identification of neural stem and progenitor cells (NPCs) by in vivo brain imaging could have important implications for diagnostic, prognostic, and therapeutic purposes. We describe a metabolic biomarker for the detection and quantification of NPCs in the human brain in vivo. We used proton nuclear magnetic resonance spectroscopy to identify and characterize a biomarker in which NPCs are enriched and demonstrated its use as a reference for monitoring neurogenesis. To detect low concentrations of NPCs in vivo, we developed a signal processing method that enabled the use of magnetic resonance spectroscopy for the analysis of the NPC biomarker in both the rodent brain and the hippocampus of live humans. Our findings thus open the possibility of investigating the role of NPCs and neurogenesis in a wide variety of human brain disorders.


The adult mammalian brain retains the ability to generate new neurons. These neurons are produced from neural stem and progenitor cells (NPCs), which reside in the hippocampus and the subventricular zone (*1*–*4*). NPCs possess the ability to self-renew and also to generate progeny that can give rise to mature cell types. The ability of NPCs to produce neurons, astrocytes, and oligodendrocytes in vitro and in vivo raises the prospect of harnessing them to repair nerve tissue damaged or lost to neurological disease or trauma (*1*, *2*, *4*). The realization of the curative potential of NPCs would benefit from the development of methods that would enable their identification and tracking in vivo. Currently, positron emission tomography, single-photon computed tomography scanning, and magnetic resonance imaging (MRI) are being examined toward this goal (*5*–*7*). These technologies require NPCs to be preloaded ex vivo with radiolabeled agents or superparamagnetic iron oxide–based derivatives, and therefore are not applied for the detection of endogenous NPCs in the human brain. We used proton magnetic resonance spectrosopy ($^1$H-MRS) to overcome the above limitations and to detect NPCs in the live human brain.

Proton nuclear magnetic resonance spectroscopy ($^1$H-NMR) has been widely used for in vitro detection of low quantities of known metabolites and the identification of unknown compounds present in body fluids or tissues in vitro (*8*). $^1$H-NMR can identify metabolites that are specific for neurons [such as *N*-acetyl aspartate (NAA)] or glia [such as choline (Cho) and myoinositol (mI)], and these compounds have been used as reliable biomarkers of the corre-


[1]SUNY Stony Brook, Stony Brook, NY 11794, USA. [2]Brookhaven National Laboratory, Upton, NY 11719, USA. [3]Cold Spring Harbor Laboratory, Cold Spring Harbor, NY 11724, USA.

*To whom correspondence should be addressed. E-mail: enikolop@cshl.edu (G.E.); mmaleticsava@notes.cc.sunysb.edu (M.M.-S.).

sponding cell types in isolated tissue samples. However, $^1$H-NMR cannot be used to analyze metabolites in live organisms; instead, its correlate, $^1$H-MRS, is used to provide information about the metabolic status of a tissue in vivo (*9*). These two techniques complement each other when physiological or pathological states are investigated (*10*–*12*). Thus, we decided to search for NPC-specific metabolites using $^1$H-NMR and then to exploit the information about these metabolites for detecting NPCs in the live brain using $^1$H-MRS.

To identify unique features in the spectroscopic profile of NPCs, we compared the $^1$H-NMR spectra of NPCs from embryonic mouse brain tissue cultivated as neurospheres in vitro (*13*) with the spectra of cultured neurons, astrocytes, and oligodendrocytes (Fig. 1A). The NPC spectra demonstrated a unique profile, including a prominent peak at the frequency of 1.28 parts per million (ppm), which was not observed in other neural cell types (Fig. 1A). Quantification of the selected signal amplitude confirmed that NPCs were strongly enriched in the 1.28-ppm biomarker as compared to other cell types, whereas, as expected, NAA (2.02 ppm) was predominant in neurons and Cho (3.22 ppm) in astrocytes (Fig. 1B). Small amounts of NAA and Cho were also observed in NPCs, most likely reflecting the presence of neuron- and astrocyte-committed progenitors in the neurospheres. The 1.28-ppm biomarker was detected, to a lesser degree, in our oligodendrocyte preparation, perhaps due to the presence of oligodendrocyte progenitor cells (OPCs; also see Fig. 1D) within the primary cultures analyzed. The amplitude of the 1.28-ppm signal on the $^1$H-NMR spectra was proportional to the number of NPCs taken for analysis (Fig. 1C); this linear correlation indicated that it is possible to quantitatively account for NPCs based on the amount of the 1.28-ppm $^1$H-NMR signal.

To further examine the specificity of the 1.28-ppm biomarker, we compared the $^1$H-NMR spectroscopic profile of NPCs with the profiles of embryonic stem cells (ESCs), cells of the hair follicle–derived sphere cultures (SPCs) (*14*), OPCs, and other types of cells that may be present in the brain, such as macrophages, T lymphocytes, and microglia. The 1.28-ppm biomarker was detected in ESCs, SPCs, and OPCs at significantly lower levels than in the NPCs and was near or below the detection limit in the resting macrophages, T lymphocytes, and microglia (Fig. 1D). We also performed experiments with cultured neurospheres derived from brains of transgenic mice expressing green fluorescent protein (GFP) under the control of nestin gene regulatory elements (*13*). Nestin-GFP neurospheres were dissociated and cells were sorted on the basis of GFP expression levels by means of fluorescence-activated cell sorting (fig. S2). NPC-enriched GFP-expressing cell populations contained higher levels of the 1.28-ppm biomarker than did GFP-negative cells (fig. S2). Together, these experiments indicate that progenitor cells of different origin (but each with neural potential) express the 1.28-ppm biomarker; that among the panel of tested cells, NPCs have the highest level of the biomarker; and that neither postmitotic differentiated cells nor cells without progenitor properties express the biomarker.

If the presence of the 1.28-ppm biomarker correlates with the progenitor status of cells, the levels of this biomarker should decrease as cells differentiate in vitro or in vivo, whereas the levels of the biomarkers of differentiated cells should increase. We cultivated neurospheres under conditions that promote their neuronal and astrocytic differentiation and analyzed their $^1$H-

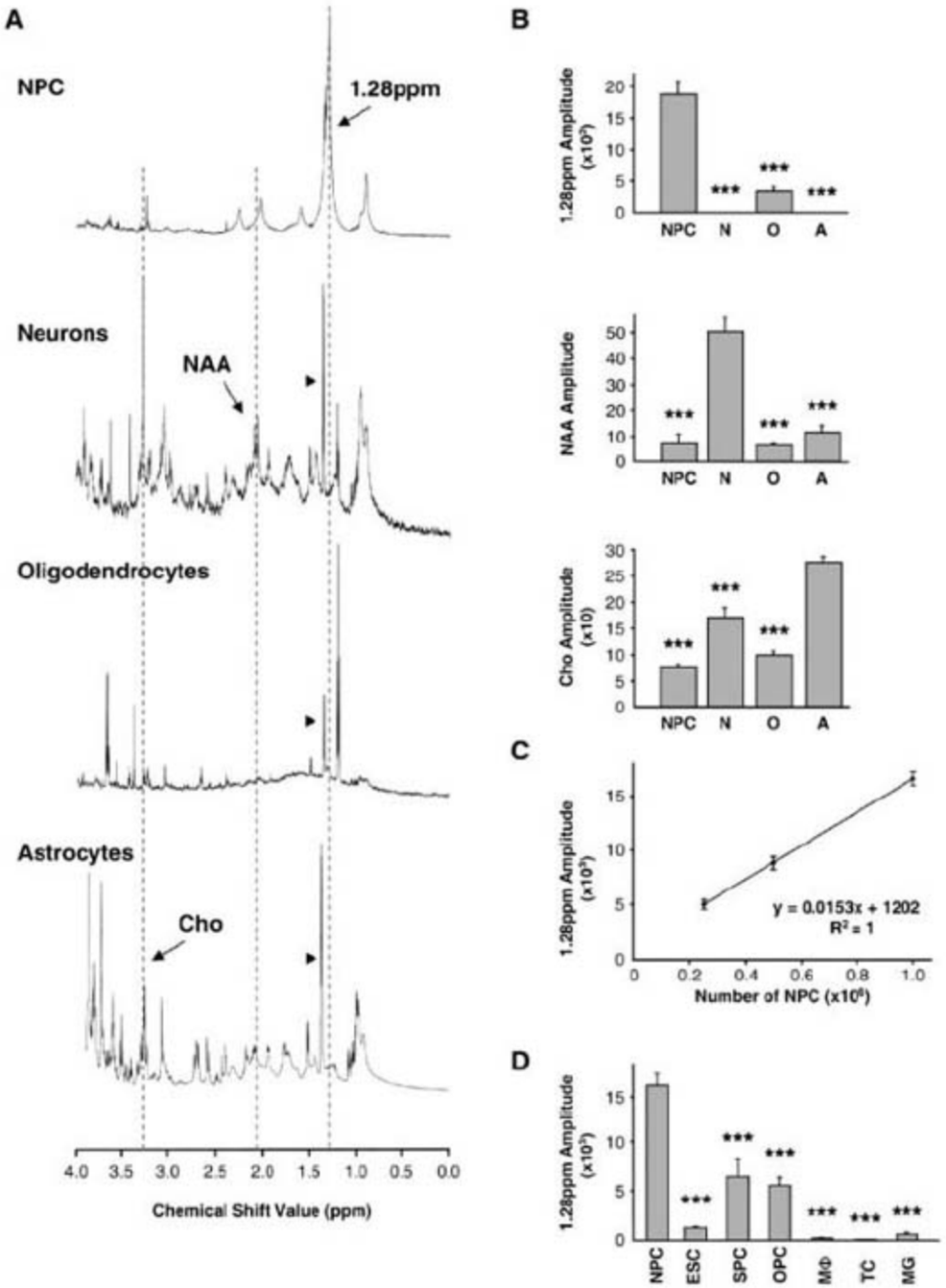


**Fig. 1.** The 1.28-ppm biomarker identifies NPCs. **(A)** Spectral profiles of cultured neural cell types: NPCs, neurons, oligodendrocytes, and astrocytes. Dotted lines outline the 1.28-ppm NPC peak, NAA (2.02 ppm), and Cho (3.23 ppm). Arrowheads denote lactate doublets (1.33 ppm). Spectra are not of equal scale. **(B)** Bar graphs show quantification of the 1.28-ppm biomarker (top), NAA (middle), and Cho (bottom) ($2.5 \times 10^5$ cells each, $n = 3$ experiments per group, done in triplicate samples per experiment). N, neurons, O, oligodendrocytes, A, astrocytes. **(C)** Quantification of the 1.28-ppm biomarker shows correlation of the number of NPCs and the 1.28-ppm signal amplitude ($n = 3$ experiments per data point, done in triplicate samples per experiment). **(D)** Quantification of the 1.28-ppm biomarker in proliferating cells: NPCs, ESCs, SPCs, OPCs, macrophages (MΦ), T lymphocytes (TC), and microglia (MG) ($1 \times 10^6$ each, $n = 3$ experiments per group, done in triplicate samples per experiment). For all figures, quantification was done with the SVD-based method; bar graphs represent mean ± SEM; *, $P < 0.05$; **, $P < 0.01$; ***, $P < 0.001$. Detailed statistics are provided in the supporting online material.

NMR spectra. The levels of the 1.28-ppm biomarker decreased, whereas the levels of the neuronal biomarker NAA and astrocytic biomarker Cho increased after several days of cultivation (Fig. 2A). We next compared the spectra of cells isolated from the mouse brain at embryonic day 12 (E12), when neurogenesis begins, and at postnatal day 30 (P30), when most of the cells in the brain have already differentiated. The levels of the 1.28-ppm biomarker were significantly reduced, whereas the levels of biomarkers of differentiated cells were significantly elevated, in the postnatal adult brain as compared to the embryonic brain (Fig. 2B).

We next examined whether neurogenic regions of the adult brain are enriched in the 1.28-ppm biomarker. We compared the $^1$H-NMR spectra of cells isolated from the adult mouse hippocampus, where continuous neurogenesis takes place, and from the cortex, where neurogenesis is not detected (*1, 2, 15*). A significantly higher amount of the 1.28-ppm biomarker was observed in the adult hippocampus as compared to the cortex (Fig. 2C), providing additional evidence that the presence of the 1.28-ppm biomarker correlates with the presence of NPCs. We then analyzed whether changes in the levels of the 1.28-ppm biomarker correlate with dynamic changes in adult neurogenesis. Neurogenesis in the adult mammalian hippocampus is sensitive to a wide range of stimuli, including electroconvulsive shock (ECS) (*16–21*). We applied ECS to adult mice and assessed cell proliferation using bromodeoxyuridine (BrdU) incorporation in the subgranular zone of the dentate gyrus and measured levels of the 1.28-ppm biomarker using $^1$H-NMR. The number of BrdU-immunoreactive cells was significantly increased in ECS-treated, as compared to control sham-operated, animals, demonstrating the effectiveness of the procedure (Fig. 2D). The levels of the 1.28-ppm biomarker in the preparation of cells from the hippocampus were also significantly increased after ECS (Fig. 2D). Together, our results with the cultured NPCs and with the developing and adult animal brain demonstrate that the amount of 1.28-ppm biomarker correlates with neurogenesis and suggest that changes in neurogenesis can be analyzed using the 1.28-ppm biomarker as a valid reference for NPCs.

We next sought to characterize the chemical nature of the 1.28-ppm biomarker. A specific group of resonances in the 0 to 2 ppm range of the $^1$H-NMR is thought to arise from macromolecules and the fatty acyl chains of triacylglycerides and cholesterol esters found in free-floating mobile lipids in the cytoplasm and in unrestricted lipid microdomains near the plasma membrane (*22*). Proton chemical shift correlation spectroscopy of NPCs showed that there was a *J*-coupling partner for the 1.28-ppm biomarker at 0.8 ppm, as would be expected for a fatty acid containing methyl (-$CH_3$) groups on the same molecule (fig. S3 and Fig. 1A). The notion that the 1.28-ppm biomarker corresponds to lipids was also supported by a decrease in the 1.28-ppm signal amplitude when neurospheres were treated with cerulenin, an inhibitor of fatty acid synthesis (Fig. 2E). To further examine whether the 1.28-ppm biomarker contains lipids, we analyzed the $^1$H-NMR spectra of NPCs extracted with a chloroform/methanol mixture. The 1.28-ppm biomarker was mainly present in the chloroform fraction, which is suggestive of a lipid metabolite (Fig. 2G). Indeed, it overlapped with some of the specific fatty acid spectra, most closely with the spectra of saturated fatty acids (SFAs), such as palmitic acid, and of monounsaturated fatty acids (MUFAs), such as oleic acid (Fig. 2G). The spectra of polyunsaturated fatty acids (PUFAs), such as arachidonic acid, which resonate in the

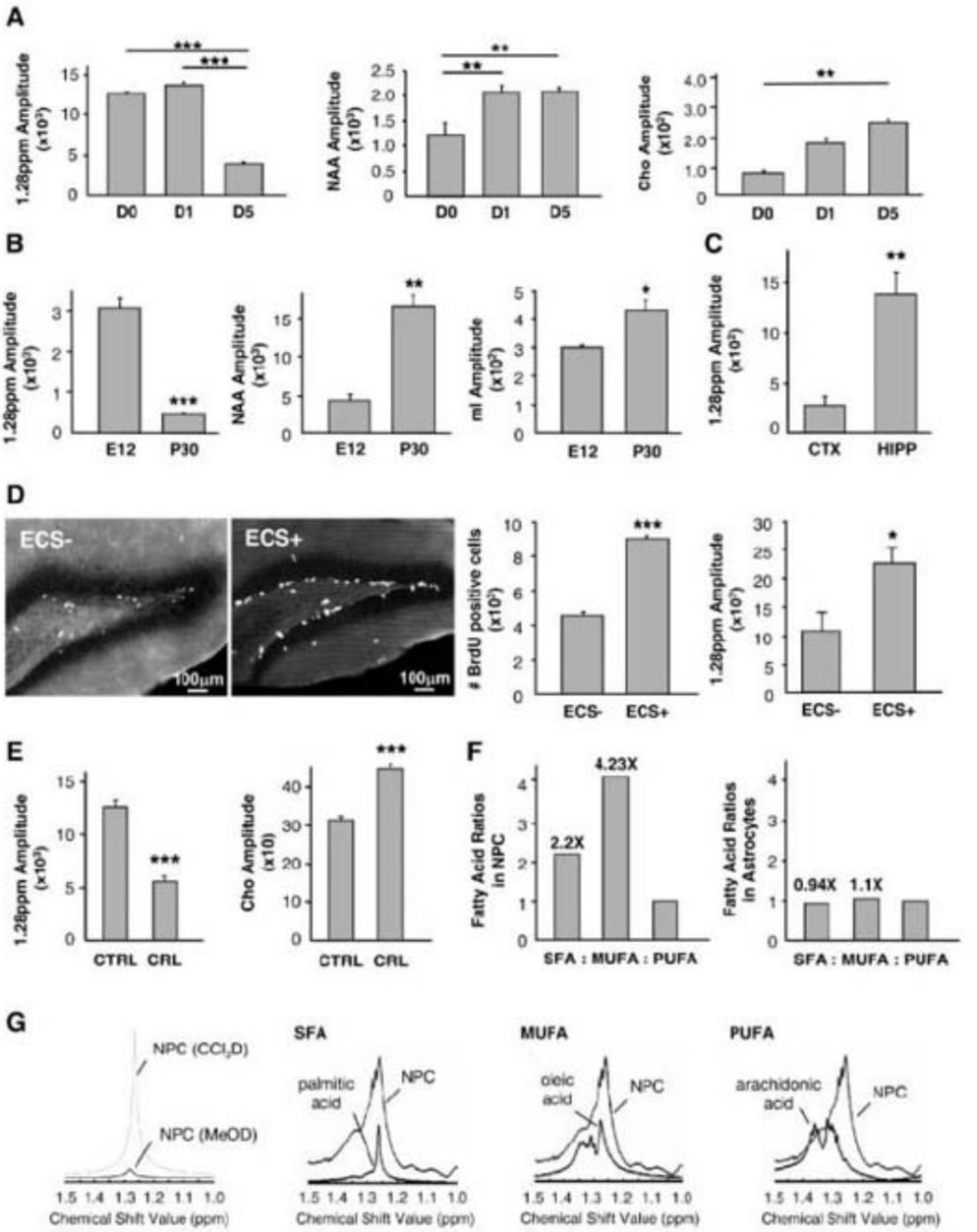


**Fig. 2.** Analysis of the specificity and molecular composition of the NPC biomarker using $^1$H-NMR. **(A)** Quantification of NPC, neuronal (NAA), and glial (Cho) biomarkers during in vitro differentiation, at 0, 1, and 5 days (D) after neurosphere plating ($1 \times 10^6$ cells per time point, $n = 3$ experiments per time point, done in triplicate samples per experiment). **(B)** Quantification of NPC, neuronal (NAA,) and glial (mI) biomarkers in whole-brain homogenates at E12 and P30 ($1 \times 10^6$ cells per time point, $n = 3$ experiments per time point, done in triplicate samples per experiment). **(C)** Quantification of the NPC biomarker in the dissociated adult mouse cortex (CTX) and hippocampus (HIPP) ($1 \times 10^6$ cells per group, $n = 3$ experiments per group, done in triplicate samples per experiment). **(D)** ECS increases both the number of BrdU-immunoreactive cells ($n = 3$ experiments; $P < 0.01$) and the 1.28-ppm biomarker ($n = 3$ experiments; $P < 0.05$) in the mouse hippocampus. **(E)** The 1.28-ppm biomarker diminishes while Cho increases upon blockade of fatty acid synthesis with cerulenin (CRL) ($n = 3$ experiments per group, done in triplicate samples per experiment, $P < 0.001$). **(F)** SFAs and MUFAs are more abundant in NPCs than in astrocytes ($n = 1$). **(G)** The 1.28-ppm biomarker belongs to a chloroform ($CCl_3D$) and not methanol (MeOD) fraction. It overlaps with SFAs and MUFAs rather than PUFAs.

1.3- to 1.4-ppm range, did not overlap (Fig. 2G). Using gas chromatography, we sought to separate and quantify specific fatty acids in NPCs and compare them to those found in astrocytes. There was a higher concentration of SFAs and MUFAs than of PUFAs in NPCs, but not in astrocytes (Fig. 2F). Together, our results suggest that the 1.28-ppm biomarker is most likely a mixture of lipids that include SFAs and/or MUFAs.

We next addressed the possibility of using the NPC biomarker for in vivo brain imaging. Using a 9.4-T micro MRI (mMRI) scanner, we obtained adult rat spectra of the hippocampus, where endogenous NPCs reside, and the parietal cortex, where dividing NPCs are undetectable (Fig. 3). Traditional Fourier transform signal processing was unable to distinguish the 1.28-ppm biomarker in the hippocampus from background noise (Fig. 3A, insets), most likely due to a low NPC density in the adult rat hippocampus. Therefore, we developed a more sensitive signal-processing algorithm in order to isolate the signal of the 1.28-ppm biomarker from the noise within the in vivo $^{1}$H-MRS spectra. We used singular value decomposition (SVD), which permits improved detection at low signal-to-noise ratios and allows better resolution of signal components (modes) that are close to one another in a given frequency domain (*23*–*25*). Based on SVD signal processing, we developed an algorithm that enables detection of the 1.28-ppm biomarker in the adult rat hippocampus in vivo (Fig. 3A, red peak). Absolute quantification of the 1.28-ppm biomarker was achieved by estimating the amplitude of the 1.28-ppm signal, whereas relative quantification was achieved by ratiometric analysis with the creatine (Cr) signal amplitude as a denominator. Both quantification methods are established as reliable indicators of a given concentration of metabolite (*26*). A large difference was observed when the absolute quantities of the 1.28-ppm biomarker were compared between the hippocampal and cortical spectra; this was paralleled by the ratiometric quantification, which confirmed that the hippocampus was highly enriched in the 1.28-ppm biomarker as compared to the cortex (Fig. 3A).

We also transplanted NPCs into the left cortical hemisphere of the adult rat brain and injected an equal volume of saline into the control right hemisphere. $^{1}$H-MRS data were obtained for both hemispheres from voxels of the same size, centered on the injected areas (Fig. 3B). Both Fourier transform (inset) and SVD-based signal processing (colored peaks) clearly detected the 1.28-ppm biomarker in the spectra of the experimental site containing NPCs (Fig. 3B). Both the direct quantification and the ratiometric analysis demonstrated that the signal in the hemisphere with the injected NPCs was more than 35 times greater than that in the corresponding region of the control cortical hemisphere (Fig. 3B).

Furthermore, to detect changes in the density of endogenous NPCs in vivo, we treated adult rats with ECS. Five days after the treatment, we injected BrdU to label dividing cells and analyzed the ECS-treated and sham-operated control animals the next day. Quantification of the 1.28-ppm:Cr signal amplitude ratios in the hippocampus showed a significant increase of the 1.28-ppm biomarker in ECS-treated rats as compared to sham-operated controls (Fig. 3C). To validate the spectroscopic findings, we quantified the number of BrdU-immunoreactive cells in the hippocampus of the same animals (Fig. 3D). A significant increase in the number of BrdU-immunoreactive cells in ECS-treated rats as compared to sham-operated controls demonstrated that, as expected, ECS increased NPC prolifera-

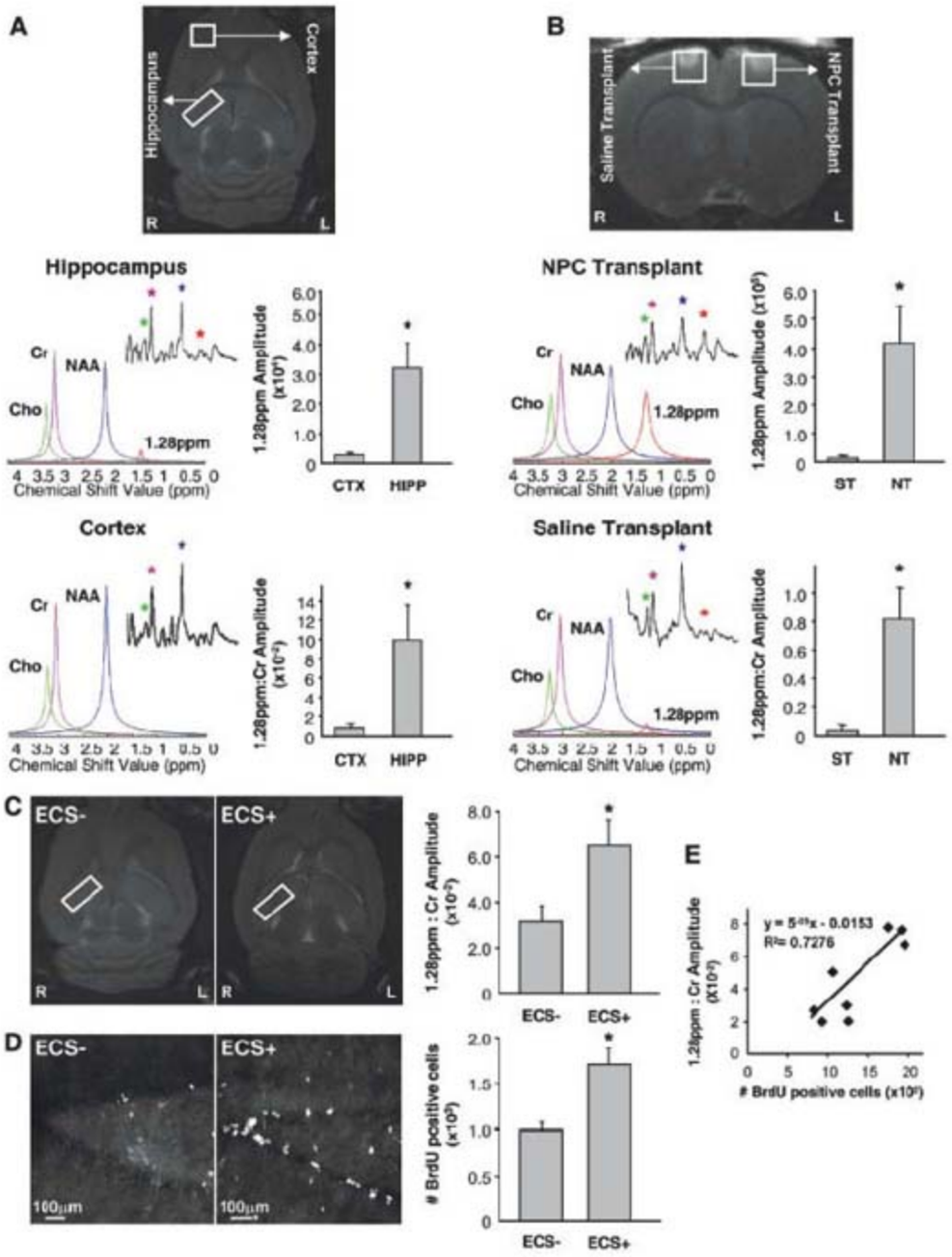


**Fig. 3.** Identification of NPCs in the rat brain in vivo, using mMRI spectroscopy. **(A)** Imaging of endogenous NPCs. Voxels are placed along the hippocampus (HIPP) and in the cortex (CTX). In the hippocampus, the 1.28-ppm biomarker (red) is evident when SVD-based signal processing is performed (colored peaks) but not when Fourier transform is done (insets). In the cortex, the 1.28-ppm biomarker is not detected by either data analysis. Colored asterisks and peaks correlate. Bar graphs show absolute (top) and relative (bottom) quantification of the 1.28-ppm biomarker ($n = 4$ experiments, $P < 0.05$). **(B)** Imaging of transplanted NPCs. Voxels are placed in the area of NPC transplant (NT; $5 \times 10^6$ NPCs in 5 μl of saline) and saline injection (ST; 5 μl). In the NT site, the 1.28-ppm biomarker (red) is observed with both Fourier transform and SVD-based signal processing. In the ST site, no significant 1.28-ppm signal is observed. Bar graphs show absolute (top) and relative (bottom) quantification of the 1.28-ppm biomarker ($n = 5$ experiments; $P < 0.05$). **(C** and **D)** Imaging of endogenous NPCs after ECS. Voxels are placed along the hippocampus in control (ECS–) and ECS-treated (ECS+) adult rats **(C)**. Quantification of the 1.28-ppm biomarker [(C) $n = 4$ experiments, $P < 0.05$] and the number of BrdU-immunoreactive cells in the dentate gyrus of the same animal [(D) $n = 4$ experiments, $P < 0.01$] indicates linear correlation **(E)**.

tion. Moreover, in the ECS-treated animals, we found a correlation between the number of BrdU-immunoreactive cells and the 1.28-ppm:Cr signal amplitude ratio in the hippocampus of the same animal (Fig. 3E). Together, these data indicate that $^1$H-MRS can be used to detect and measure changes in the density of endogenous NPCs in vivo.

We then proceeded with the identification of endogenous NPCs in the human brain. Brain $^1$H-MRS was performed on healthy adults, using a 3-T MRI scanner and SVD-based signal processing (Fig. 4A). An experimental voxel was placed along the length of the hippocampus, while a control voxel of the same volume included gray and white matter of the ipsilateral parietal cortex (Fig. 4A). The Fourier transform did not reveal the 1.28-ppm biomarker (inset) in any of the voxels (Fig. 4A). However, the SVD-based analysis (colored peaks) clearly detected the 1.28-ppm biomarker in the hippocampal spectra, indicating that this methodology can be used to identify endogenous NPCs in the human brain (Fig. 4A). For each person, we found a major difference between the hippocampus and the cortex when using either absolute or ratiometric quantification of the 1.28-ppm biomarker, indicating that both can be applied to indirectly measure NPC density in the human hippocampus. No difference in the level of the 1.28-ppm biomarker was observed when the left and right hippocampi were compared (Fig. 4A). Furthermore, when we imaged the left hippocampus of the same people after a 3-month period during which there was no major change in their daily routine, no difference was observed in the 1.28-ppm biomarker (Fig. 4B). Finally, we analyzed the age-related changes in the 1.28-ppm biomarker during human development by imaging people of varying ages: preadolescents, adolescents, and adults. Quantification of the 1.28-ppm biomarker revealed a decrease in the 1.28-ppm signal amplitude (Fig. 4C), which is compatible with data demonstrating age-related decrease in neurogenesis in animals (*27*).

In our work, we identified a spectroscopic biomarker of NPCs, developed a methodology to detect this biomarker in the live brain, and demonstrated the use of the biomarker for identifying NPCs in the live human brain. The NPC biomarker could be readily detected in vitro with $^1$H-NMR, but its detection at low concentrations in the live brain with $^1$H-MRS required the development of more refined methodology. Our SVD-based signal processing proved to be superior to the traditionally used Fourier transform and can now be applied in a variety of imaging settings where low levels of a particular metabolite preclude its reliable detection in vivo.

Our results suggest that the NPC biomarker, represented by a 1.28-ppm spectral peak, is a complex mixture of saturated and/or monounsaturated fatty acids and related compounds. The functional relevance of these molecules for the control of proliferation and differentiation of NPCs remains to be elucidated.

Finally, our data on humans provide in vivo imaging evidence for NPCs in the human hippocampus. These findings support the numerous data demonstrating continuous neurogenesis in the dentate gyrus (*1, 2, 28*). We also demonstrated that in humans the presence of the NPC biomarker in the hippocampus dramatically decreases with age. Although a decrease in neurogenesis has been reported in aging mammals, these are the first data from the living human brain that indicate a decrease in NPCs during brain development from childhood to adulthood. More generally, this biomarker can be applied to track and analyze endogenous or transplanted NPCs, to monitor neurogenesis in a wide range of human neurological and psychiatric disorders, and to evaluate the efficiency of therapeutic interventions.

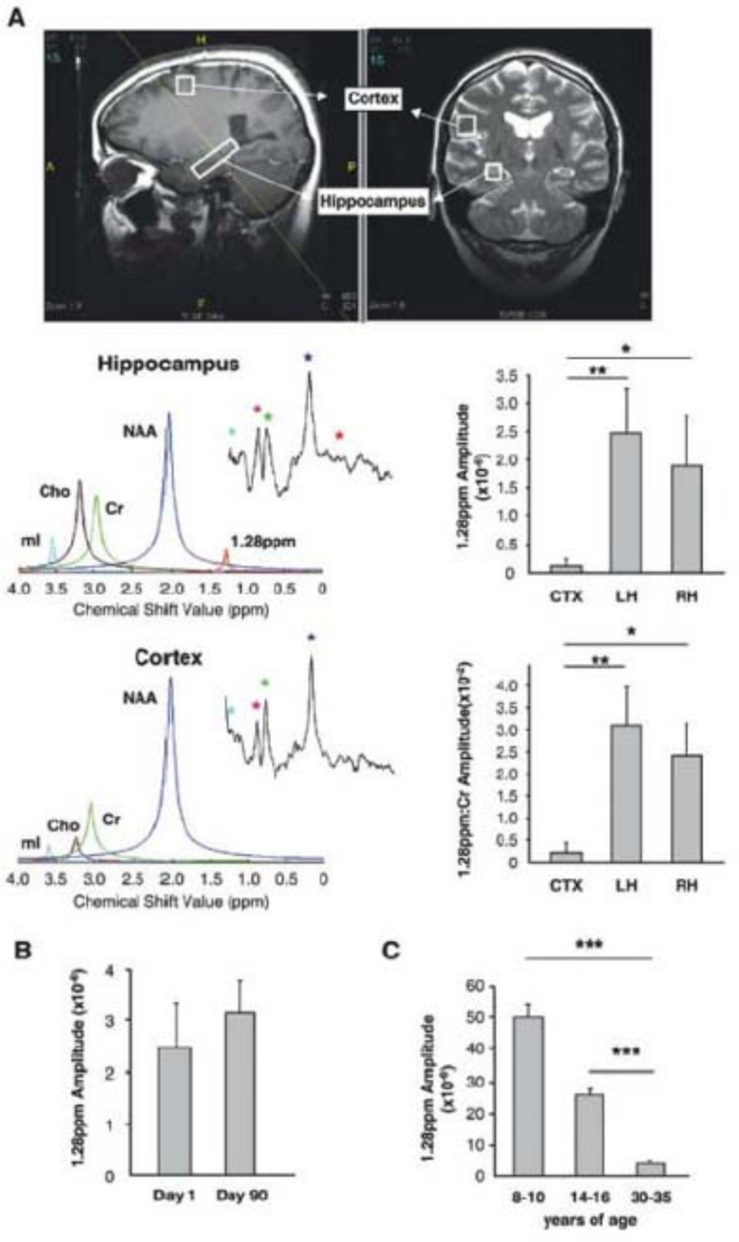


**Fig. 4.** Identification of NPCs in the human hippocampus in vivo, using $^1$H-MRS. **(A)** Voxels are placed along the hippocampus and in the cortex. In the hippocampus, the 1.28-ppm biomarker (red) is evident when SVD-based signal processing is performed but not when Fourier transform is done. In the cortex, the 1.28-ppm biomarker is not detected by either data analysis. Colored asterisks and colored peaks correlate. Bar graphs show absolute (top) and relative (bottom) quantification of the 1.28-ppm biomarker (CTX, cortex; LH, left hippocampus; RH, right hippocampus; $n = 5$ people; $P < 0.01$ and $P < 0.05$, respectively). **(B)** Quantification of the 1.28-ppm biomarker in the adult human hippocampus over time ($n = 4$ people, $P = 0.747$). The same people were imaged 90 days apart. **(C)** Quantification of the 1.28-ppm biomarker in the human hippocampus during development in preadolescent, adolescent, and adult age groups ($n = 3$ people per group; $P < 0.001$).


**References and Notes**

1. D. C. Lie, H. Song, S. A. Colamarino, G. L. Ming, F. H. Gage, *Annu. Rev. Pharmacol. Toxicol.* **44**, 399 (2004).
2. G. L. Ming, H. Song, *Annu. Rev. Neurosci.* **28**, 223 (2005).
3. M. A. Curtis *et al.*, *Science* **315**, 1243 (2007).
4. S. A. Goldman, M. S. Windrem, *Philos. Trans. R. Soc. London Ser. B* **361**, 1463 (2006).
5. F. Cicchetti *et al.*, *Contrast Media Mol. Imaging* **2**, 130 (2007).
6. B. B. Chin *et al.*, *Nucl. Med. Commun.* **24**, 1149 (2003).
7. A. S. Arbab, W. Liu, J. A. Frank, *Expert Rev. Med. Devices* **3**, 427 (2006).
8. M. R. Viant, *Methods Mol. Biol.* **358**, 229 (2007).
9. B. Ross, S. Bluml, *Anat. Rec.* **265**, 54 (2001) (New Anat).
10. H. Shinno *et al.*, *J. Neurol. Sci.* **260**, 132 (2007).
11. A. Stengel *et al.*, *Magn. Reson. Med.* **52**, 228 (2004).
12. P. A. Narayana, *J. Neuroimaging* **15**, 46S (2005).
13. J. L. Mignone, V. Kukekov, A. S. Chiang, D. Steindler, G. Enikolopov, *J. Comp. Neurol.* **469**, 311 (2004).
14. J. L. Mignone *et al.*, *Cell Cycle* **6**, 2161 (2007).
15. R. D. Bhardwaj, *Proc. Natl. Acad. Sci. U.S.A.* **103**, 12564 (2006).
16. H. van Praag, G. Kempermann, F. H. Gage, *Nat. Neurosci.* **2**, 266 (1999).
17. G. Kempermann, H. G. Kuhn, F. H. Gage, *Nature* **386**, 493 (1997).
18. J. M. Encinas, A. Vaahtokari, G. Enikolopov, *Proc. Natl. Acad. Sci. U.S.A.* **103**, 8233 (2006).
19. J. L. Warner-Schmidt, R. S. Duman, *Hippocampus* **16**, 239 (2006).
20. T. M. Madsen *et al.*, *Biol. Psychiatry* **47**, 1043 (2000).
21. T. D. Perera *et al.*, *J. Neurosci.* **27**, 4894 (2007).
22. M. L. Sparling, R. Zidovetzki, L. Muller, S. I. Chan, *Anal. Biochem.* **178**, 67 (1989).

23. H. Barkhuijsen, R. de Beer, D. van Ormondt, *J. Magn. Reson.* **73**, 553 (1987).
24. S. Cavassila *et al.*, *J. Magn. Reson. Anal.* **3**, 87 (1997).
25. P. Stoica, N. Sandgren, Y. Selen, L. Vanhamme, S. Van Huffel, *J. Magn. Reson.* **165**, 80 (2003).
26. F. Dieterle, A. Ross, G. Schlotterbeck, H. Senn, *Anal. Chem.* **78**, 4281 (2006).
27. H. G. Kuhn, H. Dickinson-Anson, F. H. Gage, *J. Neurosci.* **16**, 2027 (1996).
28. P. S. Eriksson *et al.*, *Nat. Med.* **4**, 1313 (1998).
29. We thank M. Ziliox and K. DeCock for expert technical assistance with $^1$H-NMR spectroscopy; B. Forester for mMRI assistance; H. Colognato for OPC cultures; S. Tsirka for microglial cultures; J.-H. Park for advice on ECS; and A. Sierra, J. M. Encinas, J. S. Trimmer, P. Stavropoulos, and J. Banerji for helpful discussions. This work was supported by the National Institute of Neurological Disorders and Stroke (NINDS) (grants R21NS05875-1 and 5K08 NS044276); U.S. Army Medical Research (grant DAMD170110754) (M.M.-S.); the National Institute of Diabetes and Digestive and Kidney Diseases (grant T32DK07521-16) (L.N.M.); NINDS grant R01-NS32764; NARSAD; the Seraph Foundation; the Hartman Foundation; the Hope for Depression Foundation; the Hazan Foundation (G.E.); the U.S. Department of Energy (grant FWP MO-065) (H.B.); NSF (grant CCF-0515246); and the Office of Naval Research (grant N00014-06-1-0012) (P.D.).

**Supporting Online Material**

www.sciencemag.org/cgi/content/full/318/5852/980/DC1
Materials and Methods
SOM Text
Figs. S1 to S3

16 July 2007; accepted 12 October 2007
10.1126/science.1147851

# Sex-Linked Genetic Influence on Caste Determination in a Termite

**Yoshinobu Hayashi,[1] Nathan Lo,[2] Hitoshi Miyata,[1] Osamu Kitade[1]***

**The most ecologically successful and destructive termite species are those with both a nymph caste and an irreversibly wingless worker caste. The early developmental bifurcation separating these castes is widely accepted to be strictly environmentally determined. We present evidence that genotype also influences this process. Offspring from four different crosses of nymph- and worker-derived secondary reproductive individuals had strongly differentiated caste and sex ratios, despite uniform rearing conditions. These data fit an X-linked, one-locus-two-allele model. Of five possible genotypes, one was lethal, two resulted in workers, and two resulted in either nymphs or environmentally determined workers. Caste is thus controlled both by environment and by a complex genetic inheritance pattern.**

Social insects, such as ants and termites, are characterized by the differentiation of colony members into either reproductive or sterile individuals (*1*). Kin selection theory predicts that caste results from environmentally induced differences in gene expression from a totipotent genome (*2*, *3*), a prediction supported by empirical studies of hymenopteran social insects (bees, ants, wasps) (*4*, *5*). Although genetic determination of hymenopteran queen and worker castes has been documented (*6*–*11*), these are exceptions resulting from hybridization, thelytokous parthenogenesis (asexual production of female offspring), and dimorphic queens. In termites, the reproductive and worker castes are hypothesized to be determined entirely by extrinsic factors, primarily pheromones (*12*–*14*).

Termites (Blattaria: Isoptera) are a eusocial form of cockroach (*15*). In >80% of species, a bifurcation occurs early in development (Fig. 1). The vast majority of offspring (both female and male) enter the functionally sterile, irreversibly wingless worker pathway (*13*, *16*). Alternatively, some offspring develop wing buds and enter the nymphal pathway, which leads to the alate (primary reproductive) caste. In the absence of the queen and/or king, some individuals (termed neotenics) take over the role of reproduction while retaining juvenile characteristics (*13*). Inbreeding within the colony is thus common in termites. Neotenics may arise from the nymphal and/or the worker pathway and are, respectively, termed nymphoids (with wing buds) and ergatoids (without wing buds) (Fig. 1). Workers, although functionally sterile, therefore retain the ability to occasionally become fertile in some species.

We isolated nymphs and workers from reproductive individuals, producing female (f) and male (m) nymphoids (N) and ergatoids (E) from three distinct colonies of *Reticulitermes speratus*. We crossed them (i.e., fNmN, fNmE, fEmE, fEmN) as described (*17*). Each mated pair was placed with 50 female workers from an independent, unrelated fourth colony to promote egg production. Eggs were removed daily and raised by 50 male workers from the fourth colony to identify environmental and genetic influences on developmental bifurcation (Fig. 1). The sex and caste of third-instar offspring were determined, as were survival rates. In the absence of a male reproductive, *R. speratus* females can reproduce parthenogenetically via thelytokous automixis, resulting in homozygous female nymph offspring (*18*–*20*). Therefore, we also examined the development of parthenogenetic offspring from single parents of types fN and fE.

Among replicates of a particular pair type, offspring caste and sex ratios were similar, regardless of whether they were outbred or inbred (*17*). No significant differences among offspring types were found with Fisher's exact test [fNmN, $P = 0.30$ ($n = 7$); fEmE, $P = 0.11$ ($n = 4$); fEmN, $P = 0.54$ ($n = 7$)], with the exception of fNmE ($P = 0.02$), where 1 of 5 replicates had slightly more female workers, although the pattern was similar to the other 4 replicates ($P = 0.10$ upon exclusion of the female worker–skewed replicate). Therefore, we pooled our data for comparisons with the other treatments.

All offspring of parthenogenetic fN and fE were female, and almost all differentiated into nymphs (100% and 99%, respectively) (Fig. 2). In

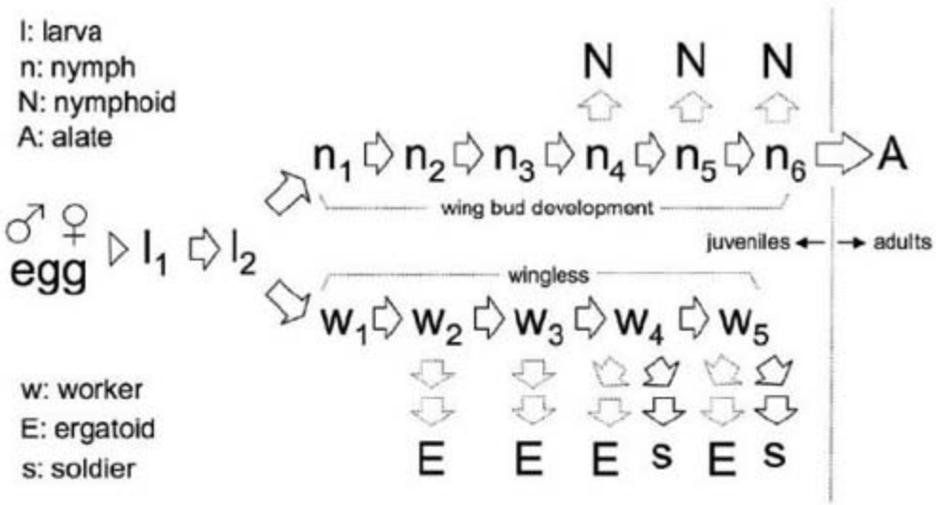


**Fig. 1.** Caste developmental pathways of *Reticulitermes* spp. (*13*). Termites are diploid and hemimetabolous; larvae of each sex follow either the worker pathway, in which individuals remain irreversibly wingless, or the nymphal pathway, leading to the alate form. Arrows indicate molts; dotted arrows indicate occasional molts to neotenic nymphoids or ergatoids, which may reproduce in the absence of the queen and/or king. Workers undergo stationary molts after $w_5$. Soldiers are derived from $w_4$ and $w_5$. Ergatoids arise from all worker stages after $w_1$.

[1]Natural History Laboratory, College of Science, Ibaraki University, Mito, Ibaraki 310-8512, Japan. [2]Behaviour and Genetics of Social Insects Laboratory, School of Biological Sciences, University of Sydney, Sydney, New South Wales 2006, Australia.

*To whom correspondence should be addressed. E-mail: kitade@mx.ibaraki.ac.jp

contrast, offspring from different pairs diverged in both caste and sex ratios. fNmN had a ~1:1 ratio of female workers to male workers [48.4 ± 1.7%: 47.7 ± 1.5% (mean ± SEM)]. fNmE had a ~1:1 ratio of female nymphs to male workers (45.9 ± 1.6%: 50.2 ± 1.4%). fEmN had a ~1:1:1 ratio of male nymphs to female workers to male workers (31.0 ± 4.0%: 35.8 ± 2.7%: 31.9 ± 1.4%). Finally, fEmE had a ~1:1:1:1 split of all four offspring types, with a slight bias of nymphs over workers (33.0 ± 5.8% female nymphs: 29.7 ± 5.2% male nymphs: 19.8 ± 4.5% female workers: 17.4 ± 4.1% male workers). We saw significant differences ($P < 0.001$) in the offspring caste and sex ratios for all six pairwise comparisons between pair types by Fisher's exact test with Bonferroni correction.

The mean survival rate (Fig. 3) of fE offspring was significantly lower than that of fN, fNmN, fNmE, and fEmE. The mean survival rate of fEmN offspring was lower than all treatments but fE, although not significantly. Death or removal of eggs by workers before hatching accounted for offspring mortality. Because larvae disappeared only rarely, it is highly unlikely that workers removed particular castes. The sensitivity of termite eggs to experimental conditions may explain the relatively low survival rate across the six treatments (≤48%) (*17*).

Our data contradict the hypothesis that termite nymph and worker caste determination is due only to environment (*12*–*14*) (Fig. 2). If maternal effects in the eggs were responsible for the different caste ratios, we should see similar patterns among offspring of fNmN and fNmE, and also of fEmE and fEmN. Similarly, paternal effects are unlikely because of the highly differentiated caste ratios of offspring between fNmN and fEmN and between fNmE and fEmE.

Our data fit a genetic model featuring a single X-linked locus, dubbed *worker* (*wk*), with two alleles, A and B (Fig. 4) [sex determination in *R. speratus* appears to involve an XY system, as found in other Rhinotermitidae and Termitidae (*13*, *19*)]. The model assumes no influence of environmental stimuli produced by reproductive individuals. Offspring with genotypes $wk^{AB}$ and $wk^{A}Y$ develop into workers; offspring with genotypes $wk^{AA}$ and $wk^{B}Y$ develop into nymphs. Allele B is homozygous lethal. Because half of the offspring produced parthenogenetically by ergatoids are $wk^{BB}$, they will be inviable; this is consistent with the significantly lower survival rate of fE offspring (Fig. 3). Similarly, one-quarter of fEmN offspring are predicted to be inviable, which is in agreement with the lower survival rate of these pairs relative to fNmN, fNmE, fEmE, and fN.

Nymph genotypes are plastic, being subject to pheromonal modification. When we placed parthenogenetically produced fN offspring ($wk^{AA}$) in the presence of a male and female nymphoid pair, 24% developed into female workers, the rest into female nymphs (*17*). Slight deviations in offspring ratios predicted by the model (as seen in Fig. 2) may be due to weak pheromonal influence from tending workers, incomplete penetrance at *wk*, other loci with weak effects on caste and sex, or a combination of these factors. We also determined a similar but less parsimonious model that fits the data of Figs. 2 and 3 (fig. S1).

We predict that offspring in queen-king colonies will be workers (i.e., $wk^{AA} \times wk^{B}Y \rightarrow wk^{AB} + wk^{A}Y$). In the event that the queen and/or king dies, ergatoid neotenics should develop, and fEmE, queen-mE, or king-fE matings should result in workers and genotypic nymphs (Fig. 4). Independent colony composition studies were consistent with these predictions. *R. speratus* queen-king incipient colonies contained workers and soldiers derived from the worker line (Fig. 1), but no nymphs (*19*). On the other hand, *R. speratus* queen-queen incipient colonies contained nymphs and workers (*19*), as predicted from our experiments showing environmental modification of nymph genotypes. In the related *R. flavipes*, queen-king colonies contained negligible numbers of nymphs (0.72 ± 0.28, $n = 17$), whereas queenless colonies (with neotenics) contained many nymphs (550 ± 86, $n = 3$) (*21*).

The bifurcated caste pathway shown in Fig. 1 is thought to have evolved from a linear pathway (*12*, *13*, *22*). Species with a linear pathway are basal (*22*) and nest and feed within one wood source. All offspring have the potential for selfish development into alates or neotenics, but they remain as sterile individuals under the influence of pheromones produced by reproductive individuals. The selective advantage of the derived *R. speratus* genetic system may be enhanced inhibition of selfish reproduction by offspring, particularly during colony development. The offspring produced in *R. speratus* queen-king colonies are presumably unable to develop into alates, and their propensity to develop into selfish neotenics is relatively low: *R. speratus* nymphs require ~12 days and a single molt to become nymphoids, whereas workers require ~30 to 40 days and two molts to become ergatoids (*23*). The evolution of the genetically influenced caste determination system may therefore have facilitated increased colony size and ecological dominance.

If having genetically (as opposed to environmentally) determined workers were advantageous, the A allele would invade the population at *wk*. Allele A would lead to colonies producing a female bias among alates, due to ≥50% of males being wingless workers. Such a bias could favor the invasion of B, which would cause an alate sex-ratio bias toward males, due to ≥50% of females within colonies being wingless workers. Eventually, primary reproductive individuals

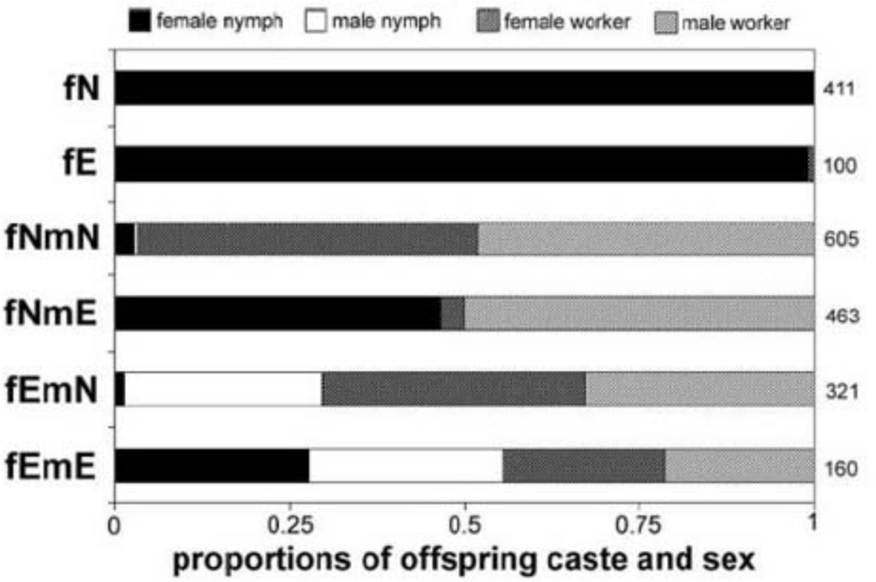


**Fig. 2.** Proportions of *R. speratus* female and male nymph and worker offspring from six experimental rearing treatments. Fifty workers raised eggs from parthenogenetic female nymphoids (fN) and ergatoids (fE), and the four possible crosses among fN, fE, male nymphoids (mN), and male ergatoids (mE) (i.e., fNmN, fNmE, fEmN, fEmE). Offspring were pooled across replicate colonies for each colony type (see text). Sample sizes (numbers of offspring produced) are shown at the right.

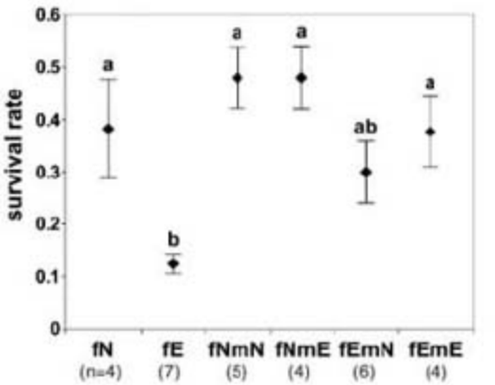


**Fig. 3.** Survival rates of offspring to the third instar (means ± SEM) in experimental treatments. Rates were determined for most replicates presented in Fig. 2. Means that bear the same letter (i.e., a or b) are not significantly different (Tukey's HSD test, $P > 0.05$); $n$ = number of replicates per treatment.

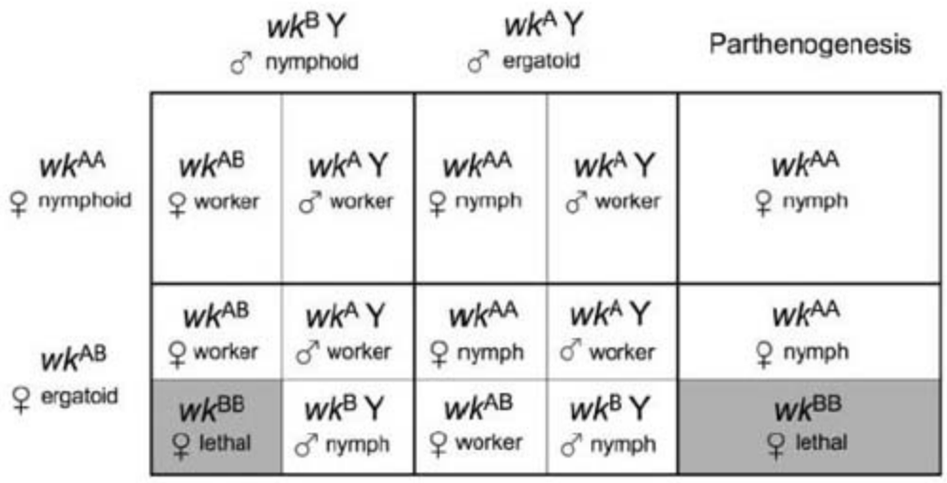


**Fig. 4.** One-locus-two-allele model of genotype affecting caste determination in *R. speratus*. This model fits the data from Figs. 2 and 3. The locus, dubbed *worker* (*wk*), is X-linked and has two alleles, A and B. Females inheriting two copies of A have a nymph genotype; females inheriting a copy of both A and B have a worker genotype (the B allele is dominant). Males inheriting a copy of A have a worker genotype; males inheriting a copy of B have a nymph genotype. The $wk^{BB}$ genotype is lethal. Genotype matches phenotype under experimental rearing conditions (i.e., in the absence of reproductive individuals). In the presence of reproductive individuals, the nymph genotype may be modified into a worker phenotype as a result of environmental stimuli. Note: *R. speratus* nymphoid and ergatoid females produce homozygous females by parthenogenesis.

carrying a combination of A and B alleles would produce workers of both sexes, outcompeting those with only one sex and allowing the alleles to spread to fixation. Because an fE always has the opportunity to mate under natural conditions (with the king, mE, or mN), lethal $wk^{BB}$ genotypes will not be produced by fE parthenogenesis. However, fE-king or fEmN crosses, if they occur, will result in 25% lethal $wk^{BB}$. The advantage of the B allele (i.e., production of female workers) presumably outweighs this potential cost.

Although some termites may have up to half their genome linked to the X and Y chromosomes (*24*), *R. speratus* appears to have at most 2 out of 21 (haploid) sex chromosomes (*19*). Thus, the presence of *wk* on a sex-linked chromosome may be important. Theory predicts that sex-linked loci are more efficient at transporting the population from a previously sexually monomorphic optimum to a complex, sex-conditional optimum, as would be the case during invasion of the A allele (*25*).

Alleles A and B have an opposite effect in each sex. Allele A results in genotypic female nymphs when homozygous, $wk^{AA}$, but results in male workers as a single copy, $wk^{A}Y$. Allele B results in male genotypic nymphs, $wk^{B}Y$, but female workers, $wk^{AB}$. Female and male alates each carry one allele type, which is passed on to offspring of the opposite sex, resulting in wingless workers. Inbreeding within the colony appears to be required to produce further alates. It is the occasional reproduction by workers (as ergatoids) that allows the cycle to continue. The existence of several termite species with ergatoids and/or workers of only one sex (*13*) suggests that genetically influenced nymph and worker caste determination may not be limited to *R. speratus*.


**References and Notes**

1. E. O. Wilson, *The Insect Societies* (Belknap, Cambridge, MA, 1971).
2. J. Seger, *J. Theor. Biol.* **91**, 191 (1981).
3. D. C. Queller, J. E. Strassman, *Bioscience* **48**, 165 (1998).
4. D. E. Wheeler, *Am. Nat.* **128**, 13 (1986).
5. R. H. Crozier, P. Pamilo, *Evolution of Social Insect Colonies* (Oxford Univ. Press, New York, 1996).
6. U. Winter, A. Buschinger, *Entomol. Gen.* **11**, 125 (1986).
7. D. Fournier *et al.*, *Nature* **435**, 1230 (2005).
8. S. Helms Cahan, L. Keller, *Nature* **424**, 306 (2003).
9. G. E. Julian, J. H. Fewell, J. Gadau, R. A. Johnson, D. Larrabee, *Proc. Natl. Acad. Sci. U.S.A.* **99**, 8157 (2002).
10. M. Pearcy, S. Aron, C. Doums, L. Keller, *Science* **306**, 1780 (2004).
11. V. P. Volny, D. M. Gordon, *Proc. Natl. Acad. Sci. U.S.A.* **99**, 6108 (2002).
12. B. L. Thorne, *Annu. Rev. Ecol. Syst.* **28**, 27 (1997).
13. Y. Roisin, in *Termites: Evolution, Sociality, Symbiosis, Ecology*, T. Abe, D. E. Bignell, M. Higashi, Eds. (Kluwer Academic, Dordrecht, Netherlands, 2000), pp. 95–120.
14. J. Korb, S. Katrantzis, *Evol. Dev.* **6**, 342 (2004).
15. N. Lo *et al.*, *Biol. Lett.* **3**, 562 (2007).
16. M. Higashi, T. Abe, in *Biodiversity: An Ecological Perspective*, T. Abe, S. A. Levin, M. Higashi, Eds. (Springer-Verlag, New York, 1996), pp. 83–112.
17. See supporting material on *Science* Online.
18. Y. Hayashi, O. Kitade, J. Kojima, *Entomol. Sci.* **6**, 253 (2003).
19. K. Matsuura, M. Fujimoto, K. Goka, *Insectes Soc.* **51**, 325 (2004).
20. Y. Hayashi, H. Miyata, O. Kitade, *Sociobiology* **48**, 849 (2006).
21. C. E. Long, B. L. Thorne, N. L. Breisch, *Bull. Entomol. Res.* **93**, 439 (2003).
22. G. J. Thompson, O. Kitade, N. Lo, R. H. Crozier, *J. Evol. Biol.* **13**, 869 (2000).
23. H. Miyata, H. Furuichi, O. Kitade, *Entomol. Sci.* **7**, 309 (2004).
24. P. Luykx, *Genome* **33**, 80 (1990).
25. H. K. Reeve, J. S. Shellman-Reeve, *Evol. Ecol.* **11**, 357 (1997).


26. We thank K. Masuko, W. O. H. Hughes, R. H. Crozier, J. Sved, S. Shafir, and the Behavior and Genetics of Social Insects lab at the University of Sydney for discussions. Supported by Grants-in-Aid for Scientific Research 06146, 17570013, and 19370009 from the Japan Society for the Promotion of Science (Y.H. and O.K.) and an Australian Research Council Postdoctoral Fellowship (N.L.).


**Supporting Online Material**

www.sciencemag.org/cgi/content/full/318/5852/985/DC1
Materials and Methods
SOM Text
Fig. S1
Table S1
References


19 June 2007; accepted 9 October 2007
10.1126/science.1146711


# Mnemonic Function of the Dorsolateral Prefrontal Cortex in Conflict-Induced Behavioral Adjustment


**Farshad A. Mansouri,[1]* Mark J. Buckley,[2] Keiji Tanaka[1,3]**



Our cognitive abilities in performing tasks are influenced by experienced competition/conflict between behavioral choices. To determine the role of the anterior cingulate cortex (ACC) and dorsolateral prefrontal cortex (DLPFC) in the conflict detection-resolution process, we conducted complementary lesion and single-cell recording studies in monkeys that were resolving a conflict between two rules. We observed conflict-induced behavioral adjustment that persisted after lesions within the ACC but disappeared after lesions within the DLPFC. In the DLPFC, activity was modulated in some cells by the current conflict level and in other cells by the conflict experienced in the previous trial. These results show that the DLPFC, but not the ACC, is essential for the conflict-induced behavioral adjustment and suggest that encoding and maintenance of information about experienced conflict is mediated by the DLPFC.


The Wisconsin Card Sorting Test (WCST) (*1*), which has been used routinely for neuropsychological assessment, is a suitable task to examine the mechanisms of the conflict-induced behavioral adjustment. In the WCST, the relevant rule and its frequent changes are not cued, and therefore the subjects face a conflict or competition between the potential

matching rules. Patients with prefrontal cortex damage typically show impaired performance on the WCST and other tasks in which they should resolve conflict between potential rules or responses (*2–4*). We trained 16 macaque monkeys to perform a close analog of the WCST (figs. S1 and S2) (*5–7*). Four monkeys received bilateral aspiration lesions to the principal sulcus within the DLPFC, four other monkeys received bilateral lesions to the sulcal region within the ACC, and six other monkeys remained as unoperated controls (Fig. 1C). In the two remaining monkeys (M1 and M2), single-cell activity was recorded from the DLPFC.

In each trial, the monkeys were required to select which one out of three different test items matched a sample, according to the currently relevant matching rule, under one of two different levels of conflict: low conflict and high conflict. In the high-conflict condition, the sample matched one of the test items in color and another test item in shape; however, it did not match the remaining test item in either color or shape (fig. S1). Therefore, the monkeys had to resolve the competition between two potential matching rules (i.e., matching by color and matching by shape) to select the target. In the low-conflict condition, the sample matched one of the test items in both color and shape, and it did not match the other two test items in either color or shape; thus, there was no conflict between matching rules. The low- and high-conflict trials were intermingled in a random order. Trial events and the feedback were similar in high- and low-conflict conditions (figs. S1 and S2).

We examined the possible role of the ACC and DLPFC in conflict-related behavioral adjustments by comparing the postoperative behavior of monkeys with bilateral lesions within the ACC (ACC group) or DLPFC (DLPFC group) (Fig. 1C) with the behavior of intact monkeys (control group). The resulting lesions were as intended in the ACC and DLPFC lesion groups (*7*) (figs. S8 and S9).

All groups successfully performed the WCST analog, as evidenced by their abilities to make numerous switches between matching rules per session (9.9 switches per daily session in the control group as compared to 9.6 and 9.6 switches in the ACC and DLPFC groups, respectively). For all groups, we observed that the level of conflict between matching rules influenced the monkeys' behavior in current as well as in subsequent trials.

With regard to current trials, we found that, in the control, ACC, and DLPFC groups, target selection was slowed by the presence of conflict (Fig. 1A): The speed of target selection (STS), which was calculated as the reciprocal of the time between the test item onset and the first screen touch, was slower in high-conflict trials. A three-way analysis of variance (ANOVA) ["monkey" (between-subject factor) × "conflict" (low/high; within-subject factor) × "group" (control/DLPFC/ACC; between-subject factor)] applied to the normalized STS in correct trials showed that there was a significant main effect of conflict ($F_{1, 256} = 509$, $P < 1 \times 10^{-62}$), but the interaction between the conflict and group factors was not significant ($F_{2, 256} = 1.9$, $P = 0.15$) (*7*). When we used only one averaged (across sessions) normalized STS value for each monkey, no significant difference was seen in the magnitude of the STS modulation (i.e., the difference in STS between high- and low-conflict trials) between the control and ACC groups ($t_{6.4} = 0.3$, $P = 0.5$, $t$ test) or between the control and DLPFC groups ($t_{7.98} = 0.61$, $P = 0.4$). These results indicate that the modulation of STS by the current conflict level was not different between control and lesion groups.

The conflict hypothesis (*8–10*) posits that the assessment of conflict and the ensuing adjustment in control should result in enhanced resolution of conflict and improved behavioral choices in subsequent circumstances where conflict arises yet again. Consequently, in order to examine whether monkeys' performance level improved when faced with repeated high-conflict situations, we compared the monkeys' behavior in high-conflict trials that followed low-conflict trials (LH trials) with that in high-conflict trials that followed high-conflict trials (HH trials). Only correct trials that were preceded by correct trials were considered in this analysis.

We observed that, in both the control and ACC groups, the STS of the second trial in HH pairings was significantly faster than that of the second trial in LH pairings; however, no such significant difference between HH and LH pairings was seen in the DLPFC group. A three-way ANOVA ["monkey" × "previous conflict" (HH/LH) × "group"] applied to the STS showed a significant main effect of previous conflict ($F_{1, 256} = 8.4$, $P = 0.004$) and no interaction between monkey and previous-conflict factors or among monkey, previous-conflict, and group factors ($P > 0.05$). However, there was a significant ($F_{2, 256} = 3.4$, $P = 0.03$) interaction between the previous-conflict and group factors. A follow-up post-hoc test (Tukey test) showed

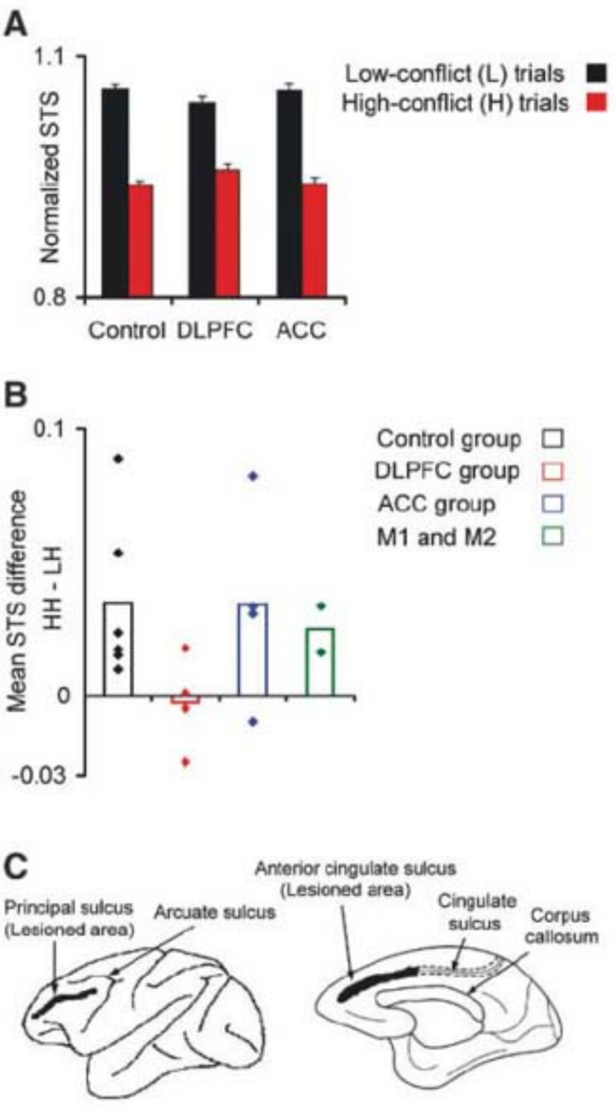


**Fig. 1.** Conflict-induced behavioral adjustments in control, DLPFC, and ACC groups. **(A)** The mean normalized STS in low-conflict (L) and high-conflict (H) trials (error bars indicate SEM). **(B)** The mean difference in STS, with respect to the second trial of HH versus LH trial sequences. Diamonds indicate the data from individual monkeys. **(C)** Black shadings show the intended lesion within the DLPFC (left) or ACC (right).

[1]Cognitive Brain Mapping Laboratory, RIKEN Brain Science Institute, Wako, Saitama 351-0198, Japan. [2]Department of Experimental Psychology, Oxford University, Oxford, OX1 3UD, UK. [3]Graduate School of Science and Engineering, Saitama University, Saitama 338-8570, Japan.

*To whom correspondence should be addressed. E-mail: farshad@postman.riken.jp

that there was a significant difference between the control and DLPFC groups ($P < 0.05$) but not between the control and ACC groups ($P > 0.9$). When we used only one averaged (across sessions) value for each monkey, there was a significant difference in the magnitude of the STS modulation (i.e., the difference in STS between HH and LH trials) between the control and DLPFC groups ($t_{7.9} = 2.44$, $P = 0.02$, one-tailed $t$ test) but not between the control and ACC groups ($t_{5.6} = 0.03$, $P = 0.5$). Figure 1B shows the mean STS modulation in the control, ACC, and DLPFC groups, as well as in the two additional monkeys (without lesions) used in the single-cell recording study (M1 and M2). These results show that, in intact monkeys and also in monkeys with lesions within the ACC, the STS was modulated by the conflict experienced in the previous trial but that this modulation was impaired after lesions within the DLPFC.

Having observed that the conflict-induced behavioral adjustment was impaired in the DLPFC lesion group, we explored the underlying neural processes by recording single-cell activity in the DLPFC of two monkeys (M1 and M2). Both monkeys successfully performed the WCST analog (fig. S2) even with the additional requirement of eye fixation, and they accrued more than 10 changes in the relevant rule per day (*7*). For both monkeys, the STS was significantly slower in high-conflict trials in all three response directions (fig. S3A), and the STS in HH trials was significantly faster than that of LH trials in all three response directions (fig. S3B).

We found that the DLPFC cell activity differed between low- and high-conflict trials in the sample and decision periods (*11*). In contrast to the lesion study, in the recording study (*7*) (fig. S2), because different samples were consistently used in the high- and low-conflict trials (fig. S4), the monkeys could know the conflict level of the trial as soon as the sample was presented. This design allowed us to compare the activity between the two conflict levels while the eye position was fixed and before the monkey had initiated its motor response. The example cell shown in Fig. 2 showed higher activities in the low-conflict trials during the sample period, regardless of the direction of the upcoming motor response. The activity difference between low- and high-conflict trials was not related to the sample identity, because higher activities were consistently observed for each of the three samples used in low-conflict conditions, and lower activities were seen for each of the seven samples in high-conflict conditions. It was also independent from the relevant rule, because the activity was higher in low-conflict conditions irrespective of the relevant rule (fig. S5).

When we applied a two-way ANOVA ("conflict" × "rule") to the activity in correct trials of 146 recorded cells, we found that 22 cells (15%) and 30 cells (21%) showed a significant ($P < 0.05$) main effect of conflict in the sample and decision periods, respectively. Only two (sample

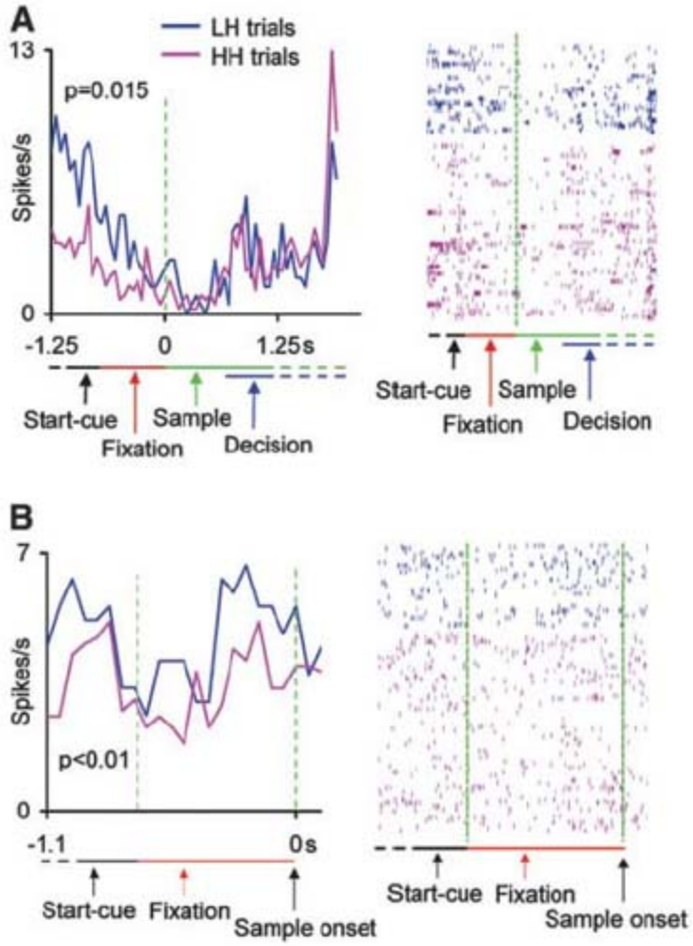


**Fig. 3.** DLPFC cell activity represented conflict experienced in the previous trial. (**A** and **B**) Activities in LH trials (blue) and those in HH trials (pink) are shown for two cells [results are shown for one cell in (A) and for the other cell in (B)]. The mean activities are aligned at sample onset. Only activities in correct trials that were preceded by correct trials were included. The $P$ values show the significance level of activity difference in the fixation period between HH and LH trials (bin width, 55 ms).

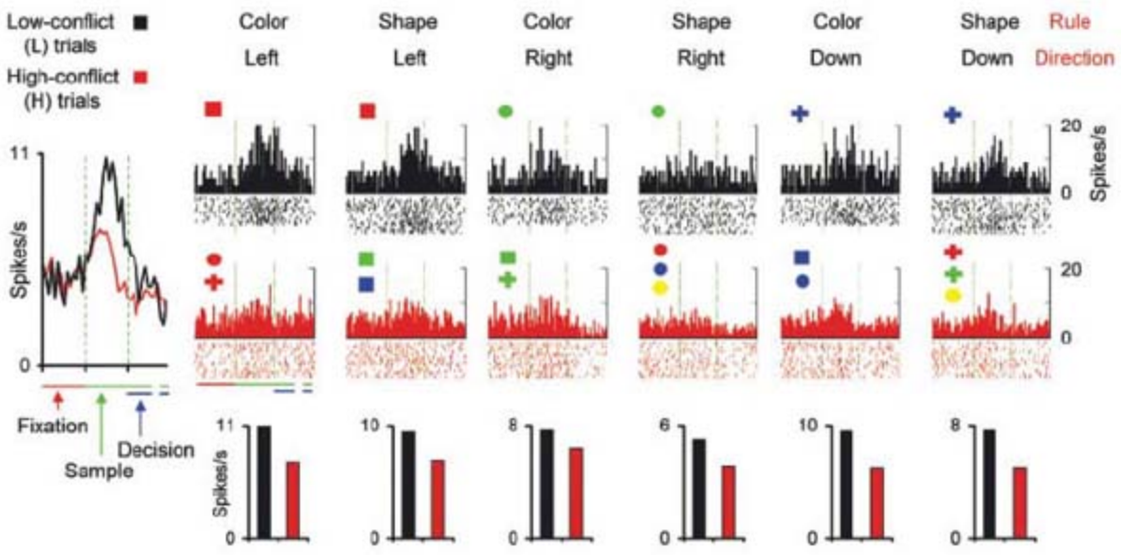


**Fig. 2.** DLPFC cell activity represented currently experienced conflict. The leftmost peri-stimulus time (PST) histogram shows activities in low-conflict (black) and high-conflict (red) trials (bin width, 55 ms). Each column shows activities in low- and high-conflict trials that required the application of the same matching rule and responses in the same direction. Left and right vertical broken lines indicate the sample onset and the onset of test items, respectively. Samples presented in each conflict condition are shown above individual PST histograms (bin width, 20 ms). Bar graphs at bottom show the mean activity in the sample period. Only correct trials were included. The recording area covered both dorsal and ventral banks of the principal sulcus.

period) and four (decision period) of the cells showed a significant interaction between the rule and conflict factors, indicating that the activity difference between low- and high-conflict trials was independent from the relevant rule (fig. S5). The activity was higher in high-conflict trials in some cells (5/22 and 14/30 cells in the sample and decision periods, respectively) and higher in low-conflict trials in others (fig. S5). Further analyses showed that the activity difference between low- and high-conflict trials was not due to selectivity for physical features of the sample stimuli (supporting online material).

The modulation of behavior in the current trial by the level of conflict experienced in the previous trial requires a purported system to hold the memory of experienced conflict across trials. The neural representation of such a memory is expected to appear in the period preceding the actual start of each trial. Thus, we also compared the cellular activity between LH and HH trials in the fixation period (a period in which the eye and hand positions of the monkey were fixed). A two-way ANOVA ("previous conflict" × "rule") showed that out of the 146 cells, 15 cells had a significant ($P < 0.025$) main effect of previous conflict or its interaction with rule. This number of cells is significantly ($P = 0.004$, binomial test) greater than the number of cells that could be obtained by chance. The activities of two examples of these cells are depicted in Fig. 3, A and B. The activity in the fixation period was higher in HH trials in 4/15 cells and higher in LH trials in 11/15 cells. Figure S6 shows the mean normalized activities of the 15 cells in preferred (i.e., whichever trial sequence, LH or HH, that had the higher activity for that cell) and nonpreferred trial sequences. At the cell population level, the activity difference between LH and HH trials could be seen during and even before the fixation period. These results suggested that DLPFC cell activities maintained, across trials, the information of the previously experienced conflict level.

Our results showed marked similarity in conflict-induced behavioral adjustment between monkeys and humans (*8*, *12*–*16*). Previous studies (*8*–*10*, *17*–*23*) have (i) shown activation of the ACC when human subjects face a conflict between behavioral choices and (ii) reported impairment of conflict-related behavioral modulations in patients with ACC lesions (*24*), which suggests the involvement of the ACC in the conflict detection-resolution process. However, humans with lesions that include the ACC do not necessarily show impairment in conflict-related behavioral modulations (*25*). We found that lesions within the ACC of the monkey did not impair the behavioral modulations that occurred after experiencing conflict in the current or previous trial. Our results indicate that, even without a functional ACC, the behavioral effects of experienced conflict can still be realized.

We observed that lesions within the DLPFC impaired the conflict-induced behavioral modulations. This suggests that in contrast to the ACC, the DLPFC plays a crucial role in mediating the behavioral effects of experienced conflict. Previous studies have shown that lesions in the principal sulcus cortex lead to impairments in short-term maintenance of spatial information (*26*–*28*). We show that the indispensable role of principal sulcus cortex in cognition extends beyond short-term storage of spatial information to support conflict-induced behavioral adjustment.

We found that DLPFC cells represented the conflict level in the current trial independently from other aspects of task, suggesting that the currently experienced conflict is encoded in DLPFC cell activity as a distinct variable. These results provide support to the hypothesis (*17*, *18*) that the DLPFC is involved in the detection of conflict.

We also found that the DLPFC cell activity maintained information regarding previously experienced conflict, and, in turn, the conflict-induced behavioral adjustment was impaired by DLPFC lesion. Based on these complementary findings, we can conclude that this region of the DLPFC is necessary for conflict-induced behavioral adjustment, and we posit that the cellular activities that we have observed in the DLPFC represent the conflict level and bring this information to bear over time to the following trial to be used in adjustment of cognitive control (*29*). In a changing environment, we need to optimize the usage of our limited cognitive resources, and the DLPFC might support an adaptive and dynamic tuning of our cognitive control processes by maintaining information of recent cognitive challenges.

### References and Notes


1. R. K. Heaton *et al.*, *Wisconsin Card Sorting Test Manual* (Psychological Assessment Resources, Odessa, FL, 1993).
2. D. T. Stuss *et al.*, *Neuropsychologia* **38**, 388 (2000).
3. A. R. Aron, S. Monsell, B. J. Sahakian, T. W. Robbins, *Brain* **127**, 1561 (2004).
4. C. M. MacLeod, P. A. MacDonald, *Trends Cognit. Sci.* **4**, 383 (2000).
5. F. A. Mansouri, K. Tanaka, *Behav. Brain Res.* **136**, 415 (2002).
6. F. A. Mansouri, K. Matsumoto, K. Tanaka, *J. Neurosci.* **26**, 2745 (2006).
7. Materials and methods are available as supporting material on *Science* Online.
8. M. M. Botvinick *et al.*, *Psychol. Rev.* **108**, 624 (2001).
9. K. R. Ridderinkhof *et al.*, *Brain Cognit.* **56**, 129 (2004).
10. W. J. Gehring, R. T. Knight, *Nat. Neurosci.* **3**, 516 (2000).
11. Firing rates were analyzed in the fixation period (600 ms, starting from 100 ms after fixation point onset), sample period (600 ms, starting from 30 ms after sample onset), and decision period (600 ms, after onset of test items). Out of 214 cells (134 from M1 and 80 from M2) that were recorded for at least six blocks, 146 cells (98 from M1 and 48 from M2) that showed significant activity modulation between the periods (sample versus fixation or decision versus fixation, $P < 0.01$, $t$ test) were included in the activity analyses.
12. T. Egner, J. Hirsch, *Nat. Neurosci.* **8**, 1784 (2005).
13. J. Lauwereyns *et al.*, *J. Exp. Psychol. Anim. Behav. Process.* **26**, 352 (2000).
14. K. Nakamura, M. R. Roesch, C. R. Olson, *J. Neurophysiol.* **93**, 884 (2005).
15. G. Gratton, M. G. H. Coles, E. Donchin, *J. Exp. Psychol. Gen.* **121**, 480 (1992).
16. T. Egner, J. Hirsch, *Neuroimage* **24**, 539 (2005).
17. M. P. Milham, M. T. Banich, E. D. Claus, N. J. Cohen, *Neuroimage* **18**, 483 (2003).
18. D. Swick, U. Turken, *Proc. Natl. Acad. Sci. U.S.A.* **99**, 16354 (2002).
19. V. van Veen, C. S. Carter, *J. Cognit. Neurosci.* **14**, 593 (2002).
20. J. D. Schall, V. Stuphorn, J. W. Brown, *Neuron* **36**, 309 (2002).
21. J. Fan *et al.*, *Neuroimage* **18**, 42 (2003).
22. C. Liston *et al.*, *Neuron* **50**, 643 (2006).
23. J. G. Kerns *et al.*, *Science* **303**, 1023 (2004).
24. G. di Pellegrino, E. Ciaramelli, E. Làdavas, *J. Cogn. Neurosci.* **19**, 275 (2007).
25. L. K. Fellows, M. J. Farah, *Brain* **128**, 788 (2005).
26. R. Levy, P. S. Goldman-Rakic, *J. Neurosci.* **19**, 5149 (1999).
27. M. Petrides, *Exp. Brain Res.* **133**, 44 (2000).
28. P. S. Goldman *et al.*, *J. Comp. Physiol. Psychol.* **77**, 212 (1971).
29. E. K. Miller, J. D. Cohen, *Annu. Rev. Neurosci.* **24**, 167 (2001).


30. This research was partly supported by a Grant-in-Aid for Scientific Research on Priority Areas from the Ministry of Education, Culture, Sports, Science and Technology of Japan; a Royal Society University Research Fellowship (M.J.B.); and a Medical Research Council (UK) program grant held by D. Gaffan (whom we also thank for support). We also thank P. G. F. Browning, H. Hoda, S. C. Kwok, M. Mahboubi, and A. Phillips for assistance with animal training in the lesion study, M. G. Baxter for assistance with anesthesia, and K. Rockland, N. Ichinohe, H. Mashiko, and Y. Abe for assistance with histology.


### Supporting Online Material

www.sciencemag.org/cgi/content/full/1146384/DC1
Materials and Methods
SOM Text
Figs. S1 to S9
References


12 June 2007; accepted 11 October 2007
Published online 25 October 2007;
10.1126/science.1146384
Include this information when citing this paper.

## Electrophysiological Guidance System

Developed to improve micro-volume injection techniques used to study connectivity and function of specific brain nuclei, the Recording Nanoject II facilitates recording of neural activity. The system enables direct displacement of neural tracer or excitotoxin from the pipet. It is engineered to mount easily on popular stereotaxic instruments and supplements instrument coordinates in guiding the placement of injections. When operated in conjunction with an extracellular amplifier, it can be used to place small volumes into targeted areas with a high degree of precision.
**Drummond Scientific** For information 800-523-7480 www.drummondsci.com

## Gel Plate Cleaner

Gelplate-clean is formulated to clean electrophoresis gel plates in a way that helps prevent poor electrophoretic migration, band distortions, and poor image development. The user simply sprays the plate and wipes it, with no need to soak plates for hours in strong and toxic solutions. It leaves no residues, while removing proteins, nucleic acids, fats, lipids, radioisotopes, and other contaminants. It is suitable for use with sequencing plates, protein gel plates, and mini gel plates.
**G-Biosciences/Genotech** For information 314-991-6034 www.GBiosciences.com

## Enhanced Image Reader Software

An enhanced version of JelMarker Image Reader Software now incorporates unique physical comparison DNA variant technology. In addition to automatically identifying gel image lands and bands, the mutation detection module of the software converts the image into a synthetic electropherogram that it then compares with a wild-type reference, thereby detecting single nucleotide polymorphisms at a sensitivity not possible with previous visual detection methodologies. JelMarker is compatible with fluorescence, chemiluminescence, and autoradiography gel image files, especially those generated by the Li-Cor 4300 DNA Analyzer and the Kodak Image Station 4000R. JelMarker can import up to two TIFF, BIP, JPEG, BMP, or TXT files for comparative analysis.
**SoftGenetics** For information www.softgenetics.com

## Literature

*Cell Signaling Application and Product Guide* includes dozens of cell signaling pathways, more than 100 pages of technical articles, an extensive troubleshooting section, and thousands of Upstate cell signaling products, including antibodies, enzymes, and kits. The range of cell-signaling research tools includes kinases, phosphatases, and G-proteins; epigenetics and chromatin function reagents; transcription factors and nuclear receptors; and multiplexing and drug-discovery services.
**Millipore** For information 800-645-5476 www.millipore.com/guides

## Solid Phase Extraction System

The MaxiLute is a 48-well solid phase extraction (SPE) system designed to bring the benefits of microplate technology to drug development, food, and environmental laboratories currently using SPE cartridges. The MaxiLute can repeatedly and precisely process up to 200 ml of sample in one go, and is up to four times faster than traditional manual SPE cartridge methods. It can be automated easily for further productivity benefits. Constructed of a single piece of high-quality molded polypropylene, the MaxiLute will not bend or distort, unlike SPE cartridges that have to be repeatedly plugged in and out. With a broad selection of packed bed volumes (250 mg to 1500 mg) and a wide choice of high performance sorbents, the MaxiLute offers the flexibility to be packed to perform optimally for almost any SPE application.
**Porvair Sciences** For information +44 1932 240255 www.porvair-sciences.com

## Stem Cell Medium

Stempro hESC SFM is a new serum-free, feeder-free medium formulated for the growth and expansion of human embryonic stem cells (hESCs). The medium has been shown to maintain these cells in a genetically normal state. It has been tested extensively and proven to keep the cells pluripotent in a number of lines, including BG01, BG02, BG03, HUES9, H1, and H9. Currently, researchers working with hESCs grow them in serum-containing undefined media using mouse or human embryonic fibroblast feeder cells. These cultures not only make it difficult to keep cells pluripotent, they are also labor-intensive and lead to challenges in scaling up cell production. The undefined nature of other cultures means scientists have a harder time controlling culture conditions and comparing results from experiment to experiment.
**Invitrogen and Novocell** For information 800-955-6288 www.invitrogen.com

## Stem Cell Passaging Tools

The StemPro EZPassage is a disposable device designed to simplify manual passaging, the process of dividing human embryonic stem cell (hESC) colonies. The new tool is designed to reduce the time required for this crucial step in stem cell research, improve the uniformity and consistency of manual passaging, and decrease the amount of training required for newcomers to the field. The ability to self-renew and continually divide is a main characteristic of embryonic stem cells. Cells replicate in culture, form colonies, and eventually outgrow the dish in which they were placed. Researchers must then "passage" the cells to a new dish to allow them to continue growing. Current manual and enzymatic passaging processes are labor-intensive, can take more than 20 minutes, and result in passaged colonies of non-uniform size. By contrast, the passaging process with StemPro EZ Passage can take less than a minute, and the resulting stem cell subcolonies are uniform.
**Invitrogen** For information 800-955-6288 www.invitrogen.com

Newly offered instrumentation, apparatus, and laboratory materials of interest to researchers in all disciplines in academic, industrial, and government organizations are featured in this space. Emphasis is given to purpose, chief characteristics, and availability of products and materials. Endorsement by *Science* or AAAS of any products or materials mentioned is not implied. Additional information may be obtained from the manufacturer or supplier.

"Scientists have to learn that it's not the science they're managing, it's the people who are doing the science that they're managing."

—Alice Sapienza, Simmons College

# Managing Scientists

Christina Hull chuckles when asked where scientists acquire their interpersonal skills. She acquired hers the same way most scientists do: They were thrust upon her when she started her laboratory at the University of Wisconsin, Madison. Suddenly she was the boss, faced with the daily challenges of motivating students, negotiating with peers in committee meetings, resolving conflicts in the lab, and a dozen other tasks that require what are broadly called "people skills."

Hull acknowledges that possessing good management ability is essential to productive scientists, but she received no formal management training prior to taking the reins. Her experience is not unusual. Fully half of U.S. postdoctoral scientists responding to a 2003 Sigma Xi survey said that they had received no training in lab or group management, and nearly all the rest had received only ad hoc or "on-the-job" training. Most wanted formal training in lab management, but only 4% had attended a workshop or done formal coursework.

"I realized there were some things I was doing that my lab expected me to do differently."

—Christina Hull, University of Wisconsin, Madison

Even established senior scientists recognize the disconnect. "Science is odd in some ways," says Robert Doms, chair of the Department of Microbiology at the University of Pennsylvania School of Medicine. "You spend all your time as a student and postdoctoral fellow learning how to be a good experimentalist. Then you become an independent scientist, and if you are successful, before long you are no longer doing experiments because you don't have any time, and personnel management becomes a major issue."

Like many scientists, Doms modeled his management style on that of his scientific mentor, Ari Helenius, a virologist at Yale University School of Medicine, whose style Doms admired. The ad hoc method can work sometimes, but it's hit-or-miss.

"There are some horrible pathologies in some labs in the relationships," says Edward O'Neil, director of the Center for the Health Professions at the University of California, San Francisco (UCSF), who offers laboratory management workshops throughout the United States. "People stay because they are inspired by the science, but they leave the training in some of these labs really wounded people. … Then they will use that as a model for leadership."

In his workshops, O'Neil tries to get scientists to change their behavior by asking them to frame a hypothesis. For example, "If I stop yelling at my technician when he makes a mistake and work together to correct the problem, he will finish experiments more quickly and completely." Then, O'Neil asks them to collect and analyze data to see if the data fit the hypothesis.

### Becoming an effective leader

Success in science is often measured by number of publications, citations, and similar metrics. But when Alice Sapienza, a chemist with a Ph.D. in organizational behavior who is now at Simmons College in Boston, Massachusetts, asked experienced scientists what qualities they most admire in a scientific leader, she got a very different answer.

Sapienza says her research suggests that the best leaders are those with the best people skills. She surveyed more than 200 scientists and engineers from the United States, Europe, and Asia, asking them to describe the most effective scientific leader they knew. Leading the list were people of "caring and compassion," followed by those who "possess managerial skills" such as effective communication and conflict resolution. Technical skill was a distant third.

Another common misperception among scientists, she says, is that managing people in a laboratory environment is somehow different from managing people in other types of workplaces. "People are people," Sapienza says. "There's a very short list of things that go wrong when people work together."

So how do you make sure those things don't go wrong? "There is no easy fix," she says. "It should not be surprising that it will take time to become an expert in the discipline of interpersonal behavior."

Carl Cohen, co-author of the book *Lab Dynamics: Management Skills for Scientists* (and a former *Science* Careers contributor), recommends taking short courses in management and reading books such as William Ury's *Getting Past No*, which he found invaluable in developing negotiation skills. There's a whole literature out there, he says, that can be very helpful.

O'Neil recommends yearly performance evaluations for everyone in the lab, including the lead investigator, using what's known as a 360-degree evaluation in which people give and get constructive feedback from supervisors and those they supervise. This kind of assessment taught Sapienza that she needed to be more explicit with her students and postdocs in setting goals and expectations.

### Formalizing training

Not long after her trial by fire at Wisconsin, Hull, a former Burroughs Wellcome Fund (BWF) Career Award recipient, got a taste of

CREDITS (TOP TO BOTTOM): GETTY IMAGES; COURTESY OF CHRISTINA HULL

# TOWARD A PHILOSOPHY OF RESOURCE MANAGEMENT

IN A COMPETITIVE RESEARCH ENVIRONMENT, THE USUAL virtues—bold ideas, solid research qualifications, a passion for discovery—can't guarantee a satisfying and lasting career. Even in an academic setting, serious researchers need financial knowledge and a businesslike attitude.

Michael McClure, former chief of the National Institute of Child Health and Human Development's Reproductive Sciences Branch, compares the modern research environment to a shopping mall in which the landlord—the university—leases space to new businesses—junior faculty members—and provides start-up assistance. The proprietor expects those fledgling operations to become self-sufficient quickly and provide a reliable source of revenue for the university. "You need to understand the principles of business and develop skills to market your business," McClure says. "In the harsh environment today, there's very little forgiveness in the system."

### A programmatic vision

Like any successful businessperson, your most important requirement is a clear plan. "It's not all about money," says Joan Lakoski, associate dean for postdoctoral education and associate vice chancellor for academic career development at the University of Pittsburgh in Pennsylvania. "It's about defining what your research goals are and then using the fiscal tools to be able to accomplish the work." "Grant reviewers will be looking for a long-term plan," agrees Maryrose Franko, senior program officer for graduate science education at the Howard Hughes Medical Institute in Chevy Chase, Maryland. "Money follows the vision."

So how do you develop a vision and a long-term plan? Your adviser probably doesn't expect you to think hard about the direction her lab ought to go in or see to day-to-day details such as preparing budgets, tracking expenses, building financially sensible collaborations, or juggling multiple funding sources, but she probably will be willing to help you learn if you express an interest.

Once your vision is in place, draw up a detailed chart of the equipment and supplies you'll need to do the work you intend to do once you're independent. Figure out where to buy it, how much it costs, and what equipment you might be able to share with other scientists.

### Funding your venture

A programmatic vision won't just help you land job offers; it will also guide your negotiations for start-up funding.

Many new faculty members are afraid to ask for too much, so instead they ask for too little, endangering their success during the critical first years of their research careers. Take the guesswork out by knowing what you need. Because you made a list, you know how much your lab will cost to start up and operate until research grants start flowing—and you can spell it out in detail for your future landlord. "You shouldn't shoot for the moon, but it does the university no good to nickel and dime you," Franko says.

When grant-writing time comes, many researchers target only funding powerhouses like the National Institutes of Health and the National Science Foundation. But it's also worthwhile to explore other possibilities

formal training when she participated in a 5-day lab management "boot camp" sponsored by BWF and the Howard Hughes Medical Institute (HHMI) in Chevy Chase, Maryland, in 2005.

"I decided to go to [the course] grudgingly," she acknowledges. "I wasn't sure it was worth a week of my time." She feared the course would be a bunch of "business-speak" that didn't apply to the issues she faced in the lab. But by the end of the course, she was glad she had come. She says she valued hearing the collective expertise of experienced scientists who had been through the same issues she faced, and she learned enough about her own personality and management style to make changes she says have improved her skills as mentor and manager.

"I realized there were some things I was doing that my lab expected me to do differently," she says. "My students pointed out that I don't manage interruptions well—that I allow them to interrupt me too much. I thought that was interesting because I was very much into my open-door policy. When I became more protective of my time, they respected my time more."

Peter Bruns, vice president for grants and special programs at HHMI, says that HHMI is unlikely to offer the lab leadership course again. Instead, the institute is trying to disseminate its model by "training the trainers": teaching the nuts and bolts of how to run such courses to a core group of 17 interested professional societies and universities that want to offer them.

**"I've become much more cognizant of what level of hands-on management people need at different stages of their training."**

—Michelle Hermiston, University of California, San Francisco

HHMI gave small seed grants to each partner and asked for evaluation data from the workshops. In aggregate, more than 90% of respondents who participated in the courses said that they would recommend them to a colleague, according to Maryrose Franko, senior program officer at HHMI.

Michelle Hermiston, a new assistant professor of pediatric hematology at UCSF, took a laboratory leadership course offered by UCSF's office of postdoctoral education this past spring. "I'm a huge cheerleader for the leadership course. I found it extremely useful, as did all of my friends who also took it," she says. She particularly appreciated the tips on how to assess work styles and how to ask difficult questions about potential weaknesses during the

CREDITS (TOP TO BOTTOM): JUPITER IMAGES; COURTESY OF MICHELLE HERMISTON

including specialized federal programs, state agencies, private foundations, industry partnerships, and community grants. Even small supplemental grants stabilize a laboratory's cash flow and support auxiliary materials, activities, or personnel that a primary grant might not. Small grants can also fund exploratory work that can lead to more significant funding later on.

Before sitting down to craft a grant proposal, it's essential to understand different funders' priorities, says James Kitchell, director of the Center for Limnology at the University of Wisconsin, Madison. The best way to gain that understanding, he says, is to read funders' strategic planning documents, study successful proposals, and talk with program officers. Program officers are eager to discuss strategic priorities with researchers; they can also advise scientists about funding possibilities at foundations and other agencies. Many funders offer online grant-writing tutorials and other lab-management tools. Some agencies host regional grant-writing workshops, and most major scientific conferences have substantive lab-management components. "As a researcher, you are an entrepreneur, and what you have to offer the marketplace is ideas," Kitchell says. "It's to your advantage to know as much about the process as possible."

Every business needs a steady and diversified supply of revenue, and a lab is no exception, so take a holistic view of your funding portfolio. One big grant is nice, but a financially healthy lab has a variety of grants, large and small, that come due at different times.

**"Grant reviewers will be looking for a long-term plan. Money follows the vision."**

—Maryrose Franko, Howard Hughes Medical Institute

**Spend wisely**

Knowing how to spend your laboratory's money is as important as knowing how to get it. A growing number of institutions provide formal financial-management training for scientists. Career-development workshops at the University of Pittsburgh, for example, help postdocs and junior faculty members prioritize research goals, develop financially manageable research programs, improve grant-writing skills, write budget justifications, and navigate fiscal policies. The Laboratory Management Institute at the University of California, Davis, offers a yearlong course for postdocs that teaches skills including writing grant proposals and protecting intellectual property.

Husbanding your resources is key. Burn through cash too quickly and you'll have to cut back on research or let people go. Play it too conservatively and you'll end up with an admirable surplus that you may not be able to roll over into the next year—along with a less-than-stellar CV.

Getting it right requires predicting how much money you'll need for the current funding period, building in overlap among multiple grants, tracking expenditures faithfully, and knowing how to save a few bucks when you can. Some tried-and-true scrimping strategies include negotiating with equipment and supply sales representatives, who are usually eager to get in on the ground floor at a new laboratory; buying used or surplus equipment online; and sharing equipment with colleagues.

**–SIRI CARPENTER**

Siri Carpenter is a freelance science writer in Madison, Wisconsin.

hiring process. "For many of us who have been trained in science, learning how to do those things can be challenging."

Hermiston says that the course has already had an effect in her lab. Her technician told her recently that she has become much more open to feedback and said how nice it has been not to have to guess what she is thinking. "I've become much more cognizant of what level of hands-on management people need at different stages of their training," she says. "It's probably changed some of my behaviors for the better in that I give and ask for feedback more often."

The United Kingdom has decided that such training should come long before a scientist finds herself running her own lab: A fundamental change is under way that aims to make "soft skills" a part of doctoral education in science. In 2002, a government-commissioned panel recommended that all science graduates receive such training. In answer to those recommendations, Research Councils UK, the nation's primary research-funding body, now disburses £21 million (about U.S. $42 million) per year to universities for professional development for graduate students and postdocs in areas such as project management, supervising others, and communicating with the public. The goal isn't to improve laboratory management per se; it is, rather, to give graduates skills that make them more attractive to potential employers in all sectors.

There is still some skepticism on the part of supervisors, and some people believe that the money would be better spent elsewhere. But the program seems to be having an effect. "We're probably about halfway there in terms of getting transferable skills into Ph.D. programs," says Iain Cameron, head of the Research Careers and Diversity Unit within Research Councils UK. "We've made a huge amount of progress since 2003, but we've still got some way to go."

Such skepticism is not confined to the United Kingdom. When Elizabeth Ellis, director of Graduate Training in Biomedical Sciences at the University of Strathclyde, U.K., gave a talk on the U.K.'s integrated-training model at an Association of American Medical Colleges meeting last year, she encountered skepticism there as well. "There seemed to be some resistance to mov[ing] towards skills-based training in the U.S., and there was little understanding of why transferable skills were needed," she writes in an e-mail.

Brian Schwartz, a physicist and vice president for research and sponsored programs at the Graduate Center of the City University of New York, has been co-teaching courses on business skills for scientists for 10 years. Schwartz says students and postdocs are often savvier than their supervisors about the need for such skills in the job market. He advises students to take such courses throughout their graduate careers. "Even while getting a Ph.D., take some other courses," he says. "A lot of students say, 'But my thesis adviser won't allow me.' I say 'Don't tell 'em.' "

"Scientists have to learn that it's not the science they're managing, it's the people who are doing the science that they're managing," says Sapienza. "Sometimes that's a quantum leap for people to understand."

**–KARYN HEDE**

Karyn Hede is a freelance writer in Chapel Hill, North Carolina.

CREDIT: CHRISTOPHER VARGAS, HHMI

## POSITIONS OPEN

### ASSISTANT PROFESSOR of BIOLOGY TWO POSITIONS: ANIMAL PHYSIOLOGIST and ECOLOGICAL GENETICIST
**Truman State University**

Position one: Assistant Professor of Biology (Animal Physiology); available August 18, 2008; nine-month, tenure-track appointment. Candidates whose research emphasizes internal physiological processes are encouraged to apply (examples include, but are not limited to reproductive physiology, endocrinology, cardiovascular physiology, and neurobiology). The successful candidate will teach junior-level physiology, sophomore-level cell biology, and upper-level elective course(s), and may teach introductory biology.

Position two: Assistant Professor of Biology (ecological genetics), available August 18, 2008; nine-month appointment, tenure-track. Candidates who possess broad training in both genetics and ecology, and whose research is at the interface of ecology and genetics are encouraged to apply. The successful candidate will teach a sophomore-level genetics course, a junior-level introduction to ecology course, and may teach introductory biology and/or an upper-level elective course(s).

Candidates for both positions should be strongly committed to maintaining both quality teaching and an active research program involving undergraduates. Successful candidates will also be encouraged to develop interdisciplinary courses and collaborative relationships with colleagues from other departments.

Required qualifications: Ph.D. in biology, or related field, by August 2008; academic preparation specifically related to animal physiology and cell biology (position one) or genetics and ecology (position two); evidence of teaching effectiveness or evidence of potential teaching effectiveness; research experience in animal physiology (for position one) or ecological genetics (for position two), as evidenced by publications in peer-reviewed venues (professional journals, successful grants); evidence of effective communication skills.

Preferred qualifications: previous experience mentoring undergraduate research students; previous teacher-scholar experience at a liberal arts institution.

Rank and salary: Assistant Professor. Salary is commensurate with experience. Truman offers a benefits package including life, health, and disability insurance, retirement contributions, and partial reimbursement for moving expenses.

More information about the positions, Truman State University, and the Biology Department can be found at **websites: http://academics.truman.edu/jobs, www.truman.edu** and **http://biology.truman.edu/.**

Application: Send a letter of application; current curriculum vitae; statement of teaching philosophy and commitment to the liberal arts and sciences and student development statement of research interests and goals; three recent letters of recommendation; and all graduate and undergraduate transcripts (copies acceptable, official copies of graduate transcripts required prior to hiring) to: **Dr. Scott Burt, Biology Faculty Search, Department of Biology, Truman State University, 100 East Normal, Kirksville, MO 63501-4221; telephone: 660-785-4597.** *Qualified applicants must be eligible to work in the United States.* Screening of applications will begin November 19, 2007, and continue until a suitable candidate is hired.

*Truman State University is an Affirmative Action/Equal Opportunity Employer committed to cultural diversity and compliance with the Americans with Disabilities Act.*

---

**POSTDOCTORAL POSITIONS in BIOPHYSICS of SIGNAL TRANSDUCTION** available at the University of Illinois-Chicago. Two positions are open immediately to study signal transduction in bacteria. Candidate should have expertise in the fields of fluorescence, total internal reflection fluorescence, single molecule biophysics, or molecular biology and biochemistry. Send curriculum vitae and names of three professional references to: **Dr. Linda J. Kenney, Department of Microbiology and Immunology, University of Illinois-Chicago, 835 S. Wolcott, M/C 790, Chicago, IL 60612.**

## POSITIONS OPEN

### FACULTY POSITION
**Gene Therapy Program**
**Lousiana State University Health Sciences Center**

The Gene Therapy Program at the Louisiana State University Health Sciences Center (LSUHSC) in New Orleans, Louisiana invites applications for open rank tenure-track faculty positions. Applicants must hold a Ph.D. and/or an M.D. degree. The position would suit an individual with interest in gene delivery and/or vaccination for modulation or prophylaxis of infectious or neoplastic disease, areas of current strength within the Program. We are particularly interested in candidates who have demonstrated translational research capacity and intramural funding is available to support developmental and ongoing translational studies. Current external funding held by Program members exceeds $23 million, mostly from the National Institutes of Health, and includes Federal and State P01 awards. The Program was founded in 2000 and is partnered with Tulane University Health Sciences Center and LSU-Shreveport in the state-funded Louisiana Gene Therapy Research Consortium (LGTRC). The Program is located in the new Clinical Sciences Research Building at LSUHSC in space adjacent to the Stanley Scott Cancer Center. The Program currently has seven faculty members, several adjunct faculty, funds three state of the art core facilities in morphology and imaging, microarray and bioinformatics and vector development, and oversees a BSL-3 facility. State-of-the-art immunology and proteomics cores have also been developed at LSUHSC. Through the LGTRC, we will have direct access to wet laboratory space in the New Orleans BioInnovation Center and a Good Manufacturing Practice Facility currently under construction that will facilitate the development of clinical trials arising from Program research. Applicants should send an e-mail including curriculum vitae to **Dr. Alistair Ramsay, Program Director** at e-mail: genetherapy@lsuhsc.edu.

*LSUHSC is an Equal Opportunity/Affirmative Action Employer.*

---

### TENURE-TRACK FACULTY POSITION
**Department of Physics**
**Morehouse College**

The Department of Physics at Morehouse College invites applications for tenure-track **ASSISTANT PROFESSOR** positions effective July 1, 2008. We seek candidates possessing a Ph.D. in physics, postdoctoral experience, and a commitment to undergraduate teaching. The succesful candidate is expected to establish a strong research program that involves undergraduates. Submit curriculum vitae and an official copy of the graduate school transcript, description of teaching experience and philosophy, description of research interests and career goals, and the names and contact information for three professional references from whom the College will request reference letters to: **The Search Committee, Department of Physics, Morehouse College, 830 Westview Drive, S.W., Atlanta, GA 30314-3773,** and must be received by December 7, 2007. For more information on the Department and College, visit our **website: http://www.morehouse.edu.** *Morehouse College is an Equal Opportunity/Affirmative Action Employer.*

---

### POSTDOCTORAL POSITIONS
**University of California, San Francisco**

(1) Embryonic stem (ES) cell commitment and differentiation into neurons (experience with mouse or ES cells required); (2) neural circuits/behavior in zebrafish (background in neurobiology required). Please send curriculum vitae and names of three references to **e-mail: peter.lu@ucsf.edu.**

National Center for Research Resources

NATIONAL INSTITUTES OF HEALTH

## Deputy Director, Clinical and Translational Research

**THE POSITION:** The National Center for Research Resources (NCRR) is seeking exceptional candidates for the position of Deputy Director, Clinical and Translational Research for the Center. The incumbent will lead NCRR efforts to integrate basic discoveries with clinical research and ensure that the resources supported by NCRR catalyze the advancement of biomedical research. He/She will advise the Director, NCRR, on the importance, policy implications, and program significance of current clinical and translational research issues, focusing on translation from basic research into pre-clinical studies and clinical trials, recommend changes in policy/operations, or follow-up actions. Areas of responsibility include sensitive biomedical and/or political issues that cut across the NIH. The NCRR provides laboratory scientists and clinical researchers with the environments and tools they need to understand, detect, treat, and prevent a wide range of diseases. www.ncrr.nih.gov This support enables discoveries that begin at a molecular and cellular level, move to animal-based studies, and then are translated to patient-oriented clinical research, resulting in cures and treatments for both common and rare diseases. This position offers a unique and exciting opportunity for an extremely capable individual to share responsibility in providing strong and visionary leadership to an organization dedicated to enhancing our understanding of health and disease, translating basic research into medical care, and improving human health. The Deputy Director, Clinical and Translational Research will be expected to represent the Director on a broad range of clinical and translational research issues related to the Center's activities before Members of Congress and their staffs, high level Government officials, leaders of national voluntary and professional health organizations, and leaders in business, science and academia.

**QUALIFICATIONS REQUIRED:** Applicants must possess an M.D., Ph.D., or equivalent degree, as well as senior-level research experience or knowledge of research programs moving research from the basic laboratory sciences into pre-clinical models and clinical trials. Candidates should be outstanding communicators and known and respected as distinguished individuals of outstanding competence. Applicants should also demonstrate the ability to think strategically, work collaboratively and use a consultative approach to problem solving and decision making.

**SALARY/BENEFITS/OTHER INFORMATION:** Salary is commensurate with experience and a full package of Civil Service benefits is available, including: retirement, health and life insurance, long term care insurance, leave and savings plan (401K equivalent). The National Institutes of Health inspires public confidence in science by maintaining high ethical principles. In addition to the Federal government's code of ethics, we have our own agency specific standards - check them out at the NIH Ethics web site. This position is subject to a background investigation.

**HOW TO APPLY:** A Curriculum Vitae, Bibliography, and two letters of recommendation must be received by **November 30, 2007**. Application packages should be sent to the **National Institutes of Health, National Center for Research Resources, ATTN: Bonnie Richards, 6701 Democracy Boulevard, Suite 1010, Bethesda, Maryland 20892**.

For further information, please call **(301) 435-0717**. All information provided by candidates will remain confidential and will not be released outside the NCRR search process without a signed release from candidates.

# Positions @ NIH

## THE NATIONAL INSTITUTES OF HEALTH

### TENURE TRACK POSITION IN IMMUNOLOGY

The Experimental Immunology Branch (EIB), Center for Cancer Research (CCR) of the National Cancer Institute (NCI), National Institutes of Health (NIH), Department of Health and Human Services (DHHS), Bethesda, MD, invites applicants to apply for a tenure track position in Immunology. The applicant should have a Ph.D., M.D. or equivalent degree, a strong record of scientific accomplishments, and the potential to establish an independent research program in any aspect of molecular or cellular immunology. The position provides salary and full funding to establish an independent research program, including laboratory space, equipment, budget, technical personnel, and support for fellows. Salary will be commensurate with education and experience. The EIB consists of 9 Principal Investigators: Alfred Singer, Triantafyllos Chavakis, Richard Hodes, Andre Nussenzweig, Paul Roche, David Segal, Stephen Shaw, Gene Shearer and Dinah Singer. Active research covers a wide range of areas of immunology including: thymic education and T cell differentiation, HIV-induced immunodeficiency, genetic recombination and chromosomal instability, inflammation biology, antigen presentation, receptor assembly and transport, signal transduction, and regulation of gene expression. Scientific interactions are encouraged and occur extensively among members of EIB as well as with other scientists at the NIH. Applicants should send a CV and bibliography, outline of a proposed research program (no more than two pages), and three letters of recommendation to **Caroline McCabe, 10 Center Drive, Bldg. 10, Room 4B36, NIH, Bethesda, MD 20892-1360**. Applications must be received by **December 15, 2007**.

### Postdoctoral Fellowship
### Experimental Transplantation and Immunology

Post-doctoral positions are available in the Experimental Transplantation and Immunology section of the National Cancer Institute in the laboratory of Dr. Dennis Hickstein. The laboratory focuses on translational research in the genetic correction of hematopoietic stem cells in animal models of human genetic diseases. Experience in molecular genetic techniques is strongly recommended. The laboratory is located on the main campus in the new Clinical Research Center in close proximity to the clinical unit, thus facilitating the clinical application of basic investigation.

The NCI offers competitive Post-doctoral stipends along with an excellent work environment. The NCI is an Equal Employment Opportunity and Affirmative Action employer that values and fosters diversity throughout the entire organization.

Interested applicants should send a CV, brief description of research interests and experience, and contact information for three references to: **Dennis D. Hickstein, M.D., Investigator, Experimental Transplantation and Immunology, Center for Cancer Research, National Cancer Institute, Bldg. 10/CRC, Room 3-3142, Bethesda, MD 20892, Email: hicksted@mail.nih.gov**.

### Postdoctoral Positions Available

The Extracellular Matrix Pathology Section of the Cell & Cancer Biology Branch, Center for Cancer Research, National Cancer Institute, National Institutes of Health, Department of Health and Human Services invites applications for two Postdoctoral Fellowship training positions. The Section's research effort focuses on the "tumor microenvironment" with particular emphasis on tumor angiogenesis and the epithelial-to-mesenchymal transition. Ongoing investigations include exploring the metalloproteinase-independent roles of the tissue inhibitors of metalloproteinases (TIMPs) in modulating the tumor-host interactions. Special emphasis is placed on understanding the role of these proteins in regulating tumor-associated angiogenesis, tumor growth and metastasis. The mechanisms of TIMPs in regulating tumor growth and angiogenesis are studied through the use of genetic mouse models, specialized in vivo angiogenesis assays, murine tumor models, flow cytometry, as well as biochemical, immuno-histochemical methods and confocal microscopy. Current projects also include the preclinical development of TIMP-derived peptides as novel cancer therapeutic agents. Experience in flow cytometry and/or scanning confocal microscopy is preferred. Postdoctoral fellowship training at the National Cancer Institute offers a unique scientific environment with significant opportunities for outstanding postdoctoral fellows to pursue innovative cancer research and provides excellent preparation for successful independent scientific careers.

Interested applicants should have a Ph.D. and/or M.D., have less than 5 years postdoctoral experience, and be either a U.S. citizen or a U.S. Permanent Resident. To apply send curriculum vitae, bibliography, cover letter with a brief description of research experience and interests, and 3 letters of references (with phone numbers) via e-mail to sstevenw@mail.nih.gov, or via post to **William G. Stelter-Stevenson, M.D., Ph.D., Cell and Cancer Biology Branch, Center for Cancer Research, National Cancer Institute, Advanced Technology Center, 8717 Grovemont Circle, Bethesda, MD 20892-4605**.

### Deputy Director, National Institute on Aging (NIA)

The Department of Health and Human Services (HHS) and the National Institutes of Health (NIH) is seeking candidates for the position of Deputy Director of the National Institute on Aging (NIA) to support NIA's mission of improving the health and well-being of older Americans by supporting and conducting high-quality research on aging processes, age-related diseases, and special problems and needs of the aged; training and developing highly skilled research scientists from all population groups; developing and maintaining state-of-the-art resources to accelerate research progress; and, developing and disseminating information, nationally and internationally, and communicating with the public and interested groups on health and research advances and on new directions for research. This position will assist the Director, NIA in coordination of all activities related to the mission and functions of the Institute, in the development and execution of plans and policies of the NIA and in the allocation of resources. Applicants may browse the NIA Home Page at http://www.nia.nih.gov for additional information on the Institute. Applicants must possess an M.D., Ph.D., or equivalent degree in a biomedical field related to the mission of NIA and have professional experience with a broad national programmatic or scientific background; have the demonstrated capability to plan and direct programs of national and international importance; and have the ability to communicate with and obtain the cooperation of public, private and national and international organizations and individuals. Salary is commensurate with qualifications and experience. Full Federal benefits available. Questions may be addressed to **Melissa Fraczkowski at kellermel@mail.nih.gov or by phone at 301-451-8413**. Application packages are to include a CV, bibliography, and statement addressing the qualifications and interest in the position. While application packages will be accepted until the position is filled, the application review process will begin in early **January, 2008**.

WWW.NIH.GOV

## Mechanistic Neuronal Cell Biology
## Tenure-Track Investigator
## Intramural Program

The Intramural Research Program of the National Institute of Neurological Disorders and Stroke invites applications from creative, interactive scientists to establish an independent research program exploring biophysical/molecular mechanisms of cellular processes in the nervous system. Candidates using a combination of structural and functional approaches interested in any area of cell biology important for nervous system function are encouraged to apply. Outstanding investigators interested in the fundamental mechanisms of membrane or cytoskeletal dynamics, or protein trafficking, are particularly of interest. New investigators will be considered at the level of tenure-track investigator, and candidates with international reputations and well-documented evidence of substantial independent accomplishments will be considered at the level of tenured senior investigator. A MD or PhD degree and at least three years postdoctoral experience are required. Laboratory facilities, start-up and sustained research funds and salary will be competitive with premier academic institutions. Applicants should send the curriculum vitae including bibliography, statement of research interests and the names of three references to: **Alan Koretsky, Scientific Director, NINDS, NIH, c/o Peggy Rollins, Building 35, Room GA908, 35 Convent Drive, MSC-3716, Bethesda, MD 20892-3716 or by email in one .pdf file to rollinsp@ninds.nih.gov. (Phone: 301-435-2232).** Applications will be reviewed beginning **November 30, 2007**.

## DEPARTMENT OF HEALTH & HUMAN SERVICES
## NATIONAL INSTITUTES OF HEALTH
## NATIONAL INSTITUTE OF MENTAL HEALTH

### Developmental Neurobiology Program

The National Institute of Mental Health (NIMH) Division of Neuroscience and Basic Behavioral Research announces an opening for a Health Sciences Administrator to guide and manage a grants program supporting basic research in developmental neurobiology. The Program Officer will lead an innovative program aimed at discovering fundamental mechanisms underlying the establishment of functional circuitry in the developing central nervous system and elucidating factors that influence neurodevelopment, especially in brain regions important for the maturation of cognitive and emotional processes implicated in psychiatric disorders. This position provides an opportunity to impact priorities, develop new research initiatives and to contribute to the advancement of a national program of neurodevelopmental research spanning molecular, cellular, physiological, and systems levels of analyses, including model systems and organisms.

Individuals are encouraged to apply who have research experience using a broad range of methods, procedures and techniques to understand the mechanisms whereby intrinsic molecules, genetic factors, and extrinsic influences impact pre- and post-natal developmental processes that determine adult brain function. General responsibilities will include administering and managing an extramural portfolio of research grants, interacting with researchers and program officers for related programs at NIMH, NIH, and other funding agencies, and developing new research initiatives.

Candidates must be U.S. citizens and have a Ph.D. equivalent degree with post-doctoral research experience relevant to developmental neurobiology. Candidates should also have experience in the grants process. The position requires working both independently and collaboratively. Strong organizational and oral and written communication skills are also required. Salary will be commensurate with experience. A full package of Civil Service benefits is available including retirement, health and life insurance, leave, and savings plan (401k equivalent).

Applications may be submitted beginning **October 9 through December 10, 2007**. Beginning October 9, official application instructions can be found at the USAJobs Web Site **(http://www.usajobs.gov)**, by searching on Vacancy Announcement **NIMH-07-222652-DE**. For further information about the application process, please contact **Ms. LaDonna Daniels (DanielsL@mail.nih.gov)** at NIH Human Resources. For more details concerning the nature of this position, please contact **Dr. Lois Winsky lwinsky@mail.nih.gov**. With nationwide responsibility for improving the health and well being of all Americans, the Department of Health & Human Services oversees the biomedical research programs of the National Institutes of Health **(http://www.os.dhhs.gov)**.

STANFORD
MATERIALS SCIENCE
AND ENGINEERING

## Stanford University
## Department of Materials Science and Engineering
## Materials for Energy Faculty Opening

The Department of Materials Science and Engineering at Stanford University invites applications for a tenure-track position at the junior (untenured) level. Applicants should hold an earned doctorate in a core engineering or science discipline and should have outstanding potential for establishing an independent research and teaching program focusing on materials for energy science and technology with connections to energy supply or demand, energy conversion or transformation, or the environmental impacts of energy.

We are especially interested in a person who would collaborate effectively with materials science faculty and students engaged in energy-related materials research, or those in other core areas of nanomaterials and biomaterials in the MSE department involving electronic, optical and photonic, magnetic, and mechanical properties. The successful candidate is expected to contribute to leadership in Stanford's multidisciplinary materials effort which spans several departments and schools, including faculty in Chemical, Electrical, Mechanical, Civil and Environmental Engineering in the School of Engineering, in Physics, Applied Physics, Chemistry and Biology in the School of Humanities and Sciences, as well as at the Stanford Synchrotron Radiation Laboratory. We seek an individual who is committed to excellence in teaching and to the mentoring of students. The successful candidate will be expected to contribute to the teaching program of the department by offering core courses in materials science, as well as by developing new curricula in their own area of specialization.

Applicants should include a summary of their educational and professional background, a current list of published work, evidence of teaching experience and the names of at least three referees who may be consulted by the search committee. An indication of how the candidate's experience matches the position described above should also be given. Applicants are encouraged to write brief descriptions of their plans for future research and how those plans might be realized in a Stanford setting, as well as to submit similar statements on teaching, focusing especially on their vision of teaching to students in the Department of Materials Science and Engineering. The appointment is expected to be made during 2008; applications should be submitted by **March 1, 2008**, to:

**Professor Reinhold H. Dauskardt**
**Chair, Search Committee**
**Department of Materials Science and Engineering**
**Stanford University**
**Stanford, CA 94305-2205**
**phone:(650) 725 – 0679**
**fax:(650) 725 – 4034**
**e-mail: dauskardt@stanford.edu**

*Stanford University is an Equal Opportunity Employer and is committed to increasing the diversity of its faculty. It welcomes nominations of and applications from women and minority groups, as well as others who would bring additional dimensions to the university's research and teaching missions.*

## FACULTY POSITIONS
## YESHIVA COLLEGE
### DEPARTMENT OF BIOLOGY

Yeshiva College, the men's undergraduate liberal arts college of Yeshiva University, invites applications for three Assistant or Associate Professor tenure-track positions in the Department of Biology to begin Fall 2008. These positions are part of the ongoing expansion and development of our department which includes new research facilities and new teaching laboratories.

Successful candidates are expected to develop vigorous, externally funded research programs involving undergraduates and to be outstanding teachers. Preferred areas of interest are neurobiology, developmental biology, and computational biology.

Review of complete applications
will begin on **January 1, 2008**.

Applicants should submit curriculum vitae, separate two-page statements of research and teaching interests, three representative publications, and arrange for three letters of recommendation to be sent to: **Biology Search Committee, Office of the Dean, Yeshiva College, 2495 Amsterdam Avenue, New York, NY 10033-3312.** EOE

Yeshiva University

THE BRAIN INSTITUTE
THE UNIVERSITY OF UTAH

## USTAR Tenure-Track Faculty Position
## Diagnostic Imaging Research

The Brain Institute at The University of Utah, Salt Lake City seeks to fill one or more tenure-track positions in diagnostic imaging research. We are particularly interested in candidates with established research programs involving the application of imaging technologies to the study of brain and spinal cord disorders. An M.D., Ph.D. or equivalent doctoral degree is required. These positions are funded by the Utah Science, Technology and Research Economic Development Initiative (USTAR). Through USTAR, the State of Utah is investing more than $15 million per year in new funds, plus additional ongoing support to recruit world-class scientists and engineers.

Interested applicants should email a CV, names of five references, a statement of research goals and statement of teaching interests to the Search Committee, USTAR Diagnostic Imaging faculty search, at brain_imaging@unite.utah.edu. Or mail to: Diagnostic Imaging Search Committee c/o The Brain Institute at The University of Utah, 383 Colorow Way, Rm. 321, Salt Lake City, UT 84108

*The University of Utah is an EO/AA employer, encourages applications from women and minorities, and provides reasonable accommodation to the known disabilities of applicants and employees.*

http://brain.utah.edu

## 2 Full-time Tenure-track Faculty Positions in Biochemistry and Organic Chemistry at the Université catholique de Louvain (Louvain-la-Neuve, Belgium) are opened (10/01/2008)

**Full-time Tenure-track Faculty Position in Biochemistry; Ref: SC/CHIM/2008/831**
**Profile:** The successful candidate will be involved in teaching mainly biochemistry and in research in biochemistry with special attention to the connection between organic chemistry and life chemistry. A multidisciplinary activity centred to bio-molecular chemistry and especially protein chemistry (structure and function) will be preferred. Collaboration with groups of the chemistry Department and/or the Institute of the Life Sciences will be an asset. Informal enquiries: **Prof. Yves-Jacques Schneider, yjs@uclouvain.be**.

**Full-time Tenure-track Faculty Position in Organic Chemistry; Ref: SC/CHIM//2008/832**
**Profile:** The successful candidate will be involved in teaching courses in general chemistry and in organic chemistry, as well as in research in organic chemistry. A multidisciplinary activity centred to organic synthesis and dealing with bio-organic chemistry and/or the study of structure-(re)activity relationship will be preferred. Informal enquiries: **Prof. Olivier Riant, riant@chim.ucl.ac.be**.

For exact application procedure, consult **http://www.uclouvain.be//en-38120.html**. Closing date: **11 January 2008**.

*The Université catholique de Louvain is committed to Equality of Opportunity in Employment.*

# FACULTY POSITIONS

## UNIVERSITY OF MICHIGAN

## MATERIALS SCIENCE AND ENGINEERING

The University of Michigan Department of Materials Science and Engineering, College of Engineering, has openings for both tenured and tenure-track faculty positions. Applicants must have a Ph.D. degree, be qualified to teach undergraduate and graduate courses in Materials Science and Engineering and are expected to develop independent and cooperative research programs. A demonstrated research record or potential is required. The preferred areas of expertise include materials for energy conversion and storage as well as photonic and phononic materials, although outstanding candidates are welcomed in all areas. We seek candidates who will provide inspiration and leadership in research and contribute actively to teaching, and are especially interested in candidates who can contribute, through their research, teaching and/or service, to the diversity and excellence of the academic community. The University of Michigan is responsive to the needs of dual career families.

**Send curriculum vitae and a list of references to:**

**Prof. David C. Martin, Chairman, Search Committee**
**Department of Materials Science and Engineering**
**The University of Michigan**
**2300 Hayward Street**
**Ann Arbor, MI 48109-2136**

*An affirmative action, equal opportunity employer.*
*The University of Michigan is a dual career-friendly institution.*

---

**Yale University** invites applications for faculty appointments at both the nontenured (tenure track) and tenured levels in its Department of Biomedical Engineering. These faculty additions represent growth of the Faculty of Engineering and the formation of unique activities uniting Yale Engineering with the Yale School of Medicine. New faculty members will collaborate with an already strong team of engineers, basic scientists, and clinical scientists providing research and education at the undergraduate and graduate levels. The areas of specialization are open, but Yale is particularly interested in candidates with research interests in biomaterials, biosensing, and biomechanics. Successful candidates will have the potential to interact with existing foci of research in biomedical imaging, biosensing, biomechanics, drug delivery, and tissue engineering.

Please send a complete CV, example publications, research/teaching plans, and the names of three references to: **Professor W. Mark Saltzman, Yale University, Department of Biomedical Engineering, P.O. Box 208284, New Haven, CT 06520**. The deadline for applications is **December 31, 2007**.

*Yale University is an Affirmative Action/ Equal Opportunity Employer and welcomes applications from women and members of minorities.*

---

UMKC
UNIVERSITY OF MISSOURI-KANSAS CITY
SCHOOL OF BIOLOGICAL SCIENCES

### Professor and Head, Division of Cell Biology and Biophysics

Applications are invited for the Head of the Division of Cell Biology and Biophysics at the School of Biological Sciences, University of Missouri-Kansas City. The successful candidate should have a proven record of sustained externally funded research, scholarly activity, and leadership potential. The candidate will be expected to participate in graduate and/or undergraduate teaching, faculty mentorship, and work closely with the Dean on decision-making matters pertaining to the growth, development and direction of the School. The School of Biological Sciences is positioning itself to become a regional leader in the areas of structural biology and molecular cell biology and welcomes applications from qualified candidates in these research areas; however, outstanding scientists from all areas of basic life sciences research are encouraged to apply. The successful candidate will receive a competitive 12-month salary, renovated research space, a start-up package commensurate with rank, and the availability of excellent research support facilities within the School of Biological Sciences. Candidates should have a Ph.D. degree and currently be in a tenured academic position at the rank of Professor.

Please direct all inquiries or nominations to **Dr. Lawrence A. Dreyfus**, Dean, School of Biological Sciences (**dreyfusl@umkc.edu**). To apply, please submit electronically (MS Word or pdf) a CV, a statement of present and future research interests, and the names and addresses of 3 references to: **dreyfusl@umkc.edu**. All materials will be handled with strict confidentiality. The position will remain open until filled.

*UMKC is an Affirmative Action/Equal Opportunity Employer.*
*Women, minorities, veterans, and individuals with disabilities are encouraged to apply.*

---

### Faculty Position
### Cell and Molecular Physiology
### The University of North Carolina at Chapel Hill

The Department of Cell and Molecular Physiology in the School of Medicine invites applications for a tenured faculty position at the level of Full Professor. This position includes full membership in the UNC Kidney Center. We seek candidates in the field of kidney physiology who will advance the field of translational kidney research and train students and postdoctoral fellows. While research will be the primary focus, this faculty member will have teaching and service obligations comparable with other full professors in the department. An attractive startup package and laboratory space is offered. Faculty members are expected to develop a strong externally funded research program and contribute to teaching graduate and medical students. Applications must hold a doctoral degree.

Please submit the names of four potential references, curriculum vitae, statement of your proposed research program, and career goals by **email** to: **research_goals@med.unc.edu; James M. Anderson, M.D., PhD, c/o Mary Wright, Executive Assistant to Chair, Department of Cell and Molecular Physiology, School of Medicine, The University of North Carolina at Chapel Hill, CB #7545, 6312 MBRB, Chapel Hill, North Carolina 27599-7545.** Closing Date: Until Filled

*UNC-CH is an Equal Opportunity Employer.*

# Dean of Engineering

The University of Delaware invites nominations and applications for the position of Dean of the College of Engineering. The Dean provides academic leadership for over 100 faculty in five departments that enroll approximately 1300 undergraduate and 500 graduate students. The College of Engineering is home to a wide range of disciplines that support world-class programs and to eight research centers; a multidisciplinary perspective is fostered and is of continued interest to the college. External funding through contracts and grants exceeds $45 million in the college. Reporting directly to the Provost, the Dean occupies a key role in the life of the University and must function effectively as part of the central administrative team, including active participation in University development activities.

The Dean should possess an outstanding academic record consistent with a senior faculty appointment, have experience in recruiting and retaining faculty of excellence, and be able to manage a complex academic enterprise. The Dean must provide vision for the college and foster both vigorous research programs and excellent undergraduate and graduate education across the breadth of disciplines within the college. An ability to develop innovative academic programs and to promote the college's interests with internal and external constituencies within the state and at the national level is important for the position. The Dean must be committed to interdisciplinary and multicultural education and have a record of promoting diversity.

With the most beautiful campus on the East Coast, the University of Delaware is a community of 15,849 undergraduate and 3,446 graduate students (www.udel.edu). It has 126 undergraduate majors, 82 master's programs and 39 doctoral programs. The University has a commitment to teaching excellence and innovation. UD is a research-extensive institution that has land grant, sea grant, urban grant and space grant status. External funding at the University exceeds $150 million.

Review of applications will begin on November 1, and will continue until the position is filled. The Dean will assume office on July 1, 2008. Nominations and expressions of interest will be held in confidence. Candidates should submit a letter of interest, a detailed resume, and the names and addresses of four references to Dean Tom Apple, Chair, Engineering Search Committee, 4 Kent Way, University of Delaware, Newark, DE 19716; or by email to engsearch@art-sci.udel.edu. For more information about the college, please visit the college's web site at www.engr.udel.edu.

***The UNIVERSITY OF DELAWARE is an Equal Opportunity Employer which encourages applications from Minority Group Members and Women.***

## THE BRAIN INSTITUTE
THE UNIVERSITY OF UTAH

### USTAR Tenure-Track Faculty Position
### Brain Circuits Research

The Brain Institute at The University of Utah, Salt Lake City seeks to fill one or more tenure-track positions in brain circuit research. We are particularly interested in candidates with established research programs in: (1) A particular circuit in the brain and its behavioral output; (2) Methods for genetic control of the activity of single cells in a circuit; and (3) Electrophysiological methods to record from such cells. An M.D., Ph.D. or equivalent doctoral degree is required. Positions are funded by the Utah Science, Technology and Research Economic Development Initiative (USTAR). Through USTAR, the State of Utah is investing more than $15 million per year in new funds, plus additional ongoing support.

Interested applicants should email a CV, names of five references, a statement of research goals and statement of teaching interests to the Search Committee, USTAR Circuits of the Brain faculty search, at brain_circuits@unite.utah.edu. Or mail to: Circuits of the Brain Search Committee c/o The Brain Institute at The University of Utah, 383 Colorow Way, Rm. 321, Salt Lake City, UT 84108.

*The University of Utah is an EO/AA employer, encourages applications from women and minorities, and provides reasonable accommodation to the known disabilities of applicants and employees.*

http://brain.utah.edu

Drexel UNIVERSITY

## FACULTY POSITION AT DREXEL UNIVERSITY
### Department of Bioscience and Biotechnology

### BIOLOGY

The Department of Bioscience and Biotechnology has tenure-track openings at the Assistant and Associate Professor Levels in the Division of Organismal, Cellular and Molecular Biology. Successful candidates will lead new growth in an expanding department that is doing dynamic research. The Assistant Professor candidates should be prepared to establish an externally funded research program. Applicants for the level of Associate Professor should have already achieved external funding and an independent research program. Candidates should be prepared to teach in both the graduate and undergraduate programs. Successful candidates should be working in the areas of cell biology of eukaryotic cells, biochemistry, stem cell biology, virology, or viral immunology.

Please send a CV, a statement of research and teaching interests, and the names of three references to:

**Chair of the Biology Search Committee**
**Department of Bioscience and Biotechnology**
**Drexel University**
**3141 Chestnut Street**
**Philadelphia, PA 19104**

**www.drexel.edu/bioscience**

*Drexel University is an Equal Opportunity/Affirmative Action Employer and encourages applications from qualified women, members of minority groups, disabled individuals, and veterans.*

Drexel UNIVERSITY

## FACULTY POSITION AT DREXEL UNIVERSITY
### Department of Bioscience and Biotechnology

### PLASMA BIOLOGY

Drexel University is searching for a biologist with experience in cell biology, especially epithelial biology or wound healing, or molecular pathogenesis. Appointment will be made at either the Assistant or Associate Professor Level. The successful candidate will be committed to develop a dedicated research program in close collaboration with an interdisciplinary research institute focusing on medical applications of electrically generated plasma. An ideal candidate will have knowledge and previous experience in the area of plasma chemistry and/or biology. Appointments at the Associate Professor level will be expected to have significant current funding in one of the described areas. Position requires a Ph.D. in an area of biology, medicine, or other plasma biology related disciplines, as well as a strong research background and a commitment to undergraduate and graduate teaching.

Please send a CV, a statement of research and teaching interests, and the names of three references to:

**Chair of the Plasma Biology Search Committee**
**Department of Bioscience and Biotechnology**
**Drexel University**
**3141 Chestnut Street**
**Philadelphia, PA 19104**

**www.drexel.edu/bioscience**

*Drexel University is an Equal Opportunity/Affirmative Action Employer and encourages applications from qualified women, members of minority groups, disabled individuals, and veterans.*

*Better thinkers;*
*Better futures*

The mission of the American University in Cairo (AUC) is to provide high quality educational opportunities to students from all segments of Egyptian society as well as from other countries, and to contribute to Egypt's cultural and intellectual life. The university offers programs at the undergraduate, graduate and professional levels as well as an extensive continuing education program. The language of instruction is English.

Founded in 1919, AUC's campus is currently located in Cairo, Egypt, but will be moving to a new, state-of-the-art campus in New Cairo beginning Fall Semester, 2008. See the New Campus website at **www.aucegypt.edu/ncd**

AUC's degree programs are accredited by the Commission on Higher Education of the Middle States Association of Colleges and Schools; Engineering programs are accredited by ABET and the Management program is accredited by AACSB. The normal teaching load is three courses per semesterand English is the language of instruction. For expatriates, benefits include housing, annual round-trip air travel for appointee and qualifying dependents, plus schooling for the equivalent of up to two children at Cairo American College. In view of AUC's protocol agreement with the Egyptian government, which requires specific proportions of Egyptian, U.S., and third-country citizen faculty, at this time preference will be given to qualified applicants who are U.S. citizens.

For more information visit our website at **www.aucegypt.edu**

The American University in Cairo is an independent, non-profit, apolitical, non-sectarian and equal-opportunity institution.

# THE AMERICAN UNIVERSITY IN CAIRO

## BIOTECHNOLOGY

The School of Sciences and Engineering has launched a new interdisciplinary Master of Science degree in Biotechnology. The School is inviting applications for a faculty position in Bioinformatics. The candidate should have a strong track record of teaching and research in bioinformatics with broad computational analysis experience including but not limited to modeling protein and DNA interactions in networks or systems and computational and statistical analysis of sequencing and microarray data. He/she is also expected to lead research activities in bioinformatics and to collaborate with the Yousef Jameel Science and Technology Research Center at AUC.

Position# BIOTECH-1-08

**Requirements:**
The candidate must hold a doctoral level degree with an educational background in biology and computer science.

The successful candidate may be a biologist with advanced degrees in information technology or a computer scientist specialized in information technology with advanced degrees in Biology.

**Additional Information:**
The faculty slot could be housed in either the Biology Department or the Department of Computer Science and Engineering.

One-, two- or three-year appointment, subject to mutual agreement will begin September 2008. Renewal of an appointment depends upon institutional needs and/or the appointee's performance.

The position will remain open until filled; however, target date for receiving applications is November 30, 2007.

**Applicants must submit the following documents via online:**
a) an updated C.V; b) a letter of interest; c) a completed AUC Personal Information Form (PIF); d) names and contact information for at least three references familiar with your professional background.

## POST DOCTORAL TEACHING FELLOWSHIPS IN ASTRONOMY, BIOLOGY, CHEMISTRY, & PHYSICS

The American University in Cairo (AUC) is pleased to announce several new Post-Doctoral Teaching Fellowships for recent Ph.D. graduates. The fellowship program is made possible by generous support from the Mellon Foundation. Successful applicants will be appointed as Post-Doctoral Teaching Fellows with the rank of visiting assistant professor, and will become part of a unique program designed to provide young scholars with the opportunity to acquire the skills and experience necessary for success in teaching. The program also supplies fellows with travel and other support for research purposes. In addition, one of its principal objectives is to provide fellows with unparalleled opportunity to observe, work in and learn about one of the most fascinating countries in the world, Egypt.

Fellows will primarily teach students engaged in AUC's freshman-level Core Curriculum. The Core is designed to introduce students to the liberal arts and sciences and includes a variety of freshman-level courses in the humanities, social sciences and sciences. Fellows will teach Core courses that reflect their personal interests and disciplinary backgrounds. They will also have the opportunity to teach additional courses in their own or related disciplines while at AUC.

**Requirements:**
Several Fellows will be appointed to AUC's program of Post-Doctoral Teaching Fellowships beginning in fall 2008.

To be eligible for appointment, applicants for Post-Doctoral Fellowships should have received their Ph.D.'s within three calendar years of the date of application. In exceptional cases A.B.D.'s will be considered. Teaching experience is not required.

**Additional Information:**
Successful applicants will hold a term of appointment for three academic years; receive support for travel associated with a job search at the end of the employment; receive special research awards of up to $5,000 per year; and participate in a monthly seminar that will provide Fellows with an opportunity to meet and exchange ideas and views with leading scholars and intellectuals from both Egypt and the wider Arab world.

**All applicants must submit the following documents via online:**
a) an updated C.V; b) a letter of interest; c) a completed AUC Personal Information Form (PIF)

For complete details and application information:

**http://aucegypt.interviewexchange.com**

## Research Faculty Position
## Division of Medicinal Chemistry and Natural Products
## The University of North Carolina at Chapel Hill
## School of Pharmacy

The University of North Carolina invites qualified scientists to apply for a Research Assistant Professor position in the Division of Medicinal Chemistry and Natural Products and Investigator in the Center for Integrative Chemical Biology and Drug Discovery.

**Roles and Responsibilities:**

- Create innovative IT and computational solutions to data creation, storage and analysis to support a team of medicinal chemists in hit discovery, SAR development and lead optimization.
- Maintain state of the art IT infrastructure and desktop tools for data visualization, analysis and decision making.
- Effectively communicate work in oral and written form for internal and external communication of Center activities.
- Collaborate effectively with scientists from across multiple disciplines.
- Contribute to an environment for interdisciplinary teamwork, constant learning and long-term excellence within the Center.

**Experience:**

- 3-5 years of IT and computational chemistry experience within the pharmaceutical industry.
- Track record of successfully enabling medicinal chemistry programs via IT and computational chemistry.
- Thorough knowledge of IT systems and computational approaches to drug discovery and structure-based drug design.
- Familiarity with basic aspects of medicinal chemistry and pharmacology with substantial knowledge of data analysis and statistical inference.
- Track record of effective publication and presentation of scientific work.

Education: Ph.D. in Computational Chemistry or Cheminformatics or demonstrated equivalency through primary authorship in peer-reviewed journals.

Applications will be reviewed upon receipt and continue until the position is filled. Applications must include: curriculum vitae, and two letters of recommendation to be sent directly to the search committee, on your behalf. Contact: **Prof. Stephen V. Frye, PhD, Chair of the Search Committee, Division of Medicinal Chemistry and Natural Products, School of Pharmacy, University of North Carolina at Chapel Hill, CB #7360, Beard Hall, Chapel Hill, NC 27599-7360; www.pharmacy.unc.edu.**

*The University of North Carolina at Chapel Hill is an Equal Opportunity Employer. Women and members of under-represented minority groups are especially encouraged to apply.*





## POSITIONS OPEN

### RESEARCH LABORATORY DIRECTOR

Looking for Research Laboratory Director at Carilion Clinic in Roanoke, Virginia dedicated to immunology, genomics, and cell biology. Will be responsible for research collaboration, oversight of the laboratory, training staff, maintaining the tissue bank. Terminal degree required with five to ten years of experience. To apply, visit website: http://www.carilion.com, for more information e-mail: cboyd@carilion.com.

### UNIVERSITY of CALIFORNIA, RIVERSIDE

**ASSISTANT COOPERATIVE EXTENSION SPECIALIST, ASSISTANT ENTOMOLOGIST, INVASIVE SPECIES ECOLOGY, University of California (UC), Riverside.** Position available July 1, 2008, 11-month, 25 percent organized research, 75 percent cooperative extension. Appointment level and salary commensurate with experience. Ph.D. in entomology or related discipline required. The successful candidate must have strong training and experience with modern approaches to the study of ecology suitable for application to management and control of invasive arthropod pests in urban, natural, and agricultural environments. A program of research could include basic and applied ecological studies of plant-herbivore-natural enemy interactions, studies of classical biological control, and integrated pest management of invasive species.

The study of invasion processes, methods of eradicating or limiting the spread of incipient populations, community ecology of host and natural enemy systems, metapopulation dynamics, and the long-term persistence of hosts/prey and parasitoids/predators at low population density levels, and nontarget effects of introduced biological control agents. It is expected that the successful individual will extend the results of the research program as well as research efforts of other scientists through educational programs to a variety of clientele including UC Cooperative Extension Advisors, pest control advisors, urban natural resource and landscape managers, commercial growers, and home owners. Send curriculum vitae, transcripts, statement of research interests, reprints, manuscripts in press, and have four letters of recommendation sent by January 31, 2008 to: **Dr. John T. Trumble, Search Committee Chair, Department of Entomology, University of California, 3401 Watkins Drive, Riverside, CA 92521; e-mail: john.trumble@ucr.edu; telephone: 951-827-5624.** This position will remain open until filled. Information about the Entomology Department and an expanded position description can be found on the **website: http://www.entomology.ucr.edu.**

*The University of California is an Equal Opportunity/Affirmative Action Employer.*

### TWO TENURE-TRACK ASSISTANT PROFESSORS POPULATION GENETICIST and PLANT ECOLOGIST/TAXONOMIST

Applications are encouraged from candidates with a Doctorate and at least two years of postdoctoral experience in (1) population genetics and (2) plant ecology or plant taxonomy. Successful candidates are expected to participate in undergraduate and graduate teaching and to develop an externally funded research program. Send letter of application, academic transcripts, statements of research interests and teaching philosophy, curriculum vitae, along with names and contact information for five references to: **Cynthia Mondragon, School of Biological Sciences, Ross Hall, P.O. Box 92, University of Northern Colorado, Greeley, CO 80639.** For details see **website: http://www.unco.edu/nhs/employment/.** For questions, contact the **Search Chair** at **e-mail: tony.schountz@unco.edu.** Review of applications begins November 30, 2007. *UNC is an Affirmative Action Equal Opportunity Employer.*

# Chair
# Department of Microbiology & Immunology
# Emory University School of Medicine

Emory University School of Medicine invites nominations and applications for the position of Chair of the Department of Microbiology & Immunology (http://www.microbiology.emory.edu/).

This is an outstanding opportunity to lead a premier basic science department with established strengths in research and training. The Department maintains a dynamic research-intensive environment that provides excellent opportunities for pre- and postdoctoral training and offers effective educational programs for Medical students and Physician Assistants students. On a national level, the department is currently ranked #7 in total NIH funding in the US and Canada, and due to steady gains in research funding has maintained a consistent presence as a top ten leading department in the fields of microbiology, immunology and vaccinology research.

The Department also holds a unique position due to extensive interactions and collaborations with the Centers for Disease Control (CDC), directly adjacent to Emory, and other external institutions in the local area; its strong interdepartmental links and collaborations, and its participation in interdisciplinary research programs and centers such as Emory Vaccine Center, Influenza Pathogenesis and Immunology Research Center and the Center for AIDS Research. The Department is also making significant contributions to Global Health. Atlanta has a reputation as a powerhouse for Global Health, and this just got another boost with the establishment of a new $110 million funded Global Health Institute at Emory. The institute will work globally to cure disease, develop vaccines, develop health infrastructures, expand research collaborations and train scientists and students. The Department has also benefited through funding of a vaccine partnership with the International Center for Genetic Engineering and Biotechnology in New Delhi, India and a consortium that includes the School of Medicine's new NIH-funded Center for Excellence for Influenza Research and Surveillance and the Harbin Veterinary Research Institute in China.

We seek an individual with outstanding leadership capabilities, proven academic and administrative experience, the vision to build and sustain programs at the forefront of microbiological and immunological research, and a commitment to excellence. Candidates must have demonstrated leadership in research, education, and administration. Salary and benefits are highly competitive.

Applicants should submit a letter of interest and a current curriculum vitae along with names and addresses of three references via email to MWILL26@emory.edu

*Emory University is an equal opportunity/affirmative action employer and encourages the application and nomination of qualified minority and female candidates.*

EMORY UNIVERSITY SCHOOL OF MEDICINE

UNC PHARMACY

## Research Faculty Position
## Division of Medicinal Chemistry and Natural Products
## The University of North Carolina at Chapel Hill School of Pharmacy

The University of North Carolina invites qualified scientists to apply for a Research Associate or Assistant Professor position in the Division of Medicinal Chemistry and Natural Products and Investigator in the Center for Integrative Chemical Biology and Drug Discovery.

**Roles and Responsibilities:**

- Direct the synthetic and medicinal chemistry efforts of a team of research associate chemists in the progression of novel biological targets of therapeutic relevance through the hit discovery to lead optimization stage of drug and/or tool compound discovery.
- Evaluate novel biological targets for tractability and validity.
- Create innovative chemical plans for efficient development of structure-activity relationships and optimization of 'drug-like' physicochemical properties.
- Maintain state of the art laboratory for parallel organic synthesis, characterization and purification of small organic compounds.
- Effectively communicate work in oral and written form for internal and external communication of Center activities.
- Collaborate effectively with scientists from across multiple disciplines.
- Develop innovative and fundable proposals for target progression and exploration of chemical biology of target systems within the Center.
- Contribute to an environment for interdisciplinary teamwork, constant learning and long-term excellence within the Center.

**Experience:**

- 5-15 years of medicinal chemistry experience within the pharmaceutical industry.
- Extensive track record of successful hit discovery and lead optimization as demonstrated by contribution to selection of drug candidates for development.
- Thorough knowledge of organic synthesis and parallel approaches to preparation, characterization and purification of organic compounds.
- Familiarity with basic aspects of cell biology and pharmacology with substantial knowledge of assay development, compound profiling and data analysis.
- Track record of effective publication and presentation of scientific work.
- Supervisory experience with a demonstrated ability to develop other scientists within the discipline of organic and medicinal chemistry.

**Education:** Ph.D. in Organic or Medicinal Chemistry or demonstrated equivalency through primary authorship in peer-reviewed journals.

Applications will be reviewed upon receipt and continue until the position is filled. Women and members of under-represented minority groups are especially encouraged to apply. Applications must include: curriculum vitae, and two letters of recommendation to be sent directly to the search committee, on your behalf. Contact:

**Prof. Stephen V. Frye, PhD**
**Chair of the Search Committee**
**Division of Medicinal Chemistry and Natural Products**
**School of Pharmacy, University of North Carolina at Chapel Hill**
**CB #7360, Beard Hall**
**Chapel Hill, NC 27599-7360**

**www.pharmacy.unc.edu**

*The University of North Carolina at Chapel Hill is an Equal Opportunity Employer. Women and members of under-represented minority groups are especially encouraged to apply.*

## POSITIONS OPEN

### JAMES BUCHANAN BRADY UROLOGICAL INSTITUTE
### The Johns Hopkins Hospital

The Department of Urology of the Johns Hopkins University School of Medicine is seeking applications from outstanding scientists for a new faculty position in the areas of stem cell biology and engineering, or developmental biology. This is a full-time tenure-track position, expected to start as an **ASSISTANT PROFESSOR,** but the rank will be commensurate with experience. Applicants should have a doctoral degree and substantial postdoctoral experience, and be committed and able to develop an independent, extramurally funded research program. Candidates with established funding support are preferred.

Please forward letters of application, with curriculum vitae and names/addresses of at least three references to:

**Robert H. Getzenberg, Ph.D.**
**Director of Urological Research**
**James Buchanan Brady Urological Institute**
**The Johns Hopkins Hospital**
**600 North Wolfe Street**
**Marburg 121**
**Baltimore, MD 21287**

*The Johns Hopkins University is an Equal Opportunity Employer and does not discriminate on the basis of race, color, gender, religion, age, sexual orientation, national or ethnic origin, disability, marital status, veteran status, or any other occupationally irrelevant criteria. The University promotes Affirmative Action for minorities, women, disabled persons, and veterans. The Johns Hopkins University is a smoke-free environment and as such, prohibits smoking in all facilities. The Johns Hopkins University is a drug-free workplace.*

---

California State University, San Marcos seeks an **ANIMAL PHYSIOLOGIST** for a tenure-track **ASSISTANT PROFESSORSHIP** beginning fall 2008. Applicants must have a Ph.D. in the biological sciences with training and research in physiology. All subdivisions of physiology will be considered; however, researchers who focus on invertebrate systems are especially encouraged to apply. Postdoctoral research and previous teaching experience is preferred. The successful applicant will have a strong commitment to undergraduate education and should have a demonstrated ability or potential to effectively instruct undergraduate and graduate students, establish community partnerships, and develop an independent research program with undergraduate and graduate students. Teaching responsibilities will include some combination of a biology major core physiology course, upper-division physiology electives (preferably with a laboratory section), upper-division general education courses, and graduate/advanced undergraduate courses in candidate's area of expertise. For position details and application instructions, please see our **website: http://www.csusm.edu/A_S/FacSearches.** Screening of applications will begin in January 2008, and continue until position is filled. *California State University, San Marcos is an Affirmative Action/Equal Opportunity/Title IX Employer. The University has a strong commitment to the principles of diversity and, in that spirit, seeks a broad spectrum of candidates including women, members of minority groups, and people with disabilities.*

---

**ASSISTANT PROFESSOR, University of California, Davis.** Tenure-track faculty position associated with the Foods for Health Initiative in Department of Chemical Engineering and Materials Science and Department of Food Science and Technology in biochemical engineering, biomaterials, biophotonics, food engineering, biochemistry, or a related field. Applicants are expected to hold a Ph.D. in a relevant area. Apply at **website: http://www.chms.ucdavis.edu/employment/.** The position is open until filled; but to assure full consideration, submit applications no later than December 3, 2007. Start date of July 1, 2008. *UC Davis is an Affirmative Action/Equal Employment Opportunity Employer and is dedicated to recruiting a diverse faculty community. We welcome all qualified applicants to apply, including women, minorities, individuals with disabilities, and veterans.*

## POSITIONS OPEN

UAF UNIVERSITY OF ALASKA FAIRBANKS

The School of Fisheries and Ocean Sciences (SFOS) at the University of Alaska Fairbanks (UAF) invites applications for two **MARINE BIOLOGIST** vacancies specializing in early life ecology and mammalogy/population genetics. Both positions are **ASSISTANT/ASSOCIATE PROFESSOR,** tenure-track faculty positions within the SFOS Institute of Marine Science located in Fairbanks, Alaska. To learn more about the School please visit **website: http://www.sfos.uaf.edu.** Complete position information can be found at **website: https://www.uakjobs.com,** reference postings 0054202 and 0054183.

---

### FACULTY POSITION in INFECTIOUS DISEASES
### Fred Hutchinson Cancer Research Center and the University of Washington

The Fred Hutchinson Cancer Research Center (FHCRC) and the University of Washington (UW) are jointly recruiting a full-time faculty position at the **ASSISTANT or ASSOCIATE MEMBER/PROFESSOR** level for a faculty position in the Program in Infectious Diseases in the Clinical Research Division of the FHCRC and the Division of Allergy and Infectious Disease at the UW, with preference being given to those who study fungal diseases. A Doctorate degree is required. The individual will be expected to develop independent research programs. University of Washington faculty engage in teaching, research, and service. Excellent collaborations are available with scientists in clinical, molecular medicine, and basic sciences at the FHCRC and the UW. Salary depends on experience and excellent benefits. Interested candidates may submit curriculum vitae, a concise statement of their research plan, and three reference letters to:

**Lawrence Corey, M.D.**
**Head, Program in Infectious Diseases**
**Fred Hutchinson Cancer Research Center**
**1100 Fairview Avenue N., LE-500**
**P.O. Box 19024**
**Seattle, WA 98109**

Application review will continue until the position is filled.

*The University of Washington and the Fred Hutchinson Cancer Research Center are Affirmative Action, Equal Opportunity Employers, dedicated to the goal of building a culturally diverse and pluralistic faculty and staff committed to teaching and working in a multicultural environment, and strongly encourage applications from women, minorities, individuals with disabilities, and covered veterans.*

---

### POSTDOCTORAL RESEARCH ASSOCIATE

Texas Tech University Health Sciences Center in Lubbock, Texas, has two positions available for a Postdoctoral Research Associate. The two Postdoctoral positions are available to conduct research on molecular and immunological aspects of helminth parasites with special emphasis on DNA vaccines for schistosomes. Another area of interest is aging genes in nematodes. A Ph.D. degree and experience in the field of molecular biology or immunology is required. Salary will be based on qualifications and experience. For additional information and to apply, log on to **website: http://jobs.texastech.edu** and refer to requisition numbers 74647 and 74648. In addition to applying online, please send resumes along with contact information of three references to: **Afzal A. Siddiqui, Ph.D., Microbiology and Immunology, Texas Tech University Health Sciences Center, 3601 4th Street, Mail Stop 6591, Lubbock, TX 79430-6591; telephone: 806- 743-2638 (office); fax: 806-743-2334; e-mail: afzal.siddiqui@ttuhsc.edu.** *TTUHSC is an Equal Employment Opportunity/Affirmative Action Employer*

## POSITIONS OPEN

### FACULTY POSITION in BIOCHEMISTRY
### University of California, San Diego

The Department of Chemistry and Biochemistry of University of Californina, San Diego **(website: http://www-chem.ucsd.edu)** invites applications for a tenure-track faculty position in biochemistry. Candidates must have a Ph.D. and a demonstrated ability for creative research and teaching at the undergraduate and graduate levels. The Department will consider applicants whose research applies experimental methods of structural analysis to biopolymers and their functional complexes, including nuclear magnetic resonance or other types of spectroscopy, diffraction, or microscopy, or combinations of these methods. Salary is commensurate with qualifications and based on University of California pay scale. Applicants are asked to submit materials online at **website: http://www-chem.ucsd.edu/recruit/index.cfm?addno-4-984.** Materials include a cover letter, curriculum vitae, complete list of publications, samples of published research, and statement of your teaching experience. Please arrange for three reference letters to be mailed directly by references to: **Chair, Biochemistry Search Committee, 4-984, University of California, San Diego, Department of Chemistry and Biochemistry, La Jolla, CA 92093-0332.** The deadline for applications is December 1, 2007, but until position is filled, all applications received will be assured full consideration. *UCSD is an Equal Opportunity/Affirmative Action Employer with a strong institutional commitment to the achievement of diversity.*

---

### FACULTY POSITIONS in THEORETICAL PHYSICAL CHEMISTRY
### University of California, San Diego

The Department of Chemistry and Biochemistry of the University of California, San Diego **(website: http://www-chem.ucsd.edu)** seeks applications for a tenure-track faculty position in theoretical physical chemistry. Candidates whose research interests are interdisciplinary are especially encouraged to apply. Candidates must have a Ph.D. in physical chemistry or a related field with a substantial record of research accomplishment and an innovative research plan. The successful candidate will be expected to teach at both the graduate and undergraduate levels. Salary is commensurate with qualifications and based on University of California pay scale. Applicants are asked to submit a cover letter, curriculum vitae, complete list of publications, samples of published research, and a statement of their teaching experience, online at **website: http://www-chem.ucsd.edu/recruit/index.cfm?addno=4-986.** Please arrange for three reference letters to be mailed directly by references to: **Chair, Physical Search Committee 4-986, Department of Chemistry and Biochemistry, University of California, San Diego, 9500 Gilman Drive, Mail Code 0332, La Jolla, CA 92093-0332.** The deadline for applications is December 1, 2007, but until the position is filled, all applications received will be assured full consideration. *UCSD is an Equal Opportunity/Affirmative Action Employer with a strong institutional commitment to the achievement of diversity.*

---

### The HEISER PROGRAM for RESEARCH in LEPROSY and TUBERCULOSIS

Beginning **POSTDOCTORAL RESEARCH FELLOWSHIPS** in leprosy and tuberculosis available at a stipend level of $40,000, and research grants in leprosy only in amounts ranging from $50,000 to $180,000.

Applicants should have M.D., Ph.D., or equivalent degree. Application deadline March 3, 2008, for awards to be activated August through December 2008. For information and forms, see **website: http://www.NYCommunitytrust.org.** Click on Grantmaking and select Special Programs. For questions or problems with application forms, **e-mail: lm@nyct-cfi.org.**

## POSITIONS OPEN

### ASSISTANT to ASSOCIATE PROFESSOR of SURGERY (RESEARCH) INFLAMMATION RESEARCH SCIENTIST
**Brown Medical School**
**Rhode Island Hospital**

The Department of Surgery at Brown University announces a research faculty position at the Assistant or Associate Professor level in inflammation and tissue injury. Research areas of interest to the Department include cellular molecular mechanisms of inflammation after injury or surgery. Candidates should have a Ph.D. and/or M.D. and at least two years of postdoctoral experience, preferably with a background in cell biology and immunology. Scientists pursuing basic research and/or clinical efforts in inflammation relevant to surgical critical care are encouraged to apply.

For a current listing of the Division of Surgical Research or the Department of Surgery members and their research interests, please visit **website: http://bms.brown.edu/surgery/research.**

All applications received by December 30, 2007, will be given full consideration. Please submit curriculum vitae, a set of representative reprints, and a concise description of research interests and goals. In addition, arrange for three letters of reference to be submitted on your behalf.

**Alfred Ayala, Ph.D.**
**c/o Ms. Courtney Coto (e-mail: ccoto@lifespan.org)**
**Professor of Surgery (Research)**
**Division of Surgical Research/Department of Surgery**
**Rhode Island Hospital/The Warren Alpert Medical School at Brown University**
**Aldrich 230, 593 Eddy Street**
**Providence, RI 02903**

*Review of applicants will begin immediately and continue until a candidate is selected or the search is closed. Rhode Island Hospital is an Equal Opportunity/Affirmative Action Employer and actively solicits applications from minorities, women, and protected persons.*

---

### CONSERVATION BIOLOGIST
**Desert Botanical Garden, Phoenix, Arizona**

Research position in one of the world's major botanical gardens specializing in desert plants. The successful applicant will include molecular genetics approaches in research on conservation biology of plants in arid regions. Responsibilities include conducting original research, seeking extramural funding, and cooperating with other departments in the development of exhibits and educational programs. Ph.D. required. Send curriculum vitae and a one-page description of research approaches and goals, along with names and contact information of three references to: **Ms. Mary Catellier, Director of Human Resources, Desert Botanical Garden, 1201 N. Galvin Parkway, Phoenix, AZ 85008.** Review of applications will begin January 15, 2008, and applications will be accepted until position is filled. *An Equal Opportunity Employer.*

---

A **POSTDOCTORAL POSITION** is available to study the role of caspase-2 in the interaction between apoptosis and aging. Research interests center on the development and use of novel instrumentation to observe real time caspase-2 activity in living cells, tissues, and small animals. A new multiphoton fluorescence lifetime optical imaging system using streak camera detection will be the major technology employed. A Ph.D. preferably in the biophysical sciences with experience in optical microscopy is desired. Send curriculum vitae and three letters of recommendation to: **Dr. Brian Herman, Professor, Cellular and Structural Biology, University of Texas Health Science Center, 7703 Floyd Curl Drive, Mail Code 7763, San Antonio, TX 78229-3900; e-mail: hermanb@uthscsa.edu; website: http://www.uthscsa.edu/research/.** *The University of Texas Health Science Center in San Antonio is an Equal Opportunity/Affirmative Action Employer.*

## POSITIONS OPEN

OHIO UNIVERSITY

The Department of Biomedical Sciences at the Ohio University College of Osteopathic Medicine invites applications for an 11-month appointment as a tenure-track **ASSISTANT/ASSOCIATE PROFESSOR in PHYSIOLOGY.** This individual will be expected to establish and maintain an active, externally funded research program. Collaborations are desirable in the College's areas of strength. Please visit our website for more information **(website: http://www.oucom.ohiou.edu/dbms).** The successful candidate should be broadly trained in systems physiology to enable participation in the delivery of our integrated medical curriculum.

A Ph.D. (or equivalent) and a minimum of two years of postdoctoral training are required. Salary will be commensurate with experience. To apply, curriculum vitae and statements of research and teaching interests and experience must be submitted online at **website: http://www.ohiouniversityjobs.com/applicants/Central?quickFind=53605.** Also mail three representative papers, and arrange to have three letters of recommendation sent to: **Sharon Inman, Ph.D., Biomedical Sciences, 228 Irvine Hall, Ohio University, Athens, OH 45701.** For questions about the position, contact **Dr. Inman** at **e-mail: inmans@ohio.edu.** Position will remain opened until filled; for full consideration apply by December 1, 2007. *We seek a candidate with a commitment to working effectively with students, faculty, and staff from diverse backgrounds. Ohio University is an Affirmative Action, Equal Opportunity Employer with a Dual Career Network* ***(website: http://www.ohio.edu/dual).***

---

### PLANT EVOLUTION and BIODIVERSITY
**Harvard University**
**Department of Organismic and Evolutionary Biology**

The Department of Organismic and Evolutionary Biology (OEB) at Harvard University invites applications for a **TENURE-TRACK FACULTY POSITION** in plant evolution and diversity. We seek to appoint an individual who uses phylogenetic approaches to address fundamental questions regarding the origin and maintenance of diversity in plant lineages and/or communities. Researchers focused on noncore eudicot lineages such as monocots, gymnosperms, nonseed land plants, and algae are especially encouraged to apply. Applicants will be expected to develop an innovative research program and contribute to teaching at the undergraduate and graduate levels. Applications from, or information about, female and minority candidates are encouraged. This search is part of a broader initiative to develop comprehensive research programs in plant biology and evolution at Harvard University. The Department has strong linkages to a number of allied institutions, including the Harvard Forest, Arnold Arboretum, Harvard University Herbaria, and Harvard Centre for the Environment.

Applicants should submit the following application materials online (to **website: http://www.lsdiv.harvard.edu/oeb/facultysearch/peb**): curriculum vitae, statements of research and teaching interests, and representative publications; and arrange for three references to be uploaded to the website. Letters of nomination from third parties are also welcome and may be sent via e-mail to: **Elena M. Kramer, Professor of Biology, c/o Katie Parodi, e-mail: kparodi@oeb.harvard.edu.** Review of applications will begin on December 15, 2007.

Further information about OEB is available at **website: http://www.oeb.harvard.edu;** information about the ongoing Plant Biology Initiative at Harvard can be found at **website: http://www.pbi.fas.harvard.edu.**

*Harvard University is an Affirmative Action/Equal Opportunity Employer.*

## POSITIONS OPEN

### INTERDISCIPLINARY SCIENTIST RESEARCH GEOLOGIST/BIOLOGIST
**Department of Paleobiology**
**National Museum of Natural History**
**Smithsonian Institution**

The Smithsonian's National Museum of Natural History seeks a **PALEONTOLOGIST** to conduct an integrative, collections-based research program in nondinosaurian vertebrates. The successful candidate is expected to utilize modern methods in pursuing research in one or more of the following areas of emphasis: evolution, paleoecology, morphology, phylogenetics, or biogeography. Frequent publication in peer-reviewed journals in specialty areas is expected, as is curation of appropriate collections and participation in the scientific community in a manner commensurate with emerging leadership in the area of specialty.

The position is initially a four-year appointment and will be filled at the GS-12 level (salary range is $66,767 to $86,801 per year, commensurate with experience.) Reference specific application procedures in actual announcement; see **website: http://www.sihr.si.edu** or contact **Audrey Davis** at **telephone: 202-633-6298.** The announcement will open on October 17, 2007. Applications must be received by November 28, 2007, and must reference announcement number: 08-AD-293537-JNT-NMNH (category rating). This is an interdisciplinary position to be filled by either a Research Geologist or a Research Biologist, depending upon the applicant's primary discipline. All applications will be notified by e-mail or telephone when their application is received. *U.S citizenship is required. The Smithsonian Institution is an Equal Opportunity Employer.*

---

### STEM CELL INITIATIVE
**University of North Carolina at Chapel Hill**

The University of North Carolina at Chapel Hill invites applications for two academic positions at the **ASSISTANT PROFESSOR** level in stem cell biology. The targeted faculty hirings are part of a Stem Cell Initiative to expand our Program in the areas of stem cell translational research. Each successful candidate will be expected to develop a vigorous, externally funded research program based on fundamental questions related to the biology of embryonic or adult stem cells. Specific areas include: (1) Research exploring the molecular regulation of embryonic stem cell pluripotentiality and differentiation, including genomic remodeling and nuclear reprogramming. (2) Active research programs focused on defining the potential of both embryonic and adult stem cells in the treatment of neurological diseases.

Applicants should have a Ph.D. or M.D./Ph.D. degree. Electronic copies of curriculum vitae, letter of interest with description of past research/future plans to **e-mail: larysa_pevny@med.unc.edu.** Four letters of recommendation (hard copy) should be sent to:

**Dr. Larysa Pevny**
**University of North Carolina at Chapel Hill**
**8109b Neuroscience Research Building**
**Campus Box #7250**
**Chapel Hill, NC 27599-7250**

*Application deadline: open until filled. The University of North Carolina at Chapel Hill is an Equal Opportunity/ADA Employer. Women and minorities are encouraged to apply.*

---

**ASSISTANT PROFESSOR in ENVIRONMENTAL CHEMISTRY, Southern Illinois University, Edwardsville.** The Department of Chemistry and the Environmental Sciences Program invite applications for a tenure-track appointment to begin in August 2008. We are a comprehensive state university offering a wide variety of undergraduate and masters programs. A Ph.D. is required; postdoctoral experience is desired. Application procedures are found at **website: http://www.siue.edu/CHEMISTRY/EnvChemSearch.** Evaluation of candidates will begin January 16, 2008.

## POSITIONS OPEN

The Department of Population Health at the University of Georgia is seeking outstanding candidates with a Ph.D. for a tenure-track faculty position at the rank of **ASSISTANT/ASSOCIATE PROFESSOR** in the area of molecular virology. The D.V.M. degree in addition to a Ph.D. is a plus. Preference will be given to those with research interests in negative-stranded RNA viruses. The applicant is required to have a Ph.D. in a biological science or a related field and should ideally have three to five years of postdoctoral experience in molecular virology, including viral molecular biology, virus structure, host-pathogen interactions, and virus evolution. Experiences in cellular biology would be valuable. Ideally, the candidate should have a record of extramurally funded independent research as evidenced by peer-reviewed publications.

The successful candidate will be expected to establish an independent and externally funded research program focused on poultry diseases and develop a graduate level course in general virology with the focus on animal viruses. Thus, experience in teaching at the undergraduate and graduate level is desirable.

In addition, the faculty member is expected to work as a team member and collaborate within the Department providing support to clinical faculty and field veterinarians, with the aim of solving disease problems in the poultry industry.

The position is located at the Poultry Diagnostic and Research Center (PDRC). The PDRC is a unit within the College of Veterinary Medicine totally focused on research, service, and instruction programs related to the poultry industry. The environment is highly interactive and productive with close ties to all basic science departments, federal research facilities, and other academic institutions nearby **(website: http://www.avian.uga.edu/).** Startup funds, state-funded salary commensurate with experience, and modern research facilities will be provided. The position is available August 2008.

Applicants should send a statement of interest detailing research and their curriculum vitae, along with names, addresses, and e-mail addresses of three references (in one PDF file) by 31 December 2007, by e-mail to: **Dr. Egbert Mundt, e-mail: emundt@uga.edu** or by mail to: **Dr. Egbert Mundt, Department of Population Health, 953 College Station Road, Athens, GA 30602.** Applications will be entertained until the position is filled. *The University of Georgia is an Equal Opportunity Affirmative Action Institution.*

---

### CHAIRPERSON
**Department of Physics**
**Morehouse College**

Morehouse College invites applications for the position of Chairperson of the Department of Physics effective July 1, 2008. Applicants should hold a Doctorate in physics, and have appropriate research and teaching experience to qualify for an appointment at either the **ASSOCIATE or FULL PROFESSOR** level. We seek an effective and imaginative Administrator. As an undergraduate institution, Morehouse values excellence in teaching, research, and mentoring. The successful applicant should demonstrate a capacity to assume a leadership role in the Department, will be expected to maintain an active research program, and to have a strong commitment to enhancing the teaching and research capacity of the Department. For more information on the Department and College, visit our **website: http://www.morehouse.edu.** Please submit full curriculum vitae and an official copy of a graduate school transcript by January 23, 2008, and also provide the names of three professional references from whom the College will request reference letters by the same date to:

**J.K. Haynes, Ph.D.**
**Dean, Division of Science and Mathematics**
**Morehouse College**
**830 Westview Drive, S.W.**
**Atlanta, GA 30314**

*Morehouse College is an Equal Opportunity/Affirmative Action Employer.*

## POSITIONS OPEN

### TENURE-TRACK AVIAN ECOLOGIST

We seek a colleague who is highly committed to teaching bright, motivated undergraduates, in lecture, field laboratory, and research venues, at a nationally ranked department in a liberal arts college with a strong sense of community. Teaching responsibilities include co-participation in our core ecology course, an upper level course in ornithology, plus two other upper-level specialty courses. The following are essential attributes: commitment to collaborative student-faculty research, to periodic leadership of trips to the tropics, and to sharing a broad understanding of natural history. Ph.D. required, postdoctoral preferred, and we will begin reading applications on December 1, 2007. Send cover letter, curriculum vitae, and teaching philosophy and research statements, and arrange to have three letters of reference sent to: **Dr. Brent Smith, Department of Biology, Earlham College, Richmond, IN 47374 (website: http://www.earlham.edu/~biol).** *Earlham eagerly solicits applications from African-Americans and other ethnic minorities, women, and Quakers.*

---

### FACULTY POSITIONS in ORGANIC CHEMISTRY
**University of California, San Diego**

The Department of Chemistry and Biochemistry of University of California, San Diego **(website: http://www-chem.ucsd.edu)** invites applications for tenure-track faculty positions in organic chemistry. A Ph.D. or equivalent degree in one of the chemical sciences is required. Candidates are expected to establish a vigorous and original research program and be capable of outstanding teaching at the undergraduate and graduate levels. Salary, commensurate with qualifications and experience, is based on University of California pay scale. Applicants are asked to submit curriculum vitae, a summary of research plans, and a list of publications online at **website: http://www-chem.ucsd.edu/recruit/index.cfm?addno=4-983.** Candidates should arrange for three reference letters to be mailed directly by references to: **Chair, Organic Search Committee, 4-983 University of California, San Diego, Department of Chemistry and Biochemistry, 9500 Gilman Drive, Mail Code 0332, La Jolla, CA 92093-0332.** Review of applications begins December 1, 2007, and will continue until the position is filled. *UCSD is an Equal Opportunity /Affirmative Action Employer with a strong institutional commitment to the achievement of diversity.*

---

### POSTDOCTORAL ASSOCIATE

Postdoctoral positions, available starting immediately, to study DNA damage and repair in the MIT Department of Biological Engineering **(website: http://web.mit.edu/engelward-lab/).** Project one - cancer and inflammation: Exploit transgenic mouse models to study the relationship between exposures, mutations, and cancer with a particular focus on DNA damage. Become involved in making novel transgenic animals designed to detect sequence rearrangements and clonal expansion. Project two - microfluidic devices for studies of DNA damage and repair: Work with engineers to invent new tools for high-throughput analysis of DNA damage levels in human cells. Exploit novel technologies to study gene-environment interactions that promote cancer. Doctorate in biology or related subject is required.

Funding at a competitive rate is guaranteed for one year; support is available for up to three years. Send application materials to: **Prof. Bevin P. Engelward, MIT Department of Biological Engineering, 56-631, 77 Massachusetts Avenue, Cambridge, MA 02139-4307;** or to **e-mail: bevin@mit.edu.** *Equal Opportunity/Affirmative Action Employer.*

## POSITIONS OPEN

### FACULTY POSITIONS in CARDIOVASCULAR BIOLOGY
**University of Cincinnati**
**Molecular Genetics/Biochemistry/Microbiology**

Cardiovascular investigators sought for tenure-track **ASSISTANT, ASSOCIATE, or FULL PROFESSOR FACULTY** positions in the Departments of Medicine or Molecular Genetics/Biochemistry/Microbiology to work with the existing Interdisciplinary Cardiovascular Center of Excellence. The University of Cincinnati, as part of its Cardiovascular Initiative, is seeking individuals who have a strong and competitive cardiovascular research programs. The University intends to supplement its already prominent cardiovascular group, which includes expertise in cell signaling, gene regulation, calcium handling, and molecular basis of cardiovascular disease, stem cell therapy, and developmental biology. Secondary and joint appointments are feasible. Candidates with expertise including, but not limited to, the areas of stem cell and regenerative biology, translational research, molecular cardiovascular biology and signaling, and who would synergize with existing investigators are encouraged to apply. Candidates should have a strong record of scholarly accomplishment, and should be able to work in a highly collaborative, interdisciplinary environment. In addition to a generous recruitment package, an **ENDOWED CHAIR** is available for the exceptional candidate. Successful candidates will be expected to maintain an innovative, externally funded research program, contribute to graduate and medical student teaching and training of fellows, and participate in clinical activities (for M.D. candidates). Submit resumes to:

**Search Committee**
**Department of Molecular Genetics**
**University of Cincinnati**
**P.O. Box 670524**
**Cincinnati, OH 45267-0524**
**E-mail: jerry.lingrel@uc.edu**
**Telephone: 513-558-5324**
**Fax: 513-558-1190**

---

### CHEMISTRY/BIOCHEMISTRY-CANCER CENTER-PHARMACY FACULTY POSITION
**University of California, San Diego**

The Department of Chemistry and Biochemistry of University of California (UC), San Diego **(website: http://www-chem.ucsd.edu),** the Moores Cancer Center **(website: http://cancer.ucsd.edu/)** and the Skaggs School of Pharmacy and Pharmaceutical Sciences **(website: http://pharmacy.ucsd.edu/)** invite applications for a tenure-track or tenured faculty position in an area of chemistry, chemical biology, or biochemistry contributing to basic knowledge in the field of oncology, translational medicine, or translational pharmacology. Candidates must have a Ph.D., Pharm.D., or M.D., and a demonstrated ability for creative research and teaching at the undergraduate and graduate levels. Senior candidates will be jointly appointed with the Department of Chemistry and Biochemistry and the Skaggs School of Pharmacy and Pharmaceutical Sciences, and will have academic commitments in both units. Salary is commensurate with qualifications and based on the University of California pay scale. Applicants are asked to submit materials online, **website: http://www-chem.ucsd.edu/recruit/index.cfm?addno=4-985.** Materials include cover letter, curriculum vitae, complete list of publications, list of current and past grant support, samples of published research, and statement of your teaching experience.

Please arrange for three reference letters to be mailed directly by references to: **Chair, Chemistry/Cancer Center Search 4-985, University of California, San Diego, Department of Chemistry and Biochemistry, La Jolla, CA 92093-0332.** The deadline for applications is December 1, 2007, but until position is filled, all applications received will be assured full consideration. *UCSD is an Equal Opportunity/Affirmative Action Employer with a strong institutional commitment to the achievement of diversity.*

## POSITIONS OPEN

### TENURE-TRACK FACULTY POSITION
### Bioinformatics
### Department of Biological Sciences
### The University of Southern Mississippi

The University of Southern Mississippi Department of Biological Sciences invites applications for a tenure-track **ASSISTANT PROFESSOR** position in computational biology. The position is tied to the development of the NSF-funded Mississippi Computational Biology Consortium (**website: http://mcbc.usm.edu/mcbc/**), a network of expertise that is collectively and cooperatively interfacing computer science and technology with the biological sciences within the State of Mississippi. We seek expertise in the application of informatics tools to biological problems that enhance a growing strength in cellular and molecular biology. Suitable research areas include, but are not limited to, comparative genomics, data mining, systems biology, or structural informatics. The successful candidate will have the opportunity to participate in the Mississippi Functional Genomics Network, a competitively funded NIH consortium that spans the disciplines of genomics, proteomics, cellomics, and bioinformatics (**website: http://mfgn.usm.edu/mfgn/**).

The University of Southern Mississippi, a Carnegie High Research Activity Institution with over 14,000 students, is located in Hattiesburg, Mississippi, near the Gulf Coast and abundant opportunities for outdoor recreation. Hattiesburg is the medical, commercial, and cultural center of south Mississippi and is ranked in the top five small metropolitan areas in the United States. The Department of Biological Sciences is comprised of over thirty faculty and offers Baccalaureate degrees in biological sciences and marine biology. Over 60 graduate students currently pursue Master's and doctoral degrees. Further information about the Department may be found at **website: http://www.usm.edu/biology/**.

The successful candidate will be expected to establish an active, extramurally funded research program, mentor graduate students, and participate in undergraduate and graduate teaching in his area of expertise. Postdoctoral research experience is required; salary is commensurate with qualifications and experience. Applicants should submit a letter of application, curriculum vitae, statement of research plans, copies of pertinent reprints, and three letters of reference to: **Dr. Shiao Wang, Bioinformatics Search Committee, Department of Biological Sciences, The University of Southern Mississippi, 118 College Drive #5018, Hattiesburg, MS 39406-0001.** Electronic submission accepted (**e-mail: shiao.wang@usm.edu**). Review of applications will begin December 11, 2007, and continue until the position is filled.

*The University of Southern Mississippi is an Affirmative Action/Equal Opportunity Employer.*

---

**BRANDEIS UNIVERSITY.** The Biochemistry Department seeks a full-time faculty member to teach introductory biochemistry lecture and laboratory classes beginning fall 2008. Candidates should have a Ph.D. in biochemistry or a related field, postdoctoral, and/or teaching experience, and be committed to undergraduate education. This will be a one-year, renewable nontenure track appointment. Salary and rank will be commensurate with experience.

Applicants should submit curriculum vitae, statement on teaching philosophy, syllabi from any courses taught by the applicant, and three letters of reference to:

**Ms. Lynn Olsen, Search Coordinator**
**Biochemistry Department, M.S. 009**
**Brandeis University**
**P.O. Box 549110**
**Waltham, MA 02454-9110**

First consideration will be given to applications received by December 15, 2007. *Brandeis University is an Equal Opportunity Employer committed to building a culturally diverse intellectual community, and strongly encourages applications from women and minorities.*

## POSITIONS OPEN

**POSTDOCTORAL POSITION.** HIV recombination creates viral diversity that obstructs therapy. We are defining the mechanisms of DNA-RNA strand interactions and viral protein activities that promote recombination within the co-packaged HIV genomes. Strong background in biochemistry and molecular biology required. Send curriculum vitae and three recommendations to: **Dr. Robert Bambara, Biochemistry and Biophysics, P.O. Box 712, University of Rochester, Rochester, NY 14642; website: http://www.urmc.rochester.edu/smd/bcbp.**

---

### POSITION ANNOUNCEMENT
### MICROBIOLOGY FACULTY POSITION
### College of Sciences and Mathematics
### Auburn University

The Department of Biological Sciences at Auburn University invites applications for a tenure-track faculty position at the **ASSISTANT PROFESSOR** level in microbiology beginning fall 2008. The successful candidate is expected to establish an internationally recognized research program in an area of microbiology, and engage in the training of graduate and undergraduate students. The successful candidate will also have teaching responsibilities in the microbiology program and will participate in teaching general microbiology.

Applicants should have a Ph.D. in microbiology or a closely related discipline with at least two years of postdoctoral experience in microbiology. Desired qualifications include a strong record of publication, teaching experience, and good interpersonal skills. *The candidate selected for this position must be able to meet eligibility requirements to work in the United States at the time appointment is scheduled to begin and continue working legally for the proposed term of employment, and be able to communicate effectively in English.*

Applicants should submit curriculum vitae, a description of research interests and teaching experience, and the names and contact information of at least three references to: **Dr. James Barbaree, Biological Sciences Search Committee Chair, Department of Biological Sciences, 101 Life Sciences Building, Auburn University, AL 36849-5407.** Review of applications will begin December 15, 2007.

*Auburn University is an Affirmative Action/Equal Opportunity Employer. Women and minorities are encouraged to apply.*

---

### TENURE-TRACK POSITION
### ASSISTANT PROFESSOR
### University of California, Davis

The Departments of Nutrition and Food Science and Technology are currently seeking to fill a faculty position by July 1, 2008. We are interested in individuals who have or can establish a strong research program focusing on metabolic regulation, specifically the physiological impact of nutritionally dependent metabolic fluxes and patterns. The candidate must have demonstrated skills and abilities related to the integration of metabolic data with high information content into physiologically meaningful results. Teaching responsibilities will include undergraduate and graduate courses in metabolic regulation, particularly those that emphasize quantitative and analytical concepts.

Full details and application information can be found at **website: http://ffh.recruitments.ucdavis.edu.** Online applications should be submitted no later than December 31, 2007.

*UC Davis is an Affirmative Action/Equal Employment Opportunity Employer and is dedicated to recruiting a diverse faculty community. We welcome all qualified applicants to apply, including women, minorities, individuals with disabilities, and veterans.*

## POSITIONS OPEN

### ASSISTANT PROFESSOR of BIOLOGY
### The University of Mississippi

The Department of Biology at the University of Mississippi invites applications for a tenure-track Assistant Professor position starting August 2008. The successful candidate will be expected to develop an active research program in any area related to immunology. Teaching responsibilities will include a course in immunology, a graduate course in the individual's area of expertise, and the opportunity to rotate through a course in cellular and molecular biology, microbiology, physiology, or freshman biology.

To apply, please visit our Online Employment Service at **website: http://www.jobs.olemiss.edu.** Address questions to: **Dr. Colin Jackson, Search Committee Chair, e-mail: cjackson@olemiss.edu.**

*The University of Mississippi is an Equal Employer Opportunity/Affirmative Action/Title VI/Title IX/Section 504/ADA/ADEA Employer.*



## MARKETPLACE

# R&D Systems: With You Every Step of the Way

**STEP 1**

## Choose from our various multiplex assays to screen for your proteins of interest.

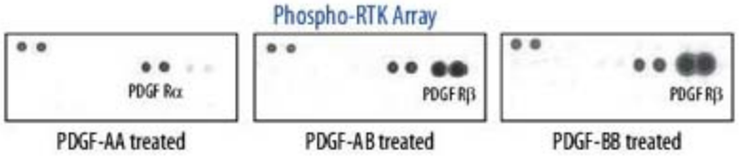



**STEP 2**

## Quantify your results with our dependable ELISA/Assay kits.

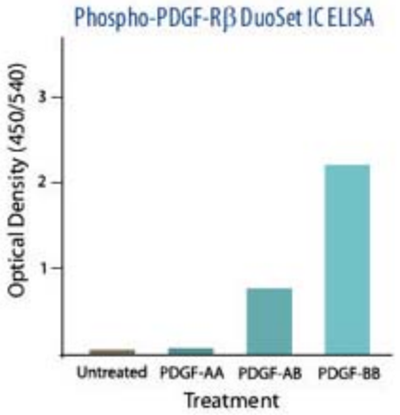


**STEP 3**

## Select from a wide range of high quality proteins and antibodies that ensure accurate results for many types of experimental procedures.

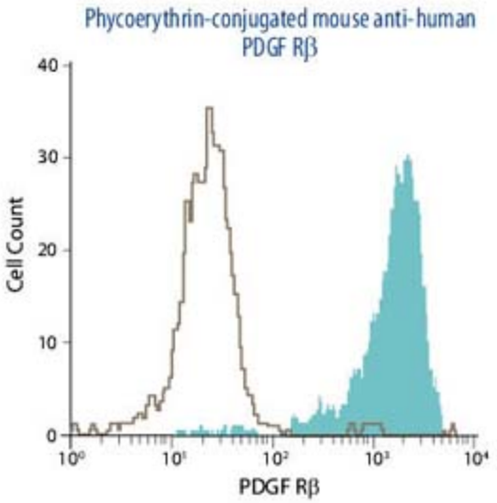


Request your poster by visiting www.RnDSystems.com/go/2007Poster


Selection expanding weekly—visit www.RnDSystems.com to sign up for weekly new product updates.


USA & Canada **R&D Systems, Inc.** Tel: (800) 343-7475 info@RnDSystems.com

Europe **R&D Systems Europe, Ltd.** Tel: +44 (0)1235 529449 info@RnDSystems.co.uk




R&D SYSTEMS®